Computational design of organic diradicals for energy applications

by Diego López Carballeira
Directed by Fernando Ruipérez and
Aurelio Mateo Alonso
Donostia, 2018

Acknowledgements

Agora que xa cheguei ó final do meu doutoramento en Donostia, hai que destacar o afortunado que me sinto de ter traballado co meu director de tese, Fernando Ruipérez. Estivo sempre ahí para dar apoio e consellos, traballou comigo incansablemente, e foi comprensivo cando foi necesario. Por iso, Fernando merece ser mencionado en primeiro lugar. Así mesmo, non podo pasar por alto a David Casanova, que gracias ós seus profundos coñecementos e a súa boa disposición, fixo grandes aportacións a esta tese.

Tamén quero destacar a aportación que tiveron na miña formación Marcos Mandado Alonso e Ignacio Pérez Juste namentres estiven en Vigo na miña etapa de master. Tamén de Vigo é José Manuel Hermida Ramón, responsable de primeira man de que puidera estar doutorandome en Polymat a día de hoxe.

Alén de toda a xente vencellada dalgunha forma na miña carreira académica, é necesario mencionar a todos aqueles que foron esenciais para que eu puidera manter a saúde psicolóxica. Por iso, sempre terei un bo recordo dos compañeiros de Trisquele, que fixeron un pouquiño máis doado que Donostia se convirtese no meu fogar.

Tamén debo agradecer ós meus pais ó seu perseverante apoio e a súa preocupación. Por último, pero

non menos importante, debo mencionar a Cristina, que estivo ó meu carón nos malos e nos bos momentos, e axudou a facer que sexa a persoa que son hoxe.

Contents

Chapter 1

Introduction

1. Radicals and diradicals

Since 1897, when Moses Gomberg synthesized for the very first time the trityl radical,[1,2,3] the chemistry of radicals has been subject of constant investigation. More than a century later, this special kind of molecules has been suggested as potential candidates for electronic devices,[4] environmentally friendly redox active materials,[5,6,7] and optoelectronic devices.[8,9] Most of the known radicals show an intrinsic instability and high reactivity in processes such as dimerization or polymerization, frequently appearing as intermediates in photochemical and thermal reactions. Nevertheless, there is a non-negligible number of radicals with longer life-times and stable enough to be characterized in solution (persistent radicals),[10] or even to be generated, isolated and stored.

Radical systems, also known as free radicals or monoradicals, are essentially those systems with an unpaired electron. Since the spin quantum number of an electron is S=1/2, the spin multiplicity (2S+1) for monoradicals is 2, that is, doublet. Those molecules with two unpaired and independent electrons are commonly denoted as diradicals or biradicals, depending on certain particularities. The long distance between the radical centers may produce an electron exchange interaction close to zero (J≈0), situation in which the appropriate denomination is biradical. Biradicals should be seen as two doublets inside the same moiety. In

the other hand, those molecules with two unpaired electrons and an electron exchange interaction different to zero (J≠0) are denominated diradicals, and may lead to two different spin multiplicities: singlet and triplet.

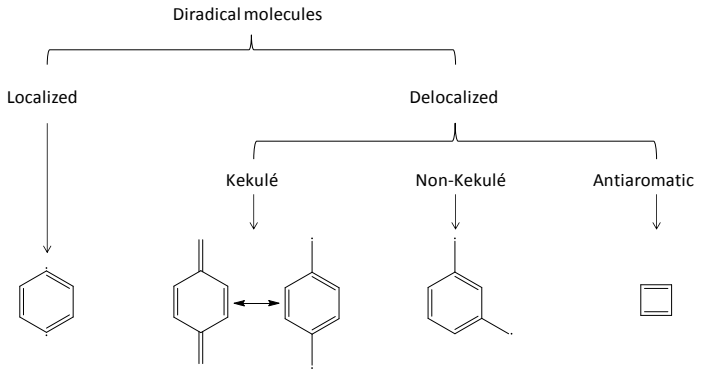

Figure 1: Different types of diradical molecules. From left to right, the represented molecules are *para*-benzyne, *para*-benzoquinone, *meta*-benzoquinone and cyclobutadiene.

Diradicals can be classified as localized and delocalized (see **Figure 1**). The latter can be further classified as Kekulé and non-Kekulé diradicals. Kekulé diradicals can be described as a structure with all the electrons paired (closed shell contribution) and as a structure with unpaired electrons (open shell contribution). Molecules such as *meta*-quinodimethane, tetramethylenemethane or oxyallyl derivatives are classified as non-Kekulé delocalized diradicals, which are not fully conjugated in their Kekulé structures. Additionally, antiaromatic molecules are also classified as delocalized systems, defined as planar cyclic molecules with 4n π-electrons. Thus, cyclobutadiene can be

represented with two rectangular isomers, where the diradical square structure plays the role of transition state.

When the two unpaired electrons are located in two non-bonding molecular orbitals, the diradical may be described by six electronic configurations: two triplets, two open-shell singlets and two closed-shell singlets (see **Figure 2**). If the molecular orbitals are degenerate, the system is denoted as diradical; when they are quasi-degenerate, the preferred term is diradicaloid.

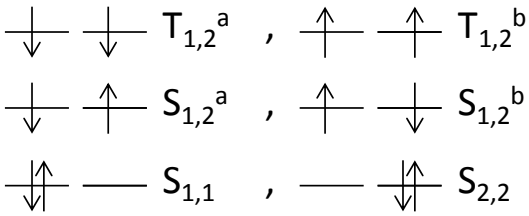

Figure 2: Electronic configurations describing the ground state of a molecule with two unpaired electrons.

Following Hund´s rule,[11] the most stable multiplicity for diradical molecules is the triplet followed by the open-shell singlet. The large electron-electron repulsion interaction (K) prevents the existence of two electrons sharing the same orbital, so that the closed-shell singlet is the least stable possibility. However, if the overlap integral between both molecular orbitals is quite small or negligible, Hund´s rule may not apply and the closed-shell singlet state might be the ground state. The electron exchange interaction (J) is proportional to the overlap integral; J<0 denotes a singlet

ground state, while J>0 states for a triplet. When the molecular orbitals are non-degenerate (diradicaloids), an energy gap appears between them. Thus, the closed-shell state appears as a possible electronic configuration for the ground state. If this energy gap is larger than the electron-electron repulsion (K), the preferred spin multiplicity is the singlet state. This means that a diradicaloid molecule can show an electronic configuration that may be described as an intermediate situation between a diradical (degenerate orbitals) and a closed-shell molecule.

One of the most important parameters for the study of diradicals is the singlet-triplet energy gap ($E[T_1]^{DFT}$), which can be calculated from J as: $E[T_1]^{DFT}=E[S_0]–E[T_1]=2J$. At this point, the diradical character appears as a magnitude to measure how important is the diradical configuration on a particular system, and it can be estimated from the occupation of the lowest unoccupied molecular orbital (LUMO).

Many experimental research has been performed to investigate this kind of molecules.[12,13,14,15,16,17,18] For instance, usual reactions as homolytic bond-cleavage or cyclization reactions depend fundamentally on localized diradicals that play the role of intermediate compounds. While triplet diradicals have been routinely investigated due to their long lifetimes, there is a lack of experimental data available for singlet diradicals. For example, molecules as *ortho*- and *para*-quinodimethanes, as well as Thiele´s[19] or Tschitschibabin´s[20]

hydrocarbons are illustrative Kekulé-type delocalized diradicals. Unfortunately, Kekulé-type diradicals are often unstable or difficult to stabilize.[21,22]

Nowadays, there is a renewed interest in diradical and multiradical systems due to the remarkable optical and magnetic properties they exhibit, in addition to their specific chemical reactivity.[23] For example, recent theoretical and experimental studies have opened a novel field of open-shell π-conjugated systems, such as polycyclic aromatic hydrocarbons and graphene, endorsing unique physico-chemical properties relevant in optoelectronics [24] and spintronics.[25,26,27] Some of these interesting properties are low-energy excited states,[28,29] tailorable low-spin/high-spin gaps,[30,31] high-yield singlet fission processes,[32,33,34] short intramolecular distances in the solid state[35,36] and large two-photon absorptions,[37] among others, and have been found to be originated in the singlet open-shell electronic structure of diradical character. Besides, singlet diradicals are involved in homolytic cleavage processes, and they are of great importance to investigate chemical reactivity and reaction mechanisms.[38]

For the sake of clarity, in this thesis, the difference between diradical and diradicaloid will be ignored and the term used to designate them will be “diradical”, despite most of the presented systems are actually “diradicaloid” molecules.

2. Photovoltaics

2.1. Solar energy harvesting. Solar cells

During the last decades, solar energy has gained acceptance as a clean and renewable alternative to the combustion of fossil fuels. Despite solar panels are already providing a large amount of energy, they still represent a small fraction of the total energy generated and consumed. In that manner, a large amount of energy is daily wasted, since the global energetic demands would be covered just by harvesting a 0.1% of the total sunlight, with an average conversion efficiency of 10%.[39] Moreover, this kind of energy can be indefinitely and ubiquitously harvested, avoiding accidents related to the inherent danger of installations such as nuclear power plants or oil refineries.

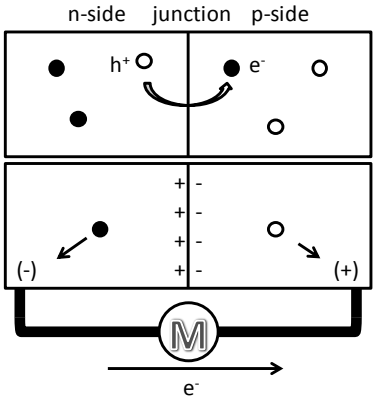

Figure 3: General structure of solar cell.

Solar cells owe their existence to the observation done by Edmond Becquerel in 1839, in which certain materials

produced small amounts of electricity after being irradiated with light. This finding was called photovoltaic effect, which is the basis of the physical process that leads to the conversion of sunlight into electrical energy. Thus, photovoltaics involves converting solar energy into electricity using semiconductor materials that exhibit the photovoltaic effect.

The general structure of a typical solar cell is shown in **Figure 3**. A layer of photoactive material is located between two electrodes. When a photon is absorbed, an electron-hole pair (exciton) is created. This pair can dissociate into separate charges that are transported to the electrodes, generating a current.

Table 1. Band gaps of several photovoltaic materials, in eV and nm (in brakets).

Material	Band gap
Silicon (Si)	1.11 (1117)
Copper oxide (CuO)	1.20 (1033)
Indium phosphide (InP)	1.35 (919)
Gallium arsenide (GaAs)	1.43 (867)
Cadmium telluride (CdTe)	1.49 (832)
Cadmium selenide (CdSe)	1.73 (717)
Selenium (Se)	1.74 (713)

In order to create the electron-hole pair, energy equal or higher than the band gap must be provided to promote the electron from the valence band to the conduction band. All wavelengths with less energy than the required will be wasted by heating the panel or just will pass through. In general, the band gaps of photovoltaic materials range between 1.1 to 1.8

eV (see **Table 1**).

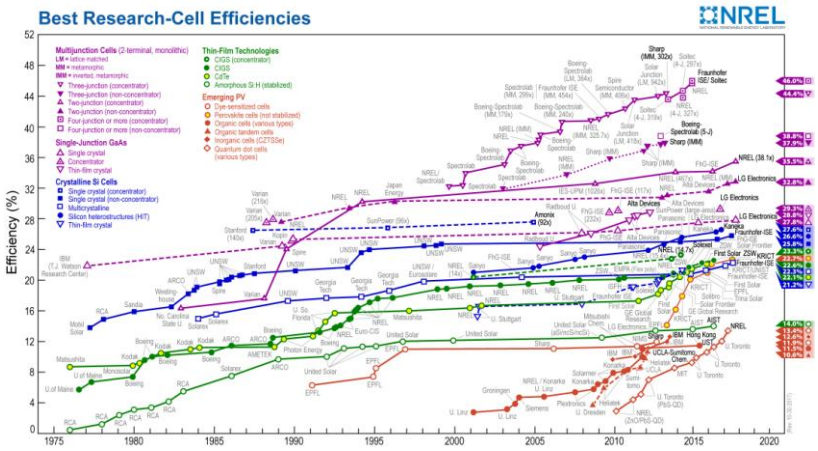

Figure 4: Conversion efficiencies of solar cells (1976-2017) for various photovoltaic technologies at research level. Taken from the National Renewable energy Laboratory (NREL).[40]

In order to overcome traditional polluting fuels and impose the solar energy as one of the main sources of electricity, it is essential to keep on reducing the cost of the solar energy by increasing the efficiency of solar devices. Traditional crystalline silicon-based solar panels have achieved a 25.6% of efficiency, approaching the maximum theoretical limit for a single-junction solar cell, set as 32% by the Shockley-Queisser limit.[41] In recent years, second- and third-generation solar cells based on organic [42] or hybrid materials [43] have been developed achieving promising efficiencies of conversion in research solar cells (22.1%),[44] see **Figure 4**. Amongst these technologies, organic-based solar cells are especially appealing due to their low

manufacturing costs, mechanical properties and design capabilities, but their conversion efficiencies are still too low.

One of the main energy losses in solar cells results from the inability to harvest and efficiently convert high-energy solar photons into electricity. Processes that can provide new paths to circumvent the energy loss are based either on the combination of two-low energy photons to generate a photon with a suitable energy or, alternatively, by splitting a high-energy photon into two energetically adequate photons. Those processes are called, respectively, upconversion and downconversion. [39,45,46,47] In the case of organic materials, the downconversion of short wavelength photons is called singlet fission (SF).[33]

2.2. Singlet fission

By definition, singlet fission is a spin-allowed photophysical process in which one spin-singlet excited state splits into two triplets, hence potentially generating two low-energy excitons per absorbed photon. The whole process can be summarized as $S_0 + S_1 \rightarrow T_1 + T_1$, and is represented in **Figure 5**. Despite the growing interest and numerous experimental and theoretical efforts towards this phenomenon, the list of requirements has limited, so far, the number of efficient singlet fission compounds to only few molecules such as tetracene,[48] pentacene,[49,50,51] hexacene[52] and, more recently, copolymer structures based on strong intramolecular donor-acceptor interactions.[53] In that manner,

the implementation of the singlet fission process might boost the solar energy harvesting thanks to a remarkable enhancement of the energy recovery efficiency, due to the overcome of the Shockley-Queisser limit.

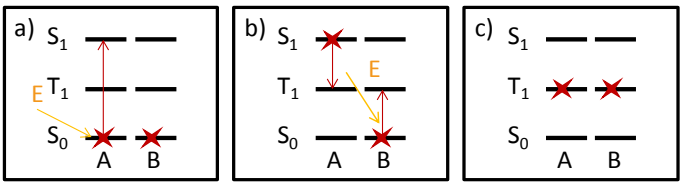

Figure 5: Stages of the singlet fission mechanism in which molecules A and B are involved. Firsly, the photon excites molecule A from S_0 to S_1 (a). Following, molecule A decays into T_1, so that the resulting energy may excite molecule B from S_0 to T_1 (b). Finally, both molecules, A and B, are in their triplet state (c).

In addition to the general requirements for solar cells sensitizers, such as good light-harvesting capabilities or photo-stability, singlet fission chromophores have to fulfill two energy conditions:[32] (i) the energy of the first singlet excited state ($E[S_1]$) should be slightly higher than (or at least equal to) twice the energy of the first triplet state ($E[T_1]$), in such a way that the process is exoergic (or isoergic). If the process is exaggeratedly exoergic the efficiency may be reduced due to energy loss by heating. (ii) The second triplet excited state ($E[T_2]$) must be higher in energy than twice the energy of the first triplet excited state ($E[T_1]$) in order to avoid no-fission decay into the triplet manifold. The deactivation channel into the quintuplet manifold is typically not considered, since the

Q_1 state in organic molecules is expected to lie at higher energies.

One of the fingerprints of diradical molecules is the small singlet-triplet gap ($E[T_1]^{DFT}$), mainly derived from the small energy difference between the HOMO and the LUMO inherent to this kind of molecules. This feature can be exploited for singlet fission.

3. Organic batteries

Since the early 90s,[54] lithium-based batteries have been gaining commercial acceptance, since they represent a big reduction on the size and weight of electronic devices. The main reason is the remarkable improvement of the energy density compared to traditional nickel-cadmium or nickel-metal hydride batteries. Together with the long cycle life, all these advantages have made lithium batteries the dominant technology to provide power for small portable devices, such as cell phones, as well as modern electric-powered cars. However, the conventional inorganic cathode materials, such as $LiCoO_2$ or $LiFePO_4$, are composed of metals, some of which come from limited resources. Thus, waste processing is a difficult and crucial issue that causes environmental concern. As an alternative to inorganic functional materials, electroactive organics or polymers involving reversible redox reactions are promising candidates as electrode materials for green lithium batteries, because of

their light weight, flexibility, higher theoretical capacity, safety and potential low cost.[55,56,57]

3.1. Working principles

Independently of how it is composed, a battery consists in a cathode (the electrode where the reduction occurs) and an anode (which supports the oxidation). The whole system is submerged on an electrolyte and, in order to avoid dead short circuit, both electrodes are separated by a separator. To assemble a rechargeable battery, there must be a voltage gap large enough between the cathode (with higher redox potential) and the anode (with lower redox potential). Among the possible cell configurations, one of the most common is the so-called n-type, where the redox reaction takes place between the neutral state and the negatively charged state. In this process, a cation (usually Li^+) is necessary to neutralize the negative charge in the organic compound (see **Figure 6**).

A rechargeable battery may be characterized by the following values:[58]

- *Cell voltage*: The common $LiCoO_2$ battery shows high voltage (≈3.9V), but in certain cases a redox potential higher than 2 V can be considered enough.

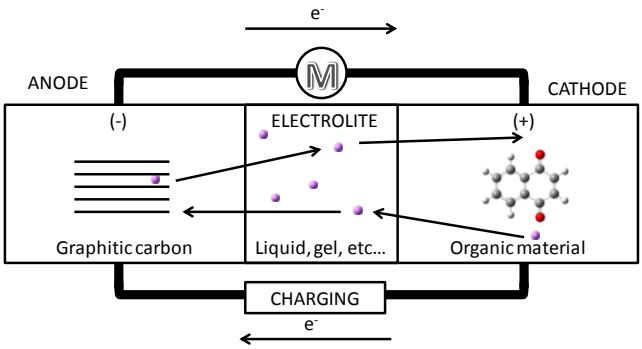

Figure 6: General structure of the discharge and charge processes of an organic battery.

- *Capacity (C):* Defined as the ratio between the charges stored by unit of mass. The specific capacity (experimental) is always lower than the theoretical one, referred as the capacity that should show a molecule to be completely reduced or oxidized. The cathode of $LiCoO_2$ battery is characterized by a capacity of 295 $mAhg^{-1}$ (around 140 $mAhg^{-1}$ if it is considered the full battery) and, considering that this magnitude is one of the weak points of the commercial Li-ion energy storage devices, batteries with high capacity can be expected in the future, expressed as shown in the formula below. There, n stands for the number of electrons transferred per molecule, F is the Faraday constant (96485 $Cmol^{-1}$) and M_W is the molecular weight ($gmol^{-1}$).

$$C_{THEO} = \frac{nF}{M_W}$$

- *Energy density:* Defined as the product of the cell voltage by the capacity. In case of $LiCoO_2$, it may reach 600 $WhKg^{-1}$.
- *Coulombic efficiency:* It is the percentage that relates the charge and the discharge capacity. It should be higher than 95%.
- *Cycle life*: Is the number of complete charge/discharge cycles that the battery is able to resist. It should be over 3000.
- *Rate capability:* Measures the necessary current to completely charge the battery on a certain period of time. For instance, 1h is expressed as 1C, while 2C means 30 min. This feature can be related with the charging time, almost as important as the cell voltage itself for a practical commercial use. $LiCoO_2$ batteries show rates between 0.1C and 5C (10 h-12 min), so higher rates would be recommended.

3.2. Organic cathodes

After almost three decades of intense development of Li-ion batteries using metal-based inorganic materials ($LiCoO_2$, $LiFePO_4$) as cathode, this technology is reaching its theoretical limit.[59,60] Thus, plenty of investigations and reviews can be found in the literature, where some promising materials are suggested.[56,61]Among them, different types of molecules can be highlighted, namely, conjugated amines,

thioethers and carbonyls, conducting polymers, organodisulfides, etc.

One of the most common sorts of organic cathodes is that composed of conjugated carbonyl compounds.[55,56,57] In 1972, Alt *et al*.[62] suggested a set of quinone molecules including *p*-benzoquinone or diphenoquinone, concluding that conjugated carbonyl molecules show adequate features to be used as cathode in secondary (rechargeable) batteries. In aqueous solution, quinones can be reduced in a two-electron step, while in an aprotic media the quinone (Q) can be reduced to the semiquinone (Q^{-}) and to the quinone dianion (Q^{-2}), in two separated monoelectronic processes. The Q^{-} molecule is reversibly obtained and shows an intrinsic instability that leads to disproportionation, producing the initial Q molecule together with Q^{-2}. In the other hand, the dianion generation by reduction of the semiquinone is a quasireversible process. The redox behavior of quinones has been profusely analyzed.[63]

The most striking disadvantage is the high solubility of the quinones on the electrolytes, reducing drastically the cyclability. Some attempts to solve this problem led fundamentally to two successful strategies. The first one is to increase the size of the molecules, for example synthesizing quinones with large substituents, or even polymers. The second strategy is to adsorb the molecules into surfaces, immobilizing them on solid substrates through physisorption

or chemisorption. Finally, solid-state organic batteries are a novel solution in which the electrolyte is a solid polymer.[64,65]

The reduction potentials of the traditionally investigated organic cathodes are determined by the stability of the reduced form, whereby the influence of the solvent, the electrolyte, etc., plays a fundamental issue. Additionally, the nature of the cathode ground state may deeply affect the reduction potential as well as other fundamental factors such as the stability.

4. Motivation and scope of the work

The continued increase in global energy demand is today one of the greatest challenges that the scientific community must face. The increasingly limited supplies of fossil fuels together with the inherent problems they present (high environmental risks, rising prices, etc.) are an indication of the need to find alternative energy sources, environmentally sustainable and cheap.

Among the plethora of materials proposed, organic singlet open-shell diradicals represent a new and promising alternative to conventional organic materials due to their unique electronic structures and fascinating properties, such as low-energy gaps between the triplet and singlet ground states, near-IR absorption, enhancement of nonlinear optical properties, etc. In particular, theoretical studies on the singlet fission process suggest the important role of open-shell

diradicals in future photovoltaic devices to enhance the efficiency of the current commercial solar cells. Furthermore, the electrochemical features of diradical molecules containing carbonyl groups deserve a close inspection, since quinones are capable to provide high reduction potentials and high energy density to design organic batteries. Nevertheless, the non-negligible diradical nature that many conjugated carbonyls present has been omitted in almost all of the published works so far. These appealing features are known to be originated in the open-shell character of the ground state.

In spite of the great experimental efforts devoted to the characterization of these systems, many of their properties remain elusive, fundamentally due to the difficulties to obtain empirical data from these unstable systems. In this context, computational approaches have emerged as a valuable tool to unravel some of the otherwise inaccessible features of diradicals. This thesis represents a contribution to this computational effort, aimed at calculating, understanding and predicting properties of singlet-open shell diradicals.

In this thesis, a systematic study is performed to:

(i) Analyze in detail the features that may tune the open-shell diradical character of organic molecules and its influence in both the ground and low-lying excited states, as well as in the electrochemistry of these molecules, to be used as a useful guideline

for the design of new efficient singlet fission sensitizers and organic cathode materials.

(ii) Accomplish a screening of a large number of diradical molecules that may be useful for the experimental community, as a first step towards the pursuit of these new materials.

The content of this thesis is organized as follows:

- In Chapter 2, the most relevant computational methods used in this work are summarized.
- In Chapter 3, different DFT and TDDFT approaches are assessed, in order to choose the best suited for the purpose of this thesis.
- In Chapter 4, an extensive and systematic study of the conditions by which the diradical character may be affected is performed.
- In Chapter 5, the carbonyl-containing molecules from Chapter 4 are selected to calculate their electron affinities, ionization potentials and their reduction potentials to evaluate their feasibility to be used as cathode materials.
- In Chapter 6, the low-lying excited states are calculated for all the molecules of Chapter 4, as required to evaluate the energy requirements for an efficient singlet fission process.
- Finally, in Chapter 7 are summarized the major conclusions of this thesis.

Chapter 2

Computational methods

1. Schrödinger equation

The most fundamental equation in quantum mechanics is the Schrödinger equation,[66] often expressed as:

$$\hat{H}\psi = E\psi$$

where $\hat{H}$ is the Hamiltonian operator and ψ is the wavefunction, a mathematical function that contains all the information of a given system and is the eigenfunction of $\hat{H}$. The application of the Hamiltonian operator to the wavefunction yields the eigenvalue *E*, the energy of the system.

For a system with *N* electrons and *M* nuclei, the non-relativistic Hamiltonian includes the kinetic energy of both nuclei ($\hat{T}_n$) and electrons ($\hat{T}_e$), the electron-nucleus attraction ($\hat{V}_{ne}$) as well as the repulsion between electrons ($\hat{V}_{ee}$) and nuclei ($\hat{V}_{nn}$):

$$\hat{H} = \hat{T}_e + \hat{T}_n + \hat{V}_{ne} + \hat{V}_{ee} + \hat{V}_{nn}$$

which, in atomic units, would be expressed as follows:

$$\hat{H} = \sum_{i=1}^{N}\left[\frac{-\nabla_i^2}{2} + \sum_{A=1}^{M}\frac{-Z_A}{|\overrightarrow{r_i} - \overrightarrow{R_A}|}\right] + \sum_{i>j}^{N}\frac{1}{|\overrightarrow{r_i} - \overrightarrow{r_j}|} + \sum_{A=1}^{M}\frac{-\nabla_A^2}{2m_A} + \sum_{A>B}^{M}\frac{Z_A Z_B}{|\overrightarrow{R_A} - \overrightarrow{R_B}|}$$

This complex equation can only be solved exactly for a one-electron system (e.g. the hydrogen atom), due to the electron-electron interaction term ($|\vec{r_i} - \vec{r_j}|$, second summation in previous Equation) and approximations must be done.

1.1. Born-Oppenheimer Approximation

The Born-Oppenheimer approximation[67] is based in the difference of mass between the electrons and the nuclei (the mass of the proton and the neutron is about 1800 times larger than the electron mass). Thereby, the motion of the electrons is several orders of magnitude faster than that of the nuclei, that is, on the time scale of the electron motion, nuclei can be considered as stationary objects. Similarly, electrons are assumed to respond instantaneously to any change in the nuclear configuration and, therefore, the nuclei are considered to move in the mean field generated by the electrons. In consequence, this allows the nuclear and electronic parts of the Schrödinger equation to be treated separately. In other words, for the electronic motion, the nuclear kinetic energy term ($\hat{T}_n$) is neglected and the nuclear repulsion term ($\hat{V}_{nn}$) is a constant, while the interaction between nuclei and electrons ($\hat{V}_{ne}$) depends parametrically on the coordinates of the fixed nuclei.

As a result, the molecular Schrödinger equation is transformed into the electronic Schrödinger equation, where the wavefunction, ψ_e, depends explicitly only on the electronic coordinates.

2. *Ab initio* methods

Besides the Born-Oppenheimer approximation, further approximations have to be made in order to solve the molecular Schrödinger equation, which are the origin of the field of quantum chemistry, in such a way that quantum chemical models differ in the nature of these approximations and span a wide range, both in terms of reliability and cost.

The most representative approximation is the Hartree-Fock (HF) method[68] which, when applied to the many-electron Schrödinger equation, leads to an important class of quantum chemical models, the molecular orbital models, and also provides the foundation for both simpler and more complex models. In the Hartree-Fock method, in order to fulfill the Pauli Exclusion Principle, the wavefunction is an antisymmetrized determinantal product (the so-called Slater determinant) of one-electron orbitals, which depends explicitly on the *3N* coordinates of the electrons, in an *N*-electron system. In this approximation, each electron moves independently in the average field created by the rest of the electrons and the nuclei, leading to a set of uncoupled single-particle equations, the Hartree-Fock equations.[69,70] Using the variational principle, we ensure that the obtained wavefunction is the best one, that is, that yields the lowest energy of the system.

HF models provide reasonably good description of equilibrium geometries and conformations, except when

transition metals are involved. However, they behave poorly in accounting for the thermochemistry of reactions involving explicit bond breaking and forming. The failures can be traced back to the incomplete description of electron correlation, that is, the way in which the motion of one electron affects the motions of all the other electrons. In order to allow for electron correlation, several quantum chemical methods have been developed. Among them, three fundamental approaches must be underlined: (i) configuration interaction (CI),[71] (ii) Møller-Plesset perturbation theory (MP)[72] and (iii) coupled-cluster approaches (CC),[73] which extend the flexibility of the HF method by mixing ground-state and excited-state wavefunctions, that is, using several Slater determinants obtained from a permutation of electron occupancies among all the molecular orbitals available. These approaches are significantly more expensive than HF but provide excellent descriptions of thermochemistry.

2.1. Density Functional Theory

A conceptually different methodology to include electron correlation is Density Functional Theory (DFT), which is based on the electron density (ρ), as opposed to the many-electron wavefunction, ψ. This is the main difference that makes DFT to be more cost-efficient: the simplest wavefunction depends on *3N* spatial coordinates, whereas the probability distribution of electrons in space depends only on three coordinates.

There are, nevertheless, similarities between wavefuntion-based and electron density-based approaches. First, the essential building blocks of a many-electron wavefunction are the one-electron orbitals, which are analogous to the orbitals used in DFT. Second, both the electron density and the wavefunction are constructed from a self-consistent field (SCF) approach. This procedure is an iterative process where an approximate Hamiltonian is constructed to solve the Schrödinger equation and to obtain a set of molecular orbitals that are used to construct another Hamiltonian producing a new, more accurate set of molecular orbitals until the process reaches convergence. The SCF procedure leads to the molecular orbitals that minimize the energy.

2.1.1. Hohenberg-Kohn Theorems

The formulation of DFT provided by Hohenberg and Kohn[74] is based on the fact that the sum of the exchange and correlation energies of a uniform gas can be calculated exactly knowing only its density. These authors enunciated the following theorems:

i) Any observable of a stationary non-degenerate ground state can be calculated, exactly in theory, from the electron density of the ground state. In other words, any observable can be written as a functional of the electron density of the ground state.

ii) The electron density of a non-degenerate ground state can be calculated, exactly in theory, determining the density that minimizes de energy of the ground state.

The first theorem is considered the foundations of DFT, as states that the energy, as all the other properties of a system, is uniquely defined by the electronic density (ρ):

$$E_0[\rho] = T[\rho] + E_{ee}[\rho] + E_{Ne}[\rho]$$

$$E_0[\rho] = F_{HK}[\rho] + E_{Ne}[\rho]$$

In this equation, the ground state energy $E_0[\rho]$ is defined as the sum of the kinetic energy ($T[\rho]$), the electron-electron repulsion ($E_{ee}[\rho]$) and the nucleus-electron attraction ($E_{Ne}[\rho]$). As $T[\rho]$ and $E_{ee}[\rho]$ are unknown, they are gathered in the so-called Hohenberg and Kohn functional $F_{HK}[\rho]$.

The second theorem provides the variational principle for E(ρ), that is, allows to obtain ρ variationally.

2.1.2. Kohn-Sham Approach

The Hohenberg-Kohn theorems are not enough to obtain information about the energy or other properties that could be calculated following the HF method, as none of them provide an explicit formula to perform the calculation of ρ. However, Kohn and Sham suggested a route to find the electronic density in the ground state using a non-interacting reference system.[75] In that manner, a Hamiltonian of a non-

interacting system could be defined as follows, in which the first term is the kinetic energy and the second is an effective local potential.

$$\hat{\mathrm{H}}_S = -\frac{1}{2}\sum_i^N \nabla_i^2 + \sum_i^N V_S(\boldsymbol{r_i})$$

Since this Hamiltonian does not contain any electron-electron interaction term, the ground state wavefunction ψ can be expressed in terms of spin orbitals (φ_i), in analogy to the HF method, that are eigenfunctions of the so-called Kohn-Sham operator ($\hat{\mathrm{h}}^{KS}$):

$$\hat{\mathrm{h}}^{KS}(i)\varphi(i) = \varepsilon_i\varphi(i)$$

$$\hat{h}^{KS}(i) = -\frac{1}{2}\nabla_i^2 - V_S(i)$$

To define the energy of a real (interacting) system, Kohn and Sham reformulated the Hohenberg-Kohn functional as:

$$F_{HK}[\rho] = T_S[\rho] + E_{ee}[\rho] = T_S[\rho] + J[\rho] + E_{XC}[\rho]$$

Following the previous equation, the electron-electron repulsion term is split into the classical Coulomb part ($J[\rho]$) and an unknown term called exchange-correlation energy ($E_{XC}[\rho]$), that basically contains the residual part of the true kinetic energy ($T[\rho] - T_S[\rho]$) and the non-classical electrostatic contributions ($E_{ee}[\rho] - J[\rho]$).

Finally, the potential due to the exchange-correlation energy ($V_{XC}[\rho]$), which is also unknown, is defined as the derivative of $E_{XC}[\rho]$ with respect to ρ:

$$V_{XC}[\rho] = \frac{\delta E_{XC}[\rho]}{\delta \rho}$$

2.1.3. Approximations to the exchange-correlation energy

The Kohn-Sham formalism is in principle exact, so it would lead to an exact energy value. However, $E_{XC}[\rho]$ and $V_{XC}[\rho]$ are unknown and approximations have to be made to decide the functional form of $E_{XC}[\rho]$. Thus, plenty of efforts have been focused on the development of an expression for the exchange-correlation term, summarized as follows:

2.1.3.1. Local Density Approximation

As a first approach, the Local Density Approximation (LDA) has been proposed. Within this method, the density is considered as a homogeneous gas, so each single position of the space is assigned to have the same constant value for the density

$$E_{XC}^{LDA}[\rho] = \int \rho(\boldsymbol{r}) \varepsilon_{XC}[\rho] d\boldsymbol{r}$$

Despite this method performs well for some systems in which the electron density decays slowly, in general this approximation is too rough for most of the systems in which

the density suffers rapid variations. Anyway, some properties can be obtained quite accurately, for instance geometries or vibrational frequencies, while the energetics (bond energies, energy barriers, etc.) are poorly represented.

For open-shell systems the Local Spin Density Approximation (LSDA) has been designed, replacing the density ρ by ρ_α and ρ_β.

2.1.3.2. Generalized Gradient Approximation

More sophisticated methods have been designed in order to reduce the errors related to the simple account of the density on the LDA approach. Thus, the first step beyond LDA was to consider the variation of the density with the distance as a gradient ($\nabla\rho(\mathbf{r})$). The functionals defined in this manner are known as Generalized Gradient Approximation (GGA) functionals. In practice, the exchange-correlation functional is split into the exchange ($E_X[\rho]$) and correlation ($E_C[\rho]$) terms:

$$E_{XC}^{GGA}[\rho] = E_C[\rho] + E_X[\rho]$$

Popular exchange and correlation functionals are the ones of Becke (B[76] and B86[77]) Perdew (P86),[78] Perdew, Burke and Ernzerhof (PBE),[79] Perdew and Wang (PW91),[80] and Lee, Yang and Parr (LYP).[81]The GGA methods can be further improved by introducing the laplacian of the electron density or the local kinetic energy density, denominated as meta-GGA methods.

2.1.3.3. Hybrid functionals

The exchange energy can be exactly calculated in Hartree-Fock, but lacks of electron correlation, which is accounted in DFT. Thus, the hybrid functionals are based on a combination of HF exchange and DFT correlation:

$$E_{XC} = E_X^{exact} + E_C^{KS}$$

where E_X^{exact} is referred to the exchange obtained from a Slater determinant built with the Kohn-Sham molecular orbitals.

One of the first hybrid functionals proposed has been the B3PW91 functional,[82,83,84] that combines the Becke three-parameter functional and the PW91 correlation as shown in the formula:

$$E_{XC}^{B3PW91} = (1-a)E_X^{LSDA} + aE_X^{HF} + b\Delta E_X^B + E_C^{LSDA} + c\Delta E_c^{PW91}$$

where *a*, *b* and *c* are 0.20, 0.72 and 0.81, respectively. The PW91 correlation may also be substituted by the LYP functional. The obtained functional is known as B3LYP,[81,82,85] and probably is one of the most popular functional nowadays:

$$E_{XC}^{B3LYP} = (1-a)E_X^{LSDA} + aE_X^{HF} + b\Delta E_X^B + (1-c)E_C^{LSDA} + cE_c^{LYP}$$

In both cases, the parameter that multiplies the E_X^{HF} is 0.2, so the percentage of HF used is 20%. However, these

parameters may be optimized for each functional and it may suffer strong variations from one to another. For instance, in the M06-2X functional developed by Truhlar and Zhao,[86] the percentage of HF exchange is enhanced to 51%, following the next expression:

$$E_{XC}^{M06-2X} = (1-a)E_X^{M06} + aE_X^{HF} + E_c^{M06}$$

Besides, new classes of hybrid functionals have been developed with the use of meta-GGA methods, leading to hybrid meta-GGA functionals.

Since all these DFT methods do not use the exact form of the exchange-correlation functional, they cannot be considered, strictly speaking, *ab initio* methods. Besides, there is no systematic way to improve the functionals and, therefore, a growing number of them is available. Nevertheless, since DFT provides with satisfactory results making use of low computational cost, is the method of choice for large systems, for which the inclusion of electron correlation by post-HF methods is prohibitive.

2.2. Time-Dependent DFT

The classic DFT formalism does not provide any information about the excited states, so only ground state properties can be predicted. Thus, the DFT fundamentals can be extended in order to describe time-dependent phenomena (TDDFT). [87,88] The time-dependent Schrödinger equation can be expressed as:

$$i\frac{\delta}{\delta t}\psi(\boldsymbol{r},t) = \hat{\mathrm{H}}(\boldsymbol{r},t)\psi(\boldsymbol{r},t)$$

$$\hat{\mathrm{H}}(\boldsymbol{r},t) = -\frac{1}{2}\sum_{i=1}^{N}\nabla_i^2 + \frac{1}{2}\sum_{i<1}^{N}\frac{1}{|r_i - r_j|} + V_{ext}(\boldsymbol{r},t)$$

The $V_{ext}(\boldsymbol{r},t)$ is the generic time-dependent potential that acts as a perturbation and can be assumed to have linear response when is weak. Often, this perturbation is modelled as a long-wavelength electric field with oscillation frequency ω.

2.2.1. Runge-Gross Theorem

Runge-Gross theorem is the time-dependent analogue of the first Hohenberg-Kohn theorem and provides a theoretical framework to construct the TDDFT formalism.[87] Hence, within this theorem can be proven that densities $\rho(\boldsymbol{r},t)$ and $\rho'(\boldsymbol{r},t)$ of two systems evolving from the same initial state $\psi(\boldsymbol{r},t_0)$ under the influence of the scalar potentials $v(\boldsymbol{r},t)$ and $v'(\boldsymbol{r},t)$, both Taylor-expandable about t_0 and differing by more than a purely time-dependent function, will always differ.

2.2.2. Time-dependent Kohn-Sham equations

In TDDFT it can be defined the action integral *A*, an analogous quantity to the ground state energy, that can be

expressed in terms of the density, as there is a unique mapping between the density and the wavefunction:

$$A[\rho(\boldsymbol{r},t)] = \int_{t_0}^{t_1} \left\langle \psi[\rho](t) \middle| i\frac{\delta}{\delta t} - \hat{\mathrm{H}}(t) \middle| \psi[\rho](t) \right\rangle dt$$

This time-dependent density should be the one which makes the action stationary ($\frac{\delta A[\rho]}{\delta \rho(\boldsymbol{r},t)} = 0$), so $A[\rho]$ could be written as:

$$A[\rho] = B[\rho] - \int_{t_0}^{t_1} \int v(\boldsymbol{r},t)\, \rho(\boldsymbol{r},t) d\boldsymbol{r} dt$$

in which $B[\rho]$ is independent of the external potential. Assuming the existence of a potential for an independent particle system in which the orbitals $\psi(\boldsymbol{r},t)$ have a density $\rho(\boldsymbol{r},t)$, $B[\rho]$ can now be written as:

$$B[\rho] = \sum_i f_i \int_{t_0}^{t_1} \left\langle \psi[\rho](t) \middle| i\frac{\delta}{\delta t} - \hat{\mathrm{H}}(t) \middle| \psi[\rho](t) \right\rangle dt - \frac{1}{2}\int_{t_0}^{t_1} \int\int \frac{\rho(\boldsymbol{r_1},t)\rho(\boldsymbol{r_2},t)}{|r_1 - r_2|} d\boldsymbol{r}_1 d\boldsymbol{r}_2 dt - A_{XC}[\rho]$$

The magnitude $A_{XC}[\rho]$ stands for the exchange-correlation term as an analogy of the KS approach in DFT, so it can be written as follows:

$$A_{XC}(\boldsymbol{r},t) = \int_{t_0}^{t_1} E_{XC}[\rho(t)] dt$$

As it was previously stated, when the external potential is weak it can be assumed a linear response, in which $\chi(\boldsymbol{r}', \omega)$ stands for the time-dependent linear response function as:

$$\delta\rho(\boldsymbol{r}, \omega) = \int \chi(\boldsymbol{r}, \boldsymbol{r}', \omega)\delta v_{ext}(\boldsymbol{r}', \omega)\, d\boldsymbol{r}'$$

For a non-interacting *N*-electron system:

$$\delta\rho(\boldsymbol{r}, \omega) = \int \chi_S(\boldsymbol{r}, \boldsymbol{r}', \omega)\delta v_{eff}(\boldsymbol{r}', \omega)\, d\boldsymbol{r}'$$

Once $\delta\rho(\boldsymbol{r}, \omega)$ has been self-consistently calculated, the frequency-dependent polarizability (α), which describes the response of the dipole moment to a time-dependent electric field with frequency ω, can be calculated:

$$\alpha(\omega) = \sum_{l} \frac{f_l}{\omega_l^2 - \omega^2}$$

It is noticeable that, at the exact excitation energy of the unperturbed system (ω_l), the equation diverges, so it is possible to obtain the excitation energies from the polarizabilities, while f_l stands for the oscillator strengths.

This formalism has been used in a wide variety of systems, as organic and inorganic molecules or metals, due to its low-time consumption compared to other methods as CASPT2. Nevertheless, TDDFT cannot describe properly

Rydberg states, charge transfer excitations or open-shell systems.

2.3. Spin-flip TDDFT

A simple extension of the TDDFT methodology is the spin-flip TDDFT (SF-TDDFT) [89] method, in which a higher spin eigenvalue is used as reference instead of the desired one. Some articles can be found in the literature in which this methodology is nicely explained more in depth.[90,91,92] The target (M_s=0) states are obtained by flipping the spin of the reference, that normally is the triplet (M_s=1) or even higher multiplicities.

Thus, the wavefunction can be represented as follows:

$$\psi_{M_S=0}^{S,t} = \hat{\mathrm{R}}_{M_S=-1}\, \psi_{M_S=+1}^{t}$$

in which $\psi_{M_S=+1}^{t}$ stands for the reference state and $\hat{\mathrm{R}}_{M_S=-1}$ is an operator that flips the spin of the electron. In **Figure 7** are shown the set of configurations obtained upon spin flip. Firstly, the first single electron configuration corresponds to the ground state singlet, followed by the configuration in which both electrons are in an excited state. Two next configurations correspond to the singlet diradical system. Then, these four configurations are the most important to describe diradical or slightly diradical systems, as both open-shell and closed-shell representations are included.

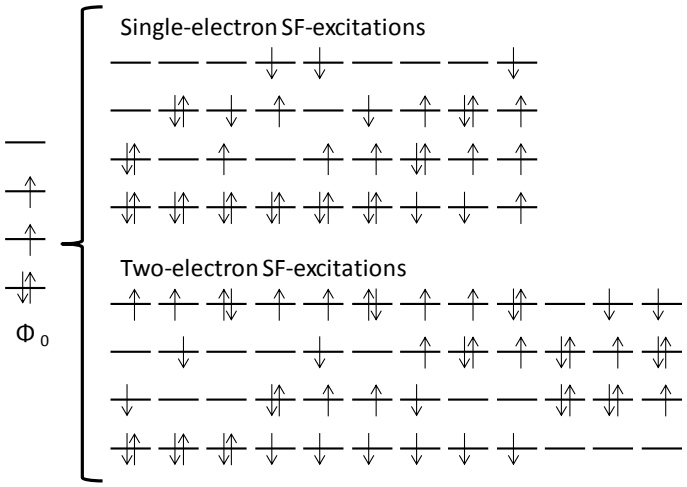

Figure 7: Configuration Φ_0 of the four electron in four orbitals system as the reference configuration, followed by the one- and two-electron excitations with spin flip.

Once all the single and double configurations are included in the model, a spin-contaminated wavefunction is obtained since the wavefunction is not eigenstate of the total spin-squared operator ($\langle \hat{S}^2 \rangle$).

SF approach has been successfully implemented in TDDFT without any increase of the computational time with respect the non-SF calculations, keeping the formulation of the original TDDFT.

In conclusion, although single-reference methods are the most widely used to characterize the electronic structure of closed-shell systems (TDDFT), the excited states of singlet diradical molecules might be qualitatively better described

with the spin-flip TDDFT wavefunction, as it includes the diradical configuration.

2.4. Broken-symmetry calculations

Many chemically interesting processes, such as dissociation and fragmentation reactions, or the formation of molecules with low-spin diradical character, involve systems with non-dynamic correlation effects and their theoretical treatment requires multiconfigurational methods. Such treatment can be provided by multiconfigurational self-consistent field methods (MCSCF), such as the complete active space second-order perturbation theory (CASPT2),[93,94] multireference configuration interaction (MRCI) [95] or MR-averaged quadratic coupled-cluster (MR-AQCC).[96] However, these methods can only be applied to relatively small systems due to their high computational cost. In the other hand, the Kohn-Sham formulation of DFT is restricted to single-reference systems

The broken-symmetry (BS) formalism proposed by Noodleman and Yamaguchi allows the representation of open-shell singlet diradicals.[97,98,99,100,101] The broken-symmetry wavefunctions are no longer eigenfunctions of the total spin operator, $\langle S^2 \rangle = \langle S(S+1) \rangle$. For a triplet state, the value of this operator is 2 and for a closed-shell singlet is 0; however, in the BS solution we look for $\langle S_{BS}^2 \rangle = 1$, which is not a pure spin state and the wavefunction is an approximate combination of the closed-shell singlet and the triplet

wavefunctions, stated in computational chemistry as spin contamination. Therefore, in order to obtain reliable singlet-state energies, this spin contamination must be corrected and, to do that, the approximation of Yamaguchi[99,100] is particularly useful:

$$J = \frac{E_{BS} - E_{T(BS)}}{\langle \hat{S}^2_{T(BS)} \rangle - \langle \hat{S}^2_{BS} \rangle}$$

where $E_{BS} - E_{T(BS)}$ is the vertical excitation energy. J is the electron magnetic exchange interaction and represents the electron-electron repulsion, which is related to the singlet-triplet gap as follows:

$$\Delta E_{ST}^{vert} = E_S - E_T = 2J$$

In order to estimate the adiabatic energy, the following expression should be used:

$$\Delta E_{ST}^{adiab} = E_{BS} - E_{T(T)} = 2J + E_{T(BS)} - E_{T(T)}$$

where $E_{T(BS)}$ is the energy of the triplet in the broken-symmetry geometry of the singlet state, and $E_{T(T)}$ is the energy of the triplet in its optimized geometry. This equation can be simplified omitting the calculation of the vertical energy and using the energy of the relaxed triplet instead:

$$J = \frac{2(E_{BS} - E_{T(T)})}{\langle S^2_{T(T)} \rangle - \langle S^2_{BS} \rangle}$$

Chapter 3

Evaluation of methods

1. Introduction

The theoretical description of singlet diradicals remains a challenging task, since the standard implementation of methods such as Density Functional Theory (DFT) or single-reference Hartree-Fock (HF) and post-HF does not describe open-shell singlet configurations properly [102] due to the multiconfigurational nature of this electronic state. A robust tool to study diradicals is the spin flip (SF) approach,[90,91,92] in which the open-shell singlet states are described within a single-reference formalism as spin-flipping excitations from a triplet state. Also, Natural Orbital Functional Theory (NOFT) [103, 104, 105] in its PNOF implementation, using the Piris reconstruction functionals,[106] has recently been successfully applied in the study of diradical species.[107,108] Nevertheless, reliable descriptions can only be obtained if a multireferential approach is used, but the applicability of multireference methods is quite limited by the size of the molecules of interest and, for practical purposes, in many cases their use is precluded.

In order to overcome the inherent limitation of DFT, the broken symmetry (BS) formalism proposed by Noodleman,[97,98] where the singlet open-shell state is a mixed state of the closed-shell singlet and the triplet states, appears as a good compromise method to describe singlet diradicals. Besides, during the last two decades, the set of composite procedures known as Gaussian-*n* (G*n*) methods[109,110,111,112,113]

have been developed for the calculation of reliable thermodynamic data. These procedures involve the combination of higher levels of theory with small basis sets and lower levels of theory with larger basis sets, in order to reach high accuracy. An extension of these procedures to study open-shell molecules (G3-RAD and G3X-RAD) was developed by Radom and coworkers [114] to improve the performance of their standard G*n* counterparts for doublet radicals and triplet biradicals.[115,116]

To our knowledge, there is a lack of any systematic study to define an efficient and computationally less demanding method to treat these complicated electronic structures. Therefore, the purpose of this chapter is the assessment of a set of recently developed DFT functionals, including long-range corrected, dispersion corrected and screened-exchange density functionals. In addition, four high-level composite methods G3-RAD, G3X-RAD, G3(MP2)-RAD and G3X(MP2)-RAD have also been tested.

This chapter will be organized as follows: (i) six well-established radicals will be used to evaluate a group of DFT functionals and G3n-RAD composite methods in the computation of adiabatic singlet-triplet gaps ($E[T_1]^{DFT}$), ionization potentials (IP) and electron affinities (EA). (ii) A reduced group of DFT functionals will be tested combined with TDDFT in the calculation of excited state energies on a set of molecules with increasing diradical character. The benchmark will be performed with available empirical results

and high-level wavefunction-based calculations, such as CASPT2.

2. Performance of modern DFT functionals and G3n-RAD methods in the calculation of $E[T_1]^{DFT}$, IP and EA

A set of 18 exchange-correlation functionals were tested, classified as follows: those functionals constructed from the gradient approximation (GA) including the exchange term in a separable way are denoted as generalized GA (GGA) functionals. In this group we have selected the popular BPW91[76, 117] and PBE.[79] Since the exchange term can be considered also in a non-separable form together with the correlation term, in this case we have non-separable GA (NGA) functionals, such as N12.[118] If the kinetic energy density is included, the functionals are denoted meta-GGA (MGGA) functionals, and the following two have been employed in this work: M11-L [119] and M06-L. [120] NGA functionals including the kinetic energy density are known as meta-NGA (MNGA), and the one used in this work is MN12-L.[121] Functionals with a given amount of Hartree-Fock (HF) exchange are designated as hybrid functionals. Usually, the functional to which the HF exchange is added is a GGA functional, denoted as hybrid-GGA (HGGA) functional. In this category we have chosen the well-known B3LYP (20% of Hartree-Fock exchange)[81,82] and B3PW91 (20%),[82,83,84] together with the recent SOGGA11-X (40.15%).[122] If the functional is a meta-GGA, we have a hybrid meta-GGA

(HMGGA) functional, such as M06 (27%),[86] M06-2X (54%)[86] and TPSSH (10%).[123] Finally, functionals that allow changing their own exchange character at long-range to account for a 100% of HF exchange are called long-range corrected (LC) functionals, and can be generated starting from any type of the previously mentioned functionals. In this work, we have chosen LC-ωPBE[124], M11[125], ωB97X,[126] and ωB97X-D[127] (including the D2 version of Grimme's dispersion[128]). In this group we also include CAM-B3LYP[129] functional, which comprises, at long range, 65% of HF exchange and 35% of Becke's 1988 gradient correction for exchange[76], and MN12-SX[130] functional, with screened exchange (SX), a version of range separation in which the electron exchange for small interelectronic distances is treated with a finite percentage of nonlocal HF exchange, but the nonlocality is screened at larger distances, where electron exchange is treated by a local approximation.

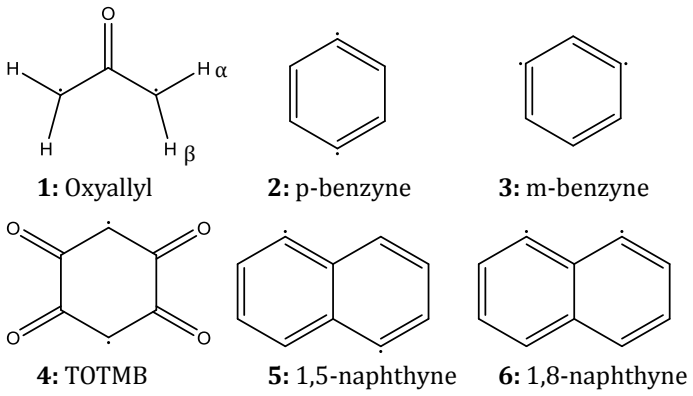

Figure 8: Singlet diradicals studied in this section.

We have chosen a set of 6 experimentally well-characterized organic singlet diradicals (see **Figure 8**): oxyallyl (**1**), two didehydrobenzenes labeled as *para*- and *meta*-benzyne (**2** and **3**, respectively), 1,2,4,5-tetraoxatetramethylenebenzene, TOTMB (**4**), and two didehydronaphthalenes, denoted as 1,5-naphthyne (**5**) and 1,8-naphthyne (**6**).

2.1. Computational details

All structures have been optimized using the 6-31+G(d,p) [131] basis set. The electronic energy is further refined by single-point calculations on the optimized structures using the aug-cc-pVTZ basis set.[132] This basis set has been selected after a small calibration using the oxyallyl diradical. Thus, starting from the M06-2X/6-31+G(d,p) optimized structure, several single-point calculations have been performed using different basis sets. In **Table 2** are collected the singlet-triplet gap ($E[T_1]^{DFT}$), electron affinity (EA), ionization potential (IP) and total spin-squared operator ($\langle \hat{S}^2 \rangle$) for this molecule together with the available experimental data. Small dependence with the basis set is accounted for EAs or IPs (>0.06 eV). However, these $E[T_1]^{DFT}$ values suggest that the required minimum-quality basis set is the aug-cc-PVXZ set, since the relative position of the triplet and the singlet state is of paramount importance, and a small difference on the energy can determine the spin multiplicity of the molecule.

Table 2: Singlet-triplet gap ($E[T_1]^{DFT}$), electron affinity (EA) and ionization potential (IP) in eV, and total spin-squared operator ($\langle \hat{\mathbf{S}}^2 \rangle$) calculated for the oxyallyl diradical at the M06-2X/BS//M06-2X/6-31+G(d,p) level of theory, where BS stands for the different basis of the table. [a]CASPT2(4,4) calculations.

Basis set	$E[T_1]^{DFT}$	EA	IP	$\langle \hat{S}^2 \rangle$
6-31+G(d,p)	0.030	1.87	9.15	0.851
6-311++G(2df,2p)	0.014	1.92	9.20	0.845
aug-cc-pVDZ	0.029	1.88	9.15	0.842
aug-cc-pVTZ	0.039	1.94	9.21	0.841
aug-cc-pVQZ	0.036	1.94	9.21	0.842
aug-cc-pV5Z	0.035	1.93	9.21	0.843
Exp	0.055	1.94	9.30[a]	

2.1.1. G3n-RAD composite methods

G3-RAD, G3X-RAD, G3(MP2)-RAD and G3X(MP2)-RAD procedures have been used following the original formulation, whose main features may be found in the literature.[114] G3X is an improvement over G3 theory, basically as an extension of the basis set. Thus, in the G3 method, the geometry optimization and the calculation of the ZPVE correction is carried out at the B3LYP/6-31G(d) level, while in the G3X method the 6-31G(2df,p) basis set is employed. G3(MP2) is a computationally less demanding variant, in which the effects of basis set extension are obtained from calculations at the MP2 level of theory. G3-RAD is the variant designed for open shell systems, and the most important changes are related to the use of URCCSD(T) single-point calculations instead of UQCISD(T). In this work, we have used the keyword UB3LYP together with guess=mix in the

geometry optimization step in order to allow a correct representation of the open-shell singlet geometry. All these calculations have been carried out using the Gaussian 09 package.[133]

2.1.2. CASSCF/CASPT2 calculations

Geometry optimizations and single-point calculations have been performed at the CASPT2 level using the aug-cc-pVDZ and aug-cc-pVTZ basis sets, respectively. Wavefunctions were obtained by means of complete active space self-consistent field calculations (CASSCF),[134,135,136] where the active space CAS(n,m) is defined by the distribution of n electrons in m orbitals. For a correct description of the molecules studied in this work, the active space must include all the bonding and antibonding π molecular orbitals plus the two orbitals and two electrons corresponding to the diradical. Thus, a CAS(4,4) space is used for oxyallyl, CAS(8,8) for *para*- and *meta*-benzyne, CAS(10,10) for TOTMB and CAS(12,12) for the naphthynes. Dynamic correlation is taken into account through complete active space second-order perturbation theory calculations (CASPT2).[93,94] All calculations have been carried out using the MOLCAS 8.0 suite of programs.[137]

2.2. Results and discussion

In the next subsection, we will accomplish an analysis of the performance of the different density functionals and the G3-based composite procedures in the modelization of

several properties of the singlet diradicals displayed in **Figure 8**, including molecular geometry, diradical character, singlet-triplet energy separation, electron affinity and ionization potential. The discussion is performed using the available experimental data or wavefunction-based CASPT2 results, both from the literature and carried out in this work. In order to get a systematic assessment, the Mean Absolute Error (MAE) is employed, calculated as the average of the absolute deviation of each property and method with respect to the reference value, for all molecules considered.

2.2.1. Diradical character

Before the discussion of the general performance of the different methodologies in the molecular properties, it is important to evaluate the diradical character and the capability of the functionals to properly represent a singlet diradical. Within the broken symmetry formalism, the value of the total spin-squared operator ($\langle\hat{S}^2\rangle$) must be 1 for a perfect singlet diradical. However, deviations of this value may give us a hint of the diradical character of a molecule, as well as of the ability of the considered functional to represent it. **Table 3** gathers the values of this operator provided by all the functionals for each molecule, together with the diradical character calculated from the weights of the main (c_0) and doubly-excited (c_d) configurations in the CASSCF expansion, in the following way:[138]

$$d = 2\sqrt{\frac{c_0^2 \cdot c_d^2}{c_0^2 + c_d^2}}$$

Table 3: Value of the $\langle \hat{S}^2 \rangle$ operator obtained for the open-shell singlet state using the broken symmetry formalism, and diradical character (d) obtained from the CASSCF calculations.

		1	2	3	4	5	6
GGA	BPW91	0.70	0.86	0.00	1.00	0.77	0.96
	PBE	0.64	0.83	0.00	1.00	0.74	0.95
NGA	N12	0.69	0.86	0.00	0.76	0.79	0.96
MNGA	MN12-L	0.77	0.98	0.00	0.96	0.92	1.00
MGGA	M06-L	0.81	0.97	0.00	0.95	0.91	1.00
	M11-L	0.72	0.97	0.00	0.93	0.90	0.99
LRC	CAM-B3LYP	0.85	0.99	0.72	1.06	0.98	1.00
	LC-ωPBE	0.91	1.03	0.83	1.09	1.05	1.01
	M11	0.84	1.00	0.75	1.05	0.99	1.00
	ωB97X	0.87	1.00	0.76	1.07	1.00	1.01
	ωB97X-D	0.84	0.99	0.69	--	0.98	1.00
	MN12-SX	0.81	0.98	0.00	1.00	0.94	1.01
HGGA	B3LYP	0.80	0.94	0.00	0.98	0.91	0.99
	B3PW91	0.83	0.97	0.48	1.00	0.93	0.99
	SOGGA11-X	0.82	0.97	0.59	0.00	0.95	0.99
HMGGA	M06	0.80	0.99	0.00	0.99	0.96	1.01
	M06-2X	0.84	1.00	0.74	1.03	0.99	1.02
	TPSSH	0.83	0.96	0.00	0.98	0.91	0.99
CASSCF	*d*	0.74	0.86	0.61	0.86	0.79	0.86

The first striking feature is that some functionals have serious problems to correctly account for the open-shell character of *meta*-benzyne (**3**), providing a value of $\langle \hat{S}^2 \rangle$=0, which corresponds to a closed-shell singlet. This feature is found to be related to a wrong geometry and will be discussed in the next subsection. In **Table 3** it is possible to observe that up to 10 funcionals, including all pure functionals (GGA, NGA,

MNGA and MGGA), calculate a closed-shell singlet for this molecule. On the other hand, the long-range corrected functionals give reasonable results, except MN12-SX, precisely the functional in which the electron exchange is screened at long distances. This suggests that the Hartree-Fock exchange at long distances plays an important role and its absence tends to bring together the radical centers to build a bicycle-like structure. It is relevant how the popular B3LYP also fails for this particular molecule. B3PW91 and SOGGA11-X provide with small values of $\langle \hat{S}^2 \rangle$, which may be a reflection of the lower diradical character of the molecule (d=0.61).

All functionals are able to represent properly the radical character of molecules **1**, **2**, **5** and **6**, but some trends can be devised. While GGA and NGA methods tend to provide with smaller $\langle \hat{S}^2 \rangle$ values, LRC functionals show values greater than 1 in several cases (especially LC-ωPBE), which may be ascribed to the contamination of the singlet with a state of higher multiplicity than triplet. It must be noted that the smallest values provided by GGA and NGA correspond to the oxyallyl molecule (**1**), which shows a less pronounced diradical character (d=0.74). Satisfactory values are accounted for by the rest of the functionals for these species. Inspecting molecule **4**, all functionals find a singlet open-shell minimum except the following two: ωB97X-D and SOGGA11-X. In the former, the optimization did not converge to a minimum (no stable open-shell singlet was found) and the

aromatic ring was split in two alkyl chains bearing two carbonyl groups each, while in the latter the reason is not obvious since the molecule retains the correct geometry, but the diradical character is lost and the result is a closed shell.

As a summary, the studied functionals are, in general, able to correctly represent the diradical character of the singlet diradicals, with particular exceptions such as molecule **3**, for which the account of long-range HF exchange is crucial to obtain a proper molecular structure and, therefore, two well-separated radicals centers.

2.2.2. Molecular geometries

We have optimized the geometries of all neutral molecules in their open-shell singlet and triplet states, as well as the cationic and anionic species. In **Table 4** are collected a selection of the geometrical parameters of the neutral molecules.

The oxyallyl diradical (**1**), a planar molecule, is a particularly complicated case and debates may be found in the literature regarding the nature of the singlet state. In general, both high-level *ab initio* calculations and experiments describe this state as a C_{2v} transition state and, following the imaginary frequency, a three-membered ring is obtained.[139,140,141,142] Although all the tested functionals could find a minimum for this molecule, suitable structures were provided and the planarity of the molecule is, in general, well represented. In **Table 4** it is observed that the predicted

dihedral angle equals to zero for most of the functionals, except for GGA and NGA functionals, which lead to C_s symmetric structures. The deviations range from 9.7º (N12) up to 15.0º (PBE). The results for the triplet and the anion structures also compare well with the reference data in the literature.[139] For the cationic species, most of the functionals predict a structure belonging to the C_{2v} point group except GGA, NGA and TPSSH functionals. Also, the optimization of this cation using BPW91, M06-L and PBE lead to transition state structures, with an imaginary vibrational frequency.

Table 4: Selected DFT- and CASPT2-optimized bond angles (in degrees) for the neutral species. O-C-C-H_α corresponds to the dihedral angle of oxyallyl.

		1	**2**	**3**	**4**	**5**	**6**
		O-C-C-H_α	C_6-C_1-C_2	C_6-C_1-C_2	C_6-C_1-C_2	C_{8a}-C_1-C_2	C_{8a}-C_1-C_2
GGA	BPW91	12.1	125.3	87.0	125.6	128.5	126.9
	PBE	15.0	125.3	75.0	125.8	128.6	127.0
NGA	N12	9.7	125.2	85.1	124.5	128.5	127.0
MNGA	MN12-L	0.0	125.2	86.8	124.1	127.2	125.9
MGGA	M06-L	0.0	125.1	71.7	124.6	127.2	125.9
	M11-L	0.0	125.1	74.1	124.7	127.4	126.0
LRC	CAM-B3LYP	0.0	125.8	106.1	123.8	127.3	126.4
	LC-ωPBE	0.0	126.0	107.5	123.8	127.1	126.3
	M11	0.0	126.1	105.8	123.6	127.3	126.4
	WB97X	0.0	125.7	106.8	123.8	127.0	126.1
	ωB97X-D	0.0	125.6	105.7	--	127.1	126.2
	MN12-SX	0.0	125.4	71.2	124.0	127.1	125.9
HGGA	B3LYP	0.0	125.6	73.2	124.2	127.7	126.5
	B3PW91	0.0	125.7	101.8	124.2	127.6	126.5
	SOGGA11-X	0.0	125.6	103.8	127.0	127.4	126.3
MHGGA	M06	0.0	125.5	69.9	124.6	127.1	126.1
	M06-2X	0.0	125.4	106.5	123.9	126.7	125.7
	TPSSH	0.0	125.6	71.8	124.1	127.7	126.5
CASPT2		0.0	124.1	103.5	124.3	126.4	125.1

Regarding *p*- and *m*-benzyne (**2** and **3**), plenty of theoretical work can be found in the literature.[143,144,145,146,147,148,149] They are described as planar

molecules belonging to the D_{2h} and C_{2v} symmetry point groups, respectively. In the case of *para*-benzyne (**2**), the geometries obtained for both the singlet and the triplet with all functionals are in very good agreement with the reference values. In **Table 4** is observed that all functionals calculate the C_6-C_1-C_2 angle (C_1 is the carbon where one of the radical electrons is located) with a deviation of around 1º with respect to the calculated CASPT2 value (124.1º). However, in *meta*-benzyne (**3**) significant deviations are found for the same angle (in this case C_1 corresponds to the carbon located between the two radical centers), where the geometry optimization leads to an almost bicycle-like structure with the radical electrons forming a single bond and, therefore, a closed-shell singlet is obtained. This distortion of the molecular geometry was previously observed in this molecule[149] as well as in pyridynes and others meta-arynes, [150,151,152,153,154,155] and it was concluded that it might be due to the lack of non-dynamical correlation. In this work, all pure functionals calculate a wrong structure. Using long-range corrected functionals reasonable geometries are calculated, with observed overestimations of 2-4º, except for MN12-SX functional, which also represents *m*-benzyne as a bycicle, emphasizing the relevance of the Hartee-Fock exchange at long distances. B3LYP also fails in this case, while B3PW91 and SOGGA11-X perform quite well. Surprisingly, only M06-2X, among HMGGA functionals, is able to correctly represent this molecule. The geometries of TOTMB (**4**), 1,5-naphthyne (**5**) and 1,8-naphthyne (**6**) were accurately calculated

compared to the reference data. The value corresponding to TOTMB using ωB97X-D is absent since, as it was previously explained, no stable molecular structure could be found. A small deviation from planarity is observed in the triplet species as well.

It is well known that the positively and negatively charged **2**, **4**, **5**, and **6** molecules suffer a lowering in its symmetry, due to the pseudo Jahn-Teller effect, [156, 157] although this reduction of symmetry may be also caused by the so-called doublet instability problem in delocalized radicals.[147] In general, GGA, MGGA and NGA functionals are not able to lower the symmetry accounting for the Jahn-Teller distortion.

2.2.3. Singlet-triplet gap

One of the most relevant parameters to study in these molecules is the singlet-triplet energy separation, which provides information about the interaction between the two radical orbitals. In that manner, in this work a positive value for $E[T_1]^{DFT}$ means a singlet ground state lower in energy than the triplet.

In **Table 5** are collected the calculated and the reference values. No experimental data were found for the singlet-triplet gap of the naphthynes (**5** and **6**) and, therefore, the CASPT2 values will be used for the assessment. In **Figure 9** are represented the mean absolute errors (MAEs) for each method in eV.

Table 5: Singlet-triplet gaps ($E[T_1]^{DFT}$), in eV, together with the available reference data. Numbers in italics refer to a closed-shell singlet state. [a]CASPT2(4,4), [b]Ref.158, [c]Ref. 159, [d]Ref. 160, [e]Ref. 142 [f]Ref. 148. The values corresponding to ωB97X, M11, and CAM-B3LYP were calculated with the simplified Yamaguchi approach due to difficulties to obtain the $E_{T(BS)}$ value.

		1	2	3	4	5	6
GGA	BPW91	0.21	0.32	*0.85*	-0.37	0.45	0.07
	PBE	0.24	0.35	*0.91*	-0.38	0.47	0.08
NGA	N12	0.20	0.36	*0.85*	-0.38	0.46	0.04
MNGA	MN12-L	0.06	0.29	*0.68*	0.27	0.39	-0.03
MGGA	M06-L	0.11	0.22	*0.92*	-0.08	0.36	0.02
	M11-L	0.22	0.28	*0.81*	0.30	0.42	0.02
LRC	CAM-B3LYP	-0.08	0.19	*0.71*	0.20	0.30	-0.01
	LC-ωPBE	-0.13	0.17	0.59	*0.17*	0.29	-0.05
	M11	-0.01	0.20	0.70	0.16	0.29	0.00
	ωB97X	-0.07	0.21	0.67	0.18	0.29	-0.03
	ωB97X-D	-0.02	0.22	0.72	--	0.31	-0.01
	MN12-SX	0.04	0.27	0.90	*0.24*	0.34	-0.01
HGGA	B3LYP	0.02	0.24	*0.64*	0.21	0.36	0.03
	B3PW91	0.00	0.22	*0.77*	0.21	0.35	0.01
	SOGGA11-X	-0.09	0.21	0.84	-0.81	0.35	0.01
HMGGA	M06	0.12	0.21	1.05	0.20	0.31	-0.02
	M06-2X	0.04	0.22	0.63	*0.19*	0.26	-0.03
	TPSSH	0.01	0.24	*0.69*	0.18	0.39	0.03
Gn-RAD	G3-RAD	-0.04	0.30	0.89	-0.05	0.50	0.05
	G3X-RAD	-0.03	0.30	*0.80*	-0.05	0.49	0.05
	G3(MP2)-RAD	0.06	0.35	0.94	0.08	0.52	0.14
	G3X(MP2)-RAD	0.06	0.34	0.80	0.07	0.52	0.13
	CASPT2	0.04[a]	0.25[b]	0.82[b]	0.16[c]	0.34[d]	0.04[d]
	Exp.	0.06[e]	0.16[f]	0.91[f]	0.15[c]	--	--

The inspection of the results shows that, as a general pattern, GGA and NGA pure functionals provide with the poorest results among all methods, and large discrepancies with the experiments are observed. In general, too positive $E[T_1]^{DFT}$ values are found, as well as the previously mentioned

problem to represent correctly the diradical character in molecule **3**. However, it is impressive how the inclusion of the kinetic energy density in their formulation to generate MNGA and MGGA functionals is decisive for an improved performance.

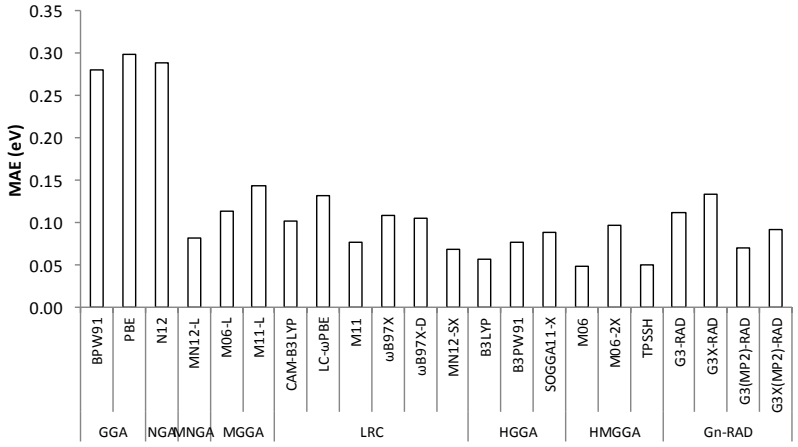

Figure 9: Mean absolute error (MAE) of the singlet-triplet gaps ($E[T_1]^{DFT}$).

On the other hand, hybrid functionals provide with very satisfactory results, which highlights the well-known fact that the incorporation of a certain amount of Hartree-Fock exchange is crucial for an accurate calculation of the singlet-triplet gap, since this energy separation is a direct measure of the electron exchange interaction. In particular, HGGAs and HMGGAs can be considered the best functionals, although B3LYP, M06 and TPSSH present the same problem with molecule **3** as pure functionals do. The great discrepancy found for SOGGA11-X in TOTMB (**4**) may be the consequence of the wrong description of the diradical nature

of the molecule. A negative $E[T_1]^{DFT}$ for oxyallyl diradical is calculated as well. Regarding long-range corrected functionals, a general good performance is observed, in the same line as HGGA and HMGGA, independently of the amount of HF exchange at long range. However, it must be noted how molecules **1**, **4** and **6** are calculated to have negative $E[T_1]^{DFT}$ values, as a result of a general trend to overestimate the singlet state. A remarkable exception is the value for oxyallyl provided by MN12-SX, which shows a value very close to the CASPT2 reference. This functional and M11 show the best performances among LR-corrected functionals.

Concerning G3n-RAD methods, an overall better performance is observed for the MP2 versions (see MAEs in **Figure 9**), at the same level of accuracy shown by hybrid functionals. G3-RAD and G3X-RAD methods predict negative singlet-triplet gaps for molecules **1** and **4** (in general, G3-RAD and G3X-RAD systematically give $E[T_1]^{DFT}$ values between 0.02 and 0.13 eV more negative than G3(MP2)-RAD and G3(MP3)-RAD). Surprisingly, the use of a bigger basis set (G3X) deteriorates the result fundamentally due to the larger errors observed in molecule **3**.

2.2.4. Electron affinity

The electron affinity (EA) is calculated as the negative of the difference in enthalpy when the neutral molecule gains an electron, in the following way:

$$\mathrm{EA} = -\Delta\mathrm{H} = -[\mathrm{H(anion)} - \mathrm{H(neutral)}]$$

In **Table 6** are gathered the calculated values and in **Figure 10** are represented the MAEs for this property.

Table 6: Electron affinities (EA), in eV, together with the available reference data. Numbers in italics refer to a closed-shell singlet state. [a]CASPT2(4,4), [b]CASPT2(8,8), [c]Ref. 159, [d]CASPT2(12,12), [e]Ref. 142, [f]Ref. 148, [g]Ref. 146.

		1	2	3	4	5	6
GGA	BPW91	1.91	1.44	0.96	4.15	1.66	1.42
	PBE	1.97	1.49	0.95	4.17	1.71	1.47
NGA	N12	1.73	1.20	0.70	4.17	1.42	1.20
MNGA	MN12-L	1.77	1.18	0.83	3.96	1.46	1.32
MGGA	M06-L	1.75	1.15	0.57	4.07	1.40	1.13
	M11-L	2.00	1.61	1.12	4.19	1.86	1.57
LRC	CAM-B3LYP	1.96	1.17	1.14	4.04	1.39	1.00
	LC-ωPBE	1.84	0.70	0.95	3.84	0.85	0.71
	M11	1.98	0.90	1.04	4.04	1.11	0.94
	ωB97X	1.86	0.91	1.04	3.84	1.08	0.90
	ωB97X-D	1.88	1.14	1.10	--	1.00	0.95
	MN12-SX	1.98	1.39	0.86	4.12	1.66	1.53
HGGA	B3LYP	1.99	1.38	1.12	4.21	1.60	1.40
	B3PW91	1.92	1.26	1.14	4.17	1.49	1.32
	SOGGA11-X	1.98	1.29	1.19	4.97	1.51	1.06
HMGGA	M06	1.89	1.18	0.50	4.12	1.44	1.34
	M06-2X	1.94	1.19	1.20	4.11	1.44	1.44
	TPSSH	1.81	1.22	0.91	4.09	1.45	1.23
Gn-RAD	G3-RAD	2.02	1.23	0.90	4.18	1.33	1.43
	G3X-RAD	2.00	1.23	0.98	4.17	1.33	1.43
	G3X(MP2)-RAD	1.97	1.25	0.91	4.08	1.36	1.40
	G3(MP2)-RAD	1.92	1.19	1.00	4.10	1.30	1.33
	CASPT2	1.80[a]	0.89[b]	0.70[b]	4.34[c]	1.00[d]	0.82[d]
	Exp.	1.94[e]	1.27[f]	0.85[g]	4.03[c]	--	--

It is well known that the calculation of EAs using DFT may be problematic due to the self-interaction error (SIE), which is the spurious interaction of an electron with itself, arising from the use of approximate exchange functionals.[161] One of the main evidences that points out this problem is a higher anion energy compared to that of the corresponding neutral species, meaning that the anion is unstable against

electron loss, and its description using standard DFT would be problematic.

In this work, all functionals show smaller anion energies. Besides, as it is observed in **Table 6** and **Figure 10**, small deviations with respect to the reference values are accounted for regardless the functional, suggesting that DFT is a useful method to calculate accurate electron affinities in these species, and the influence of the SIE error on the anion is small.

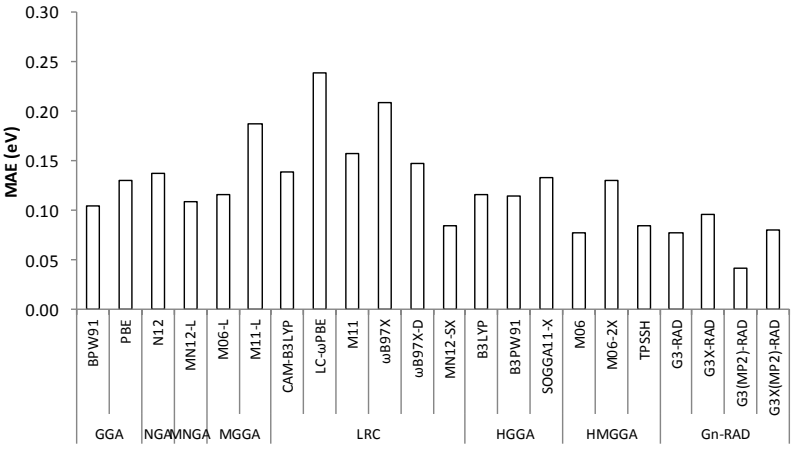

Figure 10: Mean absolute error (MAE) of the electron affinity (EA)

The results provided by the pure functionals point out that the incorporation of the kinetic energy density does not improve largely the results (MN12-L and M06-L) and, actually, M11-L shows the biggest deviation within this group. These six functionals show a satisfactory behavior, in the same line as hybrid functionals, even slightly better than long-range

corrected functionals, although one of the best results is obtained by MN12-SX. Thus, both HGGAs and pure GGAs provide with similar deviations with respect to the reference values, which means that in this case the HF exchange is not as important as it was observed in the calculation of the singlet-triplet gaps. The meta version of HGGAs (HMGGA) somewhat improve these results, as found when using pure functionals. Although the overall behavior of the functionals is very satisfactory, it should be remarked the rather large deviations of the LC-ωPBE and ωB97X functionals, a result that is improved including the dispersion correction (ωB97X-D).

Regarding the G3n-RAD composite procedures, outstanding results are obtained, especially with the computationally less demanding MP2 version, even in those cases where hybrid functionals show difficulties. An example of that is molecule **3**, in which the deviations of the HMGGAs reach up to 0.35 eV while G3n-RAD methods range between 0.05 and 0.15 eV. Very accurate results have been previously obtained in the study of radical reactions and the calculation of redox potentials of organic molecules using the G3(MP2)-RAD method.[162] Therefore, the results in this work suggest that these families of composite methods are also suitable for the calculation of accurate EAs (and then, redox potentials) in open-shell singlet diradicals. However, the computational cost may preclude their use in bigger molecules.

The results in molecules **5** and **6** are compared against CASPT2 results. However, this analysis should be done carefully, since a general underestimation of the experimental findings is found, with a mean error of around 0.25 eV. Nevertheless, almost all functionals provide with higher values than CASPT2, which may indicate a closer approximation to the experimental results and reinforcing the idea that DFT is a perfectly valid tool to calculate the EAs in singlet diradicals.

2.2.5. Ionization potential

The IP is calculated as the enthalpy change corresponding to the loss of an electron from the neutral molecule, in the following way:

$$\mathrm{IP} = \Delta\mathrm{H} = \mathrm{H(cation)} - \mathrm{H(neutral)}$$

The calculated IPs are collected in **Table 7**, together with the only available experimental data for 1,5- and 1,8-naphthyne.[163] The rest of the ionization potentials are validated using the CASPT2 calculations although it must be highlighted the unexpectedly large discrepancy of 0.69 eV found for **6**, compared to the overestimation of 0.20 eV obtained in **5**, similar to the CASPT2 deviations previously observed in the calculation of the EAs. In order to rule out any limitation or error associated to the CASSCF/CASPT2 procedure, further calculations were performed in molecule **6**, using bigger basis sets and different active spaces, but no remarkable changes were found. Besides, the chemical

structure and the molecular geometry of both molecules are very much alike, differing only in the location of the unpaired electrons (see **Figure 8**), and a difference of 0.25 eV in their IPs may be excessive. On the other hand, all of the methods used in this work show similar results for both molecules. Thus, since no reasonable explanation for this big discrepancy is found, a revision of this old experimental estimation of the IP of 1,8-naphthyne is suggested.

Table 7: Ionization potentials (IP) in eV, together with the available reference data. Numbers in italics refer to a closed-shell singlet state. [a]CASPT2(4,4), [b]CASPT2(8,8), [c]CASPT2(10,10), [d]CASPT2(12,12), [e]Ref. 163.

		1	2	3	4	5	6
GGA	BPW91	9.09	8.19	8.33	9.39	7.52	7.58
	PBE	9.11	8.20	8.37	9.43	7.53	7.58
NGA	N12	8.92	8.01	8.16	9.27	7.34	7.39
MNGA	MN12-L	8.74	8.05	7.98	9.62	8.29	7.44
MGGA	M06-L	9.07	8.13	8.33	9.52	8.32	7.55
	M11-L	9.05	8.29	8.36	9.60	8.59	7.72
LRC	CAM-B3LYP	9.19	8.58	8.27	10.66	8.09	8.11
	LC-ωPBE	9.50	8.73	8.29	10.80	8.31	8.30
	M11	9.24	8.55	8.15	10.73	8.09	8.10
	ωB97X	9.15	8.53	8.13	10.60	8.08	8.33
	ωB97X-D	9.10	8.48	8.13	--	7.97	8.00
HGGA	MN12-SX	8.97	8.29	8.39	10.14	8.71	7.74
	B3LYP	9.11	8.45	8.37	10.74	7.82	7.92
	B3PW91	9.19	8.49	8.23	10.79	7.85	7.96
	SOGGA11-X	9.22	8.50	8.21	9.62	7.98	8.02
HMGGA	M06	9.08	8.24	8.53	9.99	7.62	7.72
	M06-2X	9.21	8.52	8.14	10.70	8.02	8.06
	TPSSH	9.09	8.37	8.31	9.58	7.70	7.81
Gn-RAD	G3-RAD	9.26	8.81	8.72	10.55	8.32	8.21
	G3X-RAD	9.27	8.80	8.63	10.54	8.32	8.21
	G3X(MP2)-RAD	9.35	8.87	8.77	10.62	8.36	8.32
	G3(MP2)-RAD	9.35	8.93	8.68	10.63	8.42	8.37
CASPT2		9.30[a]	9.27[b]	8.82[b]	10.85[c]	8.38[d]	8.62[d]
Exp.		--	--	--	--	8.18[e]	7.93[e]

As a general observation, we find that the overall accuracy is decreased (see **Figure 11**) with respect to the singlet-triplet gaps and electron affinities, which implies that the description of the radical cation is not straightforward. This is reflected in the difficulties shown by several functionals in the geometry optimization step.

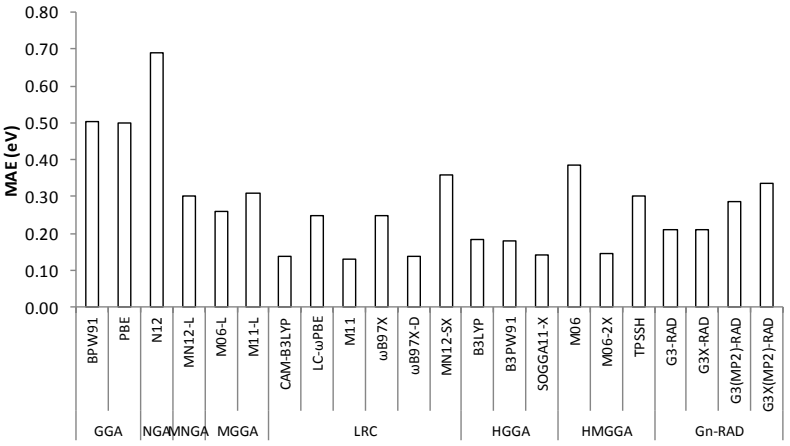

Figure 11: Mean absolute error (MAE) of the ionization potentials (IPs)

Analyzing the results of pure functionals, it is observed that both GGAs and NGAs provide with very poor IPs, with deviations of 0.5-0.7 eV. However, this result is notably improved including the kinetic energy density in the functionals (MNGA and MGGA), with deviations of 0.3 eV or smaller, a feature that was previously observed in the calculation of singlet-triplet gaps. It must be noted that the molecular structure of oxyallyl (**1**) using BPW91, PBE and M06-L was optimized to be a transition state and no stable

minimum could be found, so that these results may be handled with care.

The effect of the kinetic energy density is not accomplished in the case of HGGA functionals, which calculate rather accurate IPs, while HMGGAs provide with greater deviations, except for M06-2X. Long-range corrected functionals show the most accurate values, excepting LC-ωPBE, ωB97X and MN12-SX. It is remarkable the big discrepancy of the MN12-SX result, which suggests that the screened exchange prevents the calculation of accurate IPs. On the other hand, the poor result found in ωB97X is remarkably improved including the dispersion correction (ωB97X-D). Again, the IP of molecule **4** calculated with M11 and SOGGA11-X may be misleading, since the geometry optimization lead to a transition state structure.

Finally, the accuracy of the values calculated with G3-RAD and G3X-RAD composite methods is similar to that of the LRC and HGGA functionals, although slightly lower. The cheaper MP2 versions provide with poorer results in this case.

2.3. Summary and conclusions

In this section, a systematic analysis of the performance of 18 exchange-correlation functionals and four composite methods in the modelization of organic singlet diradicals has been performed. The difficulties associated to

the theoretical description of open-shell singlet molecules have been revealed in some of the studied molecules, which have demonstrated to be especially complex to be accurately described by means of DFT.

In general, the studied functionals are able to represent the diradical nature of these molecules. Nevertheless, the applicability of pure functionals may be more limited compared to that of the hybrid functionals due to the difficulties they show to represent the open-shell character of certain molecules (molecule **3**, for instance).

Regarding the singlet-triplet gap, the main conclusion that can be extracted from this study is the well-known fact that the incorporation of a certain amount of Hartree-Fock exchange is essential to accurately calculate this parameter, as it is a measure of the electron exchange interaction. The long-range correction does not entail improvement compared to the HGGA and HMGGA functionals. Concerning the computation of EAs, we observe that all the analyzed functionals give rather accurate results, although M11-L, LC-ωPBE and ωB97X show important discrepancies with respect to the experimental results. The analysis of the IPs is more subtle, since only two experimental results are available. Again, hybrid functionals, in general, outperform the rest, although M06 and TPSSH, as well as the screened-exchange LR-corrected MN12-SX functional show disappointingly bad results.

The effect of the dispersion correction is relevant for the computation of EAs and IPs, while is rather irrelevant for the $E[T_1]^{DFT}$ values. The long-range correction in hybrid functionals does not generally improve the results, and it is remarkable the good results obtained with the screened-exchange MN12-SX functional for $E[T_1]^{DFT}$ and EA values. The incorporation of the kinetic energy density in the formulation of the functionals (meta functionals) improves notably the results in pure functionals, while in the hybrids this trend is not obvious (actually, for the IPs, there is a clear worsening).

As a general conclusion, the inclusion of Hartree-Fock exchange seems to be crucial, although pure meta functionals are also efficient in the calculation of $E[T_1]^{DFT}$ and EA. The popular B3LYP may be still considered as a good choice. The other HGGAs (B3PW91 and SOGGA11-X), as well as the long-range corrected M11 and ωB97X-D are suggested too as good candidates for the study of open-shell singlet diradicals, although limitations have been observed.

Finally, the validation of the G3n-RAD composite procedures shows that, in general, very accurate results are obtained with G3(MP2)-RAD and G3X(MP2)-RAD methods, in particular for $E[T_1]^{DFT}$ and EA. The main drawback of these procedures is that they are computationally more demanding and their use may be precluded for bigger molecular species.

3. Evaluation of TDDFT methods for the computation of low-lying excited states

The systematic calculation of transition energies with highly correlated wavefunction-based methods is unaffordable when the number and the size of the systems considered in a study are too large. Therefore, this study relies on the energies obtained within the TDDFT framework. The calculation of excited states is very important for the study of processes such as singlet fission (SF), in which two triplet states (T_1) are created by the relaxation of an excited singlet state (S_1). Thus, the accuracy of the computed T_1 and S_1 relative energies is of vital importance and, therefore, a preliminary study must be performed in order to investigate the reliability of different exchange-correlation functionals in the calculation of vertical transitions. For this purpose, a set of linear acenes, from naphthalene to hexacene is used.

Several reasons make acenes an ideal training set for this study:

i. structural and electronic similarities with the family of molecules that are studied in this thesis (quinones, quinone dimethides, and other aromatic moieties).
ii. They contain a wide range of diradical characters that gradually increase with size.
iii. Some of them, i.e. tetracene and pentacene, are archetype examples of singlet fission chromophores.

iv. The existence of highly accurate *ab initio* results for $E[S_1]$ and $E[T_1]$ energies to use as reference.

3.1. Computational details

Time-dependent density functional theory (TDDFT) calculations have been carried out using the B3PW91/6-31+G(d) optimized structures. A set of recommended DFT functionals are tested, such as B3LYP, M06-2X, PBE0,[164] CAM-B3LYP, LC-ωPBE and BHandHLYP,[81,82] together with the 6-31G+(d,p) basis set. Additionally, Spin-Flip TDDFT (SF-TDDFT)[89] calculations have also been carried out with the 6-31G+(d,p) basis set using the Q-Chem package.[165]

3.2. Results and discussion

In **Table 8** are summarized the errors, as the average deviation with respect to the reference values, in the calculation of the energies of the first triplet ($E[T_1]$) and singlet ($E[S_1]$) excited states, together with the $2E[T_1]$-$E[S_1]$ energy difference. A good performance is observed for the M06-2X functional, especially for tetracene and pentacene (see values in italics). Moreover, the M06-2X functional shows rather balanced errors for $E[S_1]$ and $E[T_1]$ energies. The errors for the $E[S_1]$ and $E[T_1]$ states computed at the B3LYP level are systematically larger, especially for the lowest singlet.

The $2E[T_1]$-$E[S_1]$ energies are in very good agreement with reference values due to error cancelation. The SF-BHandHLYP approach exhibits very good results in the calculation of $E[S_1]$ for tetracene and pentacene, but it shows larger errors in the computation of $E[T_1]$ energies. Such behavior is also obtained with the CAM-B3LYP functional, resulting in large $2E[T_1]$-$E[S_1]$ errors, even for tetracene and pentacene. Besides, it is shown how far are the PBE0 and LC-ωPBE functionals of the reference $2E[T_1]$-$E[S_1]$ values. Also, high deviations arise from the B3PW91 functional, while the SF-B3PW91 seems to show better $2E[T_1]$-$E[S_1]$ relative energies. However, this effect appears as an artifact due to the compensation of errors in the calculated $E[S_1]$ and $E[T_1]$.

Table 8: Average absolute errors for the excitation energies of the first singlet ($E[S_1]$) and triplet ($E[T_1]$) excited states and the $2E[T_1]$-$E[S_1]$ energy difference, in eV, for linear acenes (from naphthalene to hexacene) calculated with different xc functionals with the 6-31+G(d,p) basis set. Values in italics correspond to average of errors for tetracene and pentacene.

state	B3LYP	BHandHLYP	M06-2X	CAM-B3LYP	SF-BHandHLYP	PBE0	LC-ωPBE	SF-B3PW91	B3PW91
$E[T_1]$	0.33	0.87	0.20	0.54	0.26	0.50	1.24	0.38	0.37
	0.41	*0.55*	*0.08*	*0.45*	*0.28*	*0.70*	*0.84*	*0.36*	*0.50*
$E[S_1]$	0.47	0.28	0.15	0.18	0.27	0.36	0.56	0.76	0.44
	0.45	*0.18*	*0.10*	*0.08*	*0.07*	*0.38*	*0.64*	*0.69*	*0.44*
$2E[T_1]$-$E[S_1]$	0.21	1.47	0.41	0.91	0.62	0.74	1.69	0.13	0.40
	0.38	*0.94*	*0.10*	*0.88*	*0.62*	*1.01*	*0.84*	*0.03*	*0.57*

In **Figure 12** are represented the computed errors for the $2E[T_1]$-$E[S_1]$ energy difference, depending on the number of rings in the acene. Again, the best results are obtained with M06-2X functional for tetracene and pentacene. B3LYP also

provides with reasonable results, especially in short-chain acenes. SF-BHandHLYP functional performs very well for anthracene, but for larger acenes notable errors are found.

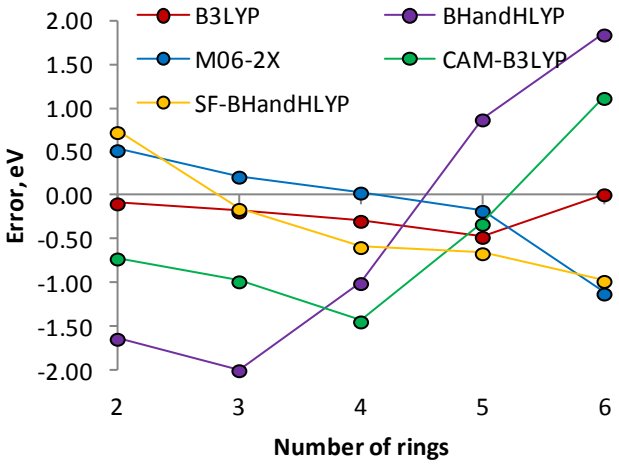

Figure 12: Computed errors for the $2E[T_1]$-$E[S_1]$ energy difference, in eV, for linear acenes calculated with selected xc functionals with the 6-31+G(d,p) basis set.

Since the M06-2X approach systematically provides $E[S_1]$ and $E[T_1]$ energies and $2E[T_1]$-$E[S_1]$ differences with small errors with respect to the reference values, we choose this approach to proceed with our study. Moreover, it is important to notice that the largest errors for $2E[T_1]$-$E[S_1]$ are obtained for naphthalene and hexacene, that are not considered as singlet fission materials. Hence, we might expect that M06-2X energies will exaggerate endoenergicity (exoenergicity) of those systems with large $|2E[T_1]-E[S_1]|$, i.e. potentially less interesting as suitable singlet fission sensitizers. Additionally, we have also considered SF-BHandHLYP energies in order to explore molecules with

strong diradical character, since this approach has shown good performance in such cases.[166]

3.3. Summary and conclusions

In this section, the effect caused by the method in the calculation of excited states was tested in order to obtain reliable $E[S_1]$ and $E[T_1]$ energies, as well as the $2E[T_1]$-$E[S_1]$ value. Data calculated with high-level computational methods were chosen from the literature and served as reference values to perform the validation. TDDFT was firstly tested combined with the B3PW91, B3LYP, M06-2X, PBE0, CAM-B3LYP, LC-ωPBE and BHandHLYP functionals. From this set, the M06-2X functional seems to give the most balanced results, accurately reproducing $E[S_1]$, $E[T_1]$ and $2E[T_1]$-$E[S_1]$. However, the enhancement of the diradical character introduces spin contamination, decreasing the quality of the obtained data. Thus, the spin-flip procedure was also utilized together with the BHandHLYP and B3PW91 functionals. Despite the spin-flip B3PW91 method shows small deviations for $2E[T_1]$-$E[S_1]$, the $E[S_1]$ and $E[T_1]$ energies are far from the reference values, leaving the BHandHLYP functional as suitable option to calculate open-shell structures.

Chapter 4

Diradical character

1. Introduction

After some decades of development of the chemistry of open-shell diradical structures,[13,14] several investigations have been focused on how certain modifications could affect the electronic structure of the ground state on a given molecule. For instance, localized singlet 1,3-diradicals were used by several authors[167,168,169] to rationalize the changes observed on the S_0-T_1 energy splitting when electron-withdrawing (EWG) or electron-donating (EDG) groups are included into the main moiety. It was sketched that the singlet ground state was favored when a EWG is used due to an interaction of the lower energy non-bonding orbital of the molecule with the low-lying unoccupied orbital of the substituent, while the opposite effect is recovered when a EDG substituent is used instead. An analogue explanation was utilized to explain the effect of heteroatoms such as silicon[170,171] or nitrogen,[172] that seemed to favor a singlet ground state as EWGs did.

The separation between singlet and triplet states was also tuned using *meta*-benzoquinone (a non-Kekulé delocalized diradical) as probe molecule, in which the oxygen atoms can be substituted by CH_2 (*meta*-benzoquinodimethane), $C(NH_2)_2$ or $C(Ph)_2$ (Schlenk diradical), among others.[173,174,175] The latter, which shows a triplet ground state, was used to elucidate how a series of EWG and EDG substituents may affect the nature of the ground state,

considering the inductive and mesomeric effects (I and M, following Ingold's notation). In this sense, substituents with -M and -I effects reduce the singlet-triplet gap ($E[T_1]^{DFT}$), while +M and +I substituents generate the opposite effect. This behavior was explained by means of the spin density.

However, very little work could be found dealing with Kekulé delocalized diradicals, such as the quinoid structures. This lack of information is noteworthy in some cases in which the diradical character is not taken into account in the calculations, or at least mentioned,[176,177,178,179,180] in order to provide a more realistic image of the ground state of these complicated systems. One of those publications was released by Canesi, [181] where it was observed that the diradical character of a bithiophene derivative could be removed introducing alkoxy groups (EDG) on the structure.

Heteroatoms have been already included into acene moieties in order to tune the diradical character (or other related properties). [182 , 183] The observed effect is that the inclusion of nitrogen atoms accomplishes an enlargement of $E[T_1]^{DFT}$ (and, then, a reduction of the diradical character), while the number and exact position of the nitrogens along the molecule can also determine the nature of the molecular ground state. Pairs of boron and nitrogen atoms have been already used to captodatively design diradical molecules taking as starting point benzene, naphthalene, azulene, fulvene and benzoquinone. [184] As it is observed for linear acenes, [185] the diradical character of quinone moieties has

been demonstrated to grow as the molecular chain is enlarged.[186]

As well as tuning the diradical character of any particular molecule, some of the mentioned chemical modifications may serve to experimentally stabilize molecules that in any other way would be impossible to synthesize. In fact, two main stabilizing strategies have been proposed, called respectively terminal functionalization and fusion.[187] The first one introduces functional groups, as cyano group, in the terminal methylene sites to block the reactive sites and delocalize the spin density. Tetracyanoquinone dimethane derivatives,[188,189] for instance, are good examples of stable *para*-quinones. The latter implies the addition of aromatic rings to enhance the rigidity of the system as well as to delocalize the spin density. In any case, the enlargement of the molecular size can reduce the solubility together with the stability.

Hence, during the last decades has been demonstrated that the diradical character can be tuned in a very controlled way, but the magnitude of the change that any structural modification can introduce in the ground state is still unknown. In that manner, the first part of this chapter represents an extensive and systematic study of the conditions by which the diradical character of conjugated quinones may be affected, generating a set of rules that may help the design of molecules with the desired diradical character by following fundamental structure-property

relationships. Namely, the effect of the number and size of the rings, the presence of heteroatoms and substituents in the rings and the substitution of the carbonyl oxygen by other heteroatoms or small moieties are studied. The second part encompasses a large number of experimentally known molecules in order to analyze the diradical character of the ground state and, besides, a large number of molecules is proposed in the pursuit of new diradical molecules that might be potential candidates to be synthesized. As a consequence of this investigation, the diradical character is established as a new, unexplored variable for the design of novel molecules with potential technological applications.

2. Computational details

All geometries have been obtained with the B3PW91 functional and the 6-31+G(d) basis set, while the electronic energy is refined with the aug-cc-pVTZ basis set. The singlet diradical character has been evaluated using the diradical index (y_i) from the spin-projected unrestricted Hartree-Fock (PUHF) theory,[190,191,192] together with the aug-cc-pVTZ basis set, as:

$$y_i = 1 - \frac{2T_i}{1 + T_i^2}$$

where T_i is defined as the orbital overlap and is calculated using the occupation number (n) of the UHF natural orbitals:

$$T_i = \frac{n_{HONO-i} - n_{LUNO-i}}{2}$$

Thus, from these equations both the diradical (y_0) and tetraradical (y_1) character can be estimated. An index value of 1 states for a perfect diradical (or tetraradical), while a value of 0 means a closed-singlet (no tetraradical character).

The aromaticity is estimated by means of the GIAO method,[193,194] at the B3PW91/6-311++G(d,p) level of theory, to perform calculations of NICS(1)[195] (nuclear independent chemical shift at 1 Å above the center of the ring) in order to better estimate the effects of the π-electron ring current while the σ-bonding contributions are diminished.[196,197] The NICS data are reported as the negative value of the absolute isotropic magnetic shielding, following NMR chemical shift conventions, where negative NICS values (magnetically shielded) indicate aromaticity, while positive values (magnetically deshielded) and values close to zero indicate antiaromaticity. Additionally, we have calculated the anisotropy of the magnetic susceptibility at the same level of theory, $\Delta\chi$, which can be used as an experimental measure of aromaticity, and is defined as:[198]

$$\Delta\chi = \chi_{ZZ} - \frac{\chi_{XX} + \chi_{YY}}{2}$$

where χ_{ZZ} is the magnetic susceptibility component corresponding to the axis normal to the molecule, while χ_{XX} and χ_{YY} are the in-plane components. Analogously to NICS(1) index, negative values of $\Delta\chi$ denote aromatic character.

3. Diradical character in conjugated quinones and methylene derivatives

In this section, a set of theoretically designed conjugated carbonyls and methylene derivatives are studied. All molecules contain one or two carbonyl groups in order to enable double-bond conjugation in the rings and are labeled using the following general nomenclature: *n,m*-C(x+y+z), where *n* and *m* refer to the positions of the carbonyl groups, and *x, y* and *z* the size of each ring, in increasing order. Additionally, an analogous set of molecules, denoted as quinone dimethides, is generated by substitution of the oxygen atom by a methylene group (CH_2). Both groups of molecules, carbonyl and methylene derivatives, will be referred as Q and QDM molecules, respectively, and the particular molecules within each group will be referred as *n,m*-C(x+y+z)/Q or *n,m*-C(x+y+z)/QDM. The monosubstituted molecules are labeled as *n*-C(x+y+z). Those structures will be also referred as Q and QDM although these molecules, strictly speaking, are not quinones or quinone dimethides. Furthermore, 26 highly symmetric molecules containing two carbonyl groups have been partially substituted with one methylene group, leading to quinone methide derivatives (QM), that will be labeled as *n,m*-C(x+y+z)/QM. For the sake of clarity, the whole collection of 206 molecules will be designated as “set”, while the label “group” will be used instead to refer the concrete case of Q molecules, QDM or QM. Finally, those molecules that can be labeled using the

same *n,m*-C(x+y+z) formula will be called “families”.

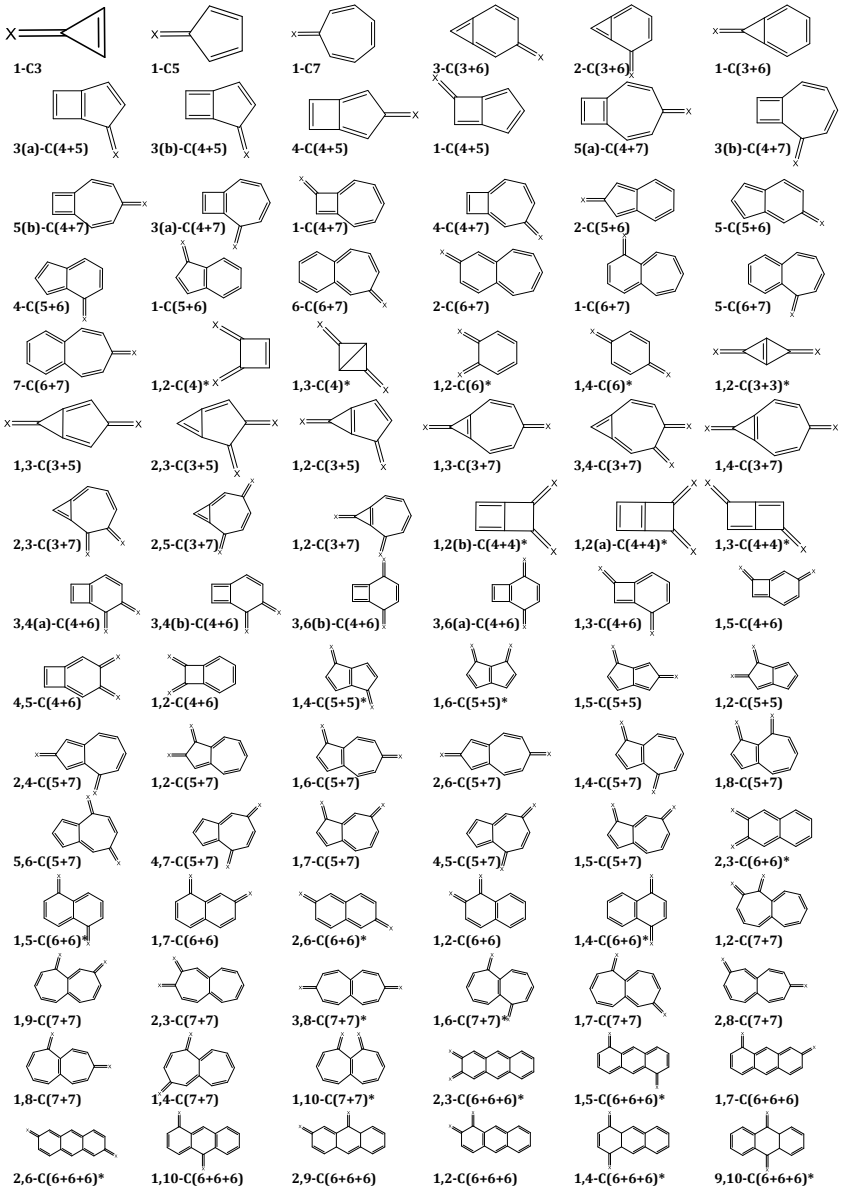

Figure 13: Whole set of molecules used in this section, with X=O, CH_2. Those molecules with a (*) are also calculated combining both O and CH_2 substituents (quinone methides).

In **Figure 13**, the investigated molecules are represented. Besides, for completeness, the bare rings are also studied in order to analyze the effect of the carbonyl and methylene substitution.

Regarding the cyclobutadiene-based molecules, the relative position of the double bonds in cyclobutadiene leads to two different isomers. In order to distinguish them, it will be used the label (a) when it exists a double bond linking the shared carbons of the two rings, while (b) will be used instead with each shared carbon having a double bond. In order to confirm this result, the energy differences between these isomers, in the Q group, have been calculated at the CASPT2 level of theory (see **Table 9**) and a good agreement is observed with the broken-symmetry DFT calculations.

Table 9: Energy differences between (a) and (b) isomers of the cyclobutadiene derivatives, in eV, calculated at the CASPT2/aug-cc-pVTZ//B3PW91/6-31+G(d) and both restricted and unrestricted B3PW91/aug-cc-pVTZ//B3PW91/6-31+G(d) levels of theory.

	CASPT2	**UB3PW91**	**RB3PW91**
1,2-C(4+4)	-1.28	-1.18	-1.43
3-C(4+5)	0.42	0.72	0.80
3,4-C(4+6)	0.00	0.00	0.17
3,6-C(4+6)	-0.02	-0.05	-0.05
3-C(4+7)	-0.59	-0.58	-0.75
5-C(4+7)	-0.23	-0.37	-0.41

In summary, this section is focused in the investigation of the diradical character in terms of nature and position of the

rings, as well as the kind of substituent employed (CH_2 or O). The diradical character (y_0) of each molecule is studied together with the spin densities (ρ) and the aromaticities, both in the full molecule (magnetic susceptibility, in $\Delta\chi$ (cgs-ppm)) and centered in the rings (NICS(1)). Firstly, the naphthalene derivatives are used to explain certain general considerations. Later, the whole set of molecules will be discussed. Finally, the aromaticity of the Q group of molecules will be discussed and related with the diradical character.

3.1. General trends

Despite the large number of molecules that are investigated in the present study, the observed trends in the diradical character can be rationalized performing a detailed analysis in selected molecules. Molecules belonging to the *n,m*-C(6+6) group, that is, derivatives of naphthalene, may be useful in this task, since the introduced modifications (position and kind of substituent) seem to play a clear role in the diradical character of the derived molecules.

In **Figure 14a**, three representative open-shell Lewis structures are depicted to analyze the distribution of the spin densities, shown in **Figure 14b**. Thus, in 2,3-C(6+6)/Q molecule **(Figure 14b,** left), large values of spin density are observed in ring positions 1 and 4, corresponding to resonance structure 2, generating an aromatic π-sextet (a benzene ring). When the carbonyls are substituted by methylene groups to form the 2,3-C(6+6)/QDM molecule

(**Figure 14b**, center), a shift of the spin density is observed towards the CH_2 groups, corresponding to an intermediate situation between resonance structures 2 and 3, anyway keeping the benzene ring. The 2,3-C(6+6)/QM molecule (**Figure 14b,** right) presents both characteristics, with an open shell structure that includes large spin density values in the CH_2 group and in the 1 and 4 positions of the rings. In this way, resonance structure 1 is unfavored due to the loss of aromaticity.

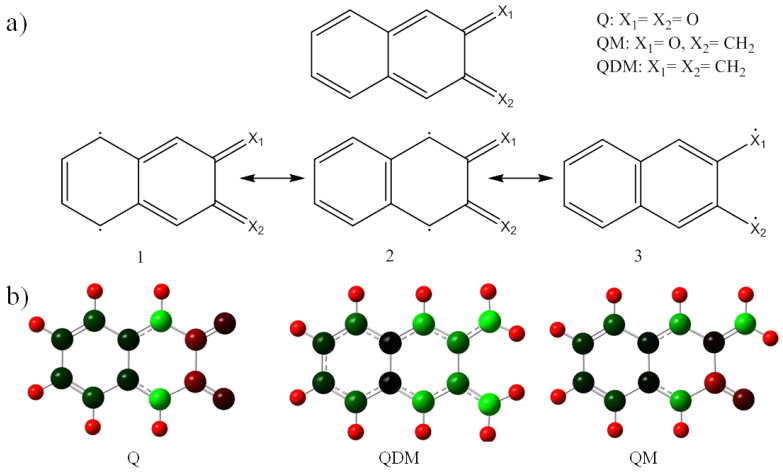

Figure 14: a) Lewis structure of the 2,3-C(6+6) molecule in the closed-shell (top) and the open-shell (bottom) resonance structures. b) Spin densities (ρ) of the 2,3-C(6+6)/Q,QDM,QM molecules. Green colour corresponds to $\rho \geq 0.9$, while red colour corresponds to $\rho \leq 0.4$. Intermediate values are denoted by intermediate colour intensities. The calculations were performed at the UHF/aug-cc-pVTZ level of theory.

The presence of substituting moieties in the naphthalene molecule has a dramatic effect in the diradical

character, increasing from y_0=0.04 in the unsubstituted molecule up to y_0=0.41 in 2,3-C(6+6)/QM, y_0=0.43 in 2,3-C(6+6)/Q and y_0=0.59 in 2,3-C(6+6)/QDM derivatives. See **Figure 15**, where the diradical character of the Q (light blue bars), QDM (dark blue bars) and QM derivatives (white bars) are displayed. This is a relevant result, since, in the acene series, in order to have diradical characters of the same magnitude, the number of rings has to be increased at least up to 4. This means that we are able to induce a remarkable change in the diradical character by introducing a slight modification into the structure of small molecules, such as naphthalene. Nevertheless, the sole presence of the substituents in naphthalene is not enough to increase the diradical character and their relative position in the rings must also be considered.

As shown in **Figure 15**, 1,2-C(6+6)/Q is a closed shell (y_0=0.00) and 1,2-C(6+6)/QDM shows only a slight diradical character (y_0=0.12). This may also be explained by using the resonant structures. As it has been mentioned before, the strong diradical character shown by the 2,3-C(6+6) structure is favored by the stabilization provided by the formation of the π-electron system.[199] In the 1,2-C(6+6) isomers, this π-electron system is already present in the closed-shell representation, which would disappear in any other resonant structure.

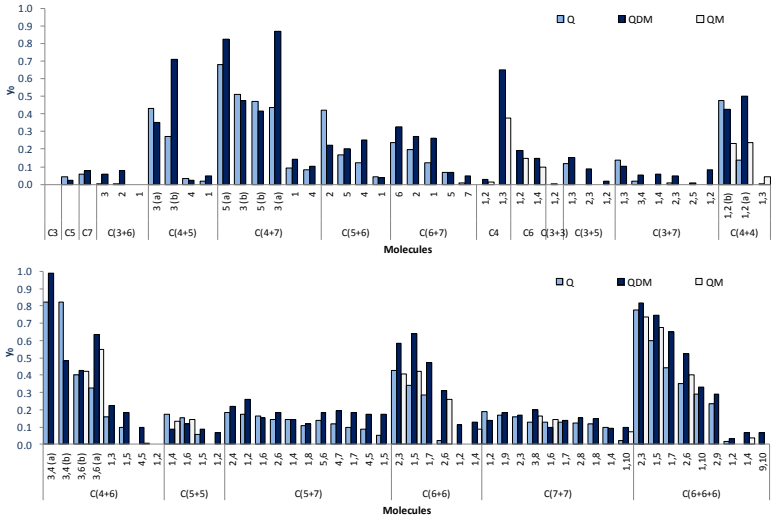

Figure 15: Diradical character (y_0) calculated at the UHF/aug-cc-pVTZ//B3PW91/6-31+G(d) level of theory, for the Q, QM and QDM derivatives.

The variation of the electronic density was studied in order to elucidate the differences between a regular closed-shell (CS) calculation with respect to a broken-symmetry open-shell (OS) calculation. This is shown in **Figure 16**, where the variation of the electron density from the closed-shell to the open-shell structures in 1,5-C(6+6+6)/Q,QDM,QM is represented. In general, the main shift takes place in the carbon rings, among adjacent double bonds, and this effect can also be observed in the methylene group of the QDM molecule. In the other hand, the double bond of the carbonyl groups shows a density loss. In the QM derivatives, an intermediate behavior is observed. This means that, in the QDM molecules, which show a general greater diradical character than the Q molecules, the unpaired electrons are

more likely to be localized in the methylene moieties, leading to a stronger aromatic stabilization, as it has been previously discussed.

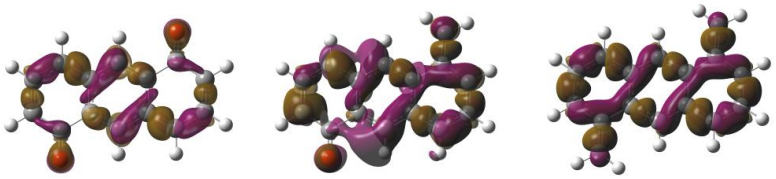

Figure 16: Variation of the electron density (isovalue=0.0004) from the closed-shell to the open-shell electronic structures in the 1,5-C(6+6+6) derivatives, namely, Q (left), QM (center) and QDM (right). Purple color indicates regions that gain density, while brown color denotes loss.

3.2. Diradical character of Q, QDM and QM molecules

Inspecting **Figure 15**, it is possible to observe that many of the carbonyl derivatives (Q) possess a non-negligible diradical character, and the ground state should be described as a singlet open-shell state. Thus, the monocycles (1-C3, *n,m*-C4, 1-C5, *n,m*-C6 and 1-C7) are basically closed-shell molecules, the same way as bicycles including a three-membered ring, except for 1,3-C(3+5) and 1,3-C(3+7), which show slight diradical character. It is remarkable the diradical character ($y_0 \geq 0.40$) of the bicycles containing a cyclobutadiene moiety, especially those fused to six- and seven-membered rings, such as 3,4(a,b)-C(4+6) or 3,4(a,b)-C(4+7). Carbonyls containing five-membered rings show small diradical character except 1-C(5+6), with a y_0 value

equal to 0.42. Three molecules with two benzene rings and six with three benzene rings show remarkable diradical character and, finally, bicycles with seven-membered rings display small diradical character.

When the carbonyl moieties are substituted by methylene, an important enhancement of the diradical character is observed. In most cases, the diradical character is increased following this general trend: y_0(QDM) > y_0(QM) > y_0(Q). In fact, 70 molecules among the full QDM group show an enhancement in the y_0 values compared to the Q group. Analogously, from the 26 QM calculated molecules, 18 show larger diradical character than the carbonyl homologues. Molecules that already showed non-negligible diradical character experience a greater increase upon substitution of the carbonyl. For example, 1,2(a)-C(4+4) with 0.14 (Q), 0.24 (QM) and 0.50 (QDM); 3,6(a)-C(4+6) (0.33, 0.55 and 0.64); 1,5-C(6+6) (0.34, 0.42 and 0.64) or 2,6-C(6+6+6) (0.35, 0.40 and 0.52). Carbonyls that are basically closed-shell molecules remain this way, in general, but still some of them are found to have a non-negligible diradical character upon substitution, such as 1,2-C(6+6), 1,4-C(6+6), 1,2-C6 or 1,4-C6. It is remarkable the case of 1,3-C4, where the QM and QDM groups show a notable diradical character (0.38 and 0.65, respectively). However, it should be noted that this trend is not always fulfilled, such in 1,2(b)-C(4+4) or in 2-C(5+6). In general, all the studied acene derivatives: benzoquinone, naphthoquinone and anthraquinone, as well as their

methylene derivatives, show in certain cases an enhancement of the diradical character when compared to the parent acene molecule.

Regarding the number of rings, it has been previously observed in fused oligoacenes that the diradical character increases with the number of benezene rings. [200] Nevertheless, this behavior becomes evident from pentacene and, therefore, it is difficult to establish a direct comparison with the set of molecules analyzed in this section. Still, we observe that the diradical character of the 2,3-, 1,5-, 1,7- and 2,6-C(6+6)/Q,QDM isomers is notably increased when the third ring is included (C(6+6+6) group). Only the 1,2- and 1,4-isomers maintain basically the same diradical character, or even a small decrease is observed. As a summary, the size of the ring does not seem to be relevant for the diradical character. Instead, the relative position and the nature of the moieties, together with the number of rings, are the key parameters for tuning this property. The variation of y_0 with the number of rings will be discussed in detail later on.

3.3. Molecular geometries and stability

Since the geometry optimization is performed using the broken-symmetry approximation, every molecule is allowed to distort its closed-shell structure to an open-shell one, lowering the energy. Nevertheless, these changes on the structures are small and only noticeable in few structures with $y_0 \neq 0$. Thus, it is observed that the C=O bond is likely to be

elongated in the open-shell state, although this variation is very small (<0.01Å). Analogously, in the QDM group is also observed a small structural effect, although the 2,3-C(6+6+6)/QDM molecule shows an elongation of 0.024 Å in their $C=CH_2$ bonds. Additionally, in the backbone of the molecules are observed modifications, with a noticeable enlargement of double bonds accompanied with a shortening of the single bonds. For instance, the single bond between the carbons labeled as 5 and 6 of the 2,3-C(6+6+6)/Q molecule is 0.032 Å longer in the open-shell calculation, while the QDM analogue shows an enlargement of only 0.020 Å. These results support the previous analysis performed using the spin densities, were the unpaired electrons are mainly delocalized in the aromatic rings.

Finally, the diradical character may be related to their stability. Thus, it is observed that a greater diradical character implies a more energetical isomer.

3.4. Aromaticity in Q molecules

The trend observed in the stability is in agreement with previously published theoretical data,[180,199,201,202] and is also reflected in the aromaticity, which provides us with a deeper insight into the ring-size effect. In order to analyze this, we have used the anisotropy of the magnetic susceptibility ($\Delta\chi$), which can be used as an experimental measure of aromaticity, together with the NICS(1) criterion, since it is also a useful indicator of aromaticity in a particular ring. In **Figure**

17, the calculated $\Delta\chi$ together with the diradical character is represented, while the NICS(1) aromaticity indexes are included in the **Table 10**. Thus, although it is not straightforward to devise a clear tendency, a general decrease in the aromaticity (shift to positive values) is observed with the increase in the diradical character.

This behavior may be explained as a combination of two factors: firstly, as it was stated in the previous subsection, the diradical character implies a delocalization of the spin density into the carbon backbone, diminishing their aromaticity, and, secondly, the disposition of the carbonyl moieties in the rings, which may lead to a less conjugated molecule and, therefore, decreasing the aromaticity.

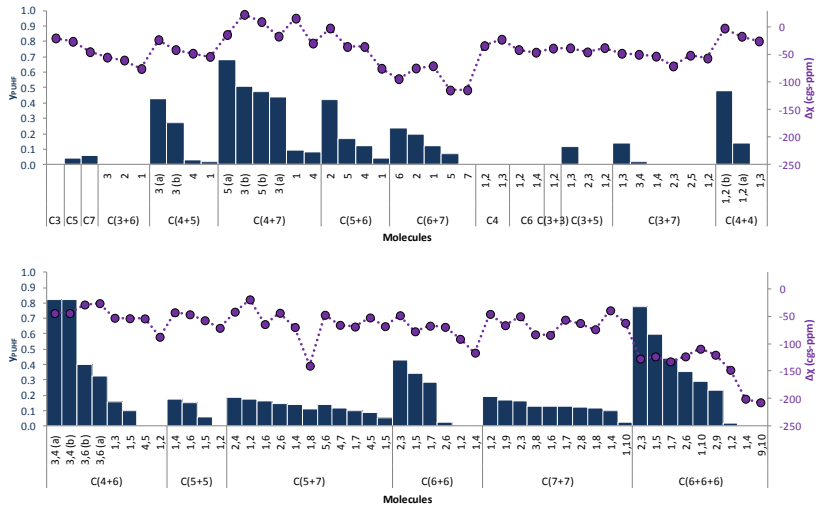

Figure 17: Anisotropy of the magnetic susceptibility ($\Delta\chi$, dotted line), in cgs-ppm, and diradical character (y_0, bars) calculated at the B3PW91/6-311++G(d,p)//B3PW91/6-31+G(d) level of theory.

Following Hückel's rule [203] for aromaticity in planar rings, 1-C3 and 1-C7 molecules are aromatic (NICS(1) values of −9.48 and −2.36), while 1-C5 is antiaromatic (4.03). In the monocycles with two carbonyl groups, 1,2-C4 is aromatic (−3.64), while *n*,*m*-C6 is antiaromatic (0.94 and 1.63 for *n*,*m*=1,2 and 1,4, respectively), in contrast to the case of cyclobutadiene and benzene.

However, in molecules with more than one ring, the relationship between aromaticity and the diradical character depends on the structure of each molecule. For instance, within the *n*,*m*-C(6+6) group, 2,3-C(6+6) molecule has one benzene-like aromatic ring (Clar sextet) in the closed-shell state, so that an eventual breaking-symmetry approach (enhancing the diradical character) may reduce the aromaticity by delocalizing the spin density on the carbon backbone. For that reason, the diradical 2,3-C(6+6) molecule is less aromatic ($\Delta\chi$=−48.4 cgs-ppm) than the closed-shell 1,2- and 1,4-C(6+6) molecules ($\Delta\chi$=−91.4 cgs-ppm and $\Delta\chi$=−116.6 cgs-ppm, respectively), even having the same number of Clar sextets. This analysis is also supported by the NICS(1) values gathered on **Table 10**. In this manner, molecules such as 1,2-C(6+6) or 1,4-C(6+6) show strongly aromatic benzene-like structures with NICS(1) ≈ -9 (this value for benzene is -10.4). However, the 2,3-C(6+6) structure shows more positive NICS(1) values, up to 1.68, indicating a non-aromatic structure.

Table 10: Nuclear Independent Chemical Shifts calculated at 1 Å over the center of the ring (NICS(1)). NPL states for non planar.

		$NICS(1)_A$	$NICS(1)_B$	$NICS(1)_C$			$NICS(1)_A$	$NICS(1)_B$	$NICS(1)_C$
C3		-9.48	--	--	**C(4+6)**	**3,6 (a)**	10.82	0.66	--
C5		4.03	--	--		**1,3**	-2.65	-1.15	--
C7		-2.36	--	--		**1,5**	-2.89	-2.03	--
C(3+6)	**3**	-11.04	-4.18	--		**4,5**	-2.46	-0.53	--
	2	-12.86	-4.73	--		**1,2**	-3.23	-10.09	--
	1	-9.44	-10.45	--	**C(5+5)**	**1,4**	3.62	3.62	--
C(4+5)	**3 (a)**	5.9	-0.79	--		**1,6**	1.83	1.83	--
	3 (b)	3.01	-8.96	--		**1,5**	-0.24	-3.83	--
	4	-4.58	-4.67	--		**1,2**	-2.65	-3.54	--
	1	-6.56	-5	--	**C(5+7)**	**2,4**	5.68	3.05	--
C(4+7)	**5 (a)**	13.17	0.6	--		**1,2**	3.38	5.43	--
	3 (b)	19.7	6.27	--		**1,6**	3.15	-1.98	--
	5 (b)	16.47	5.11	--		**2,6**	4.54	2.38	--
	3 (a)	15.32	-1.35	--		**1,4**	2.63	-2.9	--
	1	6.63	7.58	--		**1,8**	2.2	NPL	--
	4	3.33	1.39	--		**5,6**	1.46	NPL	--
C(5+6)	**2**	12.89	5.77	--		**4,7**	-0.53	1.53	--
	5	4.85	3.54	--		**1,7**	-0.77	-1.25	--
	4	3.75	4.28	--		**4,5**	0.18	NPL	--
	1	4.24	-7.77	--		**1,5**	-0.94	-1.09	--
C(6+7)	**6**	-5.77	-4.52	--	**C(6+6)**	**2,3**	5.96	1.68	--
	2	-7.17	-0.68	--		**1,5**	0.44	0.44	--
	1	-6.68	-0.32	--		**1,7**	1.43	-0.86	--
	5	-10.58	-1.72	--		**2,6**	-0.35	-0.35	--
	7	-10.18	-1.33	--		**1,2**	3.38	-8.74	--
C4	**1,2**	-3.64	--	--		**1,4**	1.86	-9.54	--
	1,3	NPL	--	--	**C(7+7)**	**1,10**	NPL	--	--
C6	**1,2**	0.94	--	--		**1,2**	NPL	--	--
	1,4	1.63	--	--		**1,9**	NPL	--	--
C(3+3)	**1,2**	-11.21	-11.21	--		**2,3**	NPL	--	--
C(3+5)	**1,3**	-4.88	3.87	--		**3,8**	-2.02	-2.02	--
	2,3	-7.16	-0.44	--		**1,6**	NPL	--	--
	1,2	-11.73	0.77	--		**1,7**	NPL	--	--
C(3+7)	**1,3**	-7.18	-1.89	--		**2,8**	NPL	--	--
	3,4	-9.44	NPL	--		**1,8**	NPL	--	--
	1,4	-8.75	-0.79	--		**1,4**	NPL	--	--
	2,3	-10.7	-1.68	--	**C(6+6+6)**	**2,3**	4.64	-0.74	-4.73
	2,5	-8.57	-0.41	--		**1,5**	-1.14	-6.13	-1.14
	1,2	-8.97	-2.04	--		**1,7**	0.44	-2.6	-1.24
C(4+4)	**1,2 (b)**	1.64	16.5	--		**2,6**	-0.78	-1.41	-0.78
	1,2 (a)	-5.81	6.97	--		**1,10**	0.11	0.9	-8.7
	1,3	-2.08	-2.08	--		**2,9**	-1.04	1.87	-8.49
C(4+6)	**3,4 (a)**	6.23	-0.74	--		**1,2**	3.44	-8.48	-9.95
	3,4 (b)	6.24	-0.74	--		**1,4**	2.09	-9.51	-10.14
	3,6 (b)	11.54	-2.18	--		**9,10**	-9.36	2.69	-9.36

On the other hand, a closed-shell representation of 1,5-, 1,7- and 2,6-C(6+6) molecules leads to structures

without any aromatic ring. However, allowing the open-shell character may provide with naphthalene-like electronic arrangements to these structures, increasing the aromaticity of the molecules. Magnetic susceptibilities support this explanation, since $\Delta\chi$ values of -77.7, -67.4 and -69.6 are found on the aforementioned structures, following the trend observed in the y_0 values (0.43, 0.00 and 0.00). Again, the NICS(1) indexes support these findings.

3.5. Summary and conclusions

In this section, the diradical character and its influence in molecular geometries, stability and aromaticity has been analyzed in a set of 206 conjugated carbonyl and methylene derivatives. We have found that, excluding the monocycles, many of the proposed molecules have a non-negligible diradical character and the ground state should be described as a singlet open-shell state.

Some of the calculated parameters such as the spin density, bond distances and aromaticity show that the radical electrons are mainly delocalized over the carbon backbone. The aromaticity shows a general decrease with the increase of the diradical character, although it is not straightforward to devise a clear tendency. The substitution of the carbonyl groups by methylene moieties enhances the diradical character, and the following trend is observed: $y_0(QDM) > y_0(QM) > y_0(Q)$.

Hence, these results highlight the singlet diradical nature shown by many conjugated cyclic compounds, and the

requirement to be properly described as singlet open-shell ground states, in contrast to the commonly assumed closed-shell nature. This feature, which has been neglected in almost all of the previously published works, has a considerable impact on molecular properties.

4. Effect of structural modifications

In this section, a systematic analysis is performed in order to elucidate how certain modifications on the molecular structure may affect the diradical nature of the ground state. The 1,5-C(6+6+6)/Q molecule has been selected due to its notable diradical character (y_0=0.60) and high symmetry. Despite a good number of quinones have been synthesized during the years, this molecule has remained elusive. However, closely related compounds could be found.[204]

In order to quantify the effect that each modification may introduce in the diradical character, the proposed structural modifications are: i) substitution of the oxygen of the carbonyl group, ii) inclusion of heteroatoms in the aromatic rings, iii) addition of substituents in different positions in the rings and iv) increase of the number of rings.

4.1. Substitution of the oxygen of the carbonyl group

In this subsection, the oxygen atom will be replaced by atoms of the groups 13 to 16 of periods 1 (B, C, N), 2 (Al, Si, P, S) and 3 (Ga, Ge, As, Se), including the required H atoms

to maintain the double bond conjugation (see **Figure 18**). The substitution by carbon (methylene group, CH_2) has been discussed in detail in the previous section. Besides, based on the methylene group, further modifications have been performed to include the following moieties: CF_2, CCl_2, CBr_2, $C(CH_3)_2$ and $C(CN)_2$.

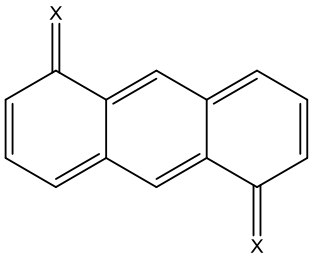

Figure 18: Derivatives of the 1,5-C(6+6+6)/Q molecule, where X=BH, CH_2, NH, O (period 1); AlH, SiH_2, PH, S (period 2) and GaH, GeH_2, AsH, Se (period 3). Besides, the following methylene derivatives have also been included: X=CF_2, CCl_2, CBr_2, $C(CH_3)_2$ and $C(CN)_2$.

In **Figure 19** are represented the diradical character, the spin density (ρ) over the substituting atoms and the NICS(1) aromaticity index, organized by periods (1, 2 and 3), and clear trends may be devised. First of all, with the exception of S and Se derivatives, all the molecules show large diradical character ($y_0 > 0.60$) and, within periods 1 and 2, both y_0 and ρ are reduced by increasing the atomic number: B>C>N>O and Al≈Si>P>S. This trend, however, is reversed in period 3 for the spin density. The variation of y_0 within each group shows a general increase with the atomic number: B < Al ≈ Ga, C < Si ≈ Ge, N < P < As, except for

group 16. The behavior of ρ is less systematic.

The unexpected behavior of S and Se has been further investigated in 1,7- and 2,3-C(6+6+6) molecules. Thus, when O is replaced by both S and Se in the 1,7-C(6+6+6) moiety, the diradical character is vanished from an original value of y_0=0.44. For 2,3-C(6+6+6), y_0 is reduced from 0.78 to 0.19 with S and is zero with Se. This feature has been further investigated using RASSCF calculations, which suggest that y_0 should increase following this trend: O<S<Se.This means that the DFT description of the singlet open-shell in these cases might be misleading and some results should be handled with care.

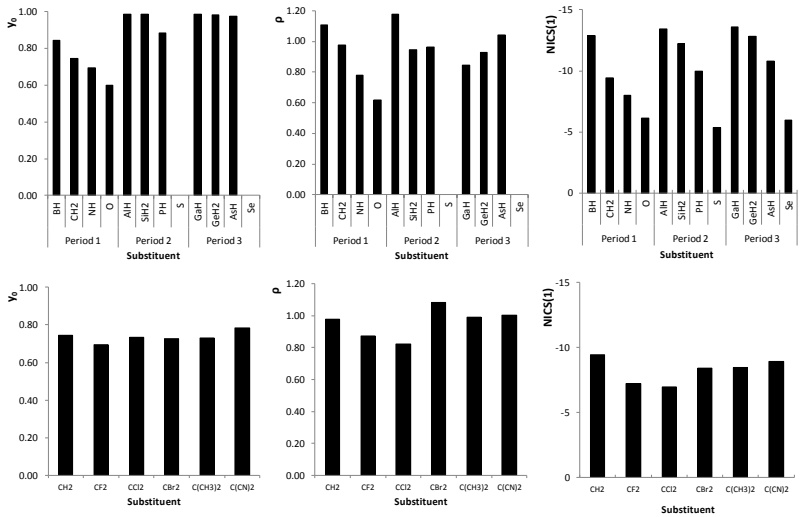

Figure 19: Diradical character (y_0), Mulliken spin densities (ρ) and aromaticity calculated on the central ring (NICS(1)).

In **Figure 19** is also observed that the aromaticity and

the diradical character follow the same trend, and larger NICS(1) values are calculated for larger y_0, as it was previously observed in the previous section, for those particular molecules in which a less aromatic closed-shell structure can be transformed into a more aromatic open-shell one. The anomalous y_0 values of S and Se derivatives are reflected in the aromaticity, and slightly lower values are accounted for with respect to the expected values.

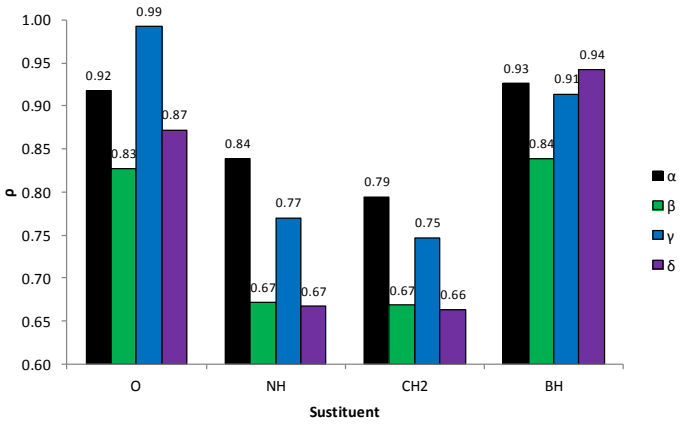

Figure 20: Spin densities (ρ) in α (black), β (green), γ (blue) and δ (purple) positions of the 1,5-C(6+6+6)/Q molecule (O) and the NH, CH_2 and BH derivatives.

In the bottom row of **Figure 19** are represented the results for the molecules obtained by the replacement of the hydrogen atoms of CH_2 moiety by halogens (F, Cl, Br), methyl (CH_3) and cyano groups (CN). Small variations in y_0 are observed, with values between 0.60 and 0.80 approximately, and no clear trend is devised. The cyano group is the only

one that provides larger diradical character than the parent CH_2 structure. Regarding ρ, small variations are also observed, almost negligible for $C(CH_3)_2$ and $C(CN)_2$ The same can be concluded for the aromaticity.

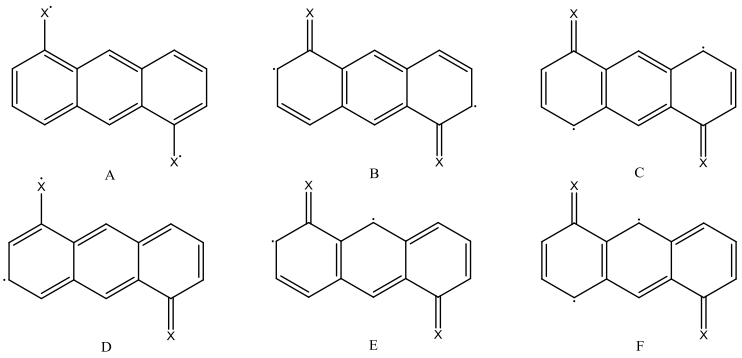

Figure 21: Selected resonance structures of the 1,5-C(6+6+6) molecule

The distribution of the spin density in the carbon backbone can be further used to analyze the variation of the diradical character. Four different positions can be noted in those structures, labeled as α (positions 2 and 6), β (positions 3 and 7), γ (positions 4 and 8) and δ (positions 9 and 10). In this manner, **Figure 20** shows how the spin density is concentrated on positions α and γ, while β and δ positions are less populated, except for the case of the boron derivative.

This behavior can be explained using the resonance structures collected on **Figure 21**, where it can be observed that structures **A**, **B** and **C** contain one Clar sextet and, therefore, are expected to be dominant in the representation of the 1,5-C(6+6+6) molecule. Structures **B** and **C** correspond

to localization of the spin density on α and γ positions, which is favored in all cases expect in the boron derivative, where structures **E** and **F** (allocation of the spin density on δ position) are preferred.

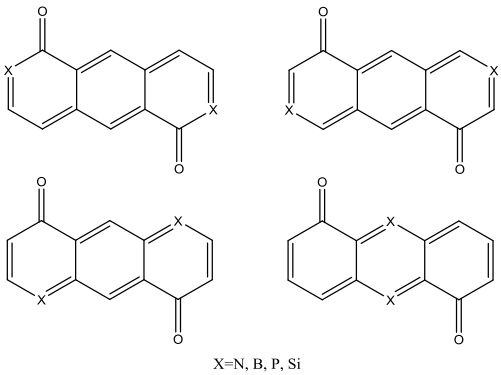

Figure 22: Derivatives of the 1,5-C(6+6+6)/Q molecule used in this study with the heteroatoms (X=N, B, P, Si) placed in α (top left), β (top right), γ (bottom left) and δ (bottom right) positions.

In general, it is observed that ρ in the carbon backbone is reduced when the atomic number of the heteroatom that substitutes the oxygen atom decreases (except for the boron derivative), as expected, since the spin density in the heteroatoms follows the opposite trend (see **Figure 20**).

4.2. Insertion of heteroatoms in the aromatic rings

The inclusion of heteroatoms in the carbon backbone has been one of the main strategies for the modification of the diradical character on a given system.[205,206,207] Thus, we have

substituted two carbons in symmetric positions of the rings with heteroatoms from the adjacent groups (B and N) and from the period below (Si and P), leading to four different isomers (see **Figure 22**) labeled as in the previous subsection: α (heteroatoms in positions 2 and 6), β (3 and 7), γ (4 and 8) and δ (9 and 10).

In general, it is observed a decrease in y_0 with the substitution (see **Figure 23**, left), although it is highly dependent on both the atom and the position. The most remarkable case is P, for which the y_0 for β and δ isomers is completely vanished (Δy_0=-0.60), while for α and γ is slightly increased with respect to the unsubstituted molecule. This trend is also observed in Si and B, while for N the opposite effect is found. Note that the Pauling electronegativities follow the trend Si (1.90) < B (2.04) < P (2.19) < C (2.55) < N (3.04). Only the nitrogen atom is more electronegative than the carbon, which may explain the deviation in the behavior. In general, the diradical character increases following N < B < C < P < Si in positions α and γ, while in positions β and δ the trend goes P << B < Si < C < N. In the other hand, the variation of the aromaticity follows the opposite trend, as expected (see **Figure 23**, right).

Again, the distribution of the spin densities may help understanding this behavior. In general, it is found that the substitution with B, P or Si in positions with high spin density (α and γ) leads to an enhancement of the diradical character,

while a decrease is found when the same atoms are inserted on low spin density positions (β or δ). For the nitrogen atom, the opposite trend is observed instead. This is reflected in **Figure 24**, where it is shown how the density over the nitrogen atom in α or γ positions is smaller (**Figure 24b**, red colour) than the density over boron (**Figure 24c**, dark green).

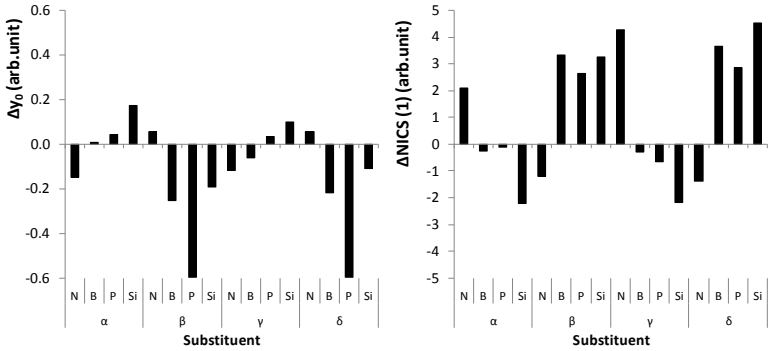

Figure 23: Variation of the diradical character, Δy_0, (left) and the NICS(1) aromaticity index calculated on the central ring (right) with respect to the 1,5-C(6+6+6)/Q molecule.

Many other previous investigations have aimed at establishing a relation between the position and nature of heteroatoms in order to modulate the diradical character or related magnitudes (like the singlet-triplet gap, for instance). However, as it was noted in the Introduction of this chapter, most of this research is focused on localized diradicals,[13] and very little work has been performed to understand the effect of substitution on delocalized diradicals. For instance, in the work of Zeng et al,[184] the captodative effect is explored to

study the variation of the diradical character after substitution. Nevertheless, this effect requires the simultaneous presence of an electron-donating and an electron-withdrawing substituent, or the substitution of a donating atom together with an acceptor atom, such as nitrogen and boron, which is out of the scope of this work.

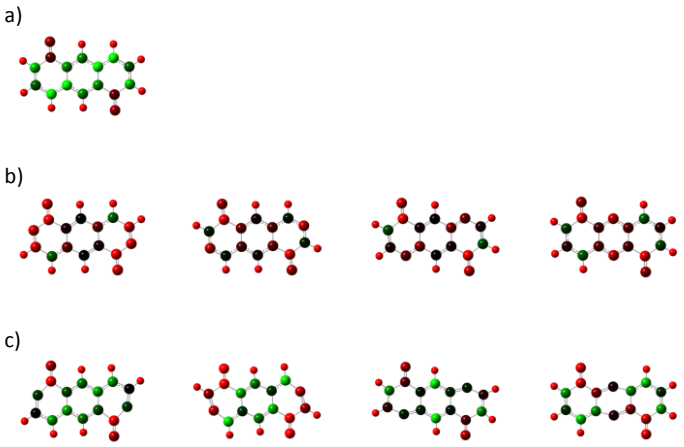

Figure 24: Mulliken spin densities (ρ) of the 1,5-C(6+6+6)/Q molecule (a), as well as the α, β, γ and δ isomers of the nitrogen (b) and boron (c) substituted derivatives. The green colour represents ρ > 1.0 while red denotes ρ < 0.5. Intermediate colours denote intermediate spin density values.

4.3. Addition of substituents

In this subsection, the effect of six different substituents in the 1,5-C(6+6+6)/Q molecule has been studied on the previously defined four positions labeled as α, β, γ and δ, as well as the fully substituted molecule, labeled as

ε (see **Figure 25**). The following substituents have been tested: two strong EWG, CF_3 and CN, three strong EDG, OH, OCH_3, and NH_2, and one weak EDG group CH_3. In order to relieve the computational effort, only the CF_3, CN, CH_3 and NH_2 groups are used to generate the fully substituted molecule (ε). Thus, in this subsection, 28 molecules are investigated.

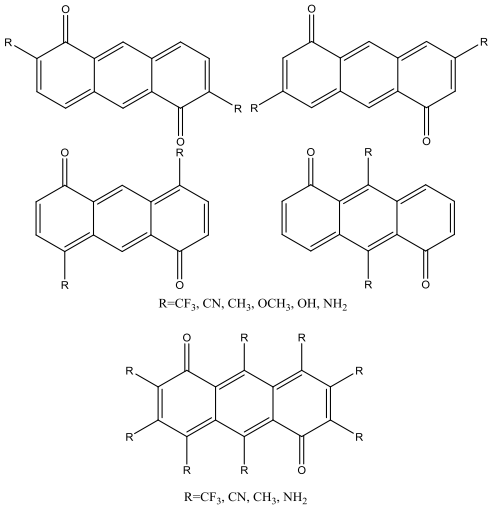

Figure 25: Derivatives of 1,5-C(6+6+6)/Q used in this study, with the substituents placed in α (top left), β (top right), γ (middle left) and δ (middle right) positions. Additionally, ε represents the fully substituted molecule (bottom).

As it has been previously observed for the α and γ substitutions, the diradical character undergoes a slight increase with respect to the unsubstituted 1,5-C(6+6+6)/Q molecule (see **Figure 26**). Despite the variations in the diradical character are small in most of cases, this effect is

more evident in the γ-substituted molecules, while the behavior of the α-substituted molecules is not that clear and some exceptions should be noted. For instance, the addition of a CF_3 substituent in α positions derives in a slight reduction of the diradical character, while the effect of the addition of a CH_3 group is negligible in that position. In the other hand, the substituents introduced in β and δ positions reduce the diradical character, especially if the substituent is an EDG group. The effect of CF_3 and CN is small (for CN a slight increase is observed). Finally, it is observed that for the fully substituted molecule (ε), the EWG substituents enhance the diradical character, while the EDG groups diminish it.

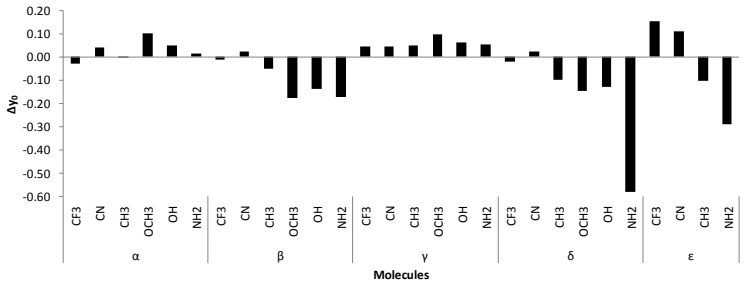

Figure 26: Variation of the diradical character (Δy_0) calculated with respect to the 1,5-C(6+6+6)/Q molecule.

Regarding the nature of the substituent, very small variations of the diradical character are observed (less than 0.2), with the exception of NH_2 in δ position, for which y_0 is remarkably decreased. This behavior might be related to the existence of a hydrogen bond interaction with the carbonyl oxygen, forming a stable six-membered ring and promoting

the enol resonance form. Thus, the N-H bond length of the interacting hydrogen is increased by 0.03 Å with respect to the other H, evidencing the existence of this interaction. In summary, the diradical character is mainly affected by the position of the substituent. This is a very relevant result from the experimental point of view, since most of the molecules proposed in this work may be difficult to synthesize, and chemical derivations may be needed in order to be isolated. With these results, we may conclude that the desired diradical character of a given molecule will remain basically unchanged after substitution.

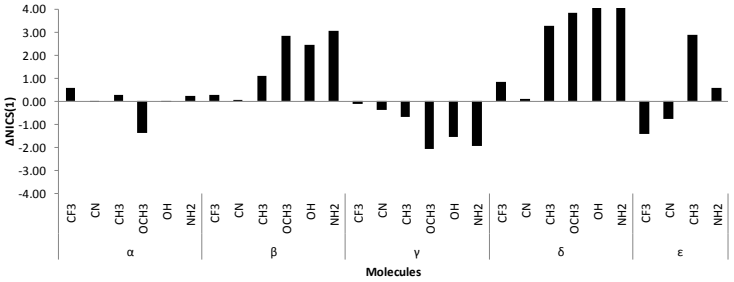

Figure 27: Variation of the NICS(1) aromaticity index with respect to the 1,5-C(6+6+6)/Q molecule.

Finally, the variation of the NICS(1) index, gathered in **Figure 27**, follows the expected trend, as in previous subsections.

4.4. Increase of the number of fused rings

In this subsection, the naphthoquinone (*n,m*-C(6+6)/Q) family of molecules is selected to study the

variation of the diradical character with the increase of the number of fused rings, starting from naphthoquinone (n=2) up to hexaquinone (n=6). Depending on the starting naphthoquinone, two different families of compounds will be generated: if the carbonyl groups are located in the same ring (1,2-, 1,4- and 2,3-C(6+6)/Q), the extra rings will be added next to the benzene without carbonyls (see **Figure 28,** top row); if the two carbonyls are located in different rings (1,5-, 1,7- and 2,6-C(6+6)/Q), the extra ones will be inserted in between, separating the carbonyl-containing rings (see **Figure 28**, bottom row).

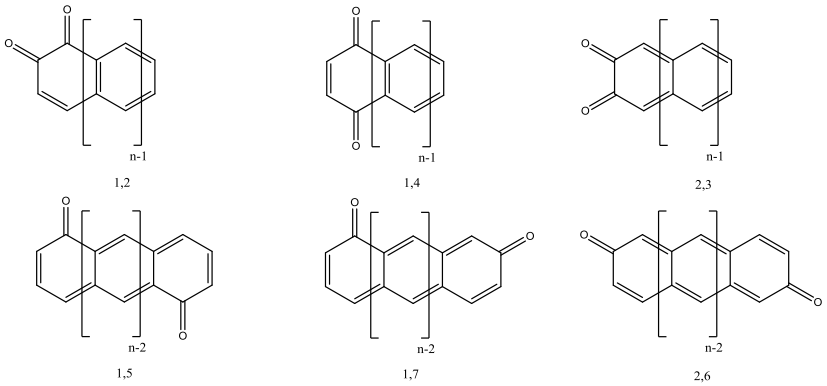

Figure 28: Naphthoquinone derivatives included in this subsection, for 2 ≤ n ≤ 6.

As it was previously discussed, the relative disposition of the carbonyls is decisive in the diradical character. Thus, the 1,5-, 1,7-, 2,6- and 2,3-C(6+6)/Q molecules show much larger y_0 values than the 1,2 and 1,4 isomers, as well as than the unsubstituted acenes. Increasing the number of rings greatly enhances y_0, especially for 2,3-C(6+6)/Q, which is a

perfect diradical for n=5 (y_0=1.00) and for the 2,6-derivative, which shows a value of y_0=0.02 with n=2 and y_0=0.72 for n=6. This effect is also found in the unsubstituted acenes, whose diradical character increases from y_0=0.05 in naphthalene to y_0=0.57 in hexacene.

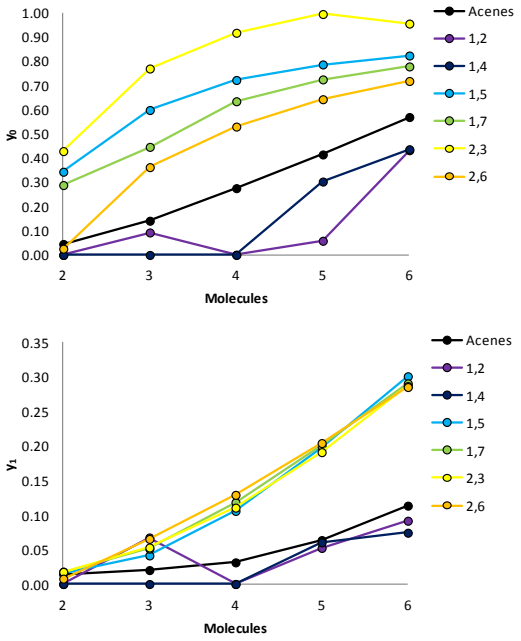

Figure 29: Diradical (y_0, top) and tetraradical (y_1, bottom) character of dicarbonyls with increasing number of rings (n=2-6) based on the 1,2-, 1,4-, 1,5-, 1,7-, 2,3- and 2,6-C(6+6)/Q naphthoquinones, together with the unsubstituted acenes.

In **Figure 29**, the diradical and tetraradical character of all studied quinone derivatives are depicted, together with the series of acenes, from naphthalene to hexacene, as a reference.

The behavior in 1,2- and 1,4- derivatives is more irregular. For instance, the diradical character of 1,2 isomer for n=3, 4, 5 is 0.09, 0.00 and 0.06, respectively. This trend is also observed in the calculated singlet-triplet gap of this molecules (1.76, 1.97 and 1.40 eV, respectively).

Additionally, in **Figure 29** is also observed that those molecules with the carbonyl groups located on separated aromatic rings show an important tetradiradical character. This feature will be of paramount importance for the application of these molecules as singlet fission sensitizers,[34, 208] that will be broadly discussed later on this thesis.

4.5. Summary and conclusions

In summary, in this section we have analyzed the variation of the diradical character after structural modifications, such as substitution of the oxygen in the carbonyl group, insertion of heteroatoms in the aromatic rings, addition of substituents and, finally, increase of the number of fused rings. For that, the 1,5-C(6+6+6)/Q molecule has been used as a reference.

The first modification introduced is the replacement of oxygen by atoms of group 13 (B, Al, Ga), group 14 (C, Si, Ge), group 15 (N, P, As) and group 16 (S, Se), and it has been found that the diradical character is enhanced in all cases except for S or Se. It has been found that, independently of the substituent, there are higher spin

densities in the positions 2, 4, 6 and 8 of the rings (positions labeled as α and γ).

Heteroatoms have been introduced in four different positions, and a relationship between the diradical character and the spin density is observed. Hence, the positions with high values of ρ are related to remarkable reductions in the diradical character when B, Si and, especially P, are inserted. When these atoms are inserted in the 2, 7, 9 and 10 positions (labeled as β and δ), the behavior of y_0 is somewhat irregular, but the general trend is an increase of this parameter. The only exception is nitrogen, which follows the opposite trend.

When EWG and EDG groups are included in different positions of the rings, a similar dependence of y_0 with the spin density is observed. Thus, the substitution in α and γ positions enhances the diradical character, while in β and δ positions y_0 is decreased. Nevertheless, it is important to emphasize that these variations are, in general, very small independently of the nature of the substituent, which may have important consequences for a hypothetical experimental synthesis of some of the molecules proposed in this work, since the desired diradical character of a given molecule will remain basically unchanged after substitution.

Finally, the increase of the number of fused rings results in the enhancement of the diradical (and tetraradical) character, but it depends on the relative position of the carbonyl groups, as it was explained previously in this chapter. Thus, those molecules with the carbonyl group inserted in separated rings experience a greater

enhancement of the diradical character.

5. Other diradical structures

During the last years, plenty of singlet open-shell molecules have been investigated, leaving an open door for the pursuit of new materials with novel applications due to their special optical, electronic and magnetic properties. Hence, in this section, we perform a screening of diradicals available in the literature and propose new derivatives in order to expand the number of open-shell molecules, in the pursuit of promising candidates to be used in organic cathode materials and as singlet fission sensitizers.

5.1. Croconate and squarate dyes

In the literature is found a considerable amount of investigations focused on the family of molecules based on squaric acid (3,4-dihydroxycyclobutenedione), denominated with several names as squarate, squaraine, or squarylium dyes.[209,210,211] This interest was mainly motivated due to their optical features, allowing their application in xerographic devices,[212] data imaging,[213] fluorescence labels,[214,215,216,217] nonlinear optics[218,219,220,221] and photovoltaics.[222,223,224,225,226,227] More information about squarates can be obtained from a few excellent reviews.[228,229,230,231] Less investigated was a structurally related group of molecules obtained from croconic acid (4,5-dihydroxycyclopentenetrione), known as croconates, croconines, croconaine, croconylium or croconium

dyes.[232,233,234] However, some reviews can still be found in the literature. [235] , [236] In any case, both categories can be considered as a group of aromatic oxocarbon-related compounds derived from oxyallyl diradical.

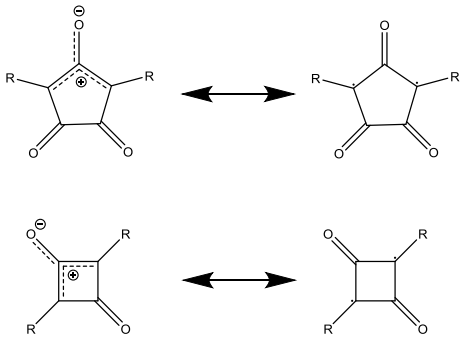

Figure 30: Molecular backbone used to design the croconate-based (top) molecules as well as the squarate derivatives (bottom). The mesoionic (left) and diradical (right) forms are depicted.

The electronic arrangement of these molecules is a combination of two isomers, the mesoionic and the diradical form (see **Figure 30**), in which the dominant one depends on the substituents selected in each case. [237]

In this subsection, a group of 22 substituents are designed to be inserted on the croconate and squarate basic moieties, leading to 44 molecules (see **Figure 31**) The substituents are arranged using the highest symmetry possible in order to save computational resources.

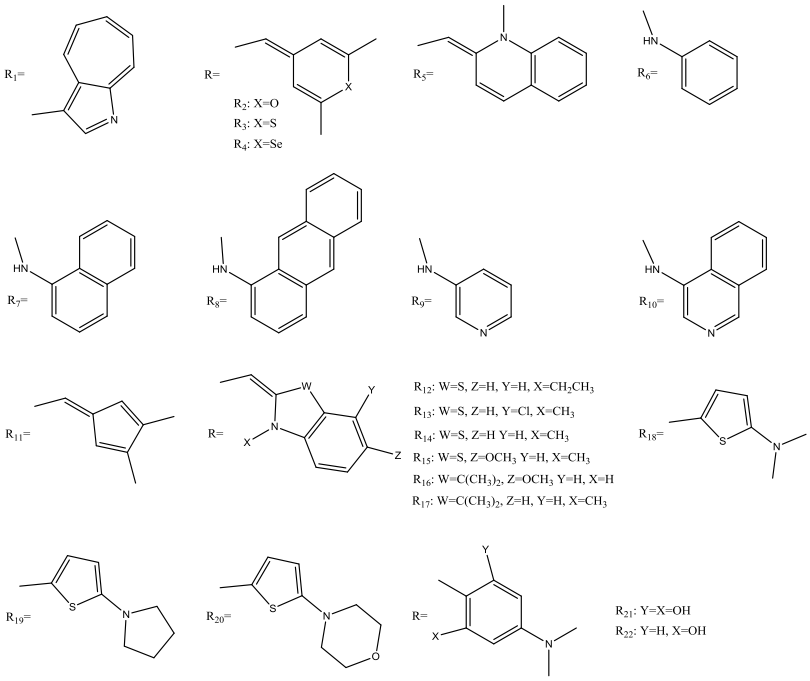

Figure 31: Substituents employed to generate the 44 squarates and croconates.

The diradical character of these molecules is collected in **Table 11**. In general, larger values of y_0 are observed for the croconate derivatives, which may be ascribed to lower HOMO-LUMO gaps, possibly due to a larger degree of conjugation in the croconates. Additionally, the existence of a non-negligible through-space radical-radical interaction between the unpaired electrons in the four-membered ring of the squarate may decrease the diradical character in these derivatives. As a consequence, only 7 squarate derivatives show significant diradical character ($y_0 \geq 0.15$). In the set formed by the croconate molecules, y_0 varies between 0.18

and 0.72.

Table 11: Diradical character (y_0) of the studied croconate derivatives. In brackets are depicted y_0 values from the literature.[233,234]

	y_0 (Squarates)	y_0 (Croconates)		y_0 (Squarates)	y_0 (Croconates)
1	0.11	0.20	**12**	0.07	0.35 (0.38)
2	0.35 (0.35)	0.63 (0.62)	**13**	0.10	0.39 (0.38)
3	0.44 (0.44)	0.70 (0.68)	**14**	0.09 (0.10)	0.38 (0.36)
4	0.46	0.71 (0.70)	**15**	0.08	0.37 (0.36)
5	0.13 (0.14)	0.41 (0.44)	**16**	0.10	0.45
6	0.02	0.27 (0.25)	**17**	0.09 (0.10)	0.45 (0.44)
7	0.08 (0.00)	0.21 (0.18)	**18**	0.20	0.45 (0.44)
8	0.17 (0.00)	0.26 (0.23)	**19**	0.18 (0.16)	0.43 (0.43)
9	0.01 (0.00)	0.27 (0.25)	**20**	0.21 (0.22)	0.47 (0.46)
10	0.08 (0.00)	0.20 (0.19)	**21**	0.00	0.18 (0.19)
11	0.44	0.72	**22**	0.03 (0.03)	0.21 (0.21)

The highest diradical characters are calculated for **R_2**, **R_3** and **R_4** derivatives, with values between 0.35 and 0.46 for the squarates and between 0.63 and 0.71 for the croconates. In these molecules, the resonant form of the closed-shell singlet involves a positively charged heteroatom (O, S or Se), destabilizing the mesoionic structure. Besides, the enhancement of y_0 from O to Se is ascribed to an increase in the electronegativity, making it more difficult to accommodate a positive charge and favoring a delocalization of the spin density along the substituents, leaving the four- or five-membered rings unchanged. This feature is observed in

Figure 32, where the spin density of the **R_2**, **R_3** and **R_4** croconate derivatives is depicted. Similar argument can be used for **R_{12}**-**R_{17}**. It is also remarkable the high diradical character of the **R_{11}** derivatives (0.72 for croconate and 0.44 for squarate), which is due to a large delocalization of the unpaired electrons in the cyclopentadiene moieties. This feature is also shared by **R_5**.

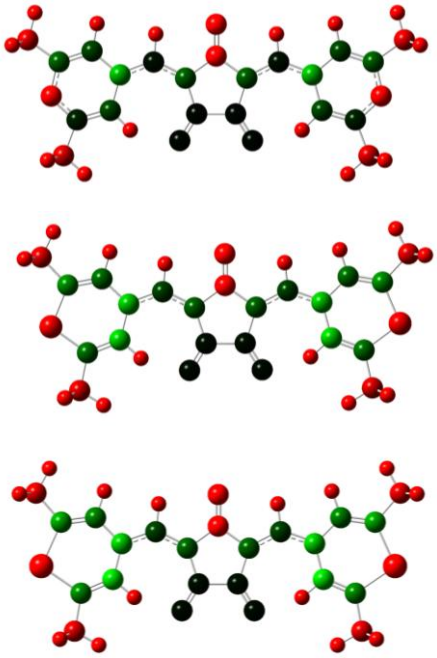

Figure 32: Variation of the spin density in the croconate derivatives due to the substitution of oxygen in R_2 (top) by sulfur (R_3, middle) and selenium (R_4, bottom). Green color corresponds to ρ=1.0, while red color corresponds to ρ=0.0. Intermediate values are denoted by intermediate color intensities. The calculations were performed at the UHF/6-311++G(d,p) level of theory

For those croconates in which the linker is an amine

group (R_6-R_{10}), the diradical character is considerably reduced, although non-negligible values are calculated, ranging between 0.17 and 0.25. This behavior can be attributed to the stabilization of the mesoionic form by π-donation of the lone pair of the nitrogen to the adjacent carbon of the central ring. Smaller y_0 values are found on their squarate counterparts, fluctuating between 0.01 and 0.17. Large diradical characters are found for those croconates in which the linker is a thiophene molecule (R_{18}, R_{19} and R_{20}), with an average of y_0=0.45 (0.20 for their squarate counterparts). The diradical form is stabilized by the aromaticity of the thiophene, while the mesoionic form would imply the formation of a quinoidal, non-aromatic, thiophene.

Finally, the low diradical character observed in **R_{21}** and **R_{22}** for both the croconate and squarate may arise from a hydrogen bond interaction between the carbonyl oxygen and the hydrogen from the alcohol groups located in *ortho* position of the phenyl rings, stabilizing the mesoionic form.[237,238] Thus, the calculated O_{carb}-H_{alc} bond distances in **R_{21}** are only of 1.67 and 1.55 Å for squarate and croconate, respectively, indicating a rather strong hydrogen bond. In **R_{22}** derivative, since only one OH group is present, less stabilization is expected and somewhat larger values of y_0 are calculated.

5.2. Oligothiophenes

Quinoidal oligothiophenes have also been investigated in this thesis, since high y_0 values have been found on this

class of molecules when two or more thiophene units are included into the structure.[28,239] This behavior, together with their optical, electronic, electrochemical and magnetic properties makes this family of compounds to be very appealing for the development of novel and versatile materials in sunlight harvesting[240] or non-linear optics.[241] The most widely used terminal group is the cyano group. For instance, the longest quinoidal oligothiophene experimentally available is a tetracyano-derivative that contains six thiophene units,[242] while other functional groups, as the dicyanovinyl group[240] or *para*-benzoquinones[243,244,245,246] have been investigated.

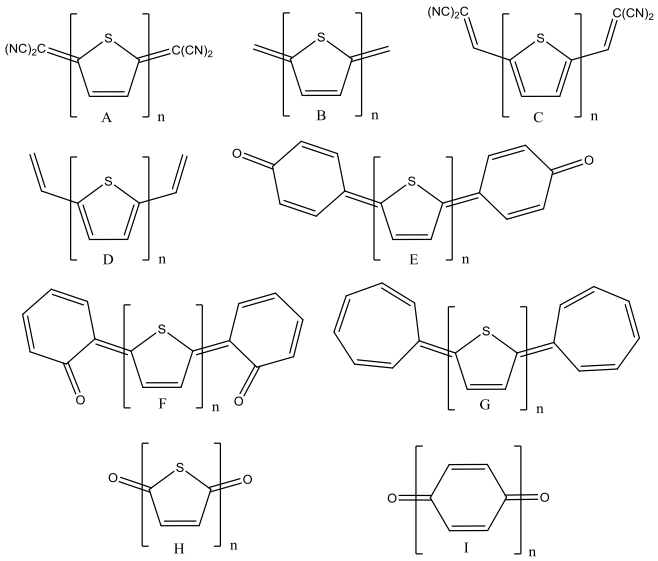

Figure 33: Studied quinoidal oligothiophenes, **A** to **H**, with n=1-4. The group **I** is included as a reference.

In this subsection, the diradical character of 32

quinoidal oligothiophenes has been investigated. All those molecules have been designed considering 1, 2, 3 and 4 thiophene monomers (n), as well as 8 different terminal substituents, labeled from **A** to **H**, as represented in **Figure 33**.

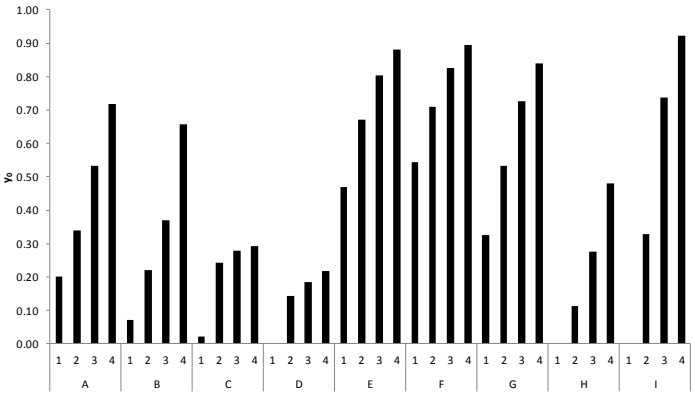

Figure 34: Diradical character (y_0) of the quinoidal oligothiophenes.

The **I** group, that can be considered as Tschitschibabin's hydrocarbon derivatives, was also included as a reference to compare the theoretically obtained data with the experimentally available work. Recently, it has been proved the experimental existence of related molecules by Zhang et al.,[247] and it was demonstrated by NMR their closed-shell character. Additionally, the dimethide analogues of **I** molecules have been already studied,[17] and a notable diradical character has been calculated. Thus, the *para*-benzoquinone (n=1), di- (n=2), tri- (n=3) and tetraphenoquinone (n=4) molecules have also been included.

The calculated y_0 values are depicted on **Figure 34**, where the expected dependence of the diradical character with the length of the chain is clearly observed.

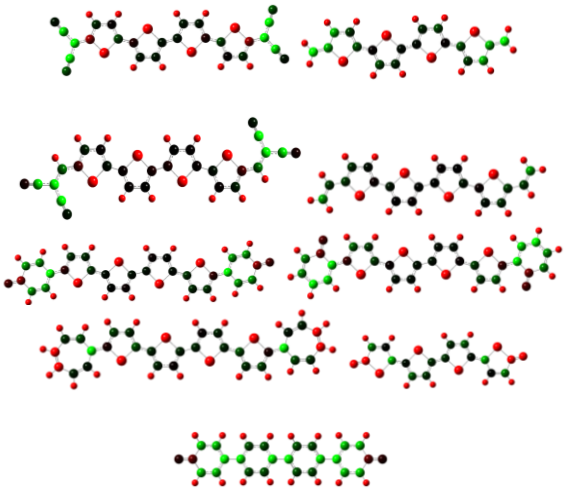

Figure 35: Spin density (ρ) of the quinoidal oligothiophenes with n=4. Green colour corresponds to $\rho \geq 0.9$, while red colour corresponds to $\rho \leq 0.5$. Intermediate values are denoted by intermediate colour intensities. The calculations were performed at the UHF/6-311++G(d,p) level of theory.

The **A**, **B** and **H** groups are characterized by y_0 values around 0.00-0.20 for n=1, 0.11-0.34 for n=2, 0.27-0.53 for n=3 and 0.48-0.72 for n=4, following this increasing trend: **H**<**B**<**A**. This behavior is in agreement with the calculations performed in the subsection 4.1, where it was demonstrated that the diradical character follows the trend: $y_0(C=C(CN)_2)$ > $y_0(C=CH_2)$ > $y_0(C=O)$. **H** group can be compared to the reference **I** group, since in both cases the molecular chain has n members with the carbonyl as terminal group, and it is

observed that the diphenoquinones have much greater diradical character than the corresponding thiophenones. Groups **E**, **F** and **G** show much higher diradical character than any other quinoidal oligothiophene studied. The reason relies on the presence of *para*- and *orto*-benzoquinone (**E** and **F**, respectively) and heptafulvene (**G**) moeties as terminal functional groups, in such a way that two extra aromatic rings are added to the oligomer, enhancing the diradical character of the whole molecule. For those groups, the tetraradical character can also reach non-negligible values, namely, y_1(**E**)=0.19, y_1(**F**)=0.21 and y_1(**G**)=0.15, for n=4.

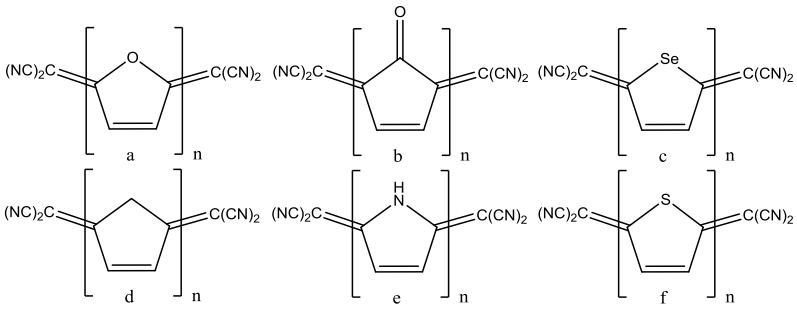

Figure 36: Derivatives of quinoidal oligothiophene A (n=2) with substituted S.

In order to explain some of the patterns observed in **Figure 34**, we can make use of the spin density, depicted in **Figure 35**. Thus, it is observed how the CH_2 group accomodates spin density more easily than the C=O group, displacing it to the thiophene moieties. In constrast, the spin density is well supported on the $C(CN)_2$ group, in both the carbon and the nitrogen, increasing the diradical character.

Similarly, **E**, **F** and **G** groups also support the major part of the spin density on the terminal group (benzoquinone or heptafulvene moieties).

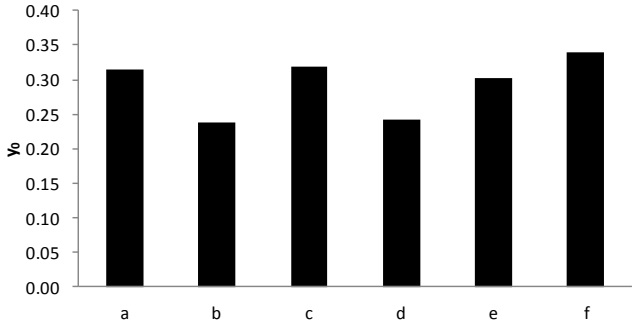

Figure 37: Diradical character (y0) of the derivatives of quinoidal oligothiophene A (n=2) with substituted S.

In order to know the effect that the S atom may introduce into the whole system, the n=2 molecule of **A** group was selected to make substitutions, as indicated in **Figure 36**. Thus, the thiophene moiety (**f**) is replaced by a furan (**a**),[248] cyclopentadienone (**b**), [249] selenophene (**c**), [250] cyclopentadiene (**d**),[251] and pyrrole (**e**).[252] In that manner, it is shown that the replacement of the sulfur atom leads to a reduction of the diradical character independently of the atom or group chosen, see **Figure 37**. However, this reduction is, in the largest case, of only 0.10 (substituting the sulfur by a sp^3 carbon).

5.3. Aromatic diimides

Another interesting type of molecules is the family of

aromatic diimides,[253] that have been investigated to be used in energy storage taking profit of their polymerization features. Since these molecules are mostly closed-shell structures, the electronic structure of their ground states has not been under debate. However, novel zethrene-based diimides have been experimentally described as open-shell structures,[254,255,256] and even an open-shell naphthalene diimide derivative has been synthesized.[257] Recently, oligorylene systems have been calculated showing that perylene, terrylene, quaterrylene and pentarylene have growing diradical character from 0.21 to 0.57.[258,259] It has been experimentally demonstrated the existence of the diimide derivatives of these molecules, and previous UV-Vis spectra suggest that the diradical character might be even higher according to absorbance in the near-IR range.[260] Finally, some novel diimines have been sketched as open-shell molecules[257] and other diimides could be identified as potential diradicals.[261]

In **Figure 38** are represented all the diimides analyzed in this thesis, and their diradical characters are gathered in **Table 12**. Attending to previous studies,[262] the polyimides **1** – **13** are classified as acene diimides, in wich **1**, and **4** – **6** are based on the PMDA (pyromellitic anhydride) moiety, and closed-shell structures are found (y_0=0.00-0.02) independently of the substituents employed. In general, the diradical character is slightly affected by the use of different substituents, so the rest of the molecules are considered using hydrogen as substituent in order to relieve the

computational effort.

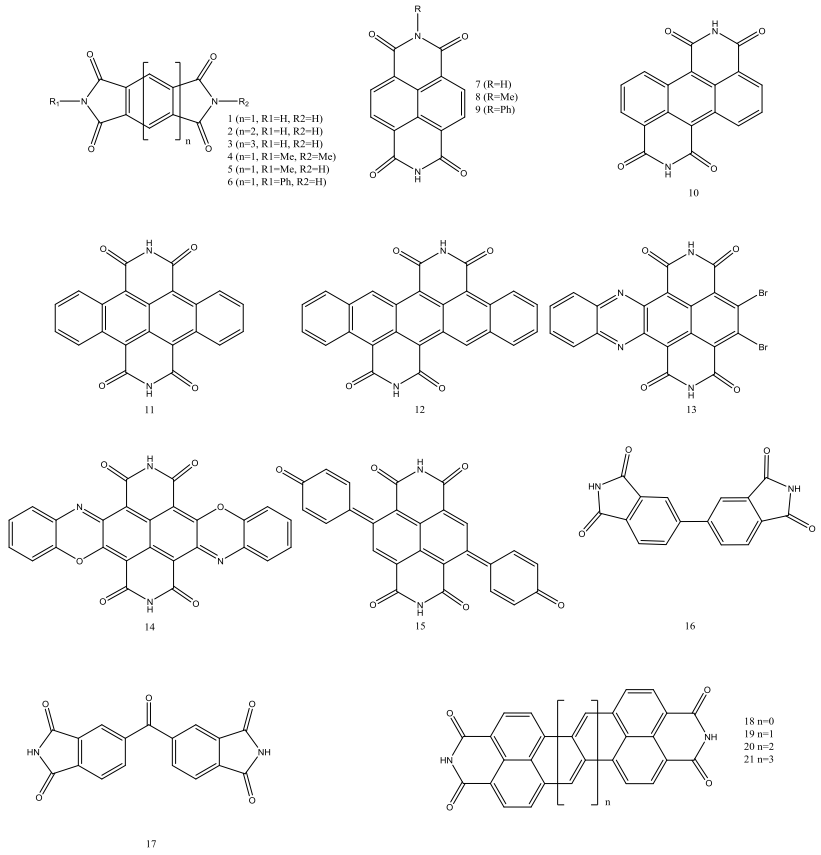

Figure 38: Diimides included on this section.

Molecules **2** and **3** are the result of the elongation of the structure by introducing aromating rings, obtaining benzene-(**1**), naphthalene-(**2**) and anthracene-(**3**) like structures, enhancing the diradical character from 0.02 to 0.15, almost equal compared to that of the unsubstituted anthracene (0.14). Analogously to the longitudinal addition of six-membered rings, the addition of rings on the transversal

axis leads to the formation of **7** (naphthalene diimide), **10** (anthracene diimide), **11** (tetracene diimide), and **12** (pentacene diimide). The presence of the diimide leaves almost unchanged the diradical character of the correspondent acene: naphthalene (y_0=0.05), anthracene (y_0=0.14), tetracene (y_0=0.28) and pentacene (y_0=0.42). In the other hand, molecules **8** and **9** are substituted derivatives of **7**, and the diradical character remains almost unchanged (y_0≈0.08).

Table 12: Diradical character (y_0) of the studied diimides

	y_0		y_0
1	0.02	**12**	0.46
2	0.00	**13**	0.30
3	0.15	**14**	0.49
4	0.01	**15**	0.97
5	0.02	**16**	0.03
6	0.02	**17**	0.00
7	0.08	**18**	0.26
8	0.08	**19**	0.45
9	0.08	**20**	0.61
10	0.19	**21**	0.71
11	0.34		

Molecule **13** can be understood as a substituted tetracene diimide, in which the diradical character is 0.30, reproducing the diradical character of the unsubstituted tetracene. Molecules **14** and **15** show high y_0 due to their naphthoquinone-like electronic arrangement (0.49 and 0.97, respectively), very similar to the previously studied 2,6-C(6+6+6) structure. The larger degree of conjugation in **15**

yields to larger value of y_0. Molecules **16** and **17** can be experimentally found on the literature,[263] and the diradical character is shown to be very low (0.00 and 0.03). Instead, the diimides based on the enlargement of the perylene diimide (**18**-**21**) show notably larger diradical characters (y_0=0.26–0.71) compared with the previous diimides, increasing with the size of the molecule. Those molecules can also be understood as zethrene derivatives, as will be discussed later. As it was previously mentioned, molecule **18** (perylene diimide) can be also understood as a rylene derivative, with a calculated y_0=0.21, slightly lower than the diradical character of **18** (0.26).

5.4. Indigo-based chromophores

The indigo molecule was sketched as a possible singlet fission sensitizer, a feature that implicitly points to a non-negligible diradical character.[33] In fact, this molecule, together with a large number of indigo-like molecules and other chromophores, have been already considered to investigate the nature of the ground state.[264] Thus, in this subsection, a set of 33 indigo-related chromophores, represented in **Figure 39**, are proposed to study their ground state and analyze the diradical character.

The indigo molecule (**1**) shows a small diradical character, y_0=0.04 (see **Table 13**), derived from the equilibrium represented in **Figure 40**, in which the structure can be understood as two radicals stabilized by captodative

substitution,[265] where both acceptor (C=O) and donor (NH) fragments coexist. In fact, the transition between the closed- and open-shell structures was experimentally reported in 2002,[266] in which an indigo-like molecule changed the colour in the solid state from yellow to red.

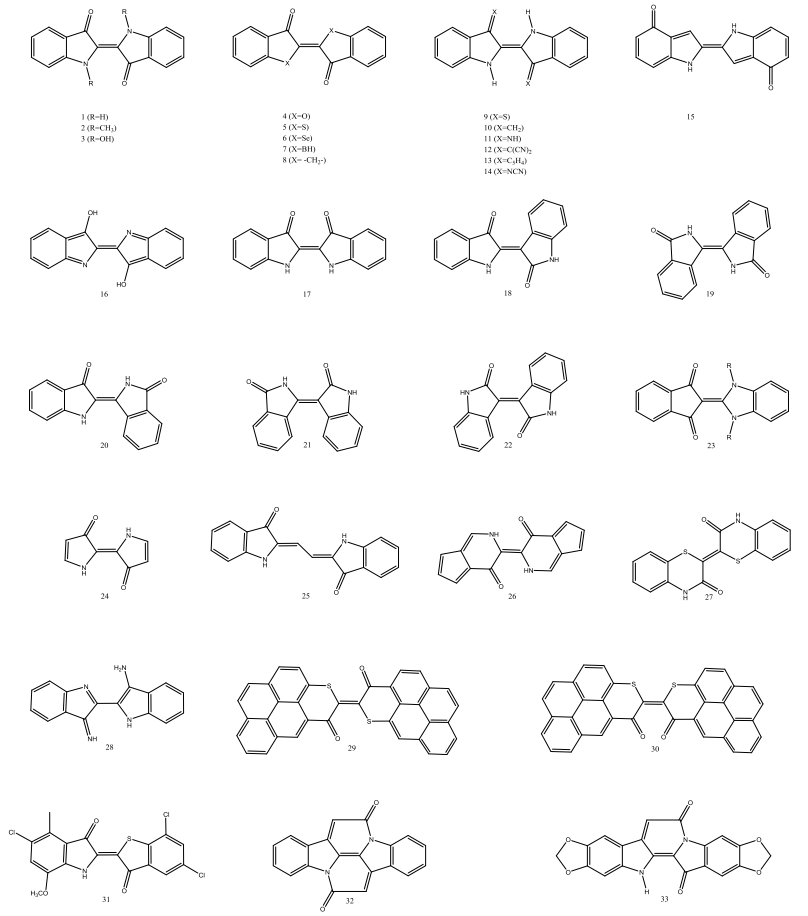

Figure 39: Indigo-like molecules studied in this work.

The C=C bond distance between the two bicycle units can be used as an extra feature, apart from y_0, to evaluate the nature of the ground state. This can be observed in **Figure**

41, where a relationship between this bond length and y_0 may be devised. It must be noted that increasing the size on the substituents directly attached to the C=C bond may enhance the diradical character on the molecule, due to the torsion of the planar structure to minimize the steric hindrance and, therefore, weakening and enlarging this bond.

Thus, indigo (**1**), characterized by an almost negligible y_0, shows a bond lenght of 1.36 Å. However, in molecule **15**, which has the largest diradical character of the whole set (y_0=0.72), this bond distance is increased up to 1.42 Å. Two molecules, **28** and **32**, are clearly out of the main trend and will be discussed below.

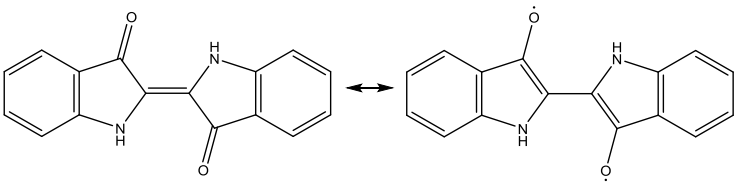

Figure 40: Closed-shell (left) and open-shell (right) resonance structures of indigo.

CH_3 (**2**) and OH (**3**) groups were used to replace the hydrogen of the amine in an attempt to modify the strength of the C=C bond. Nevertheless, small changes are observed; a subtle enhancement of y_0 (0.12) for molecule **2**, while for molecule **3** remains basically unchanged (y_0=0.05).

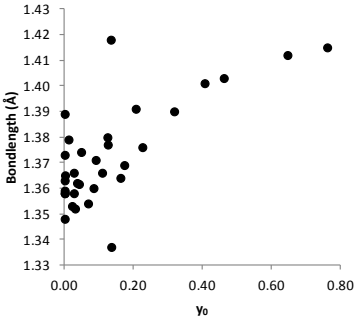

Figure 41: Relationship between the C=C bond length, in Å, and the diradical character (y_0).

The NH group has been substituted by oxygen, sulfur, boron and carbon (**4-8**), obtaining in all cases a reduction in the diradical character combined with a shortening in the C=C bond lengh. The oxygen of the carbonyl was replaced by sulfur, methylene, NH (indigoimine or nindigo),[267, 268] NCN (cyanimide),[269] $C(CN)_2$[269] and fulvene (groups **9**-**14**). A general enhancement of y_0 is observed, especially for sulfur (0.32), $C(CN)_2$ (0.41) and fulvene (0.46). It is remarkable how the substitution by sulfur enhances the diradical character, in opposition to the result found in subsection 4.1, where the replacement of oxygen by sulfur in 1,5-C(6+6+6)/Q vanishes completely the diradical character. This finding supports previous results which suggest that the selenocarbonyl and thiocarbonyl molecules have greater diradical character than their carbonyl counterpart (section 4.1).

Molecules from **15** to **23** are structural isomers of the indigo molecule. In **Table 14** are collected the relative

energies of these isomers with respect to indigo, and it is observed that more stable isomers can be found.

Table 13: Diradical character (y_0) of indigo derivatives, as well as the bond distance of the central double bond (r(C=C)), in Å. The molecule with (*) shows three central bonds, and r(C=C) is refered to one of the double bonds.

	y_0	r(C=C)		y_0	r(C=C)		y_0	r(C=C)
1	0.04	1.36	**12**	0.41	1.40	**23**	0.00	1.39
2	0.12	1.38	**13**	0.46	1.40	**24**	0.07	1.35
3	0.05	1.37	**14**	0.23	1.38	**25**	0.11	1.37*
4	0.03	1.35	**15**	0.76	1.42	**26**	0.21	1.39
5	0.03	1.36	**16**	0.65	1.41	**27**	0.01	1.38
6	0.02	1.35	**17**	0.04	1.36	**28**	0.13	1.42
7	0.00	1.36	**18**	0.09	1.37	**29**	0.00	1.36
8	0.00	1.35	**19**	0.00	1.36	**30**	0.00	1.36
9	0.32	1.39	**20**	0.00	1.37	**31**	0.03	1.37
10	0.17	1.37	**21**	0.00	1.37	**32**	0.14	1.34
11	0.16	1.36	**22**	0.13	1.38	**33**	0.08	1.36

From this group, molecule **15** is generated by the translation of the carbonyl group to the benzene ring. The result is an extraordinary enhancement of the diradical character (y_0=0.76) due to the loss of aromaticity in the six-membered rings. Additionally, a great enhancement of the diradical character (y_0=0.65) is obtained when the migration of the amino hydrogens to the carbonyl oxygen is investigated, forming the di-enol derivative (**16**). The *cis*-indigo was also studied (**17**), resulting in similar y_0 compared to the initial *trans*-indigo. However, these three isomers are less stable than the reference. Molecules from **18** to **23** are more stable isomers and are generated after the interchange of the connectivities in the C=O, C=C and NH groups. Among them, only **18** (indirubin) and **22** (isoindigo) show y_0 values different to zero (0.09 and 0.13, respectively), but still very low.

Table 14: Relative energies between indigo-like molecules and indigo, in eV

	ΔE		ΔE
15	1.62	**20**	-0.16
16	1.46	**21**	-0.69
17	0.72	**22**	-0.30
18	-0.38	**23**	-0.73
19	-0.61		

Bispyrroleindigo (**24**) and vinylogous indigo (**25**) show slightly larger y_0 that, in the case of **25** (0.11), may be ascribed to a larger conjugated system. In molecule **26**, the 5- and 6-membered rings are interchanged, and a notably larger diradical character is calculated (y_0 = 0.21). The reddish pigment thiazine-indigo (**27**) [270] is a closed-shell molecule (y_0=0.01). Molecule **28**[271] is another experimentally available indigo-like molecule, with non-negligible diradical character (y_0=0.13) and is a more energetic isomer of molecule **11** (0.23 eV). Molecules **29** and **30** possess common features with **27**, showing again a totally closed-shell ground state. Structure **31** corresponds to the pigment known as Vat Blue 36, with negligible diradical character (y_0=0.03).

Finally, two derivatives with a blocked N-C-C-N dihedral angle are considered, [272] which are simplified derivatives of cibalackrot (**32**) and its synthetic precursor, preCiba (**33**). The first one has been sketched as a singlet fission material, although further investigations are still needed.[273] Both compounds have low diradical character, but

still higher than the parent indigo molecule. In fact, the extra constrainment seems to enhance this property, since a value of y_0=0.14 is reached in molecule **33**, that can be considered as a 2,6-naphthoquinone derivative.

5.5. Other carbonyl-containing chromophores

In this subsection, the following 17 quinone-based chromophores are investigated (see **Figure 42**): quinacridone (**1**), tetrabenzodiazadiketoperylene (**2**), perinone (**3**), DPP Flame Red FD (**4**), a simplified derivative of isorenieratene (**5**), yellow 139 (**6**), carbazole dioxazine (**7**), a simplified derivative of biliverdin (**8**), a thieno[3,2-b]thiophene quinoid derivative (**9**), dibromoanthranone (**10**), indanthrene red brown RR (**11**), 7,14-dibenzpyrenequinone (**12**), pyranthrone (**13**), flavanthrone yellow (**14**), isoviolanthrone (**15**), indanthrene marine blue R (**16**), and violanthrone (**17**). The values of the diradical character are gathered in **Table 15**.

Table 15: Diradical character (y_0) of the carbonyl-containing chromphores.

	y_0		y_0
1	0.00	**10**	0.00
2	0.00	**11**	0.00
3	0.17	**12**	0.20
4	0.17	**13**	0.24
5	0.56	**14**	0.23
6	0.01	**15**	0.36
7	0.33	**16**	0.11
8	0.26	**17**	0.36
9	0.00		

It is observed that molecules **1**, **2**, **6**, **9**, **10** and **11** show closed-shell structures. These results are somewhat surprising, since molecule **2** can be related to 1,5-anthraquinone, which shows large diradical character (y_0=0.60), as well as molecule **10**, which has certain similarities with the 2,6-naphthoquinone (y_0=0.35). **3**, **4** and **16** possess very low diradical character, **7**, **8**, **12-15** and **17** show moderate values of y_0 and the largest value is accomplished by molecule **5** (y_0=0.56). In fact, molecules **15** and **17** have resemblance with the diimide **12** of subsection 5.3, but show higher y_0 values (0.36 in both cases).

5.6. Derivatives of naphthalene, pentalene, heptalene and azulene

Conjugated hydrocarbons have been widely studied during the last century, fundamentally due the optical properties conferred by the π-delocalized electronic structure. This interest has been mainly focused on tetracene and pentacene molecules, but plenty of alternatives have been proposed. For instance, acene derivatives have been theoretically designed by introducing five- and seven-membered rings on the sides of the acene chain.[274] Thus, non-alternant hydrocarbons such as pentalene, azulene and heptalene might be introduced for the seek of novel diradical structures.

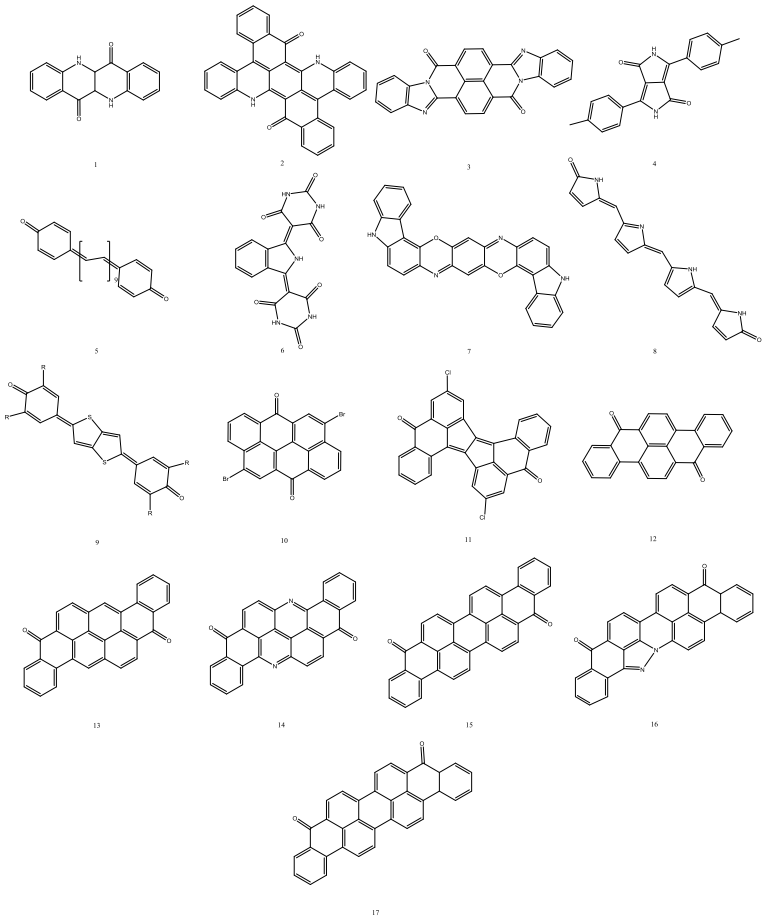

Figure 42: Carbonyl-containing chromophores.

However, while naphthalene and azulene are aromatic structures, pentalene and heptalene are not aromatic,[275] and lack the stability necessary for any practical application. For instance, pentalene molecule easily dimerizes above 140 ^{o}C.[276,277] Hence, larger efforts have been devoted in the investigation of novel applications for azulene derivatives, instead.[278,279,280,281] One of the strategies followed to synthesize stable derivatives is the inclusion of benzenoid

rings in the middle of the structure, in a process called "benzinterposition".[282,283] Following this strategy, s-indacene derivatives were synthesized as stable derivatives of the pentalene parent molecule.[284]

Therefore, in this subsection, we have studied derivatives of naphthalene, pentalene, heptalene and azulene by inserting benzene rings, as shown in **Figure 43**. In that manner, a total of sixteen molecules have been analyzed. Apart of the aforementioned s-indacene derivative and the acene molecules, only the heptalene, azulene and pentalene themselves have been synthesized, and the ground state of many of those molecules and their related features (aromaticity, diradical character, optical response, etc.) have been previously studied.[200]

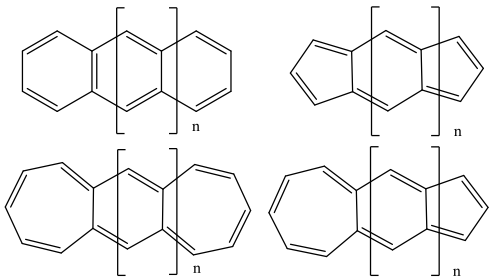

Figure 43: Derivatives of naphthalene (top left), pentalene (top right), heptalene (bottom left) and azulene (bottom right), with n=0-3.

The diradical character of the 16 hydrocarbons is represented in **Figure 44***,* in order to see the evolution of this property with the number of inserted benzene rings (n). Compared with the acene series, the derivatives of pentalene,

heptalene and azulene show, in general, larger diradical character. However, all n=1 molecules (excepting anthracene) show y_0=0, disrupting the expected progression of the diradical character with increasing molecular size. Motomura et al.[200] have obtained LUMO occupation numbers of 0.21, 0.39 and 0.60 for the n=2, 3, 4 derivatives of pentalene, indicating an increase of the diradical character with the molecular size.

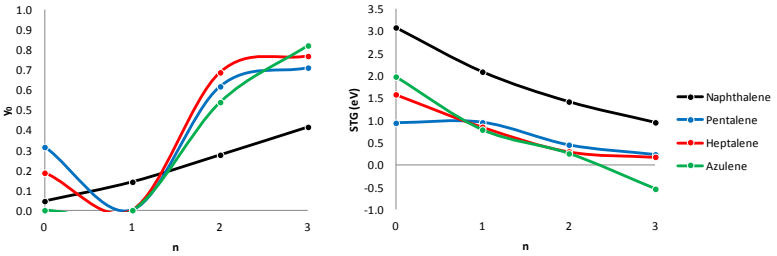

Figure 44: Diradical character (y_0, left) and singlet triplet gap ($E[T_1]^{DFT}$, right), in eV, as a function of the number of inserted benzene rings (n) for derivatives of naphthalene (black line), pentalene (blue line), heptalene (red line) and azulene (green line).

In order to validate our results, we have also performed CASSCF calculations on the n=1 isomers of the azulene and pentalene derivatives to estimate the diradical character, using the following expression shown on section 2.2.1 of Chapter 3. Thus, we have obtained *d* values of 0.35 and 0.53 for azulene and pentalene, respectively, that is, a clear diradical character, and suggesting that the present results may be an artifact of the PUHF method. Besides, singlet-triplet gaps ($E[T_1]^{DFT}$) have been also included on

Figure 44, and a decreasing trend with the molecular size is found, indicating again an increase of the diradical character. In this manner, the acene molecules would have the lowest diradical character of the group.

In conclusion, values of y_0 around 0.70-0.80 can be reached with only five rings, notably larger than with the parent acene (pentacene), which shows a value of y_0=0.42. The only exception is the n=3 azulene derivative, which has a triplet ground state.

5.7. Indenofluorenes and indolocarbazoles

Based on the previous subsection, molecular structures in which five- and six-membered rings are fused forming fully conjugated structures have motivated plenty of theoretical and experimental investigations.[285,286,287,288,289,290,291] This molecules are known as indenofluorenes, whose diradical character was recently studied.[292,293] This type of molecules displays two interesting features:[285,286] i) each five-membered ring has one carbon less compared to the corresponding acene molecule, transforming it in antiaromatic. ii) The indenofluorenes can be understood as derivatives of the unstable quinodimethane molecule. In this subsection, indolocarbazoles (nitrogen-containing derivatives of indenofluorene) are also taken into account.

A total of 16 indenofluorenes have been studied, most

of them selected from previous investigations found in the literature and are represented in **Figure 45**.

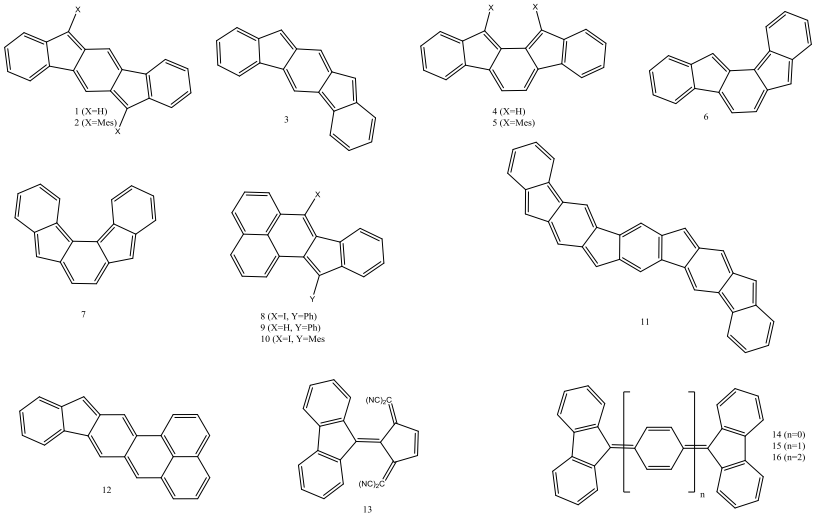

Figure 45: Studied indenofluorenes.

Haley and coworkers synthesized a series of derivatives of **1** (indeno[1,2-*b*]fluorene), a molecule with a 6-5-6-5-6 ring system[286,294,295] and fully conjugated 20 π-electrons, including the 2,8-mesityl derivative (**2**). Miyoshi et al.[293] have obtained a non-negligible y_0 value for indeno[2,1-b]fluorene (**3**). Besides, it is known that the tetraradical character may reach high values.[34,25,296] Other derivatives are: indeno[2,1-*a*]fluorene (**4**), the 2,3-mesityl derivative (**5**), indeno[1,2-*a*]fluorene (**6**), and indeno[1,2-*c*]fluorene (**7**). Additionally, other related compounds (**8-10)** have been synthesized.[297] Analogously, derivatives of **11** and **12** have been recently synthesized as black and green solids, respectively, with low diradical character.[298] However, in the present thesis, these

values have been calculated to be as high 0.46 and 0.44 respectively. Molecule **14**, commonly known as bifluorenylidene,[299,300] has been discovered long time ago and has been broadly investigated. The introduction of spacers between the fluorine units leads to a molecule (**16**) that can be understood as a derivative of the Tschitschibabin molecule, and that could be isolated as an open-shell diradical. However, superconducting quantum interference device (SQUID) measurements suggest a triplet ground state separed to the singlet by less than 0.02 eV for a similar compound.[13]

The Lewis structure of the indenofluorenes can be rearranged forming Clar sextets on the external benzene-like rings, leading to the formation of a *para*-benzoquinodimethane structure (*para*-BQDM) on molecules **1** and **7**, a *meta*-BQDM on molecules **3** and **6,** and *orto*-BQDM on molecule **4**. The diradical character has been shown to depend on these structures,[18] fundamentally due to the number of aromatic sextets presented in each case. Thus, *meta*-BQDM derived indenofluorenes have just one aromatic sextet in the closed-shell form, while the other indenofluorenes have two. Once the open-shell structure is allowed, three aromatic sextets are formed, giving special stabilization (and then, high y_0 values) to *meta*-BQDM derived molecules.

The effect of the mesityl (Mes) substituent is evaluated on molecules **1** and **4,** leading to molecules **2** and **5**

respectively. Despite the majority of indenofluorene derivatives have been experimentally described as closed-shell structures based on NMR and ESR experiments, the mesityl derivative of **3** has been demonstrated to be a diradical.[288] In fact, it has been noticed that this is the only diradical structure bearing a *meta*-quinodimethane unit in its structure.[293]

Table 16: Diradical (y_0) and tetraradical (y_1) character of the indenofluorenes and indolocarbazoles.

INDENOFLUORENES						INDOLOCARBAZOLES		
	y_0	y_1		y_0	y_1		y_0	y_1
1	0.29	0.01	**9**	0.21	0.02	**1-N**	0.26	0.04
2	0.30	0.01	**10**	0.21	0.02			
3	0.67	0.01	**11**	0.46	0.18	**3-N**	0.68	0.02
4	0.32	0.01	**12**	0.44	0.03	**4-N**	0.27	0.04
5	0.32	0.01	**13**	0.06	0.00			
6	0.97	0.03	**14**	0.22	0.01	**6-N**	0.95	0.04
7	0.28	0.01	**15**	0.50	0.02	**7-N**	0.26	0.04
8	0.26	0.02	**16**	0.89	0.03			

The values of the diradical and tetraradical character of each molecule are depicted on **Table 16**. Indenofluorenes from **1** to **7** show, despite their similarities, y_0 values from 0.28 to 0.97. However, the influence of the Mes substituents seems to be small. This behavior is again observed for compounds **8**-**10** (y_0 between 0.21 and 0.26), while the large compound **11** shows y_0=0.46, surprisingly low considering the value of pentacene (0.42). In the other hand, molecule **12** has a similar size to pentacene and also comparable diradical character (y_0=0.44). Molecules from **13** to **17** are a collection of 9-methylene-fluorene derivatives, in which the diradical character grows as the molecule becomes larger, as expected. Very small y_1 values are recorded for all cases.

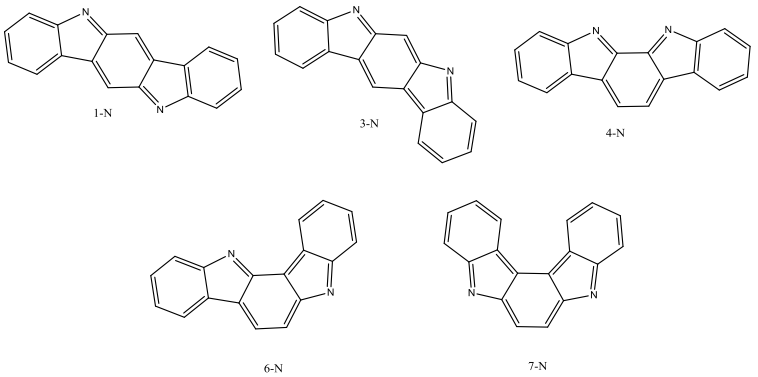

Figure 46: Studied indolocarbazoles.

The indolocarbazole class of molecules (**Figure 46**) has been less studied, although they are basically the same molecules as the indenofluorenes, only differenciated by substitution of two nitrogen atoms on the carbon backbone. However, the synthesis of derivatives of the molecules **1-N** and **3-N** can be found in the literature.[301,302,303,304] The diradical character of the indolocarbazole molecules are also included on **Table 16**, and four out of the five molecules show smaller y_0 values with respect to the parent indenofluorene. In any case, the accounted differences are small, in agreement with the findings explained on subsection 4.2.

5.8. Carbazoloquinones

The strategy of the combination of six- and five-membered rings leads to the inclusion in this thesis of the carbazole group of molecules. The carbazoles is a family of compounds in which both aromatic rings of the biphenyl molecule are linked by a NH moiety. This versatile type of heterocycles have been proposed not only as optoelectronic

materials, like photovoltaic devices, [305] sensors [306] or diodes, [307 , 308] but also in the field of energy storage. [309] However, the ground state of the carbazole molecule is clearly closed shell, therefore, in this thesis carbazoloquinone derivatives are taken into account instead,[309] which are present in some plants and have been traditionally used for their medicinal properties.[310,311,312,313,314]

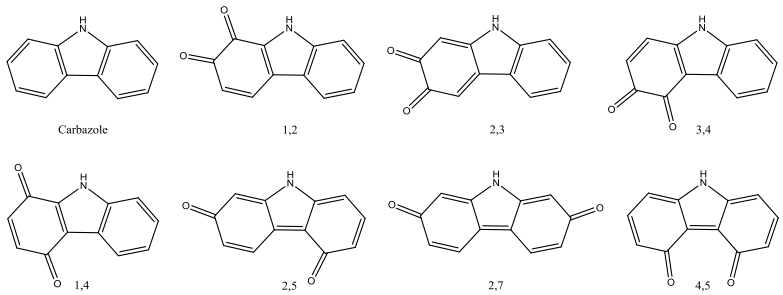

Figure 47: Studied carbazoloquinones.

Seven quinoidal derivatives of the carbazole molecule have been included in the present subsection (see **Figure 47**): three derivatives with adjacent carbonyls (1,2-, 2,3- and 3,4-carbazoloquinone), one 1,4-benzoquinone derivative (1,4-carbazoloquinone), and three derivatives with a carbonyl in each benzene ring (2,5-, 2,7- and 4,5-carbazoloquinone). The 1,4, 1,2 and 3,4 isomers have already been described in the literature.[315,316]

The diradical character of these molecules is collected in **Table 17**, where it is observed that, for the 1,2, 2,3 and 3,4 derivatives, is enhanced from y_0=0.0 to y_0=0.12-0.17.

Table 17: Diradical character (y_0) of the studied carbazoloquinones.

	y_0
Carbazole	0.00
1,2	0.14
2,3	0.17
3,4	0.12
1,4	0.00
2,5	0.36
2,7	0.01
4,5	0.58

In the other hand, the 1,4 and 2,7 isomers keep the closed-shell ground state. Finally, the 2,5 and 4,5 derivatives show important diradical character (0.36 and 0.58, respectively).

5.9. Derivatives of phenalenyl and acenaphthylene

This subsection is focused on the phenalenyl and acenaphthylene derivatives, a novel kind of polycyclic aromatic hydrocarbons (PAH) in which non-zero diradical character has been found. Thus, 23 molecules are investigated here, which are represented in **Figure 48**, and their diradical characters are collected in **Table 18**.

Thus, bisphenalenyl molecules (**1-9**) have y_0 values ranging from moderate (0.36) to very high (0.92). For instance, molecules **1** to **4** follow the expected trend of increasing y_0 with the number of rings. It is remarkable the tetraradical character of **1** (0.31). Derivatives of molecules **2**, **3** and **4** were synthesized by Kubo and coworkers, pointing to high diradical characters attending to their NMR spectra and

the values for the HOMO-LUMO and singlet-triplet gaps.[35, 317 , 318 , 319 , 320 , 321 , 322] Molecules from **5** to **9** can be compared with molecule **2** (n=1), since they have the same number of rings. In fact, molecule **5** is as molecule **2**, just with a modification in the attachment of the central benzene-like ring. The substitution of this central ring by a 5-membered ring allows the introduction of substituents that are able to tune the diradical character from 0.36 to 0.79.

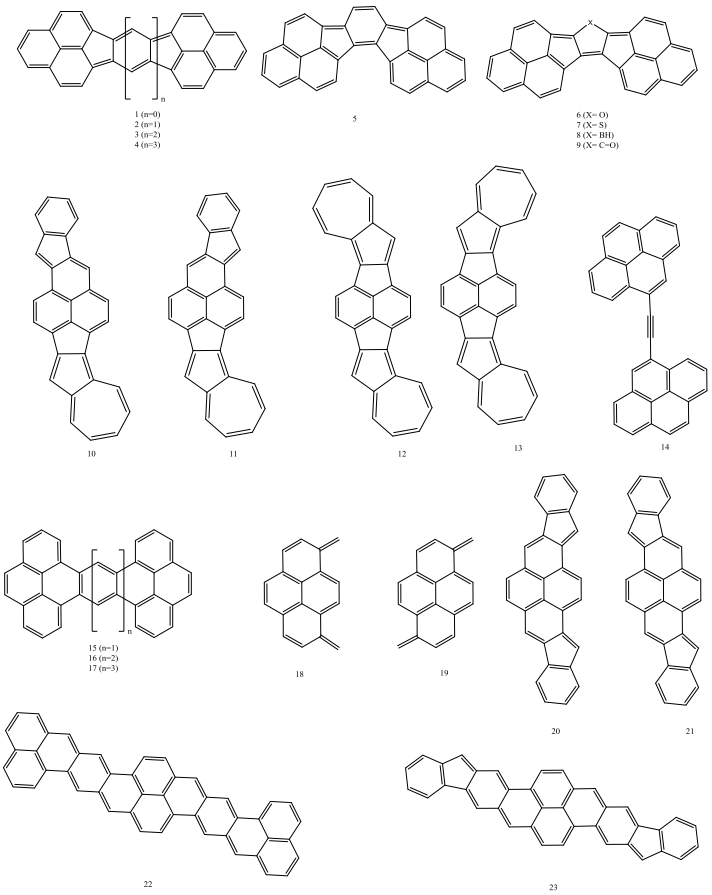

Figure 48: Studied phenalenyl and acenaphthylene derivatives.

Table 18: Diradical (y_0) and tetraradical (y_1) character of the studied phenalenyl and acenaphthylene derivatives.

	y_0	y_1		y_0	y_1
1	0.44	0.31	**13**	0.00	0.00
2	0.76	0.02	**14**	0.00	0.00
3	0.85	0.02	**15**	0.00	0.00
4	0.89	0.03	**16**	0.00	0.00
5	0.92	0.04	**17**	0.18	0.01
6	0.51	0.09	**18**	0.35	0.04
7	0.79	0.07	**19**	0.35	0.04
8	0.37	0.15	**20**	0.45	0.05
9	0.36	0.19	**21**	0.46	0.05
10	0.33	0.06	**22**	0.85	0.28
11	0.31	0.08	**23**	0.80	0.16
12	0.00	0.00			

Derivatives of molecules **10** and **11** have been synthesized by Hibi et al.[297] as dark purple solids, and in this work have been characterized as moderately open-shell molecules, with diradical characters equal to 0.33 and 0.31, respectively. In the same work is described the failed attempt to synthesize derivatives of molecules **12** and **13**, that are closed-shell molecules.

Pyrene-related derivatives (**14-16**) are closed-shell molecules, as expected, [323] while molecule **17** has low diradical character (0.18). The 1,6- and 1,8-pyrenoquinodimethanes (**18** and **19**) show intermediate diradical character (0.35 in both cases), in agreement with previous calculations.[297] However, those molecules have not been synthesized, despite the related tetracyanopyrenoquinonedimethanes can be found in the literature.[324]

Additionally, larger derivatives (**20** and **21**) are also described in the literature[297] as blue solids, and greater y_0 values (0.45 and 0.46) are calculated. Structures such as **22** and **23** have notable y_0 and derivatives of those molecules have been synthesized and already described as open-shell molecules.[298]

5.10. Zethrenes

Very interesting features have been also found in the family of zethrenes,[325,326,327] a type of molecules first reported in 1955 by Clar.[328] The original zethrene molecule (closed shell) can be seen as two naphthalene moieties linked by a *trans*-1,3-butadiene unit,[325] or as the fusion of two phenalenyl moieties. Extending the *trans*-1,3-butadiene moiety leads to larger open-shell zethrenes (heptazethrene, octazethrene, etc.), that were not possible to be synthesized,[329,330] despite the synthesis of substituted derivatives was already described in the literature.[255,256] Depending on the considered derivative, the heptazethrene molecule can be described as an open or a closed shell. In the other hand, octazethrene can be considered an open-shell molecule.[256] Further information about zethrenes and their analogues has been gathered by Hu et al.[326] The studied zethrenes are depicted on **Figure 49** and their y_0 and y_1 values are collected **Table 19**. Firstly, the importance of the chain length is observed comparing molecules from **1** to **4**, where a notable increase of y_0, from 0.21 to 0.68, is observed. Octazethrene derivatives (**4**) have been previously characterized with $y_0 \approx 0.4$.[331] The use of

experimental techniques such as NMR or SQUID demonstrated that the open-shell ground state of those derivatives emerges from the presence of a 2,6-C(6+6)/QDM-like electronic arrangement.

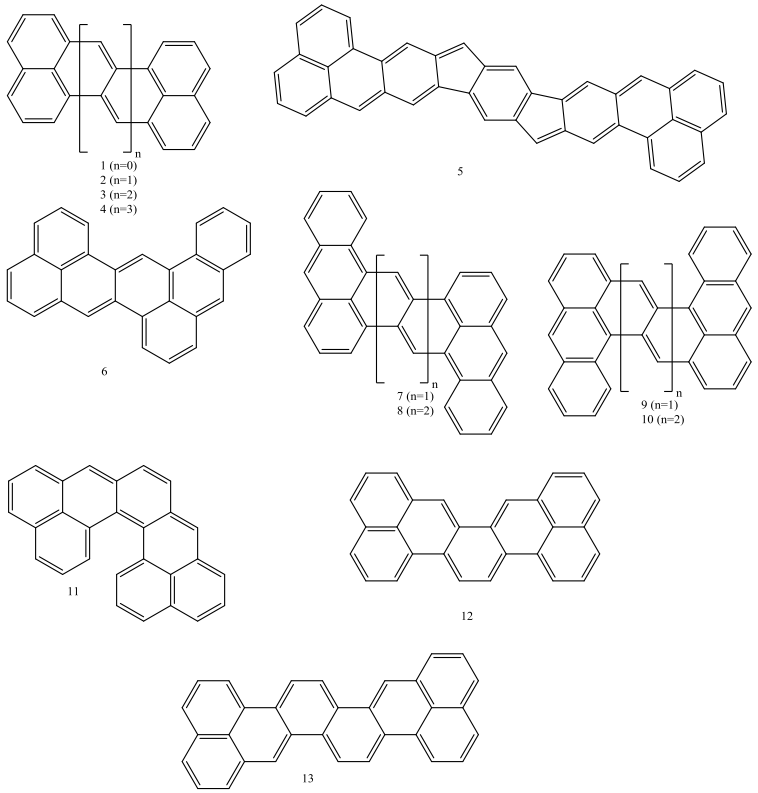

Figure 49: Studied zethrenes.

The tetraradical character may become an important factor in the understanding of these molecules. Hence, molecule **5**, whose existence has been recently reported,[298] has a y_1=0.28, while the diradical character is y_0=0.63. It is noteworthy that previously reported values of y_0 were much

lower.[298] However, high tetraradical character is more likely due to the existence of two different 1,4-quinonedimethides inside the whole system.

A side-extended zethrene was synthesized (**6**), obtaining a blue solution in hexane.[326] The synthesis of **7** was unsuccessful and it was only possible to obtain derivatives of **8** and **9**, that showed diradical character (0.58 and 0.31 respectively). [332] These values are overestimated in our calculations (0.77 and 0.48, respectively), but the trend is mantained.

Table 19: Diradical (y_0) and tetraradical (y_1) character of zethrenes.

	y_0	y_1		y_0	y_1
1	0.21	0.02	**8**	0.77	0.13
2	0.40	0.04	**9**	0.48	0.12
3	0.57	0.09	**10**	0.65	0.18
4	0.68	0.16	**11**	0.57	0.06
5	0.63	0.28	**12**	0.73	0.05
6	0.50	0.06	**13**	0.90	0.07
7	0.66	0.08			

As molecule **3**, molecules **11** and **12** can also be related to 1,4- and 1,2-quinonedimethide, that should be highlighted due to the high diradical character they show. As expected, the 1,4 derivative shows lower diradical character compared with 1,2 (0.57 vs 0.73). Note that molecule **22** of the previous section can also be described as a zethrene derivative. Despite the structural resemblance of molecule **13** with **4**, the diradical character of the latter is much higher, due to the formation of a central 1,5-C(6+6)/QDM-like moiety.[331] However, this is an unstable molecule with high reactivity.

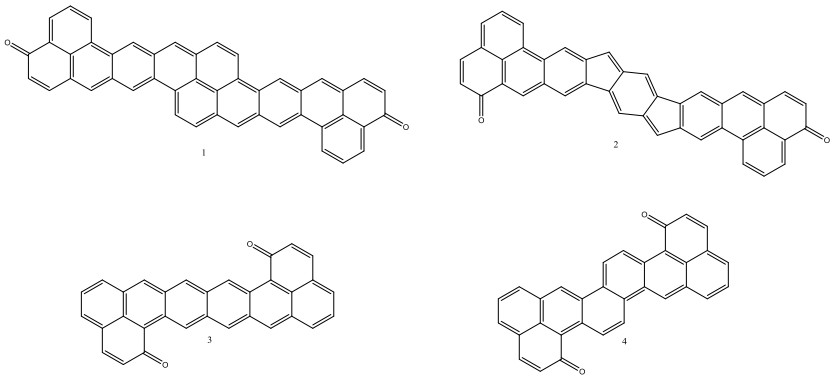

Figure 50: Studied quinone zethrene derivatives.

In the literature can be found several quinone derivatives of zethrene,[300,331] (see **Figure 50**), based on perylene (**1**), indofluorene (**2**), heptazethrene (**3**) and non-linear heptazethrene (**4**), which are characterized by intermediate y_0 values except for molecule (**4**), see **Table 20**. This can be related again with the presence of a 1,2- and 1,4-benzoquinone-like structure on the system, as well as with the formation of stable Clar sextets, once the carbonyl groups are inserted.

5.11. Other polycyclic aromatic hydrocarbons

The last group of this large screening of potential diradicals that may be promising for technological applications corresponds to a set of different polycyclic aromatic hydrocarbons (PAHs).[333, 334, 335, 336] Polyacenes longer than pentacene have been demonstrated to have open-shell ground states;[185,337,338,339] however, those large systems, that can be described as truncated graphene sheets, are unstable

and their synthesis is problematic. Larger carbon surfaces may also present diradical or even polyradical character,[340,341] and a correct description of their ground state would probably lead to the pursuit of unexpected new applications.

Table 20: Diradical (y_0) and tetraradical (y_1) character of quinone zethrenes.

	y_0	y_1
1	0.39	0.15
2	0.39	0.14
3	0.58	0.21
4	0.00	0.00

In this subsection, we have studied different PAHs (see **Figure 51**) based on previous studies found in the literature. Hence, Parac et al.[336] have calculated the value of the $S_0 \rightarrow S_1$ and $S_0 \rightarrow T_1$ transitions on a series of extended polycyclic aromatic hydrocarbons such as pyrene (**1**), dibenzocoronene (**2**), bisanthene (**3**), coronene (**4**), benzo[a]pyrene (**5**), benzo[c]tetraphene (**6**) and anthanthrene (**7**). Analogously, Naskar et al.[333] calculated the lowest excitation energies of a set of cyclopenta-fused polycyclic aromatic hydrocarbons (CP-PAH), namely, pyracylene (**8**), cycloocta-pentalene (**9**), and four dicyclo-pentacyclo-octenes (**10**-**13**).

In both investigations, they found small energy gaps between the ground singlet and the lowest triplet state, which may indicate the possibility to display an open-shell ground state. It is important to note that in both works the calculations were carried out assuming a closed-shell character, so an

eventual open-shell character was neglected. Hence, in this subsection, the y_0 values of both sets are calculated in order to establish the nature of the ground state of the proposed molecules.

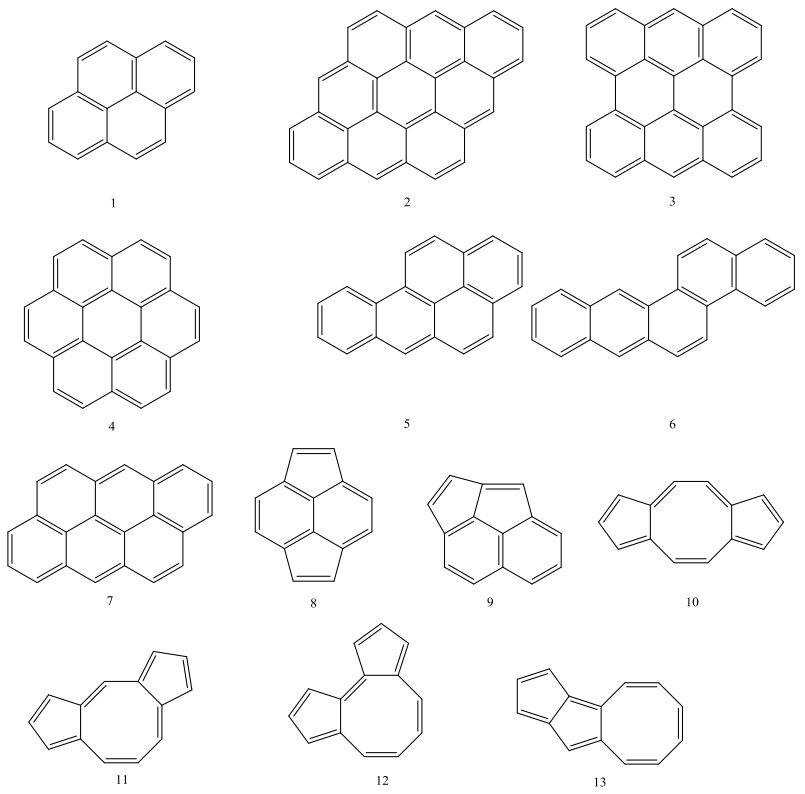

Figure 51: Polycyclic aromatic hydrocarbons (PAH) investigated in this section**.**

The diradical character of naphthalene (0.05), anthracene (0.14), tetracene (0.28), pentacene (0.42) and hexacene (0.57) can be compared with the y_0 values of larger carbon surfaces gathered on **Table 21**. It is noted that polyacenes show larger diradical character than the surfaces

with the same number of benzene-like rings (n). For instance, **1** (n=4) has lower y_0 than tetracene, the same way as **5** and **6** (n=5) with pentacene, or **7** (n=6) with hexacene. However, y_0 values comparable to those of tetracene or pentacene are calculated if larger molecules are analyzed, as **2** or **3**. Coronene (**4**) shows a surprisingly small diradical character (0.10).

Table 21: Diradical (y_0) and tetraradical character (y_1) of the studied carbon surfaces.

	y_0	y_1		y_0	y_1
1	0.12	0.03	**8**	0.16	0.01
2	0.41	0.08	**9**	0.21	0.02
3	0.51	0.05	**10**	0.07	0.00
4	0.10	0.10	**11**	0.13	0.01
5	0.17	0.04	**12**	0.21	0.17
6	0.15	0.04	**13**	0.39	0.20
7	0.25	0.04			

CP-PAH molecules have been also investigated, and moderate y_0 values (0.07-0.39) have been found. However, molecules **12** and **13** show an important tetraradical character.

5.12. Summary and conclusions

In this subsection, a screening of molecules with potential diradical character has been performed, based on previous experimental and theoretical works, in order to analyze the nature of their ground states. A large number of these structures were previously studied neglecting the possible open-shell diradical character.

Most of the analyzed molecules have been shown to have non-negligible diradical character. It is remarkable the high diradical character found among the croconates, diimides, indolocarbazoles and derivatives of pentalene, heptalene and azulene. Indigo-based and carbonyl-containing chromophores, as well as carbazoloquinones show moderate to low diradical character. Finally, groups such as zethrenes, oligothiophenes, phenalenyl derivatives or indenofluorenes have been demonstrated during the last years to show strong open-shell character. Nevertheless, scarce information can be found in the literature regarding the potential influence that this feature may have in phenomena such as singlet fission, which will be considered later in this thesis.

In conclusion, from this subsection we will select new diradical molecules to be object of further investigations in this thesis, in order to analyze their capability to be candidates for new organic cathode materials and singlet fission sensitizers.

Chapter 5

Redox chemistry

1. Introduction

The rapid development of new technologies during the last decades has boosted the investigation of new cathode materials that could satisfy the necessities of modern society in terms of price, energy density and cycle life, as well as reduce the environmental impact by designing easily recyclable cathodes produced with cheap and abundant materials.

Although singlet diradicals have been widely investigated both experimental and theoretically,[13,107,108,151,296,325,342,343,344,345,346,347,348] there is a lack of fundamental research focused to unveil the redox behavior of these open-shell systems, a key feature for the design of new organic electrode materials. Organic systems, in general, are considered a very promising type of energy storage devices due to their unique properties, such as high energy density (product of the capacity and the working potential), flexibility, processability, sustainability and structural diversity.[56]

Every organic molecule that can undergo a reversible redox reaction is a possible candidate to be an electrode material but, besides this reaction reversibility, the accomplishment of some other basic requirements is requested to improve the electrochemical performance. Thus, in order to design and evaluate new organic cathode

materials, we should look for structures with both high redox potential and theoretical capacity. The former is mainly determined by the electroactive moiety and the substituents, while the latter can be increased reducing the molecular weight of the structural unit. In this manner, conjugated carbonyl compounds are encouraging candidates for energy storage materials due to their stability, possibility of shifting the formal potential by introducing modifications in the molecule, reversibility of their redox chemistry, availability from biomass and low CO_2 footprint.[349,350,351,352,353] Also, the combination of a large number of carbonyl groups with low molecular weights results in high capacity electrodes. For practical use in a battery, there must be a voltage gap large enough between a cathode with higher redox potential and an anode with lower redox potential. Nowadays, the highest average potential that can be obtained using carbonyl-based cells is around 2.8 V[354] (vs Li/Li^+ electrode), still far from common inorganic cathode materials (3.5-4 V). Thus, in the pursuit of higher energy density, understanding carbonyl utilization and predictable engineering of the reduction potentials are desired.

In contrast to the case of inorganic electrode materials, a relatively low amount of fundamental studies have been conducted in order to understand the redox properties of organic materials,[355,356,357,358,359,360,361] although some relationships between redox voltage and properties such as electrophilicity and LUMO energy levels have already

been established from theoretical studies.[362, 363] In this manner, Aspuru-Guzik and coworkers employed a high-throughput computational approach to determine the redox potentials of a large number of quinone derivatives with different backbone lengths and functionalities.[177] Assary and coworkers also employed theoretical methods of quantum chemistry to investigate the first and second redox potentials of anthraquinone[176] and quinoxaline[364] derivates. Jang and coworkers have recently investigated the fundamental redox characteristics of model quinone derivatives to be used as positive electrodes for lithium-ion batteries, in order to understand the Li-binding properties.[365] Hernández-Burgos et al.[361] studied how some substituents (NO_2, CN, CF_3, OCH_3, CH_3, NH_2) and some heteroatoms in both aromatic (N) and non-aromatic positions (O, S, NH) could affect the reduction potential of a small set of benzoquinone derivatives. For instance, it is observed that the addition of EWG or the heterosubstitution of nitrogen lead to the enhancement of the reduction potentials. Nevertheless, we are still far from the degree of understanding regarding structure-redox activity that may be useful for a theoretically-aided selection prior to experimental characterization.

Besides, as it has been shown in Chapter 4, many conjugated carbonyls possess a non-negligible diradical character, and the lowest energy state corresponds to the open-shell singlet state. However, this important issue has been omitted in almost all of the published works so far. Thus,

the aim of this chapter is to provide with a better understanding of how the diradical nature may affect common properties such as ionization energy or coordination energy of the reduced species to metal cations, as well as the electrochemical features, in the pursuit of new organic compounds with high redox potentials useful as cathode materials.

2. Computational details

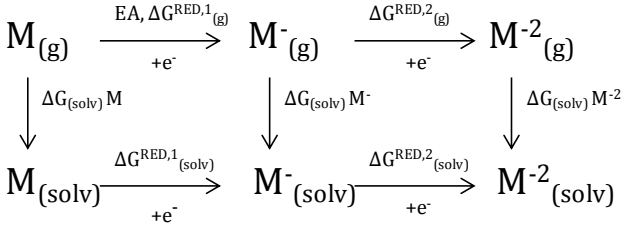

Figure 52: Thermodynamic cycle used in the calculation of the first (E_R^1) and second (E_R^2) redox potentials.

Electron affinities, ionization energies and reduction potentials are calculated at the B3PW91/6-311++G(d,p)//B3PW91/6-31+G(d) level of theory. This level of theory will be systematically used except in those cases in which something else is noted. The G3(MP2)-RAD composite method has also been employed in those molecules with mainly closed-shell character, since it has been shown to be an accurate method for the calculation of electron affinities and redox potentials of quinone derivatives.[355] The reduction potentials have been calculated using the thermodynamic cicle shown in **Figure 52**, where the Gibbs free energy of the

reduction half-reaction, $\Delta G^{RED}_{(solv)}$, consists of the free energy change in the gas phase and the solvation free energies (in acetonitrile) of the oxidized and reduced species:

$$\Delta G^{RED}_{(solv)} = \Delta G^{RED}_{(g)} + \Delta G_{(solv)}M^{-} - \Delta G_{(solv)}M$$

The relation between the Gibbs energy and the electrode potential (E) of a half-cell is:

$$E = -\frac{\Delta G}{nF} - E_{ref}$$

where *F* is the Faraday constant (96485 C/mol) and *n* is the number of electrons in the half-reaction, with the subtraction of the reduction potential of the reference electrode. In this work, we have used the reference value -1.24 V, which represents the difference between the standard hydrogen electrode (SHE, -4.28 V)[366] and the Li/Li^{+} redox couple (-3.04 V). In order to compare with the available experimental results expressed vs to the saturated calomel electrode (SCE), the reference value -4.67 V have been used. Additionally the value -4.988[367] is needed to obtain the redox potential vs ferrocene electrode.

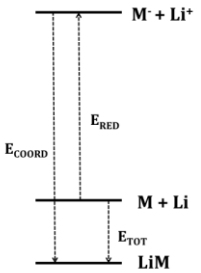

Figure 53: Lithiation mechanism in the charge/discharge process in a lithium-ion battery.

Additionally, we have studied the process of lithiation, described in **Figure 53**, since the molecules interact with Li (in lithium-ion batteries) during the charging and discharging processes. This methodology has been previously used in the literature[368] and allows a better characterization of the redox properties of these molecules. The following three parameters, reduction energy (E_{RED}), coordination energy (E_{COOR}) and total energy (E_{TOT}), are defined as:

$$E_{RED} = E(M^-) + E(Li^+) - (E(M) + E(Li))$$
$$E_{COOR} = E(LiM) - (E(M^-) + E(Li^+))$$
$$E_{TOT} = E(LiM) - (E(M) + E(Li))$$

The number of carbonyl groups defines the number of successive reductions that certain organic molecule may undergo. As previously explained, the ratio between the number of electrons and the mass of the molecule is known as theoretical capacity (C_{THEO}). Thus, this quantity will be calculated with n=2 for dicarbonyl molecules. The product of the theoretical capacity when n=2 and the reduction potential for the correspondent bielectronic process leads to the energy density (E_{DEN}), measured in $Whkg^{-1}$. For monocarbonyl molecules, E_{DEN} is calculated using C_{THEO} calculated with n=1 and E_R[1].

3. Redox properties of conjugated quinones

In this section, the redox properties of the group of 90 conjugated carbonyls labeled as *n,m*-C(x+y+z)/Q are

investigated (**Figure 13**). The discussion involving the methylene derivatives (QM and QDM) is omitted due to the observed low reduction potentials. In the next subsections, the results are presented and organized as follows: firstly, electron affinities (EA), ionization potentials (IP), as well as first and second redox potentials (E_R^1 and E_R^2) are discussed. Finally, the complexation energy with the Li^+ cation is studied, in an attempt to compare with the redox reactions that carbonyl compounds undergo in lithium-ion batteries. All these properties are discussed in terms of the diradical nature of the ground state as well as the aromaticity and some structural variations already studied in the previous chapter, such as the size and number of rings, or the relative arrangement of the carbonyls.

3.1. Electron affinities and ionization potentials.

In **Figure 54** are represented the electron affinities (EA) and the diradical character. The only available experimental data[369,370] correspond to molecules that have a closed-shell ground state. DFT calculations overestimate the experimental values around 0.3 eV, an uncertainty that may be due partly to the previously explained self-interaction error.[161]

More accurate EAs have been obtained with the G3(MP2)-RAD composite method (with an average error of only 0.04 eV) but, due to its limited application in molecules with strong diradical character, and also due to convergence

problems encountered in several molecules, we will discuss the results obtained with B3PW91 functional.

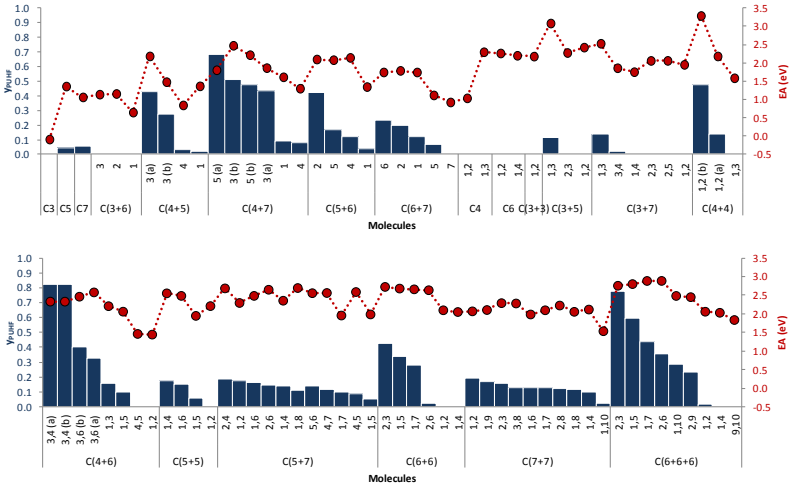

Figure 54: Electron affinities (dotted lines), in eV, and diradical character (bars).

A trend in the electron affinities may be devised in several families of molecules such as C(4+5), C(4+7), C(5+6), C(6+7), C(4+4), C(4+6), C(5+5), C(6+6) and C(6+6+6), where higher y_0 values correspond to higher EAs. This may be explained in terms of the HOMO-LUMO gap, which is small in molecules with a remarkable diradical character, mainly due to low-energy LUMO levels and, therefore, more likely to accept an electron. However, this trend is not clear in families where molecules are closed-shell singlets or in others with moderate (or small) diradical character, such as C(5+7), C(7+7), which can be ascribed to distortions in the molecular geometry of the anion with respect to the neutral molecule.

Table 22: Electron affinities (EA), in eV, calculated with the B3PW91 functional and the G3(MP2)-RAD composite method.

		EA^{B3PW91}	EA^{G3}	EA^{EXP}			EA^{B3PW91}	EA^{G3}	EA^{EXP}
C3		-0.09	-0.18	--	**C(4+6)**	**3,6 (a)**	2.58	--	--
C5		1.36	1.10	--		**1,3**	2.21	2.00	--
C7		1.06	0.90	--		**1,5**	2.06	1.81	--
C(3+6)	**3**	1.13	1.02	--		**4,5**	1.46	1.25	--
	2	1.15	1.11	--		**1,2**	1.44	1.25	--
	1	0.64	0.55	--	**C(5+5)**	**1,4**	2.55	2.20	--
C(4+5)	**3 (a)**	2.18	--	--		**1,6**	2.48	2.18	--
	3 (b)	1.48	1.36	--		**1,5**	1.95	1.71	--
	4	0.84	0.67	--		**1,2**	2.21	1.98	--
	1	1.36	1.25	--	**C(5+7)**	**2,4**	2.68	2.35	--
C(4+7)	**5 (a)**	1.80	--	--		**1,2**	2.29	2.04	--
	3 (b)	2.47	--	--		**1,6**	2.48	2.21	--
	5 (b)	2.21	--	--		**2,6**	2.65	2.30	--
	3 (a)	1.86	--	--		**1,4**	2.35	2.11	--
	1	1.61	1.44	--		**1,8**	2.69	2.04	--
	4	1.30	1.07	--		**5,6**	2.56	2.25	--
C(5+6)	**2**	2.09	--	--		**4,7**	2.56	2.27	--
	5	2.08	1.83	--		**1,7**	1.96	1.67	--
	4	2.14	1.93	--		**4,5**	2.59	2.32	--
	1	1.34	1.15	--		**1,5**	1.98	1.74	--
C(6+7)	**6**	1.74	1.60	--	**C(6+6)**	**2,3**	2.72	--	--
	2	1.78	1.66	--		**1,5**	2.68	2.43	--
	1	1.74	1.69	--		**1,7**	2.66	2.38	--
	5	1.11	0.95	--		**2,6**	2.64	2.35	--
	7	0.92	0.79	--		**1,2**	2.10	1.84	--
C4	**1,2**	1.03	0.82	--		**1,4**	2.05	1.81	1.81
	1,3	2.29	2.28	--	**C(7+7)**	**1,2**	2.07	1.86	--
C6	**1,2**	2.26	1.95	1.90		**1,9**	2.10	1.83	--
	1,4	2.20	1.89	1.85		**2,3**	2.29	2.08	--
C(3+3)	**1,2**	2.17	2.18	--		**3,8**	2.28	2.08	--
C(3+5)	**1,3**	3.08	2.81	--		**1,6**	1.98	1.77	--
	2,3	2.27	2.10	--		**1,7**	2.10	1.89	--
	1,2	2.42	2.17	--		**2,8**	2.22	1.97	--
C(3+7)	**1,3**	2.53	2.37	--		**1,8**	2.06	1.85	--
	3,4	1.86	1.60	--		**1,4**	2.12	1.87	--
	1,4	1.75	1.56	--		**1,10**	1.53	1.31	--
	2,3	2.06	1.87	--	**C(6+6+6)**	**2,3**	2.76	--	--
	2,5	2.06	1.83	--		**1,5**	2.80	--	--
	1,2	1.95	1.76	--		**1,7**	2.88	--	--
C(4+4)	**1,2 (b)**	3.28	--	--		**2,6**	2.89	2.61	--
	1,2 (a)	2.18	1.94	--		**1,10**	2.48	2.29	--
	1,3	1.58	1.41	--		**2,9**	2.45	2.23	--
C(4+6)	**3,4 (a)**	2.33	--	--		**1,2**	2.06	1.83	--
	3,4 (b)	2.33	--	--		**1,4**	2.03	1.79	--
	3,6 (b)	2.46	--	--		**9,10**	1.84	1.65	1.59

Monocarbonyl compounds show EAs between -0.09 and 2.47 eV, while dicarbonyl EAs range from 1.03 to 3.28 eV (see **Table 22**). The highest value among all the molecules considered corresponds to 1,2(b)-C(4+4), with an EA of 3.28

eV, a molecule that shows a remarkable diradical character (y_0=0.48). Large affinities are calculated for families such as C(6+6) or C(6+6+6).

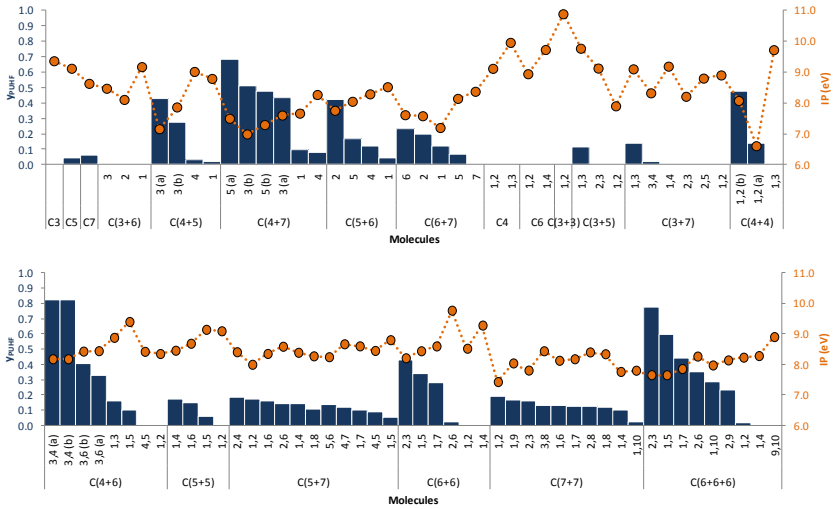

Figure 55: Ionization potentials (dotted lines), in eV, and diradical character (bars).

Analogously, we have calculated the ionization potentials (IP), which are gathered in **Figure 55** together with the diradical character. All the calculated and the available experimental data,[371,372 ,373,374] are listed in **Table 23**. In this case, both DFT and G3(MP2)-RAD calculate the IPs with similar accuracy. Monocarbonyl IPs range from 6.98 to 9.35 eV, while dicarbonyl IPs range from 6.60 to 10.88 eV, much higher than the EA values.

Table 23: Ionization potentials (IP), in eV, calculated with the B3PW91 functional and the G3(MP2)-RAD composite method.

		IP^{B3PW91}	IP^{G3}	IP^{EXP}			IP^{B3PW91}	IP^{G3}	IP^{EXP}
C3		9.35	9.38	9.47	**C(4+6)**	**3,6 (a)**	8.43	--	--
C5		9.11	9.33	9.49		**1,3**	8.87	9.03	--
C7		8.62	8.79	8.80		**1,5**	9.39	9.66	--
C(3+6)	**3**	8.46	8.50	--		**4,5**	8.41	8.68	--
	2	8.10	8.09	--		**1,2**	8.34	8.45	9.23
	1	9.16	9.29	--	**C(5+5)**	**1,4**	8.45	8.73	--
C(4+5)	**3 (a)**	7.15	--	--		**1,6**	8.68	8.95	--
	3 (b)	7.86	8.05	--		**1,5**	9.13	9.33	--
	4	9.01	9.21	--		**1,2**	9.09	8.69	--
	1	8.78	8.89	--	**C(5+7)**	**2,4**	8.40	8.71	--
C(4+7)	**5 (a)**	7.49	--	--		**1,2**	7.99	8.13	--
	3 (b)	6.98	--	--		**1,6**	8.34	8.53	--
	5 (b)	7.29	--	--		**2,6**	8.58	8.87	--
	3 (a)	7.59	--	--		**1,4**	8.38	8.59	--
	1	7.66	7.82	--		**1,8**	8.27	8.64	--
	4	8.26	8.52	--		**5,6**	8.24	8.43	--
C(5+6)	**2**	7.75	--	--		**4,7**	8.66	8.85	--
	5	8.04	8.26	--		**1,7**	8.59	8.77	--
	4	8.28	8.50	--		**4,5**	8.44	8.64	--
	1	8.51	8.68	--		**1,5**	8.79	8.96	--
C(6+7)	**6**	7.61	7.77	--	**C(6+6)**	**2,3**	8.20	--	--
	2	7.57	7.74	--		**1,5**	8.43	8.64	--
	1	7.19	7.30	--		**1,7**	8.59	8.80	--
	5	8.14	8.34	--		**2,6**	9.76	9.89	--
	7	8.36	8.54	--		**1,2**	8.51	8.78	--
C4	**1,2**	9.11	9.12	9.79		**1,4**	9.27	--	9.40
	1,3	9.95	10.05	--	**C(7+7)**	**1,2**	7.42	7.57	--
C6	**1,2**	8.93	9.11	9.60		**1,9**	8.03	8.27	--
	1,4	9.72	9.98	10.11		**2,3**	7.80	7.93	--
C(3+3)	**1,2**	10.88	10.88	--		**3,8**	8.43	8.63	--
C(3+5)	**1,3**	9.76	9.92	--		**1,6**	8.12	8.34	--
	2,3	9.12	--	--		**1,7**	8.17	--	--
	1,2	7.89	7.83	--		**2,8**	8.39	8.61	--
C(3+7)	**1,3**	9.09	--	--		**1,8**	8.33	8.53	--
	3,4	8.31	7.54	--		**1,4**	7.75	7.94	--
	1,4	9.18	9.34	--		**1,10**	7.79	8.21	--
	2,3	8.20	8.19	--	**C(6+6+6)**	**2,3**	7.65	--	--
	2,5	8.79	8.82	--		**1,5**	7.65	--	--
	1,2	8.89	9.16	--		**1,7**	7.85	--	--
C(4+4)	**1,2 (b)**	8.07	--	--		**2,6**	8.26	8.42	--
	1,2 (a)	6.60	6.75	--		**1,10**	7.97	8.20	--
	1,3	9.71	9.78	--		**2,9**	8.13	8.34	--
C(4+6)	**3,4 (a)**	8.17	--	--		**1,2**	8.22	8.39	--
	3,4 (b)	8.17	--	--		**1,4**	8.27	8.42	8.48
	3,6 (b)	8.42	--	--		**9,10**	8.90	9.32	9.00

While for the electron affinities a certain correlation with the diradical character is found within particular families,

the case of the ionization potentials is less clear. Still, it is possible to observe that higher diradical character values correspond to lower IPs in families such as C(4+5), C(5+6), C(4+6), C(6+6) or C(6+6+6). Besides, in **Figure 55** is also possible to see correlation between the number of fused rings and the IPs, which decrease as the number of fused rings increases. For example, the IPs of 1,2-C6, 1,2-C(6+6) and 1,2-C(6+6+6) are 8.93, 8.51 and 8.22 eV, respectively. Nevertheless, in the present section, molecules with up to only three fused rings are compared and, therefore, probably not enough to extrapolate to larger molecules. A similar trend is found regarding the size of the ring: bigger rings show smaller IPs (e.g. comparing monocarbonyl C3, C5 and C7 or dicarbonyl C4 and C6).

3.2. Redox potentials and coordination to Li^+.

In **Figure 56** are represented the first reduction potentials (E_R^1) and the y_0 values. In **Table 24** are gathered the calculated values of all groups together with the available experimental data.[375,376] Opposite to what was observed for the electron affinities, the first redox potentials are calculated more accurately with DFT (MAE=0.05 V) than with G3(MP2)-RAD (MAE=0.22 V), which suggests that the inclusion of the solvation effects in the composite method may be problematic.

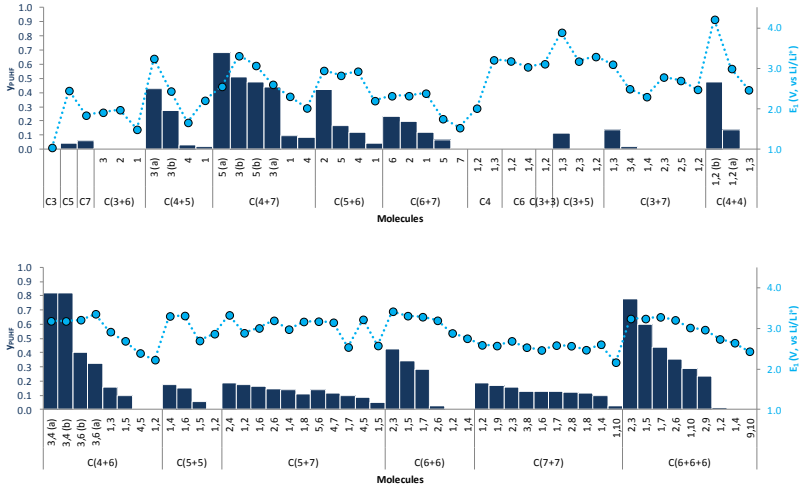

Figure 56: First redox potentials (dotted lines), in V, and diradical character (bars).

The E_R^1 values for monocarbonyls range from 1.05 to 3.32 V, while for dicarbonyls range from 2.02 to 4.22 V. The highest value calculated in this work, 4.22 V, corresponds to 1,2(b)-C(4+4), which also shows the highest electron affinity (3.28 eV) and a notable diradical character (y_0=0.48). This redox potential is considerably higher than the usual values for carbonyl-based materials (less or around 3 V) and comparable (or even greater) to common inorganic cathode materials. There are 35 molecules that show redox potentials greater than 3 V.

Table 24: First redox potential (E_R^1), in V, calculated with the B3PW91 functional and the G3(MP2)-RAD composite method. The reference electrode is Li/Li^+, while experimental references and values between parenthesis are expressed vs saturated calomel electrode (SCE).

		E_R^1 B3PW91		E_R^1 G3(MP2)-RAD		E_R^1 EXP			E_R^1 B3PW91		E_R^1 G3(MP2)-RAD		E_R^1 EXP
C3		1.05		0.97		--	**C(4+6)**	**3,6 (a)**	3.36		--		--
C5		2.46		2.20		--		**1,3**	2.92		2.71		--
C7		1.85		1.70		--		**1,5**	2.69		2.44		--
C(3+6)	**3**	1.92		1.80		--		**4,5**	2.39		2.18		--
	2	1.98		1.94		--		**1,2**	2.23		2.03		--
	1	1.50		1.40		--	**C(5+5)**	**1,4**	3.30		2.95		--
C(4+5)	**3 (a)**	3.25		--		--		**1,6**	3.31		3.01		--
	3 (b)	2.45		2.31		--		**1,5**	2.70		2.46		--
	4	1.67		1.51		--		**1,2**	2.87		2.63		--
	1	2.22		2.11		--	**C(5+7)**	**2,4**	3.33		3.00		--
C(4+7)	**5 (a)**	2.56		--		--		**1,2**	2.89	(-0.54)	2.63	(-0.80)	-0.56
	3 (b)	3.32		--		--		**1,6**	3.01		2.74		--
	5 (b)	3.08		--		--		**2,6**	3.19		2.84		--
	3 (a)	2.61		--		--		**1,4**	2.98		2.73		--
	1	2.31		2.15		--		**1,8**	3.17		2.65		--
	4	2.03		1.80		--		**5,6**	3.17		2.84		--
C(5+6)	**2**	2.95		--		--		**4,7**	3.15		2.86		--
	5	2.83		2.59		--		**1,7**	2.54		2.25		--
	4	2.94		2.73		--		**4,5**	3.22		2.93		--
	1	2.21		2.01		--		**1,5**	2.58		2.33		--
C(6+7)	**6**	2.33		2.20		--	**C(6+6)**	**2,3**	3.42		--		--
	2	2.33		2.21		--		**1,5**	3.31		3.06		--
	1	2.39		2.34		--		**1,7**	3.28		3.00		--
	5	1.76		1.61		--		**2,6**	3.19		2.91		--
	7	1.54		1.41		--		**1,2**	2.88	(-0.55)	2.63	(-0.80)	-0.56
C4	**1,2**	2.02		1.81		--		**1,4**	2.75	(-0.68)	2.53	(-0.90)	-0.71
	1,3	3.22		3.21		--	**C(7+7)**	**1,2**	2.59		2.38		--
C6	**1,2**	3.19	(-0.24)	2.88	(-0.55)	-0.31		**1,9**	2.57		2.30		--
	1,4	3.04	(-0.39)	2.74	(-0.69)	-0.51		**2,3**	2.69		2.45		--
C(3+3)	**1,2**	3.12		3.12		--		**3,8**	2.53		2.35		--
C(3+5)	**1,3**	3.90		3.59		--		**1,6**	2.47		2.24		--
	2,3	3.18		3.02		--		**1,7**	2.58		2.34		--
	1,2	3.30		2.96		--		**2,8**	2.57		2.30		--
C(3+7)	**1,3**	3.11		2.96		--		**1,8**	2.47		2.25		--
	3,4	2.50		2.21		--		**1,4**	2.61		2.35		--
	1,4	2.31		2.13		--		**1,10**	2.17		1.95		--
	2,3	2.79		2.61		--	**C(6+6+6)**	**2,3**	3.24		--		--
	2,5	2.71		2.49		--		**1,5**	3.24		--		--
	1,2	2.49		2.30		--		**1,7**	3.28		--		--
C(4+4)	**1,2 (b)**	4.22		--		--		**2,6**	3.20		2.95		--
	1,2 (a)	3.00		2.77		--		**1,10**	3.02		2.82		--
	1,3	2.48		2.29		--		**2,9**	2.97		2.75		--
C(4+6)	**3,4 (a)**	3.18		--		--		**1,2**	2.74		2.51		--
	3,4 (b)	3.18		--		--		**1,4**	2.64	(-0.78)	2.43	(-1.00)	-0.75
	3,6 (b)	3.21		--		--		**9,10**	2.43	(-1.00)	2.27	(-1.16)	-0.94

Inspecting **Figure 56**, we find the following general trend: molecules with higher diradical character, within a particular family, possess higher reduction potentials, the same correlation observed in the EAs, as expected. However, those families with low or absence of diradical character may show large reduction potentials as well, such as benzoquinones (1,2- and 1,4-C6), for example, with 3.19 and 3.04 V, respectively. This general trend is particularly clear in the following families: C(4+5), C(4+7) (with the exception of 5(a)-C(4+7)), C(6+7), C(4+4), C(4+6) (except 3,6(a)-C(4+6)), C(5+5), C(6+6) and C(6+6+6). A somewhat irregular behavior is observed in C(5+6), C(5+7) and C(7+7).

Thus, in view of these results, the effect of the diradical character may be a new, unexplored variable for tuning the redox potential in the design of new organic cathode materials. Besides the diradical character, the size of the ring and the number of fused rings may affect the redox potential as well. We observe a decrease in E_R^1 comparing C6, C(6+6) and C(6+6+6) for both 1,2 and 1,4 dicarbonyls. The same holds for 1,3-C4 and 1,3-C(4+4); however, the opposite trend is found in 1,2-C4 and 1,2-C(4+4). Regarding the size of the ring, an irregular behavior is observed in E_R^1, increasing from C3 to C5 but decreasing in C7. We have also calculated the second reduction potential (E_R^2), see **Table 25** and **Figure 57.** Monocarbonyls range from 0.72 to 2.08 V, while dicarbonyls range from 0.74 to 2.67 V. The trends are the same as in the E_R^1.

Table 25: Second redox potential (E_R^2), in V, calculated with the B3PW91 functional and the G3(MP2)-RAD composite method. The reference electrode is Li/Li^+, while experimental references and values between parenthesis are expressed vs saturated calomel electrode (SCE).

		E_2^{B3PW91}		$E_2^{G3(MP2)-RAD}$		E_2^{EXP}			E_2^{B3PW91}		$E_2^{G3(MP2)-RAD}$		E_2^{EXP}
C3		1.83		1.61		--	**C(4+6)**	**3,6 (a)**	2.33		--		--
C5		1.51		1.82		--		**1,3**	1.85		2.16		--
C7		1.65		3.92		--		**1,5**	1.76		2.13		--
C(3+6)	**3**	1.48		1.64		--		**4,5**	1.00		1.08		--
	2	1.68		1.79		--		**1,2**	1.31		1.57		--
	1	1.78		1.26		--	**C(5+5)**	**1,4**	2.29		2.51		--
C(4+5)	**3 (a)**	1.69		--		--		**1,6**	2.13		2.36		--
	3 (b)	1.69		1.91		--		**1,5**	1.73		2.01		--
	4	0.72		1.26		--		**1,2**	1.93		2.24		--
	1	1.47		1.50		--	**C(5+7)**	**2,4**	2.39		2.62		--
C(4+7)	**5 (a)**	1.66		--		--		**1,2**	2.00		2.28		--
	3 (b)	1.70		--		--		**1,6**	2.00		2.25		--
	5 (b)	1.64		--		--		**2,6**	2.25		2.51		--
	3 (a)	1.70		--		--		**1,4**	1.98		2.25		--
	1	1.34		1.64		--		**1,8**	1.94		2.60		--
	4	1.49		1.54		--		**5,6**	2.22		2.49		--
C(5+6)	**2**	2.08		--		--		**4,7**	2.20		2.49		--
	5	1.88		2.20		--		**1,7**	1.73		2.09		--
	4	1.97		2.27		--		**4,5**	2.29		2.58		--
	1	0.92		1.54		--		**1,5**	1.71		2.06		--
C(6+7)	**6**	1.57		1.45		--	**C(6+6)**	**2,3**	2.44		--		--
	2	1.28		1.58		--		**1,5**	2.44		2.80		--
	1	1.50		1.59		--		**1,7**	2.41		2.70		--
	5	1.51		1.22		--		**2,6**	2.25		2.59		--
	7	1.38		1.03		--		**1,2**	1.82		2.07		--
C4	**1,2**	1.60		1.58		--		**1,4**	1.73	(-1.70)	2.07	(-1.36)	-1.25
	1,3	1.71		1.92		--	**C(7+7)**	**1,2**	1.70		1.97		--
C6	**1,2**	2.08	(-1.35)	2.37	(-1.06)	-0.90		**1,9**	1.88		2.22		--
	1,4	1.89	(-1.54)	2.24	(-1.19)	-1.14		**2,3**	1.70		1.93		--
C(3+3)	**1,2**	2.50		2.81		--		**3,8**	1.55		1.77		--
C(3+5)	**1,3**	2.67		3.03		--		**1,6**	1.65		1.90		--
	2,3	1.97		2.46		--		**1,7**	1.75		2.07		--
	1,2	2.01		2.46		--		**2,8**	1.64		1.97		--
C(3+7)	**1,3**	1.80		2.06		--		**1,8**	1.67		1.97		--
	3,4	1.47		1.78		--		**1,4**	1.68		1.92		--
	1,4	1.47		1.75		--		**1,10**	1.73		2.07		--
	2,3	1.65		1.92		--	**C(6+6+6)**	**2,3**	2.64		--		--
	2,5	1.48		1.79		--		**1,5**	2.53		--		--
	1,2	1.62		1.96		--		**1,7**	2.48		--		--
C(4+4)	**1,2 (b)**	2.19		--		--		**2,6**	2.40		2.76		--
	1,2 (a)	2.19		2.52		--		**1,10**	2.22		2.53		--
	1,3	0.94		1.32		--		**2,9**	2.12		2.40		--
C(4+6)	**3,4 (a)**	2.20		--		--		**1,2**	1.66		1.89		--
	3,4 (b)	2.21		--		--		**1,4**	*1.68*	(-1.75)	1.95	(-1.48)	-1.25
	3,6 (b)	2.46		--		--		**9,10**	1.58	(-1.85)	1.90	(-1.53)	-1.45

Finally, we have studied the process of lithiation. In **Figure 58** are collected the values of the total binding energy (E_{TOT}) of the lithiation process together with the diradical character. In

Table 26 are collected the numerical values for E_{COOR}, E_{RED} and E_{TOT}. Inspecting the monocarbonyl compounds, very similar coordination energies (E_{COORD}) are obtained, ranging from -5.88 to -6.49 eV, revealing that the reduction energy (E_{RED}) is the main responsible of the observed pattern in the binding energies (E_{TOT}). On the other hand, this feature is not observed in the dicarbonyl compounds, as expected, since the relative position of the carbonyl moieties will affect the interaction with Li^+. This dependence of the binding energy on the position of the carbonyl groups is recognized in **Figure 58**, where molecules with neighboring carbonyls tend to show higher coordination energies, as the lithium cation is located between both oxygen atoms. For instance, while for most of the anthraquinones (group C(6+6+6)) the coordination energies vary from -5.64 to -5.88 eV, this energy for 1,2- and 2,3-C(6+6+6) molecules amounts -7.15 and -7.02 eV, respectively.

If the carbonyl groups are not adjacent, but spatially close, some extra stabilization is gained favoring the reduced complex. This can be observed comparing 1,2- and 1,9-C(7+7), where the carbonyl oxygens are separated 2.81 and 4.80 Å, respectively, and the coordination energies are -7.13 and -6.35 eV, respectively. The latter is still greater than the energies of the rest of the C(7+7) molecules, which amount less than -6 eV.

It is not easy to establish a direct relationship between binding energy and diradical character. The binding energy

depends on the reduction energy, which may be lowered with greater diradical character (due to larger electron affinities), but also on the anion-cation interaction, which is independent of the diradical character of the neutral species, and which probably is the most relevant feature. Thus, we find some groups where larger diradical characters yield larger binding energies, such as C(4+6), C(4+4), C(4+6) and C(6+6+6) groups. However, in other groups the behavior of E_{TOT} is rather irregular.

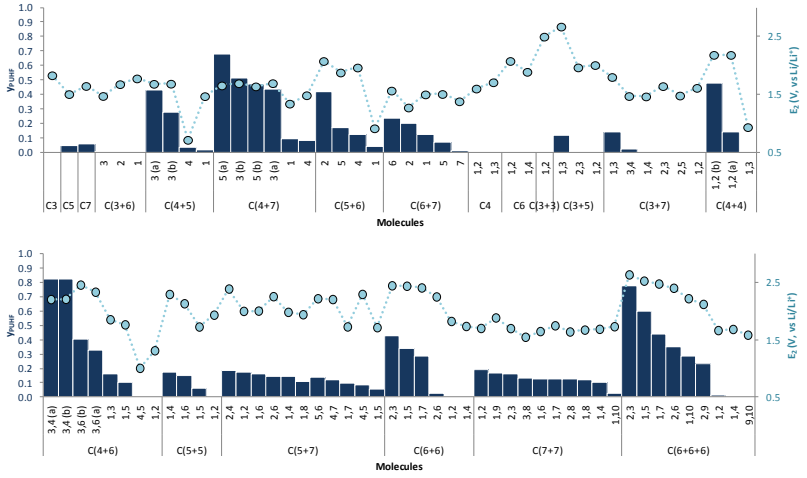

Figure 57: Second redox potentials (dotted lines), in V, and diradical character (bars).

Finally, the energy density of the whole set of 90 molecules has been gathered in **Figure 59**. There is shown that the monocarbonyl molecules have, in general, lower E_{DEN} compared to the quinones (264-837 $WhKg^{-1}$). However, some monocarbonyl molecules as 1-C5 (823 $WhKg^{-1}$) or 3(a)-C(4+5) (837 $WhKg^{-1}$) have particularly high energy density

Table 26: Reduction (E_{RED}), coordination (E_{COORD}) and total binding energies (E_{TOT}), in eV, of the lithiation process.

		E_{TOT}	E_{COORD}	E_{RED}			E_{TOT}	E_{COORD}	E_{RED}
C3		-0.75	-6.39	5.64	**C(4+6)**	**3,6 (a)**	-3.03	-6.02	2.99
C5		-2.16	-6.36	4.20		**1,3**	-2.70	-6.05	3.35
C7		-1.76	-6.26	4.50		**1,5**	-2.44	-5.94	3.50
C(3+6)	**3**	-2.00	-6.41	4.42		**4,5**	-3.38	-7.47	4.09
	2	-2.04	-6.44	4.40		**1,2**	-2.46	-6.57	4.11
	1	-1.16	-6.06	4.90	**C(5+5)**	**1,4**	-2.61	-5.62	3.01
C(4+5)	**3 (a)**	-3.12	-6.49	3.37		**1,6**	-3.99	-7.07	3.08
	3 (b)	-2.43	-6.49	4.07		**1,5**	-2.30	-5.90	3.61
	4	-1.43	-6.13	4.70		**1,2**	-3.42	-6.77	3.35
	1	-1.70	-5.88	4.19	**C(5+7)**	**2,4**	-3.05	-5.93	2.88
C(4+7)	**5 (a)**	-2.64	-6.40	3.76		**1,2**	-3.65	-6.91	3.27
	3 (b)	-3.29	-6.38	3.09		**1,6**	-2.48	-5.56	3.08
	5 (b)	-3.06	-6.40	3.34		**2,6**	-2.68	-5.59	2.91
	3 (a)	-2.68	-6.38	3.70		**1,4**	-2.54	-5.75	3.21
	1	-2.00	-5.94	3.95		**1,8**	-4.20	-7.06	2.86
	4	-1.97	-6.22	4.26		**5,6**	-4.06	-7.06	3.00
C(5+6)	**2**	-2.70	-6.17	3.46		**4,7**	-2.67	-5.67	3.00
	5	-2.68	-6.16	3.48		**1,7**	-2.24	-5.85	3.60
	4	-2.79	-6.21	3.42		**4,5**	-4.14	-7.11	2.97
	1	-1.97	-6.19	4.21		**1,5**	-2.20	-5.77	3.57
C(6+7)	**6**	-2.39	-6.21	3.81	**C(6+6)**	**2,3**	-4.23	-7.07	2.84
	2	-2.42	-6.19	3.77		**1,5**	-2.96	-5.84	2.88
	1	-2.44	-6.26	3.81		**1,7**	-3.02	-5.92	2.90
	5	-1.67	-6.11	4.44		**2,6**	-2.80	-5.73	2.93
	7	-1.61	-6.24	4.63		**1,2**	-3.74	-7.20	3.46
C4	**1,2**	-1.89	-6.41	4.52		**1,4**	-2.28	-5.79	3.51
	1,4	-2.69	-5.95	3.25	**C(7+7)**	**1,2**	-3.64	-7.13	3.49
C6	**1,2**	-4.00	-7.30	3.30		**1,9**	-2.90	-6.35	3.45
	1,4	-2.54	-5.91	3.37		**2,3**	-3.81	-7.08	3.27
C(3+3)	**1,2**	-1.22	-4.61	3.39		**3,8**	-2.18	-5.46	3.28
C(3+5)	**1,3**	-3.05	-5.53	2.49		**1,6**	-2.33	-5.90	3.57
	2,3	-3.80	-7.09	3.29		**1,7**	-2.36	-5.82	3.46
	1,2	-2.95	-6.09	3.14		**2,8**	-2.27	-5.60	3.33
C(3+7)	**1,3**	-2.68	-5.71	3.04		**1,8**	-2.28	-5.78	3.50
	3,4	-3.61	-7.31	3.70		**1,4**	-2.20	-5.64	3.44
	1,4	-1.96	-5.76	3.80		**1,10**	-3.18	-7.19	4.02
	2,3	-3.79	-7.29	3.49	**C(6+6+6)**	**2,3**	-4.22	-7.02	2.80
	2,5	-2.35	-5.85	3.50		**1,5**	-2.97	-5.73	2.76
	1,2	-2.64	-6.25	3.61		**1,7**	-3.10	-5.78	2.68
C(4+4)	**1,2 (b)**	-4.36	-6.63	2.26		**2,6**	-2.96	-5.64	2.68
	1,2 (a)	-3.25	-6.63	3.38		**1,10**	-2.72	-5.80	3.08
	1,3	-1.78	-5.76	3.97		**2,9**	-2.77	-5.88	3.11
C(4+6)	**3,4 (a)**	-4.17	-7.40	3.23		**1,2**	-3.65	-7.15	3.50
	3,4 (b)	-4.17	-7.40	3.23		**1,4**	-2.21	-5.74	3.53
	3,6 (b)	-3.09	-6.19	3.10		**9,10**	-1.98	-5.71	3.72

In the other hand, quinones yield really high E_{DEN} values (517-1882 $WhKg^{-1}$). The highest values are found on the smallest compounds 1,3-C4 (1610 $WhKg^{-1}$), 1,2-C(3+3) (1882 $WhKg^{-1}$), 1,3-C(3+5) (1660 $WhKg^{-1}$), 1,2(b)-C(4+4) (1608 $WhKg^{-1}$). Groups *n*,*m*-C(6+6+6) and *n*,*m*-C(7+7) are the largest molecules and, thus, show the lowest E_{DEN} values.

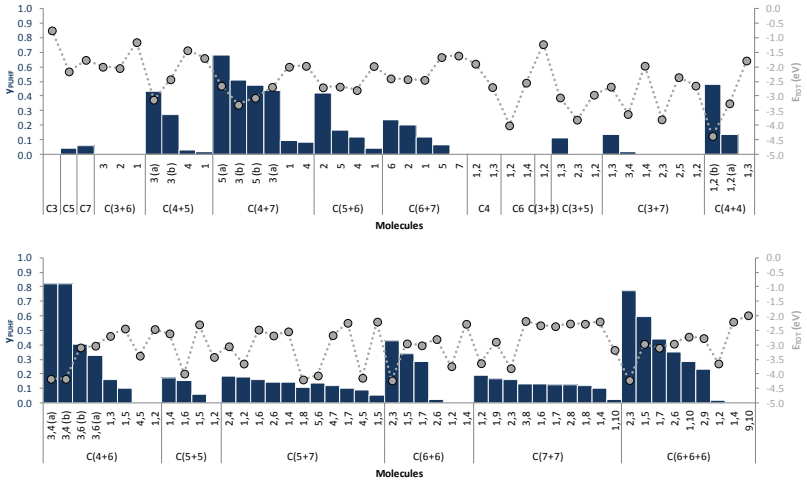

Figure 58. Total binding energy (dotted lines), in eV, of the lithiation process and diradical character (bars).

3.3. Summary and conclusions

In this section, the EAs, IPs, redox potentials and binding energies to Li^+ of a set of 90 conjugated carbonyls based on cyclic hydrocarbons have been studied and analyzed in terms of the diradical character and structural features. We have found that, in those families where several or all molecules show certain diradical character, this feature accomplishes larger EAs. Nevertheless, those molecules with closed-shell ground states may display large EAs too. With respect to the ionization potentials (IP), no clear tendency is observed related to the diradical nature of the molecules, although in some cases large values of y_0 correspond to small IPs.

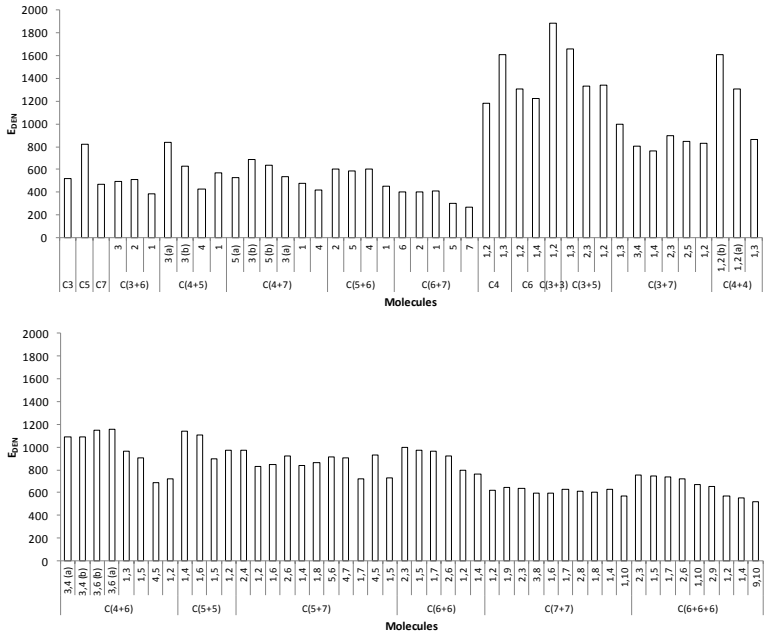

Figure 59: Energy density, in $WhKg^{-1}$.

Regarding E_R^1, we find the same trend as in the EAs, as expected, and molecules with large values of y_0 within particular family yield larger redox potentials. This behavior is clearly observed in C(4+5), C(4+7), C(6+7), C(4+4), C(4+6), C(5+5), C(6+6) and C(6+6+6), with few exceptions. Besides, some closed-shell molecules also display large redox potentials. Finally, we have observed that, for the monocarbonyls, the most relevant term is E_{RED} since E_{COORD} is very similar in all cases, while in dicarbonyls the most important feature is the relative position of the carbonyls. Thus, molecules with neighboring carbonyls show higher coordination energies, since Li^+ is located between both oxygen atoms. No clear relationship of E_{TOT} with the diradical

character is observed, because the coordination energy depends on the carbonyl anion. The E_{DEN} is greatly determined by the size of the molecule and the number of carbonyl groups. In that manner, higher E_{DEN} values are found on small dicarbonyl molecules, while large dicarbonyl systems show E_{DEN} values comparable to those of the monocarbonyls moieties.

As a summary, there are 35 molecules that show redox potentials greater than 3 V.

4. Effect of structural modifications

In this section, a systematic analysis is performed in order to elucidate how certain modifications on the molecular structure may affect the redox properties of a diradical molecule. The 1,5-C(6+6+6)/Q molecule has been previously selected due to its notable diradical character (y_0=0.60) and high symmetry, despite experimental data could not be found. However, data for similar derivatives are available.[204] Following the same scheme as in Chapter 4, the proposed structural modifications are: i) substitution of the oxygen of the carbonyl group, ii) inclusion of heteroatoms in the aromatic rings, iii) addition of substituents in different positions in the rings, iv) increase of the number of rings and v) inclusion of additional carbonyl moieties.

4.1. Substitution of the oxygen of the carbonyl group.

The oxygen atom will be replaced by atoms of the groups 13 to 16 of periods 1 (B, C, N), 2 (Al, Si, P, S) and 3 (Ga, Ge, As, Se), including the required H atoms to maintain the double bond conjugation. Further modifications have also been performed to include the following moieties: CF_2, CCl_2, CBr_2, $C(CH_3)_2$ and $C(CN)_2$.

Table 27: Electron affinities (EA) and ionization potentials (IP), in eV. First, second and two-electron reduction potentials (E_R^1, E_R^2, E_R) and oxidation potentials (E_O^1) vs Li/Li^+, in V. Theoretical capacity (C_{THEO}), in $mAhg^{-1}$, and energy density (E_{DEN}), in $Whkg^{-1}$.

		EA	IP	E_R^1	E_R^2	E_R	E_O^1	C_{THEO}	E_{DEN}
PERIOD1	BH	1.71	5.74	2.00	1.54	1.77	2.79	268	474
	CH_2	1.62	6.41	2.05	1.50	1.78	3.57	262	467
	NH	2.23	7.03	2.68	2.07	2.38	4.10	260	618
	O	2.84	7.69	3.27	2.55	2.91	4.65	257	750
PERIOD2	AlH	1.43	6.08	1.67	2.48	2.07	3.06	231	479
	SiH_2	1.89	6.36	2.28	2.84	2.56	3.46	227	580
	PH	2.18	6.85	2.57	2.43	2.50	3.97	223	558
	S	3.29	7.78	3.73	3.12	3.42	5.03	223	764
PERIOD3	GaH	1.64	6.12	1.94	2.59	2.27	2.69	169	382
	GeH2	2.10	6.39	2.48	3.05	2.77	3.50	165	456
	AsH	2.14	6.81	2.56	2.63	2.60	3.94	163	424
	Se	3.39	7.48	3.80	3.26	3.53	5.22	160	566
CH_2	CF_2	1.70	6.37	2.12	1.78	1.95	3.51	194	378
Deriv.	CCl_2	2.11	6.49	2.36	2.25	2.31	3.72	157	362
	CBr_2	2.20	6.46	2.44	1.90	2.17	3.74	103	224
	$C(CH3)_2$	1.38	5.79	1.79	1.16	1.48	3.21	206	304
	$C(CN)_2$	3.72	7.82	3.69	3.23	3.46	4.74	176	610

All the calculated redox data have been gathered on the **Table 27**, while E_R^1 and E_{DEN} have been represented in **Figure 60** and **Figure 61**.

It is observed that the substitution of the oxygen by atoms with smaller atomic number within the periods leads to

a diminution of the EA. Thus, the EA of 1,5-C(6+6+6)/Q is 2.84 eV, which is reduced to 1.71 eV when oxygen is replaced by boron. This trend is especially clear along the periods, while the variation along the groups is much smaller. The IPs follow the same trend, and the original value (7.69 eV) is greatly reduced in the boron derivative (5.74 eV). The introduction of the $C(CN)_2$ substituents lead to higher EA (3.72 eV) and IP (7.82 eV), while the other CX_2 groups show lower EAs and almost unchanged IPs.

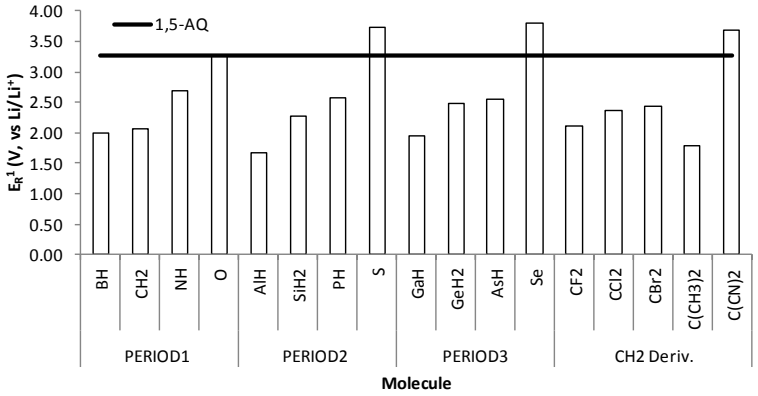

Figure 60: First reduction potential of the derivatives of 1,5-C(6+6+6)/Q.

As shown in **Figure 60**, these trends can also be found on the first reduction potentials. In that manner, is clearly shown that group 16 yields the highest E_R^1 values (up to 3.39 V), while the lowest values are found for group 13 (1.67 V on the aluminum derivative). Again, high E_R^1 is calculated for the $C(CN)_2$ derivative. For the first period elements, E_R^2 and E_R follow the trend B ≈ C < N < O, while the

in the second and third periods are found higher E_R^2 and E_R, as well as in the $C(CN)_2$ derivative.

E_{DEN} reaches its maximum on the S- and O-containing molecules (see **Figure 61**). The N- and Se-containing molecules yield also high E_{DEN} values, but the $C(CN)_2$ derivative must be highlighted, as it can be used to stabilize the open-shell structures.[187,188]

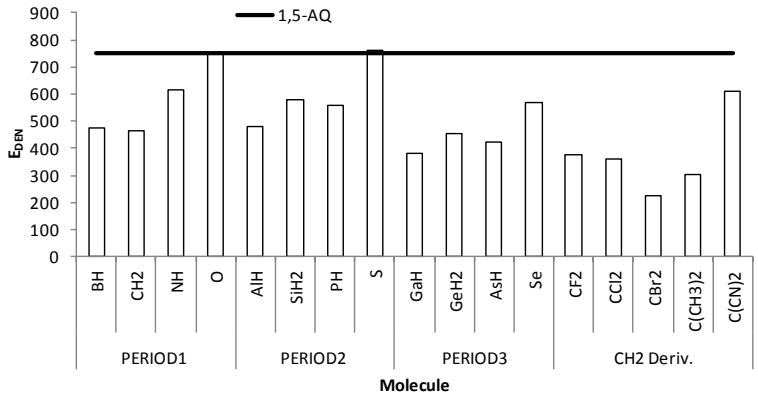

Figure 61: Energy density (E_{DEN}) of the studied molecules, in $Whkg^{-1}$.

Finally, the lithiation process is investigated in **Table 28.** There, two lithium atoms are considered, one for each substituent included in the molecule. Note that

Table 26 also deals with these magnitudes, but they are defined with only one lithium atom per molecule due to the presence of molecules with just one carbonyl group that, strictly speaking, are not quinones. The reduction energy (E_{RED}) is reduced following the trend BH > CH_2 > NH > O, showing that the better redox features are given by the

carbonyl group (O atom). However, this trend is not preserved in periods 2 and 3. At the same time, the reduction energy is decreased when descending in each group (B > Al > Ga, C > Si > Ge, N > P > As and O > S > Se). Therefore, the most favorable molecule would be the seleno derivative.

Table 28: Reduction (E_{RED}), coordination (E_{COORD}) and total energy (E_{TOT}) of the lithiation process, in eV.

		E_{RED}	E_{COORD}	E_{TOT}
PERIOD1	BH	11.81	-14.85	-3.04
	CH_2	11.55	-15.05	-3.50
	NH	10.52	-15.66	-5.14
	O	9.51	-15.17	-5.67
PERIOD2	AlH	10.51	-13.31	-2.81
	SiH_2	9.93	-13.98	-4.05
	PH	10.03	-14.23	-4.20
	S	8.39	-14.44	-6.05
PERIOD3	GaH	10.28	-13.56	-3.28
	GeH2	9.43	-13.80	-4.37
	AsH	9.98	-14.17	-4.19
	Se	8.12	-14.20	-6.08
CH_2 deriv.	CF_2	11.17	-14.43	-3.26
	CCl_2	10.05	-14.22	-4.17
	CBr_2	10.13	-15.04	-4.91
	$C(CH3)_2$	11.82	-14.69	-2.86
	$C(CN)_2$	7.01	-12.29	-5.28

The coordination energy, in general, is increased along the periods and decreased along the groups. Still, E_{TOT}, calculated as the sum of E_{RED} and E_{COORD}, shows almost the same trend as E_{RED}. In that manner, the selenium- and sulfur-containing molecules have the most negative E_{TOT}. Additionally, the substitution of the hydrogens of the methylene group leads to more favorable E_{TOT} for molecules containing heavier halogens. Despite E_{RED} of the cyano-containing molecule is the lowest, the steric effects yield an

E_{COORD} of only -12.29 eV. As a result, E_{TOT} is lower than the reference quinone structure.

In conclusion, the analyses performed in this subsection reveal that the molecules with better electrochemical features are the carbonyls (quinone) and the sulfur and selenium derivatives (C=S and C=Se). The reduction potentials are higher for S- and Se-containing molecules, and the energy density of the thiocarbonyl is even higher than that of the quinone, making these derivatives very promising candidates for the design of improved organic cathodes.

4.2. Insertion of heteroatoms in the aromatic rings

The carbon atoms of 1,5-C(6+6+6)/Q have been substituted by boron, nitrogen, silicon and potassium atoms in order to evaluate the effect that these changes may introduce in the redox features of the molecule depending on the site they are substituted, either α, β, γ or δ. In Chapter 4 was already noted that positions α and γ have higher spin density, as the unpaired electrons are majorly present in those positions. The electrochemical features are collected in **Table 29**. In **Figure 62** and **Figure 63** are represented the variation of E_R^1 and E_{DEN} with respect to the 1,5-C(6+6+6) molecule.

The N- and P-containing molecules show enhanced EAs, IPs and redox potentials (both oxidation and reduction), while these quantities are reduced in most of cases if B or Si

atoms are inserted. These analyses suggest that the nature of the heteroatom influences to a greater extent the redox features rather than the diradical character. However, it is also observable a trend for all these quantities, that shows that in α and γ positions the variations are larger than in β or δ, in agreement with the trend observed for the diradical character. To illustrate this, the E_R^1 of the molecule containing a nitrogen in α and γ position grows 0.55 V and 0.74 V, respectively, with respect to the reference molecule.

Table 29: Electron affinities (EA) and ionization potentials (IP), in eV. First, second and two-electron reduction potentials (E_R^1, E_R^2, E_R) and oxidation potentials (E_O^1) vs Li/Li^+, in V. Theoretical capacity (C_{THEO}), in $mAhg^{-1}$, and energy density (E_{DEN}), in $Whkg^{-1}$.

		EA	IP	E_R^1	E_R^2	E_R	E_O^1	C_{THEO}	E_{DEN}
1,5-AQ		2.84	7.69	3.27	2.55	2.91	4.65	257	750
α	**N**	3.50	8.53	3.82	3.12	3.47	5.32	255	886
	B	2.49	7.08	2.99	3.19	3.09	4.06	263	813
	P	3.30	7.70	3.58	3.00	3.29	4.61	220	722
	Si	2.58	6.88	2.78	2.57	2.68	3.86	223	597
β	**N**	3.31	8.26	3.64	2.90	3.27	5.02	255	834
	B	2.75	7.67	3.15	2.43	2.79	4.71	263	733
	P	3.42	7.96	3.64	2.98	3.31	4.87	220	727
	Si	2.90	7.54	3.15	2.56	2.86	4.62	223	637
γ	**N**	3.63	8.54	4.02	3.20	3.61	5.47	255	920
	B	1.47	6.70	2.02	1.56	1.79	3.73	263	470
	P	3.26	8.05	3.57	2.93	3.25	4.96	220	713
	Si	2.51	6.74	2.58	2.65	2.62	3.76	223	584
δ	**N**	3.14	8.14	3.60	2.89	3.25	5.07	255	828
	B	2.55	7.65	2.93	2.66	2.80	4.64	263	736
	P	3.13	7.68	3.47	2.76	3.12	4.70	220	684
	Si	2.61	7.31	2.83	2.20	2.51	4.36	223	561

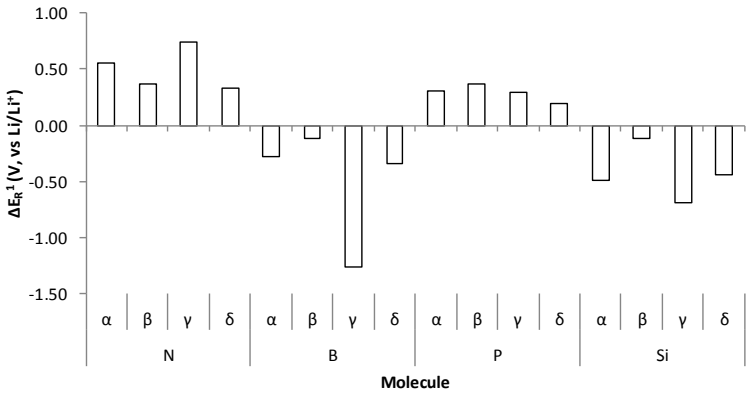

Figure 62: Variation of the first reduction potential after insertion of N, B, P and Si in α, β, γ and δ positions of the 1,5-C(6+6+6) molecule.

In the other hand, the introduction of N in β or δ positions results in an enhancement of only 0.37 and 0.33 V. This trend is not clearly shown for potassium, but the substitution of boron in γ results in the reduction of E_R^1 more than 1 V, while in α is only 0.28 V. Finally, the silicon atom reduces E_R^1 around half a volt in α, γ and δ positions.

The theoretical capacity obtained upon substitution is reduced with P or Si due to the larger size of these atoms. Thus, E_{DEN} of molecules with Si and P is lower than that of the original molecule, despite the P atom enhances the reduction potential. In the same way, boron induces higher C_{THEO} but lower E_R^1, so that E_{DEN} is reduced, except in case of the α-substituted isomer, that reaches higher E_R^1. In fact, in this case, it is observed $E_R^2 > E_R^1$, which represents an even behavior. Besides, the only molecules with positive ΔE_{DEN} are

those with the nitrogen atom, especially when the nitrogen is placed in α and γ.

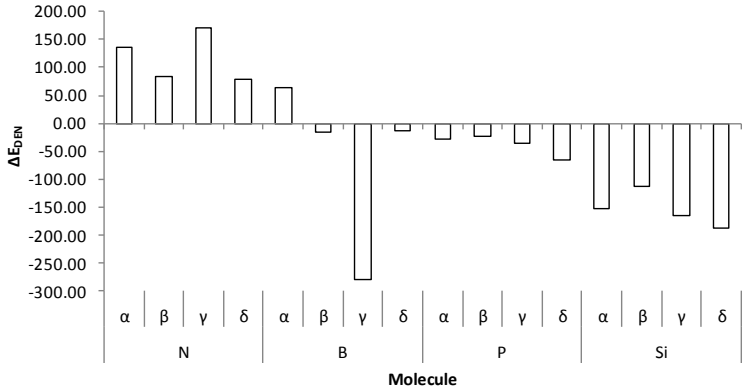

Figure 63: Variation of the energy density (E_{DEN}) after insertion of N, B, P and Si in α, β, γ and δ positions of the 1,5-C(6+6+6) molecule.

The effect of lithiation is collected in **Table 30**. According with the trends accounted for the EAs (and for the reduction potentials), the N- and P-substituted systems have higher reduction energies compared with the B or Si derivatives. Additionally, higher variations are accounted for in α and γ positions for N- and B-containing molecules, while for P and Si this trend is not clearly visible. Although the same tendencies of E_{RED} values can be observed, no clear trends are found for E_{COORD}. In that manner, it is observed that coordination energies suffer large, irregular variations depending on the heteroatoms substituted for each position.

Table 30: Reduction (E_{RED}), coordination (E_{COORD}) and total energy (E_{TOT}) of the lithiation process, in eV.

		E_{RED}	E_{COORD}	E_{TOT}
1,5-AQ		9.51	-15.17	-5.67
N	α	8.26	-16.30	-8.04
	β	8.65	-14.75	-6.10
	γ	8.11	-14.81	-6.70
	δ	8.95	-17.05	-8.11
B	α	11.41	-16.27	-4.85
	β	9.73	-14.92	-5.19
	γ	11.44	-16.34	-4.90
	δ	10.02	-15.46	-5.44
P	α	8.37	-14.73	-6.36
	β	8.23	-14.43	-6.20
	γ	8.52	-14.44	-5.92
	δ	8.89	-15.89	-7.00
Si	α	9.30	-14.13	-4.83
	β	9.14	-14.74	-5.60
	γ	9.38	-14.21	-4.83
	δ	9.85	-15.28	-5.43

Regarding E_{TOT}, it is found a shift to more negative values with respect the unsubstituted molecule when the heteroatoms inserted are N and P, in opposition to the values given by the B and Si substituents.

In conclusion, high reduction potentials are accounted for those systems that include nitrogen and potassium, in opposition to boron or silicon. However, the large size of the potassium atom diminishes the energy density of the system, and only the nitrogen atom provides energy densities higher than the unsubstituted 1,5-C(6+6+6) molecule.

4.3. Addition of substituents

In this subsection, the effect of six different substituents in the redox features of the 1,5-C(6+6+6)/Q

molecule has been studied, in the previously defined four positions labeled as α, β, γ, δ and the totally substituted molecule, labeled as ε. The following substituents have been tested: two strong EWG, CF_3 and CN, three strong EDG, OH, OCH_3 and NH_2, and one weak EDG group, CH_3. The calculation of the ε isomer including OH and OCH_3 substituents showed to be complicated to optimize due to the large number of possible conformations. Thus, these two molecules are omitted. In summary, the redox features of 30 different molecules have been investigated in this subsection.

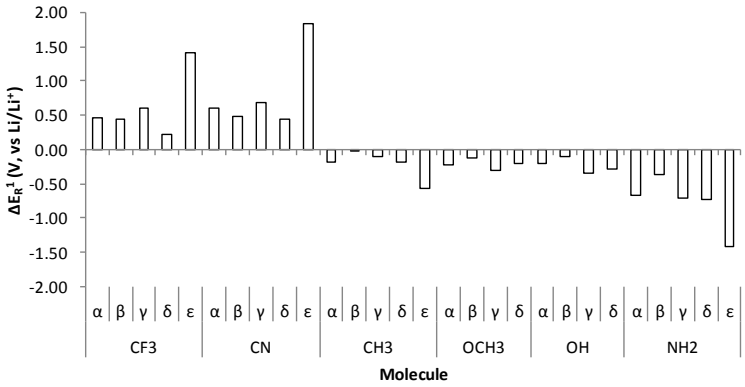

Figure 64: Variation of the first reduction potential after insertion of CF_3, CN, CH_3, OCH_3, OH and NH_2 groups in α, β, γ and δ positions of the 1,5-C(6+6+6) molecule. ε represents the fully substituted molecule.

As it was observed in the previous subsection, the nature of the substituent is more important in the variation of the redox properties than their position in the ring (see **Table 31**). The EWGs (CF_3 and CN) enhance the EAs, IPs, and redox potentials (E_R^1, E_R^2, E_R, E_O^1), while the opposite effect

is accounted for EDGs. Besides, the addition of more substituents (ε isomer) leads to a stronger enhancement (or reduction) of the properties following the trends pointed in the literature.[361]

Table 31: Electron affinities (EA) and ionization potentials (IP), in eV. First, second and two-electron reduction potentials (E_R^1, E_R^2, E_R) and oxidation potentials (E_O^1) vs Li/Li^+, in V. Theoretical capacity (C_{THEO}), in $mAhg^{-1}$, and energy density (E_{DEN}), in $Whkg^{-1}$.

		EA	IP	E_R^1	E_R^2	E_R	E_O^1	C_{THEO}	E_{DEN}
1,5-AQ		2.84	7.69	3.27	2.55	2.91	4.65	257	750
CF_3	**α**	3.63	8.29	3.74	3.03	3.39	5.14	156	527
	β	3.49	8.28	3.72	2.98	3.35	5.06	156	521
	γ	3.61	8.28	3.87	3.10	3.48	5.26	156	542
	δ	3.24	8.03	3.50	2.71	3.11	4.99	156	484
	ε	4.85	9.33	4.68	3.81	4.25	6.40	71	303
CN	**α**	3.88	8.38	3.88	3.22	3.55	5.18	208	736
	β	3.78	8.45	3.75	3.01	3.38	5.12	208	701
	γ	3.83	8.41	3.95	3.21	3.58	5.28	208	743
	δ	3.55	8.29	3.72	2.98	3.35	5.12	208	696
	ε	5.70	9.76	5.11	4.48	4.79	6.33	131	629
CH_3	**α**	2.67	7.29	3.10	2.35	2.72	4.42	227	618
	β	2.71	7.46	3.26	2.43	2.85	4.59	227	646
	γ	2.69	7.32	3.16	2.45	2.81	4.47	227	637
	δ	2.65	7.44	3.08	2.34	2.71	4.55	227	615
	ε	2.28	6.59	2.71	1.95	2.33	4.01	167	389
OCH_3	**α**	2.56	6.78	3.05	2.36	2.70	4.10	200	540
	β	2.66	7.40	3.15	2.44	2.80	4.67	200	559
	γ	2.38	6.74	2.96	2.35	2.65	4.07	200	530
	δ	2.57	7.24	3.07	2.33	2.70	4.48	200	540
OH	**α**	2.74	7.23	3.07	2.32	2.69	4.20	223	601
	β	2.81	7.61	3.17	2.49	2.83	4.65	223	631
	γ	2.45	6.99	2.92	2.31	2.61	4.03	223	583
	δ	2.66	7.52	2.99	2.24	2.61	4.50	223	583
NH_2	**α**	2.18	6.36	2.59	1.97	2.28	3.59	225	513
	β	2.53	7.14	2.91	2.29	2.60	4.40	225	586
	γ	2.17	6.41	2.56	2.01	2.29	3.49	225	515
	δ	2.15	7.37	2.54	1.92	2.23	4.50	225	502
	ε	1.52	5.54	1.85	1.43	1.64	2.99	163	267

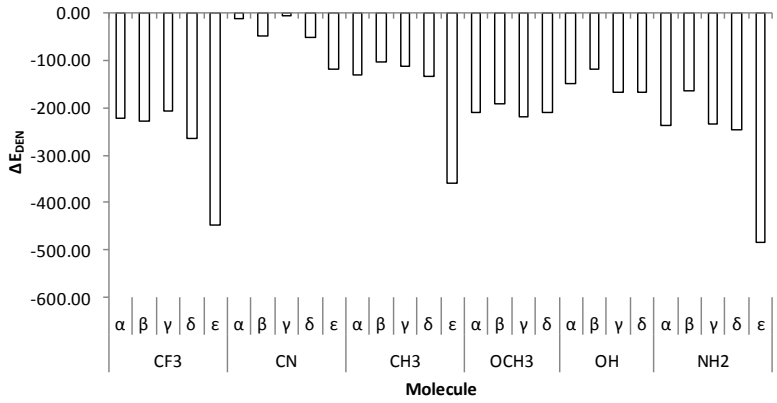

Figure 65: Variation of the energy density (E_{DEN}) after insertion of N, B, P and Si in α, β, γ and δ positions of the 1,5-C(6+6+6) molecule. ε represents the fully substituted molecule.

In **Figure 64** is represented the variation of the first reduction potential with respect to 1,5-C(6+6+6). EWG groups enhance E_R^1 (0.23-0.29 V for CF_3 and 0.45-0.68 V for CN). For the ε isomer, E_R^1 increases up to 2.01 and 2.87 V, respectively. In the other hand, the CH_3 group reduces E_R^1 between 0.01 and 0.19 V, while the reduction of the OCH_3 group fluctuates between 0.12 and 0.31 V. The OH group reduces the reduction potential between 0.10 and 0.36 V, and the NH_2 between 0.24 and 0.36 V. In summary, the strategical introduction of two substituents may vary the E_R^1 between 2.54 V (NH_2 in δ position) and 3.95 V (CN in γ position).

Similar behavior is recorded for the other parameters investigated. However, the increase of the redox potentials with EWG substituents is not enough to compensate the reduction of C_{THEO}, reducing also the value of E_{DEN} (see

Figure 65). Thus, the only substituent capable to keep E_{DEN} of the unsubstituted molecule is CN, while all the other substituents reduce the energy density more than 100 $WhKg^{-1}$. Nevertheless, in general the energy density fluctuate around 500-600 $WhKg^{-1}$, similar to the common LiCoO2 batteries.

Table 32: Reduction (E_{RED}), coordination (E_{COORD}) and total energy (E_{TOT}) of the lithiation process, in eV.

		E_{RED}	E_{COORD}	E_{TOT}
1,5-AQ		9.51	-15.17	-5.67
CF_3	α	7.71	-14.88	-7.18
	β	7.99	-14.25	-6.26
	γ	7.79	-14.51	-6.72
	δ	8.64	-15.63	-6.99
	ε	5.07	-13.45	-8.39
CN	α	7.14	-15.02	-7.88
	β	7.48	-13.91	-6.43
	γ	7.34	-14.21	-6.87
	δ	7.98	-15.91	-7.93
	ε	3.16	-12.87	-9.71
CH_3	α	9.70	-15.11	-5.41
	β	9.59	-15.16	-5.57
	γ	9.64	-15.18	-5.54
	δ	9.74	-15.18	-5.43
	ε	10.17	-13.64	-3.48
OCH_3	α	9.67	-15.97	-6.30
	β	9.69	-15.02	-5.33
	γ	10.08	-15.46	-5.38
	δ	9.79	-16.45	-6.66
OH	α	9.64	-14.74	-5.10
	β	9.44	-14.96	-5.53
	γ	10.09	-15.51	-5.42
	δ	9.83	-16.81	-6.97
NH_2	α	10.43	-16.06	-5.63
	β	9.91	-15.22	-5.31
	γ	10.27	-15.32	-5.05
	δ	10.64	-15.80	-5.16
	ε	11.40	-15.87	-4.46

In the reduction process, two lithium atoms can also be considered. In that manner, it is observed that the reduction energy behaves following the same trends that were observed for the reduction potentials, as expected (see **Table 32**). However, no clear trend is found regarding the variation in the coordination energy. In most cases, this variation is smaller than that in the reduction energy, leading to a E_{TOT} that follows, in general, the same trends as the reduction potentials. The exception is the δ isomer, which shows the most exoergic coordination energy, in such a way that the process is more favorable for those molecules containing EWG groups, in the following order: $\varepsilon > \alpha > \delta > \gamma > \beta$. In the other hand, EDG groups slightly disfavor this process by shifting E_{TOT} to more positive values. Nevertheless, only the ε configuration for the CH_3 and NH_2 substituted molecules enhances E_{TOT} to more positive values (>1 eV).

In summary, the inclusion of EWG groups yields to an enhancement of the reduction potential. However, large differences are accounted for depending on the position in the molecule. As expected, the ε isomers show larger modifications of the redox-related parameters, followed in most of the cases by the α and γ configurations. The coordination energy is enhanced for δ substitutions. Although both CH_3 and CN substituents can enhance the reduction potentials, the large size of those substituents reduce the energy density.

Table 33: Electron affinities (EA) and ionization potentials (IP), in eV. First, second and two-electron reduction potentials (E_R^1, E_R^2, E_R) and oxidation potentials (E_O^1) vs Li/Li^+, in V. Theoretical capacity (C_{THEO}), in $mAhg^{-1}$, and energy density (E_{DEN}), in $Whkg^{-1}$.

		EA	IP	E_R^1	E_R^2	E_R	E_O^1	C_{THEO}	E_{DEN}
1,2	**2**	2.12	8.59	2.91	1.83	2.37	5.50	339	803
	3	2.08	8.25	2.76	1.68	2.22	5.08	257	572
	4	2.09	7.57	2.70	1.49	2.09	4.55	208	434
	5	2.19	7.05	2.59	1.52	2.05	4.16	174	357
	6	2.42	6.66	2.54	1.73	2.13	3.88	150	319
1,4	**2**	2.09	9.34	2.80	1.76	2.28	6.11	339	773
	3	2.07	8.32	2.69	1.68	2.19	5.17	257	563
	4	2.08	7.54	2.65	1.54	2.10	4.55	208	435
	5	1.95	7.00	2.46	1.57	2.01	4.14	174	350
	6	2.10	6.60	2.54	1.60	2.07	3.84	150	310
1,5	**2**	2.71	8.48	3.34	2.46	2.90	5.26	339	983
	3	2.84	7.69	3.27	2.55	2.91	4.65	257	750
	4	2.88	7.21	3.16	2.59	2.87	4.31	208	596
	5	2.89	6.88	3.03	2.60	2.82	4.08	174	490
	6	2.88	6.62	2.95	2.61	2.78	3.90	150	416
1,7	**2**	2.69	8.63	3.32	2.43	2.87	5.33	339	973
	3	2.92	7.89	3.32	2.50	2.91	4.81	257	749
	4	2.97	7.41	3.21	2.55	2.88	4.46	208	598
	5	2.98	7.05	3.11	2.57	2.84	4.20	174	494
	6	2.97	6.78	3.01	2.58	2.79	4.00	150	418
2,3	**2**	2.75	8.24	3.44	2.46	2.95	4.89	339	1000
	3	2.79	7.68	3.27	2.65	2.96	4.56	257	763
	4	2.90	6.41	2.80	2.58	2.69	3.76	208	559
	5	2.80	7.12	3.16	2.50	2.83	4.21	174	492
	6	2.84	6.85	3.11	2.43	2.77	3.99	150	414
2,6	**2**	2.68	9.82	3.24	2.29	2.76	6.54	339	937
	3	2.93	8.29	3.25	2.44	2.84	5.20	257	732
	4	3.04	7.68	3.21	2.51	2.86	4.71	208	594
	5	3.07	7.26	3.15	2.54	2.85	4.36	174	495
	6	3.06	6.95	3.04	2.56	2.80	4.15	150	419

4.4. Increase of the number of fused rings

The naphthoquinone family of molecules (*n,m*-C(6+6)/Q) is selected to study the variations of the redox properties with the increase of the number of fused rings,

from naphthoquinone (n=2) to hexaquinone (n=6). Starting from naphthoquinone, six different relative positions of the carbonyls have been studied (1,4-, 1,2-, 1,5-, 1,7-, 2,3- and 2,6-), so a total of 30 molecules have been investigated. The calculated data are gathered on the **Table 33**.

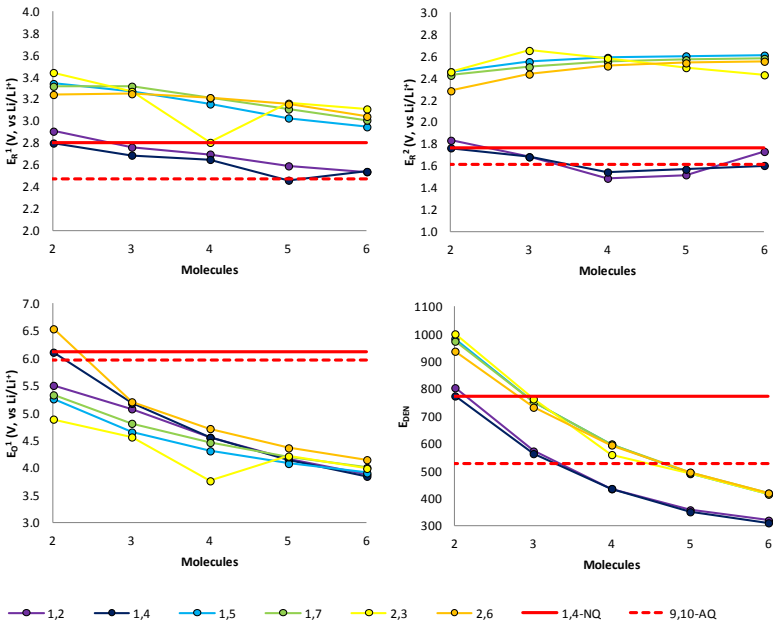

Figure 66: First and second reduction potentials (top left and right), first oxidation potential (bottom left), in V, and energy density (bottom right), in $Whkg^{-1}$, for the quinones with 2≤n≤6 number of fused rings. Straight and dotted red lines correspond to the reference values of 1,4-NQ and 9,10-AQ, respectively.

It is observed that the EAs in 1,2- and 1,4-quinones are considerably lower (about 2 eV). This effect can be related to the diradical character, as they have y_0 values close to zero. The other quinones investigated show EAs between

2.70 and 3.10 eV, approximately. In any case, it is observed a large dependence of the open-shell quinones with the molecular size, as higher EAs are accounted for larger molecules. The same is observed for the IPs.

In **Figure 66**, the variation of E_R^1 (top left), E_O^1 (bottom left), E_R^2 (top right) and E_{DEN} (bottom right) is represented. Same trends as in the EAs are observed for the reduction and oxidation potentials, increasing with the diradical character.

The resulting E_R (see **Table 33**) is almost constant for the open shell structures 1,2-, 1,4-, 1,5-, 1,7- and 2,3-, while they have maxima at n=3 (1,2-, 1,4-, 1,5- and 1,7-) and n=4 (2,3-). The closed-shell molecules show decreasing values for E_R until a minimum is reached at n=5. The resulting E_{DEN} (see **Figure 66,** bottom right) shows that the E_R of open-shell molecules is high enough to improve the energy density about 200 $Whkg^{-1}$ for the smaller quinones or 100 for the larger ones. In fact, some 1,2- and 1,4- quinones have lower E_{DEN} compared with larger open-shell molecules, as it happens when comparing 1,5-tetraquinone (596 $Whkg^{-1}$) and the 1,2-anthraquinone (572 $Whkg^{-1}$).

In **Table 34**, can be observed that E_{RED} of n=6 molecules are 1.84-2.42 eV lower than the n=2 molecules. This trend could be adequate for the design of future organic cathodes, but the coordination energy is also reduced with the enlargement of the system and in similar magnitude (2.30-

2.51 eV). In that manner, E_{TOT} remains almost unchanged upon the enlargement of the molecules.

Table 34: Reduction (E_{RED}), coordination (E_{COORD}) and total energy (E_{TOT}) of the lithiation process, in eV.

		E_{RED}	E_{COORD}	E_{TOT}
1,2	**2**	11.74	-17.95	-6.20
	3	11.43	-17.44	-6.00
	4	11.03	-16.94	-5.91
	5	10.34	-16.20	-5.86
	6	9.61	-15.44	-5.83
1,4	**2**	11.84	-16.45	-4.62
	3	11.53	-16.01	-4.48
	4	11.33	-15.74	-4.42
	5	10.45	-14.83	-4.39
	6	9.76	-14.13	-4.37
1,5	**2**	10.35	-16.02	-5.67
	3	9.51	-15.17	-5.67
	4	8.93	-14.53	-5.60
	5	8.52	-14.04	-5.52
	6	8.21	-13.66	-5.45
1,7	**2**	10.39	-16.00	-5.60
	3	9.43	-15.16	-5.73
	4	8.85	-14.52	-5.68
	5	8.43	-14.04	-5.61
	6	8.12	-13.65	-5.54
2,3	**2**	10.36	-17.51	-7.15
	3	9.57	-16.72	-7.15
	4	9.12	-16.12	-7.01
	5	8.79	-15.58	-6.80
	6	8.53	-15.20	-6.68
2,6	**2**	10.45	-15.95	-5.51
	3	9.43	-15.13	-5.70
	4	8.78	-14.51	-5.74
	5	8.34	-14.03	-5.69
	6	8.03	-13.65	-5.62

In summary, the size enlargement does not bring evident benefits for the design of a better cathode material, as long as the calculated E_R^1, E_R^2, E_R and E_{TOT} values show a slow variation. Moreover, the energy density diminishes as the molecular size grows.

4.5. Summary and conclusions

In this section we have analyzed the variation of the redox characteristics after structural modifications, such as substitution of the oxygen in the carbonyl group, insertion of heteroatoms in the aromatic rings, addition of substituents and increase of the number of fused rings.

It has been found that the reduction potentials are diminished with any replacement of the oxygen in all cases except for S or Se.

Heteroatoms were introduced in four different positions of the carbon backbone. In general, N- and P-containing molecules show higher reduction potentials (and lower E_{TOT} values). However, the energy density is increased only for N-substituted molecules.

When EWGs and EDGs are included into the 1,5-C(6+6+6)/Q moiety is observed that EWG-containing molecules show higher reduction potentials and lower E_{TOT} values, but lower E_{DEN} values are obtained anyway.

Finally, the augmentation of the carbon backbone decreases the reduction potentials (related with more positive E_{TOT} values).

As a summary, the following molecules can be highlighted:

- 1,5-C(6+6+6)/Q with the oxygen of the carbonyl substituted by S and Se.
- 1,5-C(6+6+6)/Q with N and P in α and γ positions

- 1,5-C(6+6+6)/Q with CF_3 and CN groups in α and γ positions

5. Other diradical structures

From the whole set of structures studied in Chapter 4, those carbonyl-containing molecules will be analyzed in this section using the calculated values of 9,10-C(6+6+6)/Q and 1,4-C(6+6)/Q molecules as a reference.

5.1. Croconate and squarate dyes

Although very few works have been focused in the redox behavior of the croconate derivatives, some interesting publications can be found in the literature dealing with this type of carbonyl molecule. For instance, Fabre et al.[377] characterized the redox states of the croconate blue, croconate violet, and croconate dianion, highlighting the large number of electron transfers. Analogously, Simard et al.[378] analyzed the effect of the inclusion of heteroatoms on the croconate derivatives together with their squarate-related molecules. They observed little changes on the first reduction potential as well as in the oxidation potential. Recently, Punzi et al.[379] synthesized and characterized (both theoretically and experimentally) a reduced number of indolenine-based croconates.

Table 35: Electron affinities (EA) and ionization potentials (IP), in eV. First, second and two-electron reduction potentials (E_R^1, E_R^2, E_R) and oxidation potentials (E_O^1) vs Li/Li^+, in V. Theoretical capacity (C_{THEO}), in $mAhg^{-1}$, and energy density (E_{DEN}), in $Whkg^{-1}$, for the studied croconates.

	EA	IP	E_R^1	E_R^2	E_R	E_O^1	C_{THEO}	E_{DEN}
1	3.08	6.98	3.26	2.36	2.81	4.42	147	414
2	2.33	5.99	2.72	1.87	2.29	3.67	153	351
3	2.57	5.99	2.85	2.08	2.46	3.59	140	345
4	2.66	6.01	2.93	2.18	2.56	3.63	113	288
5	2.36	5.78	2.55	1.83	2.19	3.53	127	279
6	2.32	7.18	2.68	1.77	2.23	4.43	183	409
7	2.46	6.80	2.76	1.81	2.28	4.28	137	312
8	2.56	6.49	2.76	1.83	2.30	4.09	109	250
9	2.65	7.57	2.86	1.92	2.39	4.61	182	435
10	2.64	7.10	2.88	1.91	2.39	4.50	136	325
11	3.55	7.48	3.87	2.93	3.40	4.94	168	573
12	2.17	5.82	2.52	1.82	2.17	3.57	97	210
13	2.32	6.00	2.58	1.89	2.24	3.75	107	239
14	2.13	5.86	2.51	1.78	2.15	3.63	124	266
15	2.04	5.65	2.40	1.74	2.07	3.60	109	226
16	2.31	5.87	2.53	1.68	2.10	3.58	111	233
17	2.41	6.05	2.66	1.77	2.21	3.80	118	262
18	2.24	6.00	2.64	2.05	2.35	3.65	149	349
19	2.06	5.83	2.60	1.86	2.23	3.59	130	289
20	2.44	6.02	2.76	2.07	2.42	3.65	121	291
21	2.93	6.69	3.20	2.51	2.86	4.20	130	371
22	2.63	6.47	2.93	2.18	2.56	4.06	141	360

The electrochemistry of squarates has been more extensively investigated due to their suitability for the construction of dye-sensitized solar cells.[380] For instance, Buschel et al.[381] have described the oxidation and reduction of three squarates and noted the limited stability of the obtained anion, while Chen et al.[382] compared the effect of the OH group on three squarates. There could be observed how the introduction of alcoxy groups reduced the reduction potential and enhanced the oxidation potential. A small

number of investigations deal with the practical application of the croconic acid as a cathode,[383,384] in general with modest results.

Table 36: Electron affinities (EA) and ionization potentials (IP), in eV. First, second and two-electron reduction potentials (E_R^1, E_R^2, E_R) and oxidation potentials (E_O^1) vs Li/Li^+, in V. Theoretical capacity (C_{THEO}), in $mAhg^{-1}$, and energy density (E_{DEN}), in $Whkg^{-1}$, for the studied squarates.

	EA	IP	E_R^1	E_R^2	E_R	E_O^1	C_{THEO}	E_{DEN}
1	2.48	6.88	2.70	1.71	2.21	4.36	159	352
2	1.82	5.95	2.23	1.21	1.72	3.58	166	286
3	2.15	5.96	2.45	1.52	1.99	3.52	151	300
4	2.27	5.97	2.55	1.64	2.10	3.55	120	251
5	1.86	5.72	2.09	1.23	1.66	3.44	137	226
6	1.24	7.09	1.61	0.93	1.27	4.27	203	258
7	1.55	6.75	1.83	0.86	1.34	4.19	147	198
8	1.84	6.44	1.91	1.10	1.50	4.01	115	174
9	1.60	7.50	1.80	1.05	1.43	4.47	201	287
10	1.76	7.02	1.97	1.07	1.52	4.40	146	222
11	3.16	7.19	3.48	2.45	2.96	4.54	185	547
12	1.60	5.74	2.03	1.11	1.57	3.47	102	160
13	1.74	5.91	2.10	1.11	1.60	3.66	113	182
14	1.55	5.77	1.98	1.03	1.51	3.54	133	200
15	1.45	5.56	1.92	1.05	1.48	3.49	115	171
16	1.66	5.82	1.97	0.85	1.41	3.47	117	165
17	1.76	5.98	2.05	1.05	1.55	3.65	126	196
18	1.71	5.93	2.15	1.36	1.75	3.53	161	283
19	1.51	5.74	2.06	1.30	1.68	3.53	139	235
20	1.93	5.97	2.26	1.46	1.86	3.58	129	240
21	2.06	6.55	2.37	1.38	1.87	4.14	139	261
22	1.91	6.37	2.30	1.40	1.85	4.02	152	281

Both reversible and irreversible reduction[381,382,385] and oxidation[382, 386 , 387] processes have been found on these molecules. Additionally, the redox behavior of the croconates has also been already described as a mechanism in which two successive monoelectronic transfers are involved.[377] High voltages have been found upon the reduction of these

molecules, that can reach values as high as -0.29 V vs Fc/Fc^+ (around 3.5 V vs Li/Li^+). Additionally, croconates have shown slightly higher reduction potentials (around 0.3 V) when compared with the corresponding squarate.[378]

In this subsection are investigated a total of 44 derivatives (22 for each backbone, squarate and croconate). As a result, several molecules are proposed as candidates for the design of an efficient energy storage device.

All the croconates studied (see **Table 35**) have an EA between 2.04 eV and 3.08 eV, except $\mathbf{R_{11}}$ (3.55 eV). The same feature has been noticed for squarates, in which the $\mathbf{R_{11}}$ substituent shows EA=3.16 eV, while the others fluctuate between 2.48 and 1.24 eV (see **Table 36**). In general, the squarates possess EAs about 0.4-1.0 eV lower than the croconates. Some trends can be identified in the rest of the molecules. For example, $\mathbf{R_2}$, $\mathbf{R_3}$ and $\mathbf{R_4}$ follow the same trend due to the heteroatom (O, S and Se). Additionally, molecules with substituents $\mathbf{R_6}$ to $\mathbf{R_{10}}$ show an increase in the EA with the size of the conjugated chain. The inclusion of nitrogen into the acene-like chain also enhances EA. Finally, low EAs are observed on thiophene-containing molecules ($\mathbf{R_{18}}$, $\mathbf{R_{19}}$, $\mathbf{R_{20}}$) as well as in molecules containing the indole group ($\mathbf{R_{12\text{-}17}}$).

Regarding the ionization potentials, both in the croconates and squarates, the $\mathbf{R_{11}}$ substituent shows an outstanding value, although high IPs are also found with the substituents linked by an amino group ($\mathbf{R_{6\text{-}10}}$). Besides the

OH-containing molecules (**R_{21-22}**) and **R_1** show IPs higher than 6.3 eV. The rest of substituents give low IPs.

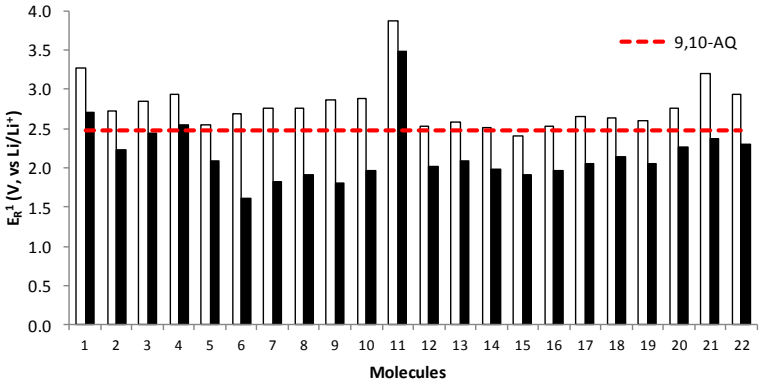

Figure 67: First reduction potential (E_R^1) for squarates (black bars) and croconates (white bars). The red line stands for the E_R^1 of 9,10-anthraquinone (2.48 V). Values in V vs Li/Li$^+$.

In the literature, very few data dealing with the IP and the EA of these systems are available. For example, squarates with experimental EAs around 3.2 eV and IPs around 4.7 eV could be found.[385] It must be noted that the oxidation on air may be a problem for those materials with IP below 5.2 eV, and IPs between 5.2 and 5.8 eV are typically wanted in photovoltaics. Nevertheless, the simple replacement of the substituent by a more (or less) electron-deficient group would reduce (or enhance) the IP value. Both squarates and croconates show IPs that could be interesting for matching the range 5.2-5.8 eV. Thus, **R_5**, **R_{12}**, **R_{14}**, **R_{15}** and **R_{19}** substituents give IPs inside (or near) this range.

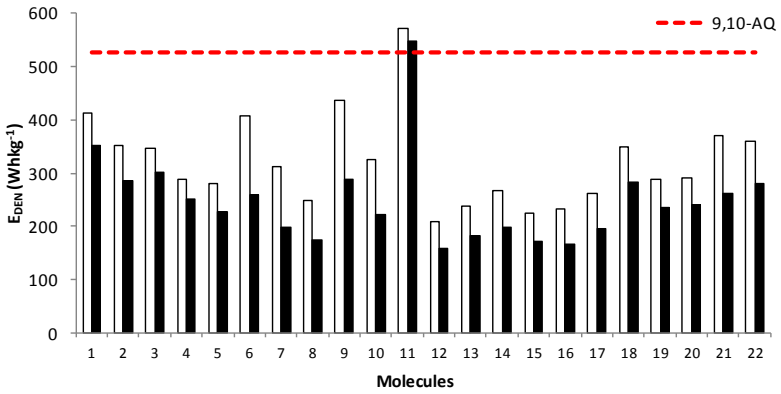

Figure 68: Energy density (E_{DEN}), in$Whkg^{-1}$, for squarates (black bars) and croconates (white bars). The red line stands for the value of 9,10-anthraquinone (526 $Whkg^{-1}$).

The trends noticed for EAs and IPs are transferable to E_R^1 and E_O^1. Thus, apart from the $\mathbf{R_{11}}$-containing molecules, the E_R^1 of squarates fluctuate between 1.61 and 2.70 V, while croconates vary between 3.26 and 2.40 V. Analogously, the E_O^1 of squarates fluctuate between 3.44 and 4.54 V, while the oxidation potentials of croconates fluctuate between 3.53 and 4.94 V. Again, the highest reduction potentials are found for croconates with $\mathbf{R_1}$, $\mathbf{R_{21}}$ and $\mathbf{R_{22}}$ substituents, as well as $\mathbf{R_3}$, $\mathbf{R_4}$, $\mathbf{R_9}$, $\mathbf{R_{10}}$ and $\mathbf{R_{11}}$, that can overcome a value of 2.8 V. These substituents on the squarate moiety also give the highest reduction potentials, but only overcome 2.26 V. All those features are more clearly shown on **Figure 67**. There is observed that only $\mathbf{R_{11}}$-containing molecules can overcome the first reduction potential of the 9-10-C(6+6+6)/Q. Both E_R^2 and E_R show the same trends as E_R^1.

Table 37: Electron affinities (EA) and ionization potentials (IP), in eV. First, second and two-electron reduction potentials (E_R^1, E_R^2, E_R) and oxidation potentials (E_O^1) vs Li/Li^+, in V. Theoretical capacity (C_{THEO}), in $mAhg^{-1}$, and energy density (E_{DEN}), in $Whkg^{-1}$, for the quinoidal thiophenes.

		EA	IP	E_R^1	E_R^2	E_R	E_O^1	C_{THEO}	E_{DEN}
A	1	3.62	9.28	3.62	2.81	3.22	5.86	255	820
	2	3.72	8.14	3.52	2.97	3.24	4.98	183	595
	3	3.78	7.45	3.47	3.05	3.26	4.47	143	467
	4	3.78	7.01	3.42	3.17	3.30	4.16	117	387
B	1	0.46	7.58	1.29	0.69	0.99	4.36	487	480
	2	1.35	6.57	1.86	1.15	1.50	3.70	279	419
	3	1.89	6.00	2.18	1.50	1.84	3.35	195	359
	4	2.12	5.76	2.25	1.75	2.00	3.27	150	301
C	1	3.20	8.82	3.19	2.48	2.84	5.57	227	644
	2	3.14	8.05	2.93	2.45	2.69	4.99	168	453
	3	3.07	7.51	2.75	2.39	2.57	4.62	134	344
	4	3.03	7.14	2.63	2.33	2.48	4.35	111	276
D	1	0.60	7.46	1.30	0.69	0.99	4.38	330	328
	2	1.11	6.85	1.54	1.02	1.28	4.06	246	315
	3	1.42	6.50	1.66	1.22	1.44	3.91	178	257
	4	1.63	6.27	1.73	1.35	1.54	3.82	140	216
E	1	3.13	7.48	3.27	2.69	2.98	4.57	201	600
	2	3.26	6.91	3.27	2.85	3.06	6.46	154	470
	3	3.30	6.58	3.20	2.97	3.09	3.96	124	384
	4	3.31	6.36	3.11	3.08	3.10	3.88	105	324
F	1	3.04	7.29	3.39	2.82	3.11	4.47	201	625
	2	3.19	6.79	3.34	2.96	3.15	6.07	154	485
	3	3.25	6.47	3.27	3.05	3.16	3.97	124	394
	4	3.27	6.27	3.19	3.10	3.15	3.89	105	329
G	1	1.41	5.54	1.69	0.89	1.29	2.95	204	264
	2	1.76	5.28	1.95	1.20	1.58	2.85	156	245
	3	1.94	5.17	2.01	1.52	1.77	2.85	126	222
	4	2.07	5.11	1.99	1.71	1.85	2.91	105	195
H	1	1.96	10.07	2.81	1.74	2.27	6.46	470	1067
	2	2.75	8.08	3.17	2.20	2.68	4.85	273	733
	3	2.83	7.34	2.99	2.46	2.72	4.38	193	524
	4	3.03	6.75	3.02	2.63	2.82	3.99	149	420
I	1	2.25	9.80	3.09	1.92	2.51	6.31	496	1244
	2	2.95	8.43	3.31	2.56	2.94	7.73	291	854
	3	3.24	7.47	3.40	2.88	3.14	6.89	206	647
	4	3.21	7.12	3.27	3.08	3.18	4.39	159	506

The energy density (E_{DEN}) is represented in **Figure 68**. It is observed that only $\mathbf{R_{11}}$ can overcome the E_{DEN} of the 9,10-anthraquinone, while the rest of the substituents give E_{DEN} values that are much smaller. However, the slightly higher size of the croconates is compensated by their higher reduction potentials, giving higher energy densities. In this group, no clear relationship of the EA, IP or the redox potentials with the y_0 has been observed, as in other systems.

In summary, the E_R^1 of the croconates (between 2.40 and 3.87 V) are higher than those of the squarates (between 1.61 and 3.48 V), while in any case the substituents that yield the highest potentials are $\mathbf{R_1}$, $\mathbf{R_3}$, $\mathbf{R_4}$, $\mathbf{R_9}$, $\mathbf{R_{10}}$, $\mathbf{R_{21}}$, $\mathbf{R_{22}}$ and, especially, $\mathbf{R_{11}}$. However, the energy density of these molecules is small due the large size of these systems. Similar E_O^1 are found in both groups of molecules, and values larger 4 V are found for substituents $\mathbf{R_1}$, $\mathbf{R_{6\text{-}11}}$ and $\mathbf{R_{21\text{-}22}}$.

5.2. Oligothiophenes

Quinoidal oligothiophenes have been widely investigated for their wide range of applications, related with their open-shell character, such as singlet fission[388] or non-linear optics.[241] In that manner, a large variety of quinoidal oligothiophenes have been synthesized and some information about their redox features is available. Thus, it is well known that they show high electron affinities[241, 389 ,390,391] and that the reduction takes place by two monoelectronic processes that can reach high values. [392] One example is the quinoidal

bithiophene, whose reduction potentials are E_R^1=-0.23 V and E_R^2=-0.52 V vs SCE,[243] which expressed in terms of Li/Li^+ might overcome 3.0 V, higher than other organic molecules broadly investigated as cathode materials, such as the aforementioned anthraquinone.[393,394]

In this subsection, the set of quinoidal oligothiophenes defined in Chapter 4 is investigated to unveil their redox behavior depending on the number of thiophenes as well as the nature of the terminal group.

Thiophenes containing the CN group have the highest EA values (**A** and **C**), see **Table 37***,* followed by carbonyl-containing quinoidal oligothiophenes (**E**, **F**, **H** and **I**), as expected. The remaining groups (**B**, **D** and **G**) are formed only by conjugated carbons. With the exception of group **C**, the addition of thiophene units results into the increase of the electron affinity. In some groups of the set, the EA of the n=4 structure is only by about 0.2 eV more than the n=1 (**A**, **E**, **F**), while groups **B**, **D**, **H** or **I** are strongly affected by the number of thiophene units. The calculated IPs (see **Table 37**) show large differences between different groups. In that manner, IPs of group **G** fluctuate between 5.11 and 5.24 eV, while in group **H** vary between 6.75 and 10.07 eV. Anyway, it is observed in all groups that the IP values decay from n=1 until n=4.

Figure 69 shows that the enlargement of the molecules leads to the diminution of the E_R^1 potentials in

groups **A**, **E** and **F**, while the first reduction potential of group **C** decays more rapidly. Those groups have the highest E_R^1 values, so that the pursuit of high reduction potentials in quinoidal oligothiophenes might be restricted to small chains of carbonyl- or cyano-containing molecules.

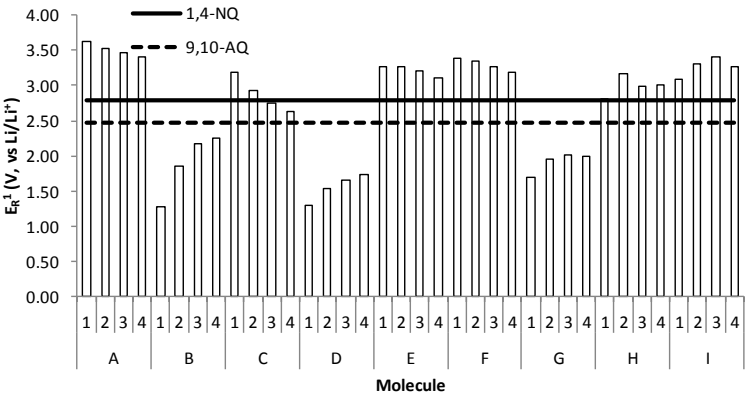

Figure 69: First reduction potential of the oligothiophenes (V, vs Li/Li^+).

The E_R^2 in groups **A**, **E** and **F** follows an increasing trend with the number of thiophenes, approaching the E_R^1 values. Inspecting the data in **Table 37**, $\mathbf{E_4}$ has E_R^1=3.11 V, while E_R^2 is only 0.02 V lower. This behavior has been experimentally observed.[242] Additionally, the reduction potentials calculated for the cyano and carbonyl derivatives agree well with the experimental data:[243] E_R^1=-0.12 and E_R^2=-0.21 V, vs SCE (calculated E_R^1=-0.16 and E_R^2=-0.74 V vs SCE) for $\mathbf{E_1}$; E_R^1=-0.32 and E_R^2=-0.52 V, vs SCE (calculated E_R^1=0.09 and E_R^2=-0.46 V vs SCE) for $\mathbf{A_2}$.

Thus, 19 of the studied molecules have E_R^1 higher than 3.00 V and, in 13 molecules, even the two-electron reduction is favored enough to yield E_R > 3.00 V, fundamentally in groups **A**, **E**, **F** and **I**.

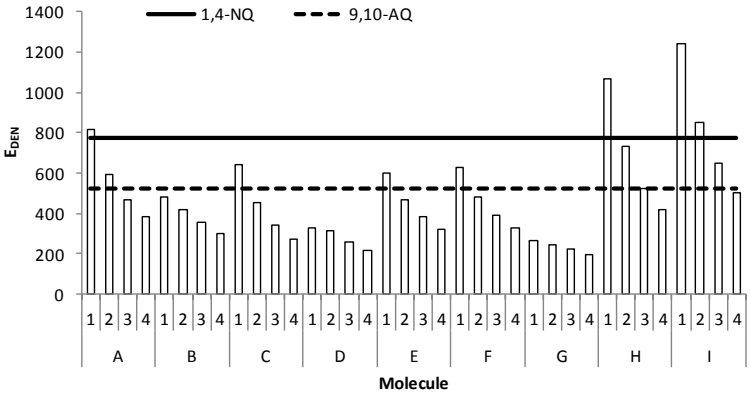

Figure 70: Energy density of the oligothiophenes studied ($WhKg^{-1}$).

The energy density of the n=1,3 molecules of groups **H** or **I** are equal or higher than that of the 9,10-anthraquinone (526 $WhKg^{-1}$), see **Figure 70**, as well as n=1,2 molecules of group **A** or n=1 of **C**, **E** and **F**. The E_{DEN} of $\mathbf{A_1}$, $\mathbf{H_1}$, $\mathbf{I_1}$, and $\mathbf{I_2}$ molecules is even higher than that of the 1,4-naphthoquinone (733 $WhKg^{-1}$). It should be noted that the molecules of group **I** are not thiophenes and are included as reference.

As done in Chapter 4, the sulfur atom of the thiophene has been substituted by oxygen, carbonyl group, selenium, carbon and nitrogen, see **Table 38**. Thus, the original thiophene molecule (**f**) shows the highest EA. The reduction potentials of the thiophene are also the highest of the set,

followed by **a**, **b** and **c** molecules. However, the energy density of **a** and **e** systems are more adequate, due to lower molecular weights.

Table 38: Electron affinities (EA) and ionization potentials (IP), in eV. First, second and two-electron reduction potentials (E_R^1, E_R^2, E_R) and oxidation potentials (E_O^1) vs Li/Li^+, in V. Theoretical capacity (C_{THEO}), in $mAhg^{-1}$, and energy density (E_{DEN}), in $Whkg^{-1}$.

	EA	IP	E_R^1	E_R^2	E_R	E_O^1	C_{THEO}	E_{DEN}
a	3.64	8.26	3.46	2.82	3.14	5.09	206	647
b	3.60	8.90	3.38	2.76	3.07	5.57	189	579
c	3.69	8.10	3.48	2.91	3.19	4.93	139	443
d	3.22	8.20	3.03	2.45	2.74	4.95	209	573
e	3.44	7.85	3.22	2.60	2.91	4.68	208	604
f	3.72	8.14	3.52	2.97	3.24	4.98	183	595

In summary, 13 molecules with $E_R^1 > 3.00$ V are found in this group. The largest value is accomplished by $\mathbf{A_1}$ (E_R^1=3.62 V). Such high reduction potentials lead to high energy densities for small-chain oligothiophenes, but it suffers a fast decay with the enhancement of the molecular weight.

5.3. Aromatic diimides

Among the large number of organic materials that have been proposed during the last decades, diimides are one of the most promising carbonyl materials for the consecution of an efficient and cheap battery cathode material. Several reviews have been published describing these molecules as feasible cathode materials.[56,393, 395 , 396] Besides, great efforts have been focused to enhance the loss

of capacity due to the dissolution of the cathode into the electrolyte,[397,398,399] via polymerization of the diimide units[253] or adsorption into 2D surfaces, among others.[400,401]

Table 39: Electron affinities (EA) and ionization potentials (IP), in eV. First, second and two-electron reduction potentials (E_R^1, E_R^2, E_R) and oxidation potentials (E_O^1) vs Li/Li^+, in V. Theoretical capacity (C_{THEO}), in $mAhg^{-1}$, and energy density (E_{DEN}), in $Whkg^{-1}$, for the diimides.

	EA	IP	E_R^1	E_R^2	E_R	E_O^1	C_{THEO}	E_{DEN}
1	2.37	9.75	2.68	1.87	2.28	6.75	248	565
2	2.14	8.97	2.76	1.60	2.18	5.19	201	439
3	2.27	8.11	2.30	1.49	1.90	4.94	169	322
4	2.25	9.33	2.64	1.78	2.21	6.18	220	485
5	2.31	9.57	2.66	1.82	2.24	6.37	233	522
6	2.42	8.42	2.65	1.78	2.21	5.43	183	406
7	2.71	9.06	2.90	2.26	2.58	5.77	201	520
8	2.64	8.94	2.87	2.20	2.54	5.75	191	485
9	2.67	8.65	2.85	2.14	2.50	5.71	157	391
10	2.89	8.21	3.02	2.42	2.72	5.16	169	461
11	3.19	7.63	3.34	2.65	2.99	4.78	146	438
12	3.26	7.23	3.37	2.76	3.07	4.48	129	395
13	3.48	8.00	3.55	2.75	3.15	5.25	102	321
14	3.10	7.21	3.12	2.46	2.79	4.64	113	315
15	3.80	7.76	3.55	3.25	3.40	5.02	120	406
16	2.11	8.86	2.20	1.76	1.98	5.64	183	363
17	2.39	9.20	2.39	1.78	2.08	6.23	167	349
18	3.28	7.39	3.23	2.45	2.84	7.11	137	390
19	3.23	7.16	3.09	2.63	2.86	4.26	122	348
20	3.30	6.83	3.07	2.69	2.88	4.04	109	315
21	3.31	6.63	3.02	2.71	2.87	3.92	99	284

The redox processes involved in those systems are mostly reversible, and proofs of reductions in a two-electron step as well as in two consecutive monoelectronic processes can be found in the literature,[253,402,403] while the most usual is the successive formation of the anion and the dianion.

Although it could be expected, the formation of the tetraanion moiety has not been proved as the main mechanism.[395] However, some examples can be found of imides that may be reduced more than the number of carbonyl groups present in the structure,[404 405] leading to higher theoretical capacities. Additionally, experimental works show that electrowithdrawing substituents such as CN have the ability to enhance the reduction potentials while the electrodonating moieties yield the opposite behavior.[397] Such modifications, as the polymerization of the diimide units, might influence the cyclability of an eventual battery.[397,253]

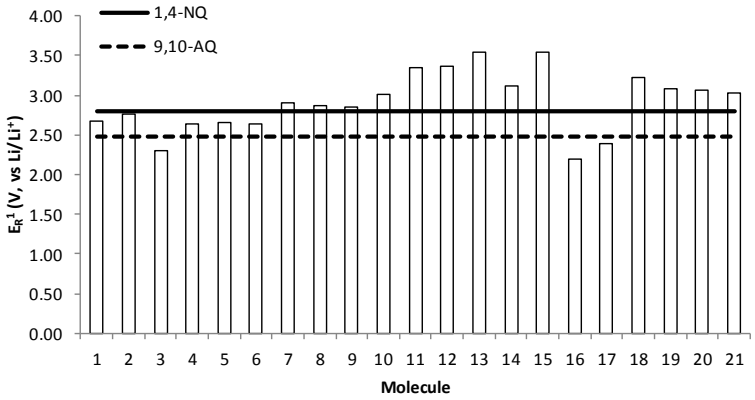

Figure 71: First reduction potential of the diimides (V, vs Li/Li$^+$).

Few experimental or theoretical data regarding EAs or IPs can be found in the literature. Thus, oligorylenes have been theoretically predicted to show values of EA=2.27 eV and IP=8.72 eV for the naphthalene diimide, and EA=2.57 eV and IP=7.42 eV for the perylene diimide.[260] These data agree quite well with the values obtained in this thesis, see **Table**

39. The diradical character seems to be related with both EAs and IPs, while large IPs and low EAs are found on closed-shell molecules (**1**-**6**, **16**-**17**), while open-shell ground state molecules have low IPs and high EAs (**10**-**15**, **18**-**21**). In that manner, EAs fluctuate between 2.11 and 3.80 eV while IPs vary between 6.63 and 9.75 eV.

Table 40: Theoretical and experimental E_1 and E_2 values for selected diimides (V, vs Fc/Fc^+). Experimental data from Ref. 255, 406, 407, 408, and 409.

	E_1^{CALC}	E_2^{CALC}	E_1^{EXP}	E_2^{EXP}
7	-0.84	-1.49	-0.99	-1.41
10	-0.73	-1.33	-1.02	-1.39
11	-0.41	-1.10	-0.74	-1.08
12	-0.37	-0.99	-0.68	-1.00
13	-0.20	-1.00	-0.60	-0.96
18	-0.52	-1.30	-0.68	-0.91
20	-0.68	-1.06	-0.65	-0.69

The reduction potentials are greatly affected by the behavior of the EA, and the same trends can be observed in both E_R^1 and E_R^2 (see **Figure 71**). In that manner, the calculated E_R^1 values vary between 2.20 V and 3.55 V, and E_R^2 ranges between 1.49 V and 3.25 V. This is a broad range of potentials, that can be even wider considering the possibility of adding electro-withdrawing or electro-donating substituents, as it has been previously described. This effect has been already observed on naphthalene diimides, and the first redox potential of molecule **7** substituted with four donor

amine groups is -1.85 V, while four sulfone groups enhance the redox potential to -0.36 V vs ferrocene electrode.[410,411,412]

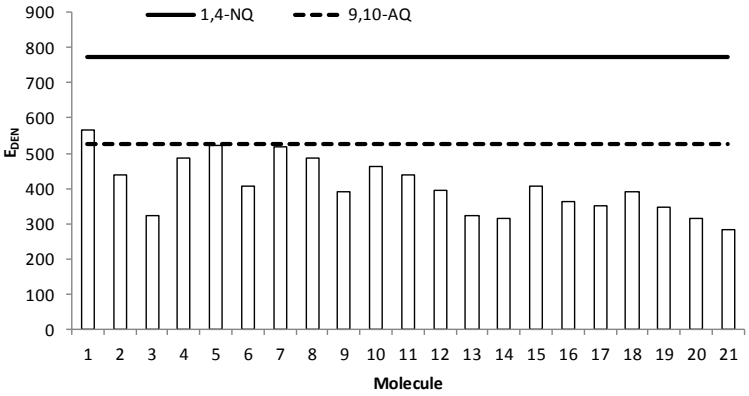

Figure 72: Energy density of the diimides studied ($WhKg^{-1}$).

Experimental reduction potentials (vs Fc/Fc^{+}) have been found in the literature that compare well with the calculated data (see **Table 40**). Thus, MAEs of 0.24 and 0.14 V for first and second reduction potentials are obtained, respectively, suggesting that the chosen methodology is appropriate for this kind of molecules. High reduction potentials are found for molecules with large y_0. For instance, those molecules with $y_0 \leq 0.15$ have E_R^1 between 2.20 and 2.90 V, while the rest of the diimides fluctuate between 3.02 and 3.55 V. The highest E_R^1 have been found on molecules **13** and **15**, both with large diradical character. A total of 13 molecules have an E_R^1 higher than the 1,4-naphthoquinone molecule, while up to ten overcome 3.00 V. The E_R^2 and E_R systems show the same trends as the first reduction potentials. Nevertheless, small E_{DEN} are calculated for these

systems, in general (see **Figure 72**). Thus, only molecules **1**, **5** and **7** surpass or almost reach the E_{DEN} of 9,10-C(6+6+6).

Table 41: Electron affinities (EA) and ionization potentials (IP), in eV. First, second and two-electron reduction potentials (E_R^1, E_R^2, E_R) and oxidation potentials (E_O^1) vs Li/Li^+, in V. Theoretical capacity (C_{THEO}), in $mAhg^{-1}$, and energy density (E_{DEN}), in $Whkg^{-1}$, for the indigo derivatives.

	EA	IP	E_R^1	E_R^2	E_R	E_O^1	C_{THEO}	E_{DEN}
1	2.03	7.05	2.52	1.67	2.10	4.17	204	428
2	1.94	6.70	2.50	1.67	2.09	4.03	185	385
3	2.44	6.87	2.59	2.47	2.53	4.10	182	461
4	2.18	7.97	2.78	1.90	2.34	5.17	203	474
5	2.26	7.52	2.82	1.97	2.39	4.75	181	433
6	2.25	7.40	2.79	1.95	2.37	4.64	137	326
7	2.46	8.04	2.93	2.25	2.59	5.38	210	543
8	1.10	8.27	1.60	2.62	2.11	5.55	206	435
9	2.75	7.07	3.25	2.61	2.93	4.30	182	533
10	1.12	6.01	1.49	0.67	1.08	3.18	208	225
11	1.51	6.48	1.97	1.18	1.57	3.70	206	324
12	3.54	7.24	3.54	3.18	3.36	3.99	150	503
13	2.72	6.26	2.92	2.50	2.71	3.51	150	406
14	3.01	7.39	3.19	2.48	2.83	4.43	173	490
15	2.84	6.85	3.09	2.66	2.88	3.94	204	588
16	2.77	6.89	3.21	2.37	2.79	4.08	204	570
17	1.83	7.11	2.39	2.66	2.53	4.09	204	516
18	2.00	7.24	2.52	1.65	2.08	4.41	204	426
19	1.64	7.34	1.96	1.41	1.68	4.39	204	344
20	1.76	7.27	2.21	1.47	1.84	4.22	204	375
21	1.77	7.44	2.23	1.58	1.90	4.49	204	389
22	2.04	7.36	2.57	1.93	2.25	4.56	204	459
23	0.96	7.28	1.60	1.55	1.57	4.42	204	321
24	1.77	7.75	2.52	1.58	2.05	4.54	331	678
25	1.99	6.66	2.53	1.66	2.09	3.92	186	390
26	2.60	7.09	2.96	2.18	2.57	4.28	204	525
27	1.48	6.73	2.04	1.63	1.83	4.04	164	301
28	1.72	6.60	2.17	1.28	1.73	3.70	206	356
29	2.42	6.28	2.69	1.96	2.32	3.93	98	229
30	2.19	6.23	2.57	2.27	2.42	3.96	98	239
31	2.55	7.03	2.86	1.94	2.40	4.36	121	290
32	2.16	7.34	2.47	1.84	2.15	4.57	173	372
33	1.97	6.90	2.36	1.58	1.97	4.15	143	282

In summary, high reduction potentials are found for molecules with large y_0. Ten molecules show E_R^1> 3.00 V (**11-15** and **18-21**), that reach 3.55 V in case of **13** and **15**. However, the big size of these molecules reduces the energy density.

5.4. Indigo-based chromophores

As the aromatic diimides, indigo derivatives have also been widely investigated. In fact, the addition of two sulfonate groups in the benzene-like rings leads to the molecule popularly known as indigo carmine, that has been used satisfactorily to design Li-ion and Na-ion batteries (2.2 vs Li/Li^+ and 1.8 vs Na/Na^+, respectively), [413] in which two electrons are transferred. Both lithium and sodium batteries showed high stability, good cycle stability and poor solubility in common organic solvents. For that reason, indigoid molecules have been included in many reviews together with other promising organic molecules in energy storage.[56,404,395,414.]

Nevertheless, the theoretical capacity of the indigo molecule is not high compared to other carbonyl compounds as anthraquinone (204 vs 257 $mAhg^{-1}$, respectively) and the addition of sulfonate groups leads to a real capacity of around 100 $mAhg^{-1}$.[413] The diversity of indigo-like molecules might help the pursuit of a promising cathode material and, thus, in this subsection a group of molecules based on experimentally known derivatives of indigo is analyzed.

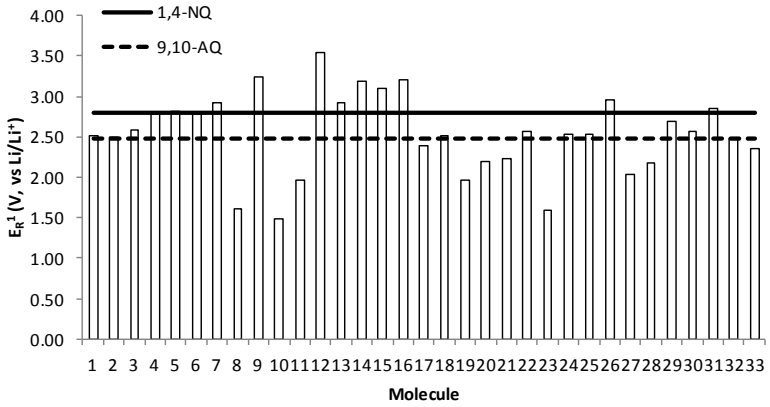

Figure 73: First reduction potential of the indigo-like molecules (V, vs Li/Li$^+$).

In **Table 41** is observed a large range of electron affinities. Thus, values from 0.96 to 3.54 eV have been obtained, while the EA of the original indigo molecule (**1**) is 2.03 eV. Most of the molecules show slight variations of this value, but some structural modifications show quite large changes into their electrochemical features. For instance, the introduction of OH functional group (**3**) enhances the EA more than 0.40 eV, while the substitution of the carbonyl oxygen by sulfur or the substitution of the nitrogen by boron has similar effects, in agreement with the findings gathered on sections 4.2 and 4.3 of this chapter. Molecules **12**-**16** also show much higher EAs than **1**, in some cases due to the presence of CN and OH groups (**12**, **14**, **16**), as well as the presence of fulvene moieties and the translation of the carbonyl groups (**13** and **15**). Molecules **26** and **31** also have EAs about 0.5 eV higher than **1**. In the other hand, substitution of any of the functional groups by carbon or nitrogen leads to the reduction

of the electron affinity (**8**, **10**, **11**). Additionally, despite the structural similitude, molecule **23** shows an EA 1.07 eV lower than **1**, while the substitution of the five-membered ring by a six-membered ring leads to a diminution of 0.57 on the EA.

These variations can be approximately translated to the reduction potentials (see **Figure 73**), since lower values are accounted for molecules **10** and **11**, and higher reduction potentials are found in molecules **12**-**16**, as well as in **5**, **7**, **9**, **26** and **31**, all of them with first redox potential higher than that of 1,4-naphthoquinone. It is still unclear if the experimental reduction of the indigo derivatives occurs in one (E_R) or two steps (E_R^1 and E_R^2). In fact, the experimental value of the reduction is 2.2 V, but this value could match both E_R^1 (2.52 V) and E_R (2.10 V). Both E_R and E_R^2 follow the same trend than E_R^1. In fact, the highest E_R^2 has been found on molecule **12**, which is as high as 3.36 V.

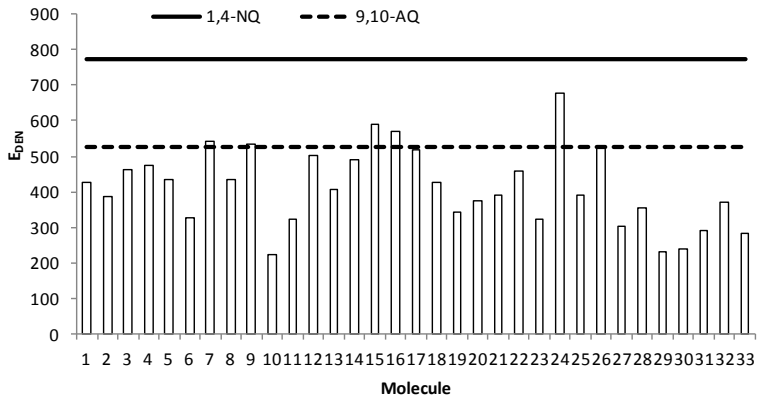

Figure 74: Energy density of the diimines studied ($WhKg^{-1}$).

The ionization potentials of these molecules have been also calculated and much smaller variations have been accounted, from 6.01 eV in molecule **10** to 8.27 eV in molecule **8**. Those values are related with oxidation potentials of 3.18 V and 5.55 V respectively. The experimental oxidation potential of **1** is 0.67 vs Fc/Fc^+, agreeing well with the calculated value of 4.17 V vs Li/Li^+ (0.43 vs Fc/Fc^+).

Table 42: Electron affinities (EA) and ionization potentials (IP), in eV. First, second and two-electron reduction potentials (E_R^1, E_R^2, E_R) and oxidation potentials (E_O^1) vs Li/Li^+, in V. Theoretical capacity (C_{THEO}), in $mAhg^{-1}$, and energy density (E_{DEN}), in $Whkg^{-1}$, for other carbonyl-containing chromophores.

	EA	IP	E_R^1	E_R^2	E_R	E_O^1	C_{THEO}	E_{DEN}
1	1.55	7.01	1.94	1.28	1.61	4.16	172	277
2	1.94	6.24	2.13	1.63	1.88	3.80	110	207
3	2.73	7.55	2.86	2.26	2.56	4.95	130	333
4	1.71	6.73	2.08	1.27	1.68	4.11	169	284
5	3.21	6.23	2.78	2.65	2.71	3.71	128	348
6	3.03	8.46	3.11	2.52	2.82	5.40	146	411
7	1.76	6.02	2.20	1.27	1.73	3.64	115	200
8	2.50	6.62	2.49	1.88	2.18	3.91	162	354
9	3.14	6.61	2.99	2.36	2.67	4.17	98	262
10	2.66	7.75	2.88	2.20	2.54	4.97	115	294
11	3.00	7.51	3.06	2.49	2.77	4.79	113	313
12	2.36	7.69	2.68	2.07	2.38	4.96	161	383
13	2.46	7.41	2.65	2.12	2.39	4.75	132	315
14	2.78	7.83	2.96	2.41	2.68	5.16	131	352
15	2.65	6.88	2.73	2.30	2.52	4.33	117	295
16	2.59	6.93	2.71	2.18	2.44	4.32	120	293
17	2.65	6.86	2.75	2.31	2.53	4.30	117	297

High energy densities are found in molecules with high reduction potentials (**7**, **9**, **12**, **13**, **16**), see **Figure 74**. However, small-sized molecules also show high energy densities, as molecule **24**.

In summary, 10 molecules have E_R^1 higher than the 1,4-naphthoquinone, but most of them are too large to keep a low value for E_{DEN}.

5.5. Other carbonyl-containing chromophores

During decades, the redox features of small dye molecules like indigo have been investigated.[415] However, less research efforts have been devoted to the investigation of the redox features of larger pigments.[416] Thus, this subsection is devoted to study a set of 17 well-known larger pigments.

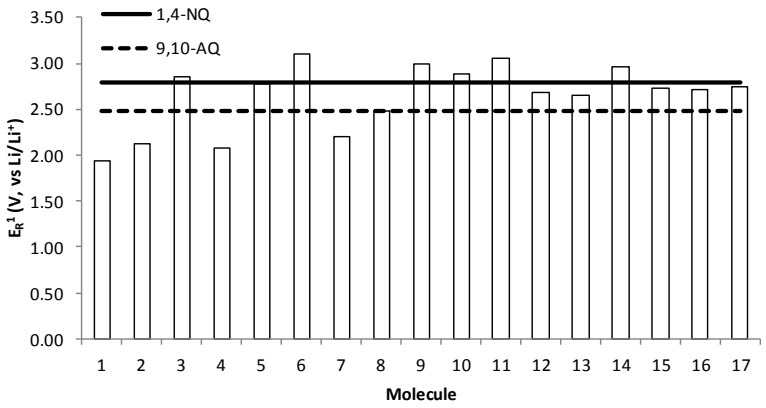

Figure 75: First reduction potential of the cromophores studied (V, vs Li/Li^+)

The EAs fluctuate between 1.55 and 2.51 eV, and only molecules **1**, **2**, **4**, and **7** have EAs lower than 2.00 eV, while molecules **5**, **6**, **9** and **11** have EAs above 3.00 eV (see **Table 42**). The large value calculated for molecule **5** (3.21 eV) is

ascribed to the presence of six carbonyl groups instead of two.

All molecules show reduction potentials (E_R) higher than **1** (see **Table 42** and **Figure 75**), that should result in a better battery performance than indigo if it is assumed that the reduction process includes only a single two-electron step (E_R=2.10 V). Anyway, up to six molecules show higher E_R^1 than the 1,4-naphthoquinone, namely **3**, **6**, **9**-**11** and **14**. For molecule **9**, a comparison with experimental data can be performed. In that manner, the calculated values vs SCE are: E_R^1=-0.44 V, E_R^2=-1.07 V and E_O=-0.76 V, in good agreement with the experimental values (E_R^1=-0.42 V, E_R^2=-0.55 V and E_O^1=1.04 V),[417] except for the rather large deviation observed in E_O.

Some comparisons with previously studied molecules can also be performed. For instance, molecule **2** shares the basic backbone with 1,5-C(6+6+6)/Q and the addition of extra benzene-like rings seems to negatively affect the performance as organic cathode. Thus, the original E_R^1 is reduced from 3.27 V to 2.13 V, analogously as it happens with E_R and E_R^2. At the same time, molecule **3** can be considered as a derivative of the aromatic diimide labeled as **7**, and small differences are observed. The only difference to note is the variation of E_O from 4.95 V to 5.77 V. Analogously, molecule **9** can be compared with the oligothiophene labeled as **E_2**. Slightly lower redox potentials are found for molecule **9**. For instance, the E_R^1 is reduced from 2.85 V to 2.36 V, and

the E_O is lowered from 6.46 V to 4.17 V. All these features, added to the fact that these three molecules (**2**, **3** and **9**) are bigger than their counterparts, will reduce their efficiency in the field of energy storage.

Molecules **13** and **14** can be compared as they are only differentiated by the substitution of two nitrogens into the structure. This modification leads to slightly higher reduction potentials, as it is observed in the pair of molecules **16** and **17**. This finding agrees with previous calculations, in which the substitution of nitrogen into the aromatic structure leads to higher reduction potentials.

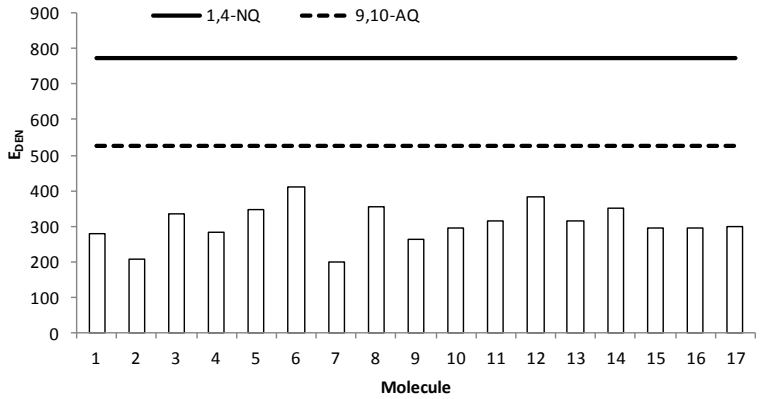

Figure 76: Energy density of the carbonyl-containing chromophores ($WhKg^{-1}$).

Due to the large size of these molecules, the high positive value of the reduction potentials cannot mantain a high energy density (see **Figure 76**). While the indigo molecule has an energy density of 428 $WhKg^{-1}$, none of these

selected five molecules have an energy density more than 411 $WhKg^{-1}$.

Summarizing, adequate reduction potentials have been found for all molecules (E_R^1 around 2.7 V) although the large molecular weights yield low energy density values.

5.6. Carbazoloquinones

Seven quinoidal derivatives of the carbazole molecule have been included in the present subsection, three 1,2-benzoquinone derivatives (1,2-, 2,3- and 3,4-carbazoloquinone), one 1,4-benzoquinone derivative (1,4-carbazoloquinone), and three diphenoquinone derivatives (2,5-, 2,7- and 4,5-carbazoloquinone), that can be compared with the molecule labeled as **I_2** from the subsection devoted to the oligothiophenes.

Table 43: Electron affinities (EA) and ionization potentials (IP), in eV. First, second and two-electron reduction potentials (E_R^1, E_R^2, E_R) and oxidation potentials (E_O^1) vs Li/Li^+, in V. Theoretical capacity (C_{THEO}), in $mAhg^{-1}$, and energy density (E_{DEN}), in $Whkg^{-1}$, for carbazoloquinones.

	EA	IP	E_R^1	E_R^2	E_R	E_O^1	C_{THEO}	E_{DEN}
CARB.	-0.14	7.45	0.56	1.26	0.91	4.37	321	291
1,2	2.23	7.95	2.94	1.81	2.38	4.73	272	646
2,3	2.26	7.84	2.98	1.89	2.44	4.59	272	662
3,4	2.09	7.95	2.83	1.71	2.27	4.79	272	616
1,4	2.18	8.22	2.84	1.75	2.30	5.01	272	624
2,5	2.81	7.70	3.36	2.47	2.92	4.49	272	792
2,7	2.77	8.16	3.20	2.35	2.78	4.93	272	755
4,5	2.63	7.42	3.29	2.49	2.89	4.32	272	786

The 1,2 and 1,4-benzoquinone derivatives have EAs

between 2.09 and 2.26 eV, while diphenoquinone derivatives show EAs from 2.63 to 2.81 eV (see **Table 43**). This difference is also observed in the redox features, as the highest reduction potentials from these three molecules are found on 2,7-carbazoloquinone (E_R^1=3.20 V and E_R^2=2.35 V), anyway, below the values recorded for diphenoquinone (E_R^1=3.31 V and E_R^2=2.56 V). Besides, these three molecules lead to high energy densities (750-800 $WhKg^{-1}$).

Table 44: Electron affinities (EA) and ionization potentials (IP), in eV. First, second and two-electron reduction potentials (E_R^1, E_R^2, E_R) and oxidation potentials (E_O^1) vs Li/Li^+, in V. Theoretical capacity (C_{THEO}), in $mAhg^{-1}$, and energy density (E_{DEN}), in $Whkg^{-1}$, for quinone zethrenes.

	EA	IP	E_R^1	E_R^2	E_R	E_O^1	C_{THEO}	E_{DEN}
1	2.63	6.44	2.40	2.06	2.23	3.88	88	197
2	2.86	6.64	2.79	2.33	2.56	4.11	96	247
3	2.76	6.45	2.88	2.38	2.63	3.96	124	326
4	2.37	7.05	2.47	1.98	2.22	4.48	124	276

The inclusion of the carbonyl groups to the carbazole moiety does not strongly affect the IPs. However, the 1,4 and 2,7-carbazoloquinones show higher values (8.22 and 8.16 eV, respectively), that also leads to high oxidation potentials (5.01 and 4.93 V).

5.7. Zethrenes

Due to their electrochemical features, carbonyl-containing aromatic molecules such as zethrenes have conformed the target of investigations in the field of novel

battery materials. [394,395] In this subsection, the redox features of some zethrene derivatives containing carbonyl groups have been studied (see **Table 44**).

Table 45: Redox potentials together with the available experimental results, in brackets, from Refs. 298 and 331. Values in V vs Fc/Fc^+.

	E_1	E_2	E_O
1	-1.35 (-1.67)	-1.69 (-2.27)	0.13 (0.14)
2	-0.96 (-1.41)	-1.42 (-1.59)	0.36 (0.49)
3	-0.87	-1.37	0.21
4	-1.28 (-1.54)	-1.77 (-2.32)	0.73 (0.88)

The E_R^1 values fluctuate between 2.40 and 2.88 V, while E_R^2 vary between 1.98 and 2.38 V. However, these molecules are very large, and low energy density values are found, 326 $WhKg^{-1}$ in the best of the cases. Since several carbonyl zethrene derivatives have been proposed as battery cathode,[298, 331] in **Table 45** are collected the experimental and the computed redox potential vs Fc/Fc^+ electrode. The MAEs are 0.35 V, 0.43 V and 0.10 V for the E_R^1, E_R^2 and E_O^1, respectively.

5.8. Summary and conclusions

This section was devoted to unveil the redox features of several different carbonyl-containing systems in order to evaluate their potential to be used as organic cathode materials. For that purpose, the 1,4-anthraquinone and 1,4-naphthoquinone molecules have been used as reference.

In general, high reduction potentials could be found, but the large size of the molecules reduces the E_{DEN} below the values of the reference molecules.

Firstly, 22 substituents were inserted into the croconate and squarate moieties, and high reduction potentials have been found. In general, the reduction potentials of the croconates (between 2.40 and 3.87 V) are higher than those of the squarates (between 1.61 and 3.48 V), while high energy density is reached when **R_{11}** is used (573 and 547 $WhKg^{-1}$ for croconates and squarates, respectively). From the 22 substituents used, 8 croconates and 2 squarates have $E_R^1 > 2.80$ V.

Regarding the quinoidal oligothiophenes, high reduction potentials were found for carbonyl- and cyano-containing molecules. The increase of the molecular size leads to a decrease of E_R^1 in case of **A**, **C**, **E** and **F**, while in the remaining groups the opposite effect is accounted. 22 molecules have $E_R^1 > 2.80$ V, while only **A_1**, **H_1**, **I_1** and **I_2** have an energy density higher to that of the 1,4-naphthoquinone.

Aromatic diimides show E_R^1 values between 2.20 and 3.55 V, and 13 have $E_R^1 > 2.80$ V. E_{DEN} ranges from 284 to 565 $WhKg^{-1}$ due to the large size of some of the molecules.

33 indigo-like molecules were investigated, 10 of them with E_R^1 over 2.80 V, and E_{DEN} as high as 678 $WhKg^{-1}$ are reached. Something similar was accounted for seventeen quinoidal-related chromophores ($1.94 \text{ V} < E_R^1 < 3.11$ V), six of

them with E_R^1> 2.80 V. Yet, the values of energy density are lower, varying between 200 and 411 $WhKg^{-1}$.

Seven carbazoloquinones were studied, all of them with high reduction potentials above 2.80 V and E_{DEN} up to 792 $WhKg^{-1}$, very similar compared with the diphenoquinone molecule. Finally, four large-sized quinone zethrenes lead to low E_{DEN} values. From the four molecules, only one has E_R^1 > 2.80 V.

Thus, in this thesis, a total of 69 molecules are proposed for further investigations in order to get a cheap, clean and efficient battery cathode material. These molecules were chosen using the reduction potential of the 9,10-anthraquinone molecule as lower bound (E_R^1=2.80 V).

Chapter 6

Singlet fission

1. Introduction

As it was previously mentioned in the Introduction of this thesis, in addition to the general requirements for solar cell sensitizers, such as good light-harvesting capabilities or photo-stability, singlet fission (SF) chromophores have to fulfill two energy conditions:[32] (i) the energy of the first singlet excited state (E[S_1]) should be slightly higher than (or at least equal to) twice the energy of the first triplet state (E[T_1]), in such a way that the process is exoergic (or isoergic). If the process is exaggeratedly exoergic, the efficiency may be reduced due to energy loss by heating. (ii) The second triplet state (E[T_2]) must be higher in energy than twice the energy of the first triplet excited state (E[T_1]) in order to avoid no-fission decay into the triplet manifold. The deactivation channel into the quintuplet manifold is typically not considered, since the E[Q_1] state in organic molecules is expected to lie at higher energies. The fulfillment of these energy conditions is considerably influenced by the diradical character of the molecule and compounds with an intermediate diradical character have been proposed as one of the main classes of promising singlet fission sensitizers, [33,32,34, 418 , 419 , 420] fundamentally due to their inherent small singlet-triplet gaps that help the accomplishment of the aforementioned requirements. Since the energies of the singlet and triplet states are related to the diradical character of the ground state, this characteristic is suggested as a useful guideline for the design of new efficient SF molecules.

As it has been already demonstrated in Chapter 4, the diradical character can be tuned by introducing structural modifications and, therefore, the energies of the low-lying excited states may be modulated to fulfill the required energy conditions. In the literature, few articles can be found pointing to that direction and the acenes (especially tetracene and pentacene) have been used as a tool to probe that relation.[421] For instance, it was found that the substitution of silicon atoms into an acene moiety leads to the diminution of the singlet-triplet gap,[422,423] reducing the value of the $2E[T_1]$-$E[S_1]$ energy difference. The opposite behavior was observed when sp^2-conjugated nitrogen atoms are inserted into the backbone of the acene molecule.[424] Besides, the effect of the heteroatom strongly depends on the site of substitution. Similarly, the introduction of thiophene rings also shifts the $2E[T_1]$-$E[S_1]$ to more negative values due to the enlargement of the molecule,[182,183,424] favoring the SF process. In general, it has been observed that electron-withdrawing groups slightly shift the $2E[T_1]$-$E[S_1]$ to more negative values, especially for CN or NO_2 substituents.[425,426] Very interesting results were also obtained using the captodative effect on various molecules as azulene, fulvene or benzene,[184] reducing the $2E[T_1]$-$E[S_1]$ energy difference. Hence, the introduction of boron and nitrogen atoms was found to be a viable way to create new singlet fission materials starting from a multitude of conjugated molecules

As in previous chapters, we will start from the set of conjugated carbonyls and methylene derivatives and perform a detailed investigation of the low-lying excited states, in order to unravel the best strategy to design adequate SF materials that could be experimentally efficient. Then, the same modifications introduced in previous chapters are investigated in order to know their influence in the SF energy conditions ($2E[T_1]-E[S_1]\leq 0$ and $2E[T_1]-E[T_2]<0$). It is important to keep in mind that commonly SF systems present extended structures, e.g. molecular crystals or thin films, which typically present redshifted transition energies with respect to the gas phase. In linear acenes, the S_1 energies in the gas phase are 0.3-0.5 eV higher than in the crystal, while this shift is one order of magnitude smaller for the triplet state.[33,427] This fact makes the $2E[T_1]-E[S_1]$ energy difference around 0.4 eV more endoergic in the solid state, disfavoring the SF process in some cases, and favoring it in other cases with $2E[T_1]-E[S_1] > 0$. The case of tetracene is paradigmatic, since this molecule shows an almost isoergic $2E[T_1]-E[S_1]$ value in the gas phase but becomes endoergic in the solid state.[428] The SF phenomenon can be activated anyway with soft heating.

2. Computational details

All geometry optimizations have been performed in gas phase using the B3PW91 functional in combination with the 6-31+G(d) basis set. Harmonic vibrational frequencies were obtained at the same level of theory to confirm that all the structures were minima in the potential energy surfaces

(no imaginary frequencies were found) and to evaluate the zero-point vibrational energy (ZPVE) and the thermal corrections to the Gibbs free energy (T=298 K, 1 atm) in the harmonic oscillator approximation. Single point calculations using the aug-cc-pVTZ basis set were carried out on the optimized structures to refine the electronic energy.

Time-dependent density functional theory (TDDFT) calculations have been carried out using the M06-2X functional together with the 6-31G+(d,p) basis set, while the B3PW91 could be used if required with the same basis set. Additionally, in order to improve the description of the non-dynamic correlation effects, Spin-Flip TDDFT (SF-TDDFT) calculations have been also carried out with the BHandHLYP functional and the 6-31G+(d,p) basis set.

3. Singlet fission in conjugated quinones and methylene derivatives

The structural and electronic features, in the ground and low-lying excited states, of the previously designed set of 206 molecules belonging to the groups labeled as *n,m*-C(x+y+z)/Q, *n,m*-C(x+y+z)/QDM and *n,m*-C(x+y+z)/QM have been studied. In **Figure 77**, some representative molecules of each family are shown (the whole set of molecules is depicted in **Figure 13**, in Chapter 4). As previously done, the bare rings are also studied in order to analyze the effect of the carbonyl and methylene substitution.

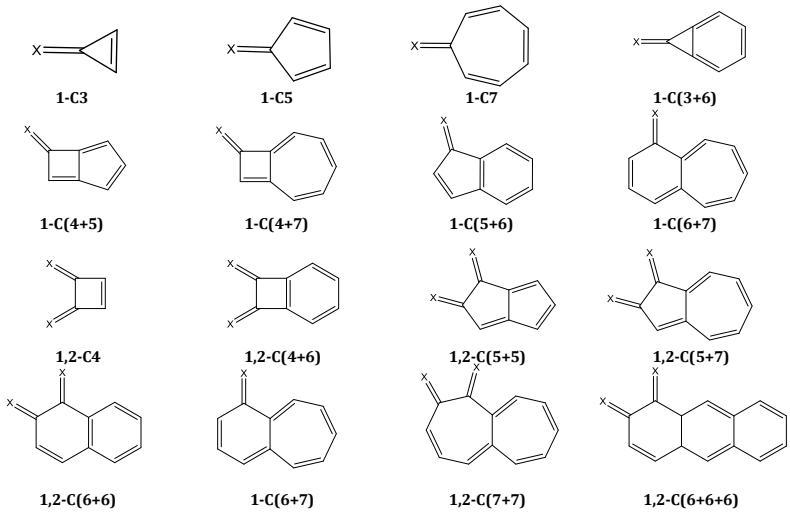

Figure 77: Representative molecules of each family, where X=O, CH_2.

In the next sections, the results are presented and organized as follows: firstly, a thorough study of the low-lying excited states is performed, followed by an analysis of those systems that can be proposed as promising candidates to undergo singlet fission.

As it was mentioned in Chapter 4, many of the carbonyl derivatives (Q) possess a non-negligible diradical character, and the ground state should be described as a singlet open-shell state. It has also been noted the importance of an intermediate y_0 value to get an exoergic singlet fission process. Two acenes, tetracene (Tc) and pentacene (Pc), will be used as guidelines for the pursuit of adequate SF sensitizers, since they are archetypal examples of singlet fission chromophores.

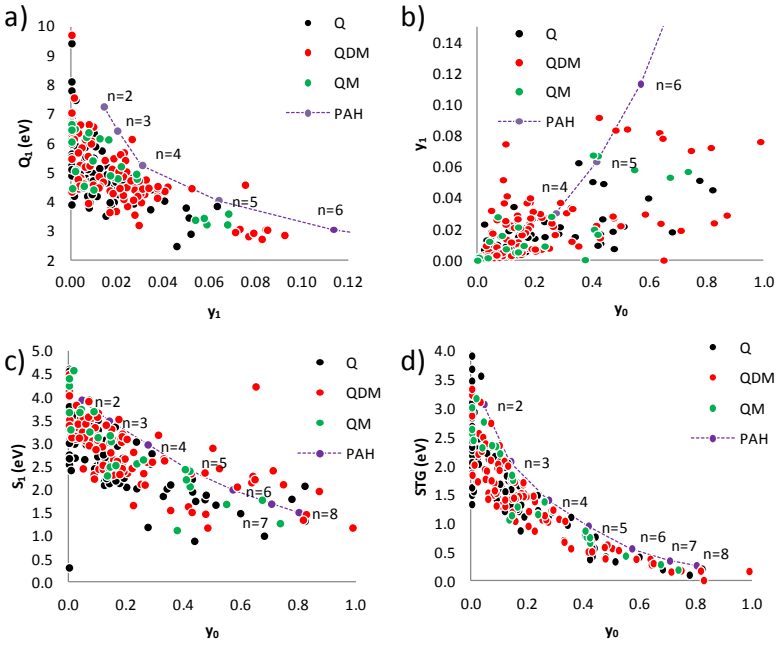

Figure 78: Relation between a) the tetraradical character (y_1) and the energy of the first quintet state (Q_1), in eV; b) the diradical (y_0) and tetraradical characters; c) y_0 and the energy of the first singlet state (S_1), in eV and d) y_0 and the singlet-triplet gap ($E[T_1]^{DFT}$), in eV, for Q, QM and QDM derivatives. For comparison, the values of the acene series up to octacene (n=8) have been included.

We have also computed the tetraradical character (y_1), which measures the ability of a molecule to place four unpaired electrons in different atoms. An increase of this parameter is related with the presence of a low-lying quintet state (Q_1), which may negatively interfere on an eventual SF process, reducing the efficiency as a competing state. In **Figure 78a** and **Figure 78b** are represented the relation between y_1 and the energy of Q_1 with respect to the ground

state, and the relation between y_0 and y_1, for all the Q, QM and QDM derivatives, together with the acenes. In general, larger y_0 values accomplish larger y_1 values; however, all the systems studied in this section show low y_1 values, less than 0.10, although larger values than those of the acenes are observed, regarding the same number of fused rings. Nevertheless, most of the molecules show Q_1 energies greater than 4 eV, still smaller than those of the acene series.

3.1. Low-lying singlet and triplet states

In order to study the singlet fission process, the nature of the lowest singlet (S_1) and triplet (T_1) excited states is of paramount importance. The energy and character of the $S_0 \rightarrow S_1$ and $S_0 \rightarrow T_1$ transitions, as well as the oscillator strength for the Q, QDM and QM molecules, are collected in **Table 46**, **Table 47** and **Table 48,** respectively. Since the large majority of the molecules show a small or intermediate diradical character, the main discussion will be performed at the TDDFT level. The data for molecular structures with large diradical character is obtained with SF-TDDFT and is included in the Tables in italics.

Table 46: Energies of the first singlet ($E[S_1]$) and triplet ($E[T_1]$) excited states, as well as $2E[T_1]$-$E[S_1]$ (C1) and $2E[T_1]$-$E[T_2]$ (C2) energy conditions, in eV. Nature of the $S_0 \rightarrow S_1$ and $S_0 \rightarrow T_1$ transitions, and oscillator strength (*f*) of the Q molecules calculated with TDDFT. The spin-contaminated values are substituted by those obtained by SF-TDDFT and highlighted in italics.

		$E(S_1)$	S_0->S_1	*f*	$E(T_1)$	S_0->T_1	$E(T_2)$	C1	C2			$E(S_1)$	S_0->S_1	*f*	$E(T_1)$	S_0->T_1	$E(T_2)$	C1	C2
C3		4.40	n->π*	0.00	4.09	π->π*	4.92	3.79	3.27	**C(4+6)**	**3,6 (a)**	1.85	π->π*	0.01	0.46	π->π*	2.09	-0.93	-1.17
C5		2.73	n->π*	0.00	2.08	π->π*	2.32	1.44	1.85		**1,3**	2.80	n->π*	0.00	1.68	π->π*	2.44	0.56	0.92
C7		3.74	n->π*	0.00	2.43	π->π*	3.10	1.11	1.75		**1,5**	3.01	n->π*	0.00	2.17	π->π*	2.66	1.32	1.68
C(3+6)	**3**	3.36	n->π*	0.00	2.46	π->π*	3.08	1.56	1.84		**4,5**	2.60	n->π*	0.00	2.22	n->π*	2.75	1.84	1.70
	2	3.24	π->π*	0.08	1.97	π->π*	2.95	0.69	0.98		**1,2**	2.82	n->π*	0.00	2.48	n->π*	3.48	2.13	1.47
	1	3.88	n->π*	0.00	3.63	n->π*	3.95	3.38	3.31	**C(5+5)**	**1,4**	2.04	π->π*	0.01	1.08	π->π*	2.04	0.11	0.11
C(4+5)	**3 (a)**	*1.54*	--	--	*0.15*	--	*0.77*	*-1.23*	-0.46		**1,6**	2.29	π->π*	0.01	1.20	π->π*	2.01	0.11	0.39
	3 (b)	2.30	π->π*	0.01	1.05	π->π*	1.99	-0.21	0.10		**1,5**	2.72	n->π*	0.00	1.77	π->π*	2.23	0.81	1.30
	4	3.64	n->π*	0.00	3.02	π->π*	3.26	2.41	2.79		**1,2**	2.06	n->π*	0.00	1.67	π->π*	1.79	1.28	1.55
	1	3.35	π->π*	0.00	2.47	π->π*	3.04	1.58	1.89	**C(5+7)**	**2,4**	2.33	π->π*	0.04	1.25	π->π*	2.00	0.17	0.50
C(4+7)	**5 (a)**	*1.45*	--	--	*-0.46*	--	*0.31*	*-2.36*	-1.22		**1,2**	2.11	n->π*	0.00	1.47	π->π*	1.76	0.83	1.17
	3 (b)	*1.46*	--	--	*0.09*	--	*0.64*	*-1.28*	-0.46		**1,6**	2.52	π->π*	0.02	1.40	π->π*	2.35	0.28	0.45
	5 (b)	*1.62*	--	--	*0.13*	--	*0.75*	*-1.35*	-0.48		**2,6**	2.49	π->π*	0.00	1.46	π->π*	2.13	0.43	0.79
	3 (a)	1.72	π->π*	0.02	0.08	π->π*	2.51	-1.57	-2.36		**1,4**	2.68	π->π*	0.07	1.54	π->π*	2.37	0.40	0.71
	1	2.22	π->π*	0.01	1.49	π->π*	2.47	0.75	0.50		**1,8**	2.41	n->π*	0.00	1.76	π->π*	2.07	1.11	1.46
	4	3.36	n->π*	0.00	2.22	π->π*	2.91	1.07	1.53		**5,6**	2.35	n->π*	0.01	1.44	π->π*	2.03	0.53	0.86
C(5+6)	**2**	*1.65*	--	--	*0.12*	--	*0.68*	*-1.41*	-0.44		**4,7**	2.75	π->π*	0.03	1.72	π->π*	2.39	0.69	1.04
	5	2.33	π->π*	0.03	1.26	π->π*	2.31	0.20	0.21		**1,7**	3.04	n->π*	0.00	2.10	π->π*	2.65	1.15	1.54
	4	2.38	π->π*	0.01	1.32	π->π*	1.64	0.27	1.00		**4,5**	2.27	n->π*	0.00	1.55	π->π*	1.76	0.83	1.35
	1	3.00	n->π*	0.00	2.50	π->π*	2.60	2.01	2.40		**1,5**	3.14	n->π*	0.00	2.30	π->π*	2.60	1.46	2.00
C(6+7)	**6**	2.78	π->π*	0.09	1.23	π->π*	2.71	-0.33	-0.25	**C(6+6)**	**2,3**	1.71	n->π*	0.00	0.52	π->π*	1.36	-0.68	-0.33
	2	2.57	π->π*	0.07	1.49	π->π*	2.26	0.41	0.72		**1,5**	2.33	n->π*	0.00	0.65	π->π*	2.05	-1.03	-0.75
	1	2.11	π->π*	0.04	1.28	π->π*	1.83	0.45	0.72		**1,7**	2.43	n->π*	0.00	1.01	π->π*	2.10	-0.42	-0.09
	5	3.63	n->π*	0.00	2.45	π->π*	3.25	1.27	1.65		**2,6**	2.70	n->π*	0.00	1.50	n->π*	2.34	0.30	0.66
	7	3.53	n->π*	0.00	3.00	π->π*	3.03	2.47	2.98		**1,2**	2.21	n->π*	0.00	1.84	n->π*	2.35	1.47	1.33
C4	**1,2**	3.41	n->π*	0.00	3.03	n->π*	3.11	2.65	2.95		**1,4**	2.92	n->π*	0.00	2.54	n->π*	2.75	2.15	2.33
	1,3	4.46	n->π*	0.00	4.04	n->π*	4.43	3.61	3.64	**C(7+7)**	**1,2**	2.40	π->π*	0.05	1.52	π->π*	1.80	0.64	1.24
C6	**1,2**	1.94	n->π*	0.00	1.57	n->π*	1.90	1.21	1.24		**1,9**	3.14	π->π*	0.14	1.71	π->π*	2.77	0.29	0.65
	1,4	2.70	n->π*	0.00	2.30	n->π*	2.50	1.91	2.11		**2,3**	2.54	π->π*	0.07	1.56	π->π*	2.13	0.59	1.00
C(3+3)		3.54	n->π*	0.00	3.22	σ->π*	3.31	2.91	3.13		**3,8**	3.25	π->π*	0.09	1.90	π->π*	2.77	0.54	1.02
C(3+5)	**1,3**	1.94	n->π*	0.00	1.37	π->π*	1.60	0.80	1.14		**1,6**	3.43	π->π*	0.27	2.06	π->π*	2.77	0.68	1.34
	2,3	2.11	n->π*	0.00	1.74	n->π*	2.14	1.37	1.34		**1,7**	3.18	π->π*	0.03	1.91	π->π*	2.46	0.64	1.36
	1,2	2.56	n->π*	0.00	2.20	n->π*	2.58	1.84	1.81		**2,8**	3.21	n->π*	0.00	1.93	π->π*	2.50	0.64	1.35
C(3+7)	**1,3**	2.48	n->π*	0.00	1.57	π->π*	2.22	0.66	0.91		**1,8**	3.45	π->π*	0.13	2.06	π->π*	2.80	0.67	1.32
	3,4	2.84	n->π*	0.00	2.38	π->π*	2.58	1.91	2.17		**1,4**	2.73	π->π*	0.06	1.85	π->π*	2.18	0.97	1.52
	1,4	3.44	n->π*	0.00	2.83	π->π*	2.92	2.22	2.75		**1,10**	3.61	n->π*	0.00	2.47	π->π*	2.77	1.34	2.18
	2,3	2.54	n->π*	0.00	1.76	π->π*	2.16	0.99	1.37	**C(6+6+6)**	**2,3**	*1.33*	--	--	*-0.50*	--	*0.15*	*-2.33*	-1.15
	2,5	3.05	n->π*	0.00	2.46	π->π*	2.65	1.86	2.26		**1,5**	*2.10*	--	--	*-0.01*	--	*0.70*	*-2.12*	-0.72
	1,2	3.20	n->π*	0.00	2.55	π->π*	2.87	1.90	2.23		**1,7**	*2.21*	--	--	*0.45*	--	*1.12*	*-1.32*	-0.23
C(4+4)	**1,2 (b)**	*1.50*	--	--	*0.02*	--	*0.54*	*-1.47*	-0.50		**2,6**	2.69	n->π*	0.00	0.59	π->π*	1.97	-1.50	-0.78
	1,2 (a)	2.81	π->π*	0.00	1.49	π->π*	2.67	0.18	0.32		**1,10**	2.59	n->π*	0.00	1.06	π->π*	2.31	-0.47	-0.19
	1,3	3.55	n->π*	0.00	3.16	π->π*	3.20	2.76	3.11		**2,9**	2.66	n->π*	0.00	1.38	π->π*	2.32	0.10	0.44
C(4+6)	**3,4 (a)**	*1.16*	--	--	*-0.43*	--	*0.24*	*-2.02*	-1.10		**1,2**	2.31	n->π*	0.00	1.94	n->π*	2.42	1.56	1.45
	3,4 (b)	*1.16*	--	--	*-0.43*	--	*0.24*	*-2.01*	-1.10		**1,4**	3.00	n->π*	0.00	2.62	n->π*	2.80	2.23	2.44
	3,6 (b)	2.02	π->π*	0.01	0.50	π->π*	2.17	-1.01	-1.16		**9,10**	3.16	n->π*	0.00	2.79	n->π*	3.01	2.42	2.57

The main striking difference of substituted molecules with respect to pristine compounds is the nature of the transition in carbonyl-containing molecules due to the

presence of the lone pairs of the oxygen atoms. Concretely, 51 Q and 10 QM molecules show a S_1 excited state with n $\rightarrow$ π^* character and redshifted transition energies with respect to the unsubstituted counterpart. Moreover, the computed oscillator strengths for S_1 in these cases is considerably lower since the n $\rightarrow$ π^* transitions are less intense than $\pi \rightarrow \pi^*$ excitations. On the other hand, the promotion of lone pair electrons into π^* orbitals in the T_1 state is only obtained for 15 Q molecules.

Comparing the $S_0 \rightarrow S_1$ transition energies in the acenes with those calculated in the Q, QM and QDM derivatives, a general decrease is observed upon substitution. This stabilization of the S_1 state may be related to a larger diradical character, see **Figure 78c**. In this way, QDM molecules are expected to show lower $E(S_1)$ values than Q molecules, due to the larger y_0 values they exhibit. The nature of the transition plays a relevant role, and the presence of the oxygen lone pairs in carbonyl-containing molecules destabilizes the HOMO having as a consequence a shift to lower transition energies, which, in many cases, exceeds the stabilization accomplished by y_0, in such a way that, in those cases, the following trend is observed: $E(S_1,QDM) > E(S_1,QM) > E(S_1,Q)$. In the case of the $S_0 \rightarrow T_1$ transitions, this behavior is less clear and in many cases the trend is reversed: $E(T_1,QDM) < E(T_1,Q)$. This may be ascribed to two features: first, a greater stabilization of the T_1 state due to the

diradical character and, second, most of the transitions in the Q derivatives are of $\pi \rightarrow \pi^*$ type, as in QDM derivatives.

Table 47: Energies of the first singlet ($E[S_1]$) and triplet ($E[T_1]$) excited states, as well as $2E[T_1]$-$E[S_1]$ (C1) and $2E[T_1]$-$E[T_2]$ (C2) energy conditions, in eV. Nature of the $S_0 \rightarrow S_1$ and $S_0 \rightarrow T_1$ transitions, and oscillator strength (*f*) of the QDM molecules calculated with TDDFT. The spin-contaminated values are substituted by those obtained by SF-TDDFT and highlighted in italics.

		$E(S_1)$	S_0->S_1	*f*	$E(T_1)$	S_0->T_1	$E(T_2)$	C1	C2			$E(S_1)$	S_0->S_1	*f*	$E(T_1)$	S_0->T_1	$E(T_2)$	C1	C2
C3		4.48	π->π*	0.02	3.54	π->π*	4.74	2.59	2.34	**C(4+6)**	**3,6 (a)**	2.21	π->π*	0.01	0.48	π->π*	2.06	-1.24	-1.10
C5		3.54	π->π*	0.01	2.42	π->π*	3.00	1.31	1.85		**1,3**	3.27	π->π*	0.19	1.39	π->π*	2.99	-0.49	-0.21
C7		2.82	π->π*	0.01	1.86	π->π*	2.63	0.89	1.08		**1,5**	3.65	π->π*	0.35	1.67	π->π*	3.12	-0.32	0.21
C(3+6)	**3**	2.78	π->π*	0.08	1.69	π->π*	3.57	0.60	-0.19		**4,5**	3.98	π->π*	0.05	2.27	π->π*	2.88	0.56	1.66
	2	3.05	π->π*	0.13	1.62	π->π*	2.90	0.20	0.34		**1,2**	4.49	π->π*	0.16	3.26	π->π*	3.50	2.04	3.02
	1	4.49	π->π*	0.38	3.04	π->π*	3.99	1.59	2.09	**C(5+5)**	**1,4**	2.49	π->π*	0.02	1.59	π->π*	2.63	0.68	0.54
C(4+5)	**3 (a)**	1.72	π->π*	0.00	0.54	π->π*	2.72	-0.64	-1.64		**1,6**	2.58	π->π*	0.01	1.55	π->π*	2.47	0.53	0.64
	3 (b)	*1.17*	--	--	*-0.42*	--	*0.30*	*-2.01*	-1.14		**1,5**	3.18	π->π*	0.01	2.15	π->π*	2.43	1.12	1.87
	4	3.85	π->π*	0.03	2.67	π->π*	2.80	1.48	2.54		**1,2**	2.85	π->π*	0.03	1.92	π->π*	2.29	1.00	1.56
	1	3.02	π->π*	0.01	2.15	π->π*	2.73	1.27	1.56	**C(5+7)**	**2,4**	2.88	π->π*	0.07	1.55	π->π*	1.98	0.22	1.12
C(4+7)	**5 (a)**	*0.98*	--	--	*-0.76*	--	*0.04*	*-2.50*	-1.55		**1,2**	2.08	π->π*	0.01	1.30	π->π*	1.98	0.51	0.61
	3 (b)	*1.66*	--	--	*0.08*	--	*0.79*	*-1.49*	-0.63		**1,6**	2.13	π->π*	0.01	1.28	π->π*	2.48	0.43	0.08
	5 (b)	1.58	π->π*	0.00	0.35	π->π*	2.11	-0.88	-1.41		**2,6**	3.05	π->π*	0.00	1.77	π->π*	2.05	0.50	1.50
	3 (a)	*0.87*	--	--	*-0.85*	--	*-0.08*	*-2.57*	-1.62		**1,4**	2.24	π->π*	0.03	1.42	π->π*	2.35	0.60	0.49
	1	2.36	π->π*	0.01	1.55	π->π*	2.43	0.73	0.66		**1,8**	2.46	π->π*	0.02	1.64	π->π*	2.56	0.81	0.71
	4	3.60	π->π*	0.12	2.06	π->π*	2.59	0.52	1.53		**5,6**	2.61	π->π*	0.05	1.65	π->π*	2.33	0.68	0.96
C(5+6)	**2**	2.11	π->π*	0.02	1.03	π->π*	2.51	-0.04	-0.44		**4,7**	2.75	π->π*	0.05	1.68	π->π*	2.18	0.61	1.17
	5	2.51	π->π*	0.06	1.31	π->π*	2.26	0.10	0.35		**1,7**	2.65	π->π*	0.04	1.64	π->π*	1.95	0.62	1.32
	4	2.46	π->π*	0.04	1.12	π->π*	1.86	-0.23	0.38		**4,5**	2.55	π->π*	0.01	1.74	π->π*	1.85	0.93	1.62
	1	3.78	π->π*	0.03	2.67	π->π*	3.14	1.56	2.20		**1,5**	2.60	π->π*	0.02	1.65	π->π*	1.98	0.70	1.33
C(6+7)	**6**	1.84	π->π*	0.02	0.71	π->π*	2.26	-0.41	-0.84	**C(6+6)**	**2,3**	*2.21*	--	--	*-0.01*	--	*0.63*	*-2.24*	-0.66
	2	2.13	π->π*	0.05	1.06	π->π*	1.93	-0.01	0.20		**1,5**	*2.01*	--	--	*-0.22*	--	*0.49*	*-2.45*	-0.93
	1	2.11	π->π*	0.03	1.16	π->π*	1.70	0.22	0.62		**1,7**	*2.55*	--	--	*0.24*	--	*0.93*	*-2.07*	-0.44
	5	3.70	π->π*	0.09	2.49	π->π*	3.26	1.28	1.73		**2,6**	3.43	π->π*	1.03	0.84	π->π*	2.77	-1.75	-1.09
	7	3.36	π->π*	0.01	2.56	π->π*	2.58	1.76	2.53		**1,2**	3.71	π->π*	0.14	2.20	π->π*	3.44	0.70	0.97
C4	**1,2**	5.12	π->π*	0.12	3.15	π->π*	3.90	1.19	2.41		**1,4**	4.32	π->π*	0.65	2.10	π->π*	3.65	-0.11	0.56
	1,3	*0.30*	--	--	*-1.69*	--	*-0.70*	*-3.67*	-2.67	**C(7+7)**	**1,2**	2.75	π->π*	0.02	1.80	π->π*	2.02	0.84	1.58
C6	**1,2**	3.31	π->π*	0.14	1.53	π->π*	3.68	-0.26	-0.62		**1,9**	2.74	π->π*	0.11	1.58	π->π*	2.56	0.42	0.59
	1,4	4.34	π->π*	0.87	1.81	π->π*	3.77	-0.73	-0.16		**2,3**	2.50	π->π*	0.06	1.56	π->π*	2.33	0.63	0.79
C(3+3)	**1,2**	2.91	π->π*	0.00	2.12	π->π*	3.07	1.32	1.17		**3,8**	2.05	π->π*	0.02	1.14	π->π*	2.36	0.24	-0.08
C(3+5)	**1,3**	3.25	σ->π*	0.00	1.72	π->π*	2.27	0.19	1.17		**1,6**	3.14	π->π*	0.13	2.10	π->π*	2.82	1.06	1.38
	2,3	2.74	π->π*	0.03	1.72	π->π*	3.57	0.71	-0.13		**1,7**	2.97	π->π*	0.02	1.90	π->π*	2.29	0.82	1.50
	1,2	2.77	π->π*	0.01	2.05	π->π*	2.87	1.32	1.22		**2,8**	2.52	π->π*	0.02	1.56	π->π*	2.03	0.59	1.09
C(3+7)	**1,3**	2.30	π->π*	0.02	1.45	π->π*	2.40	0.60	0.49		**1,8**	2.56	π->π*	0.04	1.61	π->π*	2.55	0.67	0.68
	3,4	2.84	π->π*	0.03	2.16	π->π*	3.02	1.47	1.30		**1,4**	3.08	π->π*	0.02	2.20	π->π*	2.29	1.33	2.11
	1,4	2.44	π->π*	0.01	1.64	π->π*	2.26	0.84	1.03		**1,10**	3.06	π->π*	0.01	2.08	π->π*	2.49	1.11	1.68
	2,3	2.66	π->π*	0.04	2.08	π->π*	2.44	1.51	1.73	**C(6+6+6)**	**2,3**	*1.78*	--	--	*-0.47*	--	*0.22*	*-2.72*	-1.16
	2,5	2.99	π->π*	0.02	2.39	π->π*	2.48	1.79	2.31		**1,5**	*1.47*	--	--	*-0.51*	--	*0.31*	*-2.49*	-1.32
	1,2	2.62	π->π*	0.05	1.77	π->π*	2.47	0.92	1.07		**1,7**	*1.74*	--	--	*-0.26*	--	*0.52*	*-2.26*	-1.03
C(4+4)	**1,2 (b)**	1.68	π->π*	0.00	0.16	π->π*	2.76	-1.35	-2.43		**2,6**	*2.09*	--	--	*0.09*	--	*0.83*	*-1.91*	-0.65
	1,2 (a)	*2.12*	--	--	*0.24*	--	*0.86*	*-1.65*	-0.38		**1,10**	2.59	π->π*	0.29	1.03	π->π*	2.76	-0.52	-0.69
	1,3	4.29	π->π*	0.00	2.91	π->π*	3.31	1.53	2.51		**2,9**	3.01	π->π*	0.47	1.19	π->π*	2.73	-0.63	-0.35
C(4+6)	**3,4 (a)**	*1.31*	--	--	*-0.61*	--	*0.11*	*-2.53*	-1.33		**1,2**	3.77	π->π*	0.10	2.33	π->π*	3.07	0.88	1.59
	3,4 (b)	*2.06*	--	--	*0.31*	--	*0.95*	*-1.43*	-0.32		**1,4**	3.93	π->π*	0.00	2.18	π->π*	2.95	0.42	1.40
	3,6 (b)	1.85	π->π*	0.01	0.42	π->π*	2.16	-1.01	-1.32		**9,10**	4.52	π->π*	0.01	2.86	π->π*	3.49	1.19	2.22

Table 48: Energies of the first singlet ($E[S_1]$) and triplet ($E[T_1]$) excited states, as well as $2E[T_1]$-$E[S_1]$ (C1) and $2E[T_1]$-$E[T_2]$ (C2) energy conditions, in eV. Nature of the $S_0 \rightarrow S_1$ and $S_0 \rightarrow T_1$ transitions, and oscillator strength (*f*) of the QM molecules calculated with TDDFT. The spin-contaminated values are substituted by those obtained by SF-TDDFT and highlighted in italics.

		$E(S_1)$	S_0->S_1	*f*	$E(T_1)$	S_0->T_1	$E(T_2)$	C1	C2
C4	**1,2**	3.84	n->π*	3.30	3.30	π->π*	3.45	2.76	3.15
	1,3	*1.11*	--	--	*-0.86*	--	*0.07*	*-2.83*	-1.79
C6	**1,2**	2.96	n->π*	0.00	1.72	π->π*	2.64	0.48	0.80
	1,4	3.11	n->π*	0.00	2.15	π->π*	2.73	1.19	1.57
C(3+3)		3.65	π->π*	0.00	2.83	π->π*	3.47	2.01	2.19
C(4+4)	**1,2 (b)**	2.36	π->π*	0.01	1.10	π->π*	3.50	-0.16	-1.30
	1,2 (a)	2.35	π->π*	0.01	1.09	π->π*	3.49	-0.17	-1.31
	1,3	3.95	n->π*	0.00	2.93	π->π*	3.17	1.91	2.69
C(4+6)	**3,6 (b)**	1.77	π->π*	0.01	0.36	π->π*	2.09	-1.05	-1.37
	3,6 (a)	*1.67*	--	--	*0.07*	--	*0.71*	*-1.54*	-0.57
	4,5	3.40	n->π*	0.00	2.47	π->π*	2.97	1.54	1.97
	1,2	3.64	n->π*	0.00	3.27	π->π*	3.28	2.90	3.26
C(5+5)	**1,4**	2.22	π->π*	0.02	1.30	π->π*	2.33	0.38	0.27
	1,6	2.38	π->π*	0.01	1.32	π->π*	2.37	0.26	0.27
C(6+6)	**2,3**	2.21	π->π*	0.07	0.54	π->π*	2.43	-1.13	-1.35
	1,5	2.37	π->π*	0.22	0.44	π->π*	2.51	-1.49	-1.63
	2,6	2.94	n->π*	0.00	1.15	π->π*	2.59	-0.64	-0.29
	1,4	3.29	n->π*	0.00	2.39	π->π*	2.92	1.49	1.86
C(7+7)	**3,8**	2.41	π->π*	0.03	1.46	π->π*	2.48	0.51	0.44
	1,6	3.12	π->π*	0.20	1.89	π->π*	2.88	0.66	0.90
	1,10	3.50	π->π*	0.02	2.45	π->π*	2.81	1.40	2.09
C(6+6+6	**2,3**	*1.26*	--	--	*-0.31*	--	*0.36*	*-1.87*	-0.97
	1,5	*1.76*	--	--	*-0.24*	--	*0.51*	*-2.25*	-1.00
	2,6	*2.42*	--	--	*0.55*	--	*1.22*	*-1.33*	-0.13
	1,4	3.33	n->π*	0.00	2.40	π->π*	2.93	1.47	1.87
	9,10	3.46	n->π*	0.00	2.80	π->π*	3.08	2.14	2.52

In **Figure 78d** is represented the variation of the singlet-triplet gap ($E[T_1]^{DFT}$) with the diradical character. It is well known that the molecules with notable diradical character display small singlet-triplet gaps, due to a stabilization of the T_1 state. Inspecting **Figure 78d**, we find that the optimal y_0

values according to the energy requirements discussed above vary between 0.2 and 0.4.

The shift of the transition energy to lower energies due to the enhancement of y_0 may also be used to tune the optoelectronic properties of conjugated hydrocarbons, to include a broader range of wavelengths. Nevertheless, the n $\rightarrow \pi^*$ character of the $S_0 \rightarrow S_1$ transition may negatively affect the light harvesting power of the material, since the oscillator strength is very low. In such cases, it can be considered the possibility to excite to a higher $S_0 \rightarrow S_n$ transition, which may relax to the desired S_1 state. Finally, it must be mentioned that 1,3-C(3+5)/QDM molecule shows a $S_0 \rightarrow S_1$ transition with $\sigma \rightarrow \pi^*$ character and the same is observed for the $S_0 \rightarrow T_1$ transition in 1,2-C(3+3)/Q. Nevertheless, these transitions are only 0.02 and 0.09 eV, respectively, lower than the $\pi \rightarrow \pi^*$ transition.

3.2. Singlet fission suitability

In this section, the feasibility of each group of molecules to be potential candidates as singlet fission sensitizers will be analyzed. First of all, those molecules with a moderate diradical character (less than 0.4) will be the main target of the discussion, since an intermediate diradical character has been found to be optimal for singlet fission.[34] Molecules with strong diradical character are not likely to be good candidates since the $2E[T_1]$-$E[S_1]$ values tend to be too negative (exoergic), reducing the efficiency of the process. All

values discussed in this section have been obtained at the TDDFT level.

The analysis of the SF performance will be done considering the energetic conditions $2E[T_1]-E[S_1]\leq 0$ and $2E[T_1]-E[T_2]<0$ discussed above, that will be referred as first (C1) and second (C2) conditions, respectively. It is experimentally seen that these conditions can be slightly relaxed, since tetracene, which is able to undergo SF, shows C1=0.14 eV and C2=0.07 eV. Therefore, in order to not exclude potential candidates, a margin of 0.2 eV will be introduced. In this manner, molecules with slightly positive C1 and C2 values will be also labeled as potential singlet fission sensitizers, as well as those molecules that could be discarded due excessive exoergicity. In the following, we will use C1 as the main criteria and C2 as a secondary condition.

From the 206 molecules studied, only 6 molecules have a quintet state (Q_1) below the energy of $2E[T_1]$, that may be a competitive state. Therefore, these molecules will be excluded from the analysis. Also, some other molecules such as 1,4-C(6+6+6)/Q, 1,2-C(6+6+6)/QDM and 1,2-C(5+5)/Q have a low energy Q_1, close to $2E[T_1]$, that may reduce the efficiency of the process and, therefore, will be also excluded. The graphical representation of the $2E[T_1]-E[S_1]$ and $2E[T_1]-E[T_2]$ energy differences are displayed in **Figure 79** and **Figure 80**. The computed $2E[T_1]-E[S_1]$ values for tetracene (0.14 eV) and pentacene (-0.42 eV) (red lines in **Figure 79**)

will be used as a guide to evaluate the SF suitability of the studied compounds.

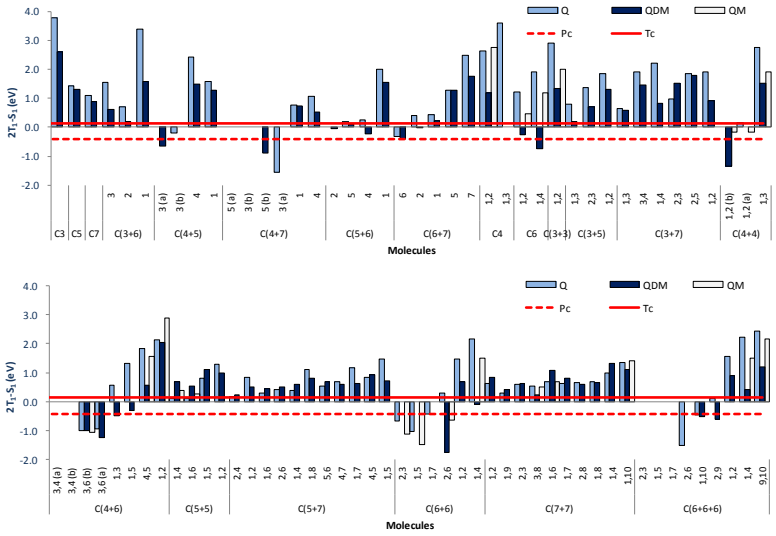

Figure 79: 2E[T_1]-E[S_1] energy differences values calculated with TDDFT, in eV, of the Q, QDM and QM systems. Red straight and dashed lines represent the values for tetracene and pentacene, respectively

Starting with the acene derivatives, in the *n,m*-C(6+6)/Q family, three molecules show negative values for the C1 and C2 conditions, namely, 2,3-, 1,5- and 1,7-derivatives. However, the C1 condition is too negative for the first two compounds and only 1,7-C(6+6) can be appointed as a good candidate for singlet fission. When the carbonyls are substituted by methylene groups, the diradical character is notably increased and three molecules should be rejected.

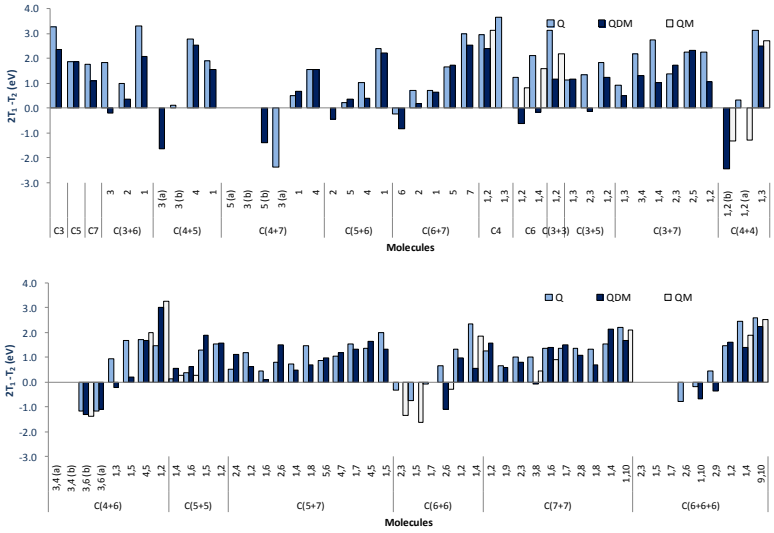

Figure 80: 2E[T_1]-E[T_2] energy differences values calculated with TDDFT, in eV, of the Q, QDM and QM systems.

From the remaining molecules, only the 2,6 isomer fulfills both conditions, but C1 is again too negative. Considering the QM group, too negative C1 values are recorded in general. Regarding the anthracene derivatives, *n,m*-C(6+6+6)/Q,QM,QDM, none of them accomplishes the conditions for several reasons: large y_0 values, positive C1 and C2 or too negative C1 values. Nevertheless, 1,10-C(6+6+6)/Q,QDM show values for C1 of -0.47 eV (Q) and -0.52 eV (QDM), rather close to the value of pentacene (-0.42 eV), and could eventually be considered as possible candidates. The enhancement of y_0 in QDM with respect to Q derivatives in the *n,m*-C6 family facilitates the fulfillment of the C1 condition in 1,2-C6/QDM. Analyzing the results from the SF-TDDFT calculations in the acenes and attending to their

$2E[T_1]$-$E[S_1]$ values (see **Table 46**), SF-TDDFT results suggest that 1,10-C(6+6+6)/Q should be also included in the list of candidates.

Amongst the family of explored compounds, 2,6-C(6+6)/Q [429] and derivatives of 1,7-C(6+6)/Q [430] and 1,5-C(6+6)/Q [431] have been synthesized, while 2,3-C(6+6)/Q [432] and 2,6-C(6+6+6)/Q[433] molecules have shown to be difficult to synthesize or isolate. The QM derivatives 2,3-, 1,5- and 2,6-C(6+6) have also been synthesized.[434,435] Finally, the *n,m*-C6/QDM molecules have also been found in the literature,[436] despite it is well known that they are very reactive. Molecules including a four-membered ring, such as *n*-C(4+5), *n*-C(4+7), *n,m*-C(4), *n,m*-C(4+4) or *n,m*-C(4+6), show high diradical character in most cases and, therefore, they are probably not good candidates for singlet fission, with the only exception of 3(b)-C(4+5)/Q.

On inspecting the molecules containing three-membered rings (*n*-C(3+6), *n,m*-C(3+3), *n,m*-C(3+5) and *n,m*-C(3+7)), none of them could be considered as potential candidates. A similar behavior is accounted for the families *n,m*-C(5+7) and *n,m*-C(7+7). In these examples, the diradical character is small or moderate, but the energetic conditions are not fulfilled. Nevertheless, it is important to notice that the 1,6-C(5+7)/Q compound has been isolated experimentally as a stable yellow crystalline solid,[437] and shows a C1 value close to that of tetracene. In the literature it is also possible to find experimental data for a derivative of the 2,6-C(5+7)/QM

molecule,[438] as well as some other derivatives.[439] Our results are not conclusive for 1,6- and 1,8-C(5+7)/Q, 1,4-C(5+7) (both Q and QDM) and 3,8-C(7+7) (both Q and QDM), since we find important discrepancies between the TDDFT and the SF-TDDFT computed energies. This disagreement has been also obtained for the *n,m*-C(5+5) family, where some of them are classified as good candidates by SF-TDDFT (1,4- and 1,6-C(5+5)/QDM), while they should be discarded using TDDFT. It must be highlighted that 1,4-C(5+5)/Q accomplishes both C1 and C2 conditions and has been synthesized.[440] None of the molecules within the *n*-C(5+6)/Q family shows promising interstate energy gaps. However, in the QDM derivatives, 2-, 4- and 5-C(5+6) fulfill the C1 condition, while in certain cases the T_2 state is placed excessively low. Thus, only 2-C(5+6) isomer (isobenzofulvene) seems to be appropriated to host singlet fission. This compound has been experimentally described[441] as a blue compound that easily dimerizes at low temperatures.

Other molecules from this family are also experimentally available, as 1-C(5+6)/QDM (benzofulvene[442]) and 1-C(5+6)/Q (indenone[443,444]), but should be discarded. Regarding the C(6+7) family, three molecules can be considered as potential candidates: 6-C(6+7)/Q,QDM and 2-C(6+7)/QDM. Among them, the carbonyl 6-C(6+7)/Q should be highlighted, as it can be found in the literature[445] as an orange compound that easily dimerizes in solution.

3.3. Summary and conclusions

In this section, the electronic and structural properties of 206 conjugated carbonyl (quinone, Q), methylene (quinone dimethane, QDM) and mixed (quinone methide, QM) derivatives have been analyzed including the diradical character, singlet-triplet gap, low-lying excited states and their feasibility to undergo singlet fission, for the pursuit of new singlet fission sensitizers that may improve the performance of archetype molecules such as tetracene and pentacene.

As it was investigated in Chapter 4, an important number of the studied molecules show a non-negligible diradical character, which is mainly affected by the nature of the substituents and their relative position. Thus, methylene moieties enhance the diradical character at a greater extent than the carbonyl ones and the following trend is observed: y_0(QDM) > y_0(QM) > y_0(Q). This characteristic affects the electronic structure of the ground and excited states and has implications in the possibilities of the molecules to undergo singlet fission. As it was previously known,[34] an intermediate diradical character is optimal for singlet fission, that is, the fulfillment of the energetic conditions $2E[T_1]-E[S_1] \leq 0$ (C1) and $2E[T_1]-E[T_2] < 0$ (C2) is favored. Besides, larger diradical characters imply a shift of the absorption energy to larger wavelengths, from UV to visible or even near-IR, which may be useful for the design of new optical devices.

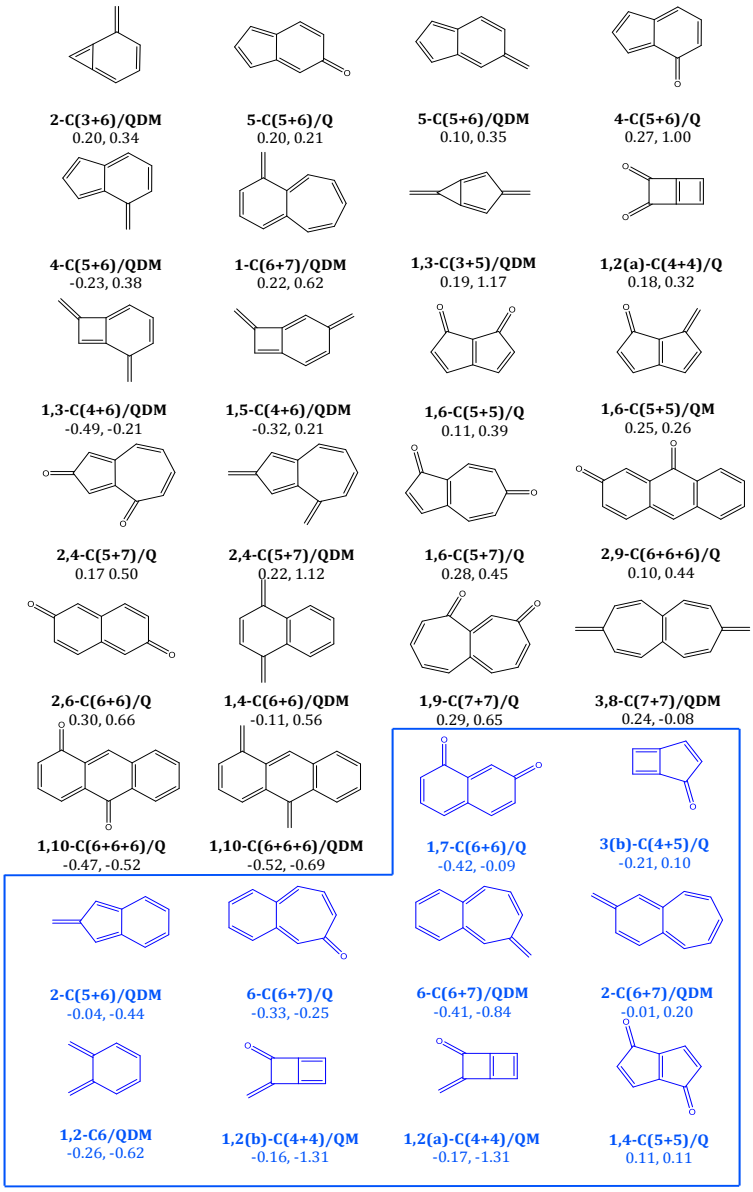

Figure 81: Set of promising candidates to undergo an efficient singlet fission process. In black, those molecules that fulfill only the condition: -0.62 eV < C1 < 0.34 eV (C2 may be positive). In blue, those molecules that also fulfill the conditions: -0.42 eV ≤ C1 ≤ 0.14 eV and C2 ≤ 0.2 eV.

The character of the $S_0 \rightarrow S_1$ and $S_0 \rightarrow T_1$ transitions of the QDM molecules is $\pi \rightarrow \pi^*$, while in some carbonyl-containing molecules (51 Q and 10 QM) these transitions show $n \rightarrow \pi^*$ character. This feature is relevant for the selection of a suitable singlet fission sensitizer, since the $n \rightarrow \pi^*$ transitions appear, in general, at lower energies than the $\pi \rightarrow \pi^*$ transitions, which, in some cases, may help to fulfill the energetic conditions

From the total set of 206 molecules discussed on this section, 48 molecules are predicted to fulfill the first condition using TDDFT. However, for those molecules with a remarkable diradical character, this value is often too negative, which may be related to a loss of efficiency. Hence, using the tetracene and pentacene values as boundaries for the first condition, up to 15 molecules can be selected with a C1 in between 0.14 and -0.42 eV. If we expand these boundary values just 0.2 eV, up to 32 molecules can be taken into account, which are represented in **Figure 81**. Besides, 12 of these molecules can be found in the literature as experimentally available, although sometimes as very reactive intermediates. Out of these 32 molecules, 10 fulfill the following, more restrictive conditions: $-0.42\ eV \leq C1 \leq 0.14\ eV$ and $C2 \leq 0.2\ eV$. Namely, 1,7-C(6+6)/Q, 3(b)-C(4+5)/Q, 2-C(5+6)/QDM, 6-C(6+7)/Q, 6-C(6+7)/QDM, 2-C(6+7)/QDM, 1,2-C6/QDM, 1,2(a,b)-C(4+4)QM and 1,4-C(5+5)/Q, which are highlighted with blue color in **Figure 81**. Some of this molecules have been experimentally obtained, i.e. 1,7-

C(6+6)/Q, 6-C(6+7)/Q, 2-C(5+6)/QDM and 1,2-C6/QDM. It is worth noting that a derivative of 1,2-C6/QDM was already proposed as a potential SF sensitizer,[32] and it has been experimentally shown to undergo efficient singlet fission.[446,447,448]

In this manner, these systems can open new avenues for understanding singlet fission and be used to develop new SF sensitizers that may improve the performance of tetracene and pentacene.

4. Effect of structural modifications

Only a few of the whole set of molecules presented in the previous section have been experimentally synthesized. It is well known that unstable molecules with large diradical character can be stabilized by means of structural modifications, such as the addition of substituents, heteroatoms, etc. For instance, Nishida obtained stable derivatives of the 1,5-C(6+6+6) structure,[204] showing intense absorption in the visible region, with maxima at 2.14 eV. Using TDDFT and SF-TDDFT calculations, this value is calculated to be 2.32 and 2.68 eV, respectively. The obtained $2E[T_1]$-$E[S_1]$ values are -1.38 (TDDFT) and -1.61 eV (SF-TDDFT), far from the reference value of pentacene. For comparison, the $E[S_1]^{SF\text{-}TDDFT}$ has been calculated to be 2.10 eV for the unsubstituted 1,5-C(6+6+6) molecule, leading to $2E[T_1]$-$E[S_1]$=-2.12 eV, that is, 0.51 eV more exoergic.

Thus, the introduction of chemical modifications may help in the design of singlet fission materials in which the optical features can be tuned to enhance the efficiency of the process. Following the same scheme as in previous chapters, the proposed structural modifications are: i) substitution of the oxygen of the carbonyl group, ii) inclusion of heteroatoms in the aromatic rings, iii) addition of substituents in different positions in the rings and iv) increase of the number of rings. The calculations in the present section have been performed with SF-TDDFT instead of TDDFT due to the high spin contamination present in such open-shell structures.

4.1. Substitution of the oxygen of the carbonyl group

In this subsection, the oxygen atoms in 1,5-C(6+6+6)/Q molecule will be replaced by atoms of groups 13, 14, 15 and 16 of period 1 (B, C, N, O), period 2 (Al, Si, P, S) and period 3 (Ga, Ge, As, Se). The required H atoms are included to maintain the double bond conjugation (see Chapter 4). Besides, further modifications have been performed to include the following moieties: CF_2, CCl_2, CBr_2, CF_2, $C(CH_3)_2$ and $C(CN)_2$.

The numerical values of the low-lying excited states ($E[S_1]$, $E[T_1]$, $E[T_2]$ and $E[Q_1]$), as well as the $2E[T_1]$-$E[S_1]$ and $2E[T_1]$-$E[T_2]$ energy differences used to evaluate the C1 and C2 conditions, are gathered in **Table 49**. For period 1, $E[S_1]$ increases with the atomic number. This behavior was already

observed when comparing the Q and QDM molecules in previous sections. Those molecules containing elements from periods 2 and 3 show a more irregular behavior, with an increase from group 13 to 14 and then a decreasing trend for the rest of the groups. Besides, atoms with lone pairs allow the existence of low-lying n $\rightarrow \pi^*$ transitions, such as in the amino (NH_2) derivative.

Table 49: Energies of the first singlet ($E[S_1]$) and two triplet ($E[T_1]$ and $E[T_2]$) excited states, and the $2E[T_1]$-$E[S_1]$ (C1) and $2E[T_1]$-$E[T_2]$ (C2) energy conditions, in eV, calculated with SF-TDDFT. $E[Q_1]$ and $E[T_1]^{DFT}$ have been calculated with DFT.

		$E[S_1]$	$E[T_1]$	$E[T_1]^{DFT}$	$E[T_2]$	$E[Q_1]$	$2E[T_1]$-$E[S_1]$	$2E[T_1]$-$E[T_2]$
1,5-C(6+6+6)/Q		2.10	-0.01	0.42	0.70	4.07	-2.12	-0.72
PERIOD1	BH	0.89	-0.60	0.00	0.00	1.83	-2.09	-1.20
	CH2	1.47	-0.51	0.18	0.31	2.97	-2.49	-1.33
	NH	1.78	-0.36	0.27	0.48	3.33	-2.50	-1.20
	O	2.10	-0.01	0.42	0.70	4.07	-2.12	-0.72
PERIOD2	AlH	1.77	-0.31	0.00	0.00	2.03	-2.39	-0.62
	SiH2	2.36	-0.41	0.01	0.01	2.20	-3.17	-0.82
	PH	1.29	-0.52	0.05	0.05	2.41	-2.34	-1.10
	S	0.61	-0.23	0.02	0.36	2.57	-1.08	-0.82
PERIOD3	GaH	1.74	-0.16	0.00	0.00	2.02	-2.06	-0.32
	GeH2	2.40	-0.29	0.01	0.01	2.19	-2.99	-0.60
	AsH	1.50	-0.40	0.04	0.04	2.32	-2.30	-0.84
	Se	0.28	-0.29	0.44	0.21	2.22	-0.86	-0.80
CH_2	CF_2	1.67	-0.39	0.25	0.45	3.23	-2.44	-1.22
Deriv.	CCl_2	1.45	-0.46	0.19	0.35	2.97	-2.37	-1.26
	CBr_2	1.50	-0.43	0.20	0.35	3.04	-2.35	-1.21
	$C(CH_3)_2$	1.44	-0.45	0.20	0.34	2.98	-2.35	-1.24
	$C(CN)_2$	1.40	-0.42	0.16	0.28	2.81	-2.23	-1.12

In **Table 49** it is observed that all these molecules show a triplet ground state. Nevertheless, this feature may be ascribed to a previously observed additional stabilization of the triplet states accounted for by SF-TDDFT. Thus, the

calculation of the $E[T_1]^{DFT}$ values points to singlet ground states, although for those derivatives containing Al, Si, Ga or Ge, almost degenerated singlet and triplet states are observed.

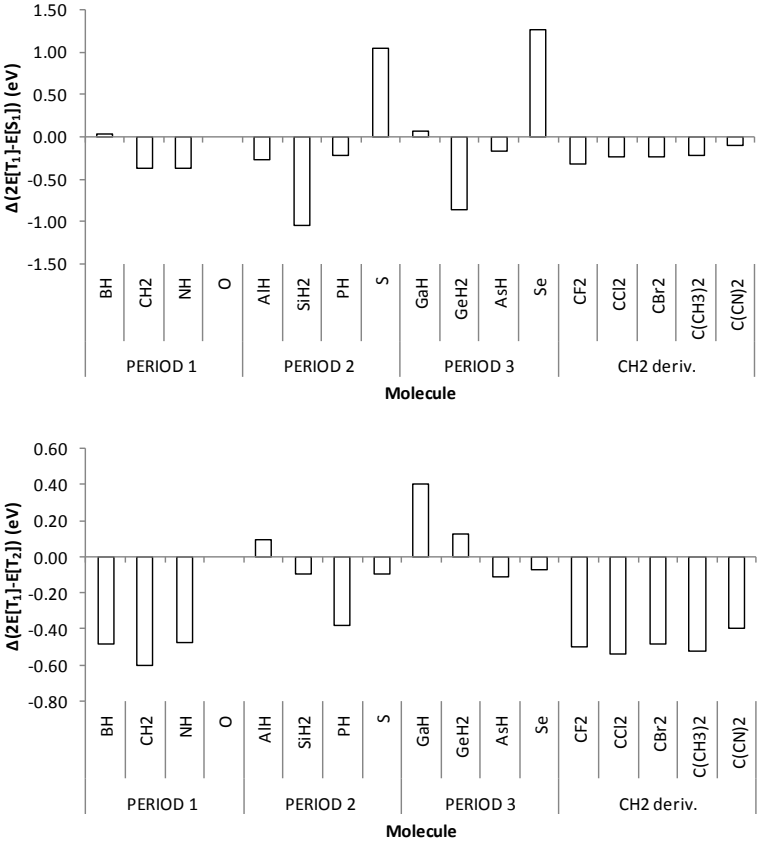

Figure 82: Variation of the $2E[T_1]$-$E[S_1]$ and $2E[T_1]$-$E[T_2]$ energy differences with respect to the 1,5-C(6+6+6) molecule, in eV, calculated with SF-TDDFT

Hence, substitution of oxygen leads to a diminution of the $2E[T_1]$-$E[S_1]$ energy difference (see **Figure 82**), with the

exception of sulfur and selenium atoms, while for boron a slight increase is found. The reduction on the $2E[T_1]$-$E[S_1]$ value upon substitution with nitrogen is very similar to that of the methylene moiety. In the other hand, for silicon and germanium more negative shifts are observed. Finally, small variations are accounted for the CF_2, CCl_2, CBr_2, CF_2, $C(CH_3)_2$ and $C(CN)_2$ groups with respect to 1,5-C(6+6+6)/Q. In that manner, the only substitutions able to shift the $2E[T_1]$-$E[S_1]$ energy difference close to those of tetracene and pentacene are sulfur and selenium (see **Figure 83**).

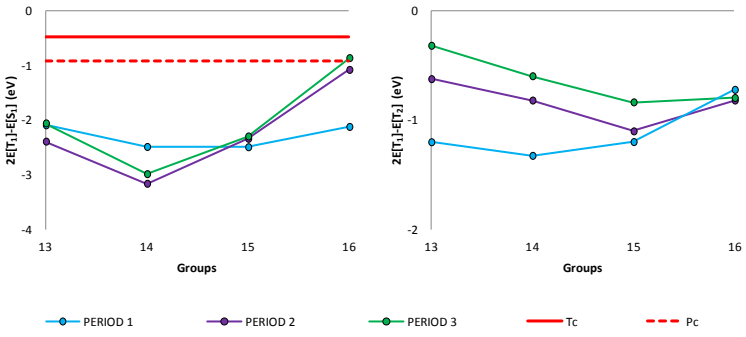

Figure 83: $2E[T_1]$-$E[S_1]$ (left) and $2E[T_1]$-$E[T_2]$ (right) energy differences, in eV, calculated with SF-TDDFT. Red straight and dashed lines represent the values for tetracene and pentacene, respectively. In the X axis are represented the groups from the periodic table.

4.2. Insertion of heteroatoms in the aromatic ring

As in previous chapters, B, N, Si and P atoms are inserted into the 1,5-C(6+6+6)/Q molecule (see Chapter 4), using the same nomenclature: α (heteroatoms in positions 2

and 6), β (positions 3 and 7), γ (positions 4 and 8) and δ (positions 9 and 10).

Table 50: Energies of the first singlet ($E[S_1]$) and two triplet ($E[T_1]$ and $E[T_2]$) excited states, and the $2E[T_1]$-$E[S_1]$ (C1) and $2E[T_1]$-$E[T_2]$ (C2) energy conditions, in eV, calculated with SF-TDDFT. $E[Q_1]$ has been calculated with DFT.

		$E[S_1]$	$E[T_1]$	$E[T_2]$	$E[Q_1]$	$2E[T_1]$-$E[S_1]$	$2E[T_1]$-$E[T_2]$
1,5-C(6+6+6)/Q		2.10	-0.01	0.70	4.07	-2.12	-0.72
α	**N**	2.26	0.48	1.13	4.22	-1.29	-0.16
	B	1.73	0.02	0.60	3.68	-1.68	-0.55
	P	1.64	-0.05	0.54	3.37	-1.75	-0.64
	Si	1.40	-0.43	0.16	3.41	-2.26	-1.01
β	**N**	1.64	-0.22	0.54	3.25	-2.08	-0.98
	B	2.30	0.68	1.25	4.01	-0.93	0.12
	P	2.07	0.33	1.02	3.71	-1.42	-0.37
	Si	2.18	0.72	1.29	3.98	-0.73	0.16
γ	**N**	2.12	0.44	1.20	4.37	-1.24	-0.31
	B	1.27	0.09	0.59	4.30	-1.10	-0.41
	P	2.21	-0.08	0.52	3.83	-2.37	-0.67
	Si	2.01	-0.18	0.31	3.60	-2.37	-0.66
δ	**N**	1.65	-0.28	0.51	2.83	-2.21	-1.06
	B	1.81	0.89	1.48	2.92	-0.02	0.31
	P	1.69	0.24	0.90	2.99	-1.22	-0.43
	Si	2.13	0.78	1.34	2.83	-0.56	0.23

The energies of the low-lying excited states are gathered on **Table 50**, as well as the $2E[T_1]$-$E[S_1]$ and the $2E[T_1]$-$E[T_2]$ energy differences. Besides, the variation of $2E[T_1]$-$E[S_1]$ and the $2E[T_1]$-$E[T_2]$ with respect to the 1,5-C(6+6+6)/Q reference molecule is represented in **Figure 84**, while the C1 and C2 values have been plotted together with those of tetracene and pentacene (see **Figure 85**).

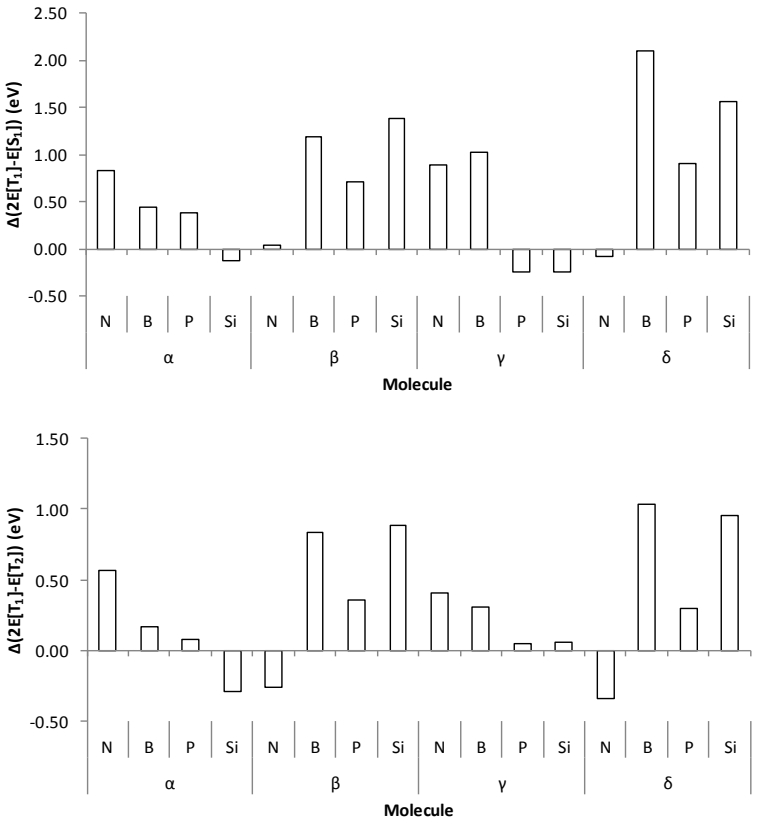

Figure 84: Variation of the $2E[T_1]$-$E[S_1]$ and $2E[T_1]$-$E[T_2]$ energy differences with respect to the 1,5-C(6+6+6) molecule, in eV, calculated with SF-TDDFT.

It is observed a general lowering of $E[S_1]$ compared to the unsubstituted 1,5-C(6+6+6)/Q. The only molecules that show an enhancement of $E[S_1]$ are: N in α position, B and Si in β position, N and P in γ position and Si in δ position. This behavior cannot be easily related to the trend observed in the diradical character. For instance, the substitution of P in β positions drastically reduces the diradical character (see

Figure 23, Chapter 4), so an enhancement of $E[S_1]$ is expected, while it remains basically unaffected.

Similarly, the molecule containing boron on γ position shows a large decrease of $E[S_1]$, while the diradical character is slightly modified.

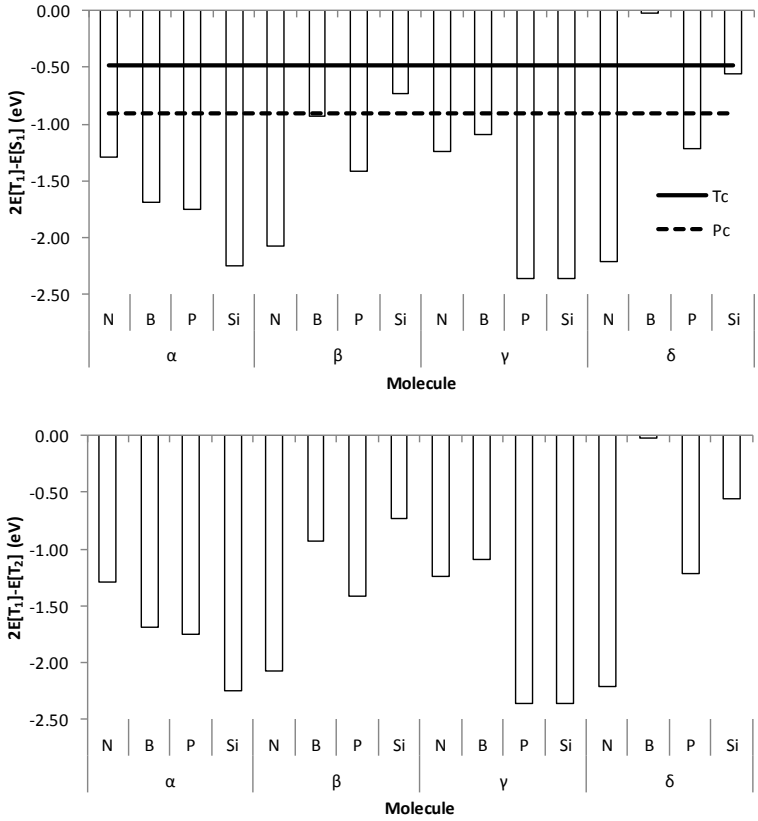

Figure 85: $2E[T_1]$-$E[S_1]$ and $2E[T_1]$-$E[T_2]$ energy differences, in eV, calculated with SF-TDDFT. Black straight and dashed lines represent the values for tetracene and pentacene, respectively.

Table 51: Energies of the first singlet ($E[S_1]$) and two triplet ($E[T_1]$ and $E[T_2]$) excited states, and the $2E[T_1]$-$E[S_1]$ (C1) and $2E[T_1]$-$E[T_2]$ (C2) energy conditions, in eV, calculated with SF-TDDFT. $E[Q_1]$ has been calculated with DFT.

		$E[S_1]$	$E[T_1]$	$E[T_2]$	$E[Q_1]$	$2E[T_1]$-$E[S_1]$	$2E[T_1]$-$E[T_2]$
1,5-AQ		2.10	-0.01	0.70	4.07	-2.12	-0.72
α	CF_3	2.19	0.09	0.77	4.11	-2.01	-0.59
	CN	1.95	-0.06	0.63	4.06	-2.07	-0.75
	CH_3	2.02	-0.01	0.66	4.09	-2.04	-0.68
	OCH_3	1.72	-0.23	0.38	3.53	-2.19	-0.85
	OH	1.85	-0.07	0.51	3.63	-2.00	-0.65
	NH_2	1.88	0.04	0.52	3.45	-1.81	-0.45
β	CF_3	2.01	-0.04	0.73	3.97	-2.08	-0.80
	CN	1.96	-0.06	0.70	3.87	-2.08	-0.82
	CH_3	2.19	0.15	0.84	4.16	-1.89	-0.53
	OCH_3	2.44	0.56	1.17	4.33	-1.33	-0.05
	OH	2.31	0.44	1.07	4.24	-1.42	-0.18
	NH_2	2.11	0.56	1.17	4.08	-0.98	-0.04
γ	CF_3	1.82	-0.16	0.61	3.96	-2.14	-0.92
	CN	1.90	-0.16	0.61	3.88	-2.21	-0.93
	CH_3	2.01	-0.17	0.52	3.93	-2.36	-0.87
	OCH_3	2.03	-0.28	0.35	3.85	-2.59	-0.91
	OH	2.07	-0.20	0.44	3.86	-2.47	-0.84
	NH_2	2.06	-0.17	0.37	3.75	-2.40	-0.71
δ	CF_3	1.99	-0.04	0.75	3.60	-2.07	-0.84
	CN	1.86	-0.10	0.63	3.18	-2.07	-0.84
	CH_3	2.32	0.34	1.00	3.89	-1.64	-0.31
	OCH_3	1.67	0.22	1.34	3.82	-1.23	-0.90
	OH	2.32	0.57	1.23	3.83	-1.19	-0.09
	NH_2	2.34	1.25	1.73	4.00	0.15	0.76
ε	CF_3	1.71	-0.58	0.29	3.14	-2.86	-1.44
	CN	1.55	-0.29	0.53	2.88	-2.13	-1.12
	CH_3	2.12	0.35	0.96	3.66	-1.43	-0.27
	NH_2	2.34	0.87	1.28	3.77	-0.60	0.45

In the chapter devoted to the diradical character, it was noticed how this feature depends not only on the nature but also in the position of the heteroatom. In that manner, the

nitrogen was able to enhance the diradical character in positions β or δ and reduce it in positions α and γ, while the reversed effect was noted in the rest of the elements.

The trends observed in the $E[T_1]$ energies can be related with those accounted for the diradical character, and those molecules that enhance their diradical character after the substitution have also lower singlet-triplet gap. Some examples can be cited, as Si in positions α and γ, or N in positions β or δ.

The variation of the $2E[T_1]$-$E[S_1]$ and $2E[T_1]$-$E[T_2]$ energy differences (see **Figure 84**) describes a general shift to more positive values (especially for B and Si in β or δ positions), that could be interesting to reduce the large exoergicity observed in systems such as 1,5-C(6+6+6)/Q. Thus, only Si (α and γ positions), P (γ position) and N (α position) induce more negative C1 values. Four of the investigated molecules can be emphasized, with C1 conditions close to the limits of tetracene and pentacene (see **Figure 85**): molecules with B and Si in β position, the one with B in γ and the molecule with Si in δ position. It is remarkable how the molecule with B in δ position greatly reduces the exoergicity in C1, from the original -2.12 eV value of 1,5-C(6+6+6)/Q to only -0.02 eV. As a consequence, this can be an option to tune the C1 requirement to improve the SF process, with minimum energy losses. Nevertheless, this molecule shows a somewhat too positive C2 value.

Similar variations were accounted for the C2 condition; while most of the molecules show negative values, as required, some of them are shifted to positive values, such as those molecules with B and Si β position, B in γ and B and Si in δ.

4.3. Effect of the addition of substituents

The effect that the electron-withdrawing (CF_3 and CN) and the electron-donating groups (OH, OCH_3, CH_3 and NH_2) may introduce in the low-lying excited states is analyzed in this section. These substitutions were performed in α, β, γ, and δ positions, while the ε label stands for the totally substituted molecule, using only CF_3, CN, CH_3 and NH_2.

In the literature can be found some examples in which the low-lying states of diradicaloid molecules are modified by substitution. For instance, the absorption energy of oligothiophenes[181] and squarates[382] is redshifted upon the introduction of OH groups

As it was previously noticed, the nature has a secondary importance compared to the position of the substitution, in such a way that the substitutions in α and γ yield, in most of cases, to a slight enhancement of the diradical character, while the substitutions in β and δ positions accomplish a diminution of this feature. Inspecting **Table 51**, where the values of $E[S_1]$ and $E[T_1]$ are collected, it is observed that the substituents (both EWG and EDG) in α and

γ positions decrease the energies of both the singlet and the triplet, while the opposite effect is noticed when the substitution is on β and δ positions, as expected from the variation of y_0. This trend is more irregular in the $E[S_1]$ energies.

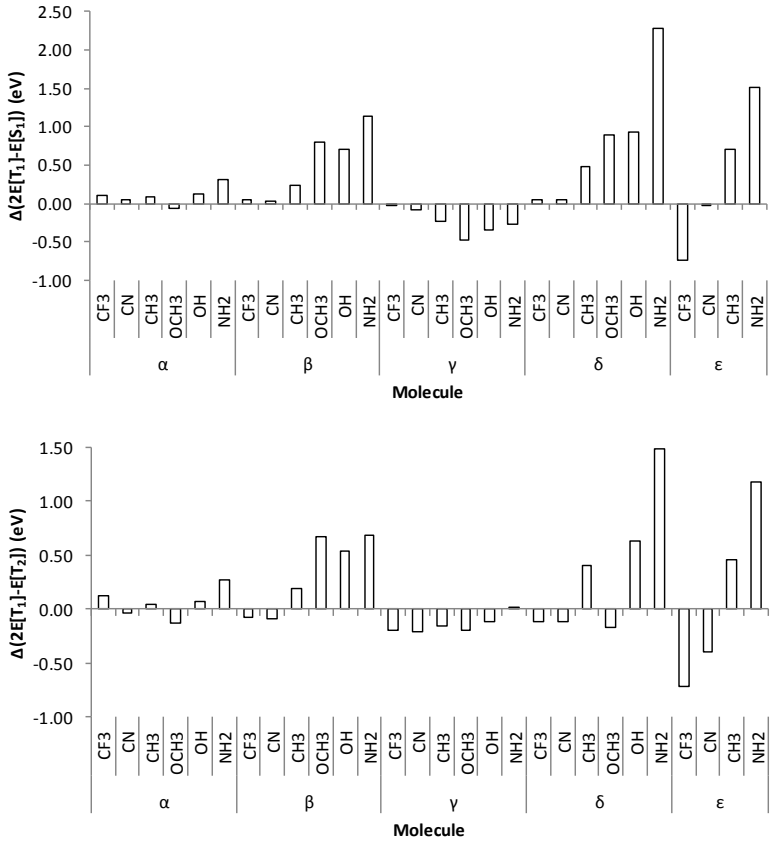

Figure 86: Variation of the $2E[T_1]$-$E[S_1]$ and $2E[T_1]$-$E[T_2]$ energy differences with respect to the 1,5-C(6+6+6) molecule, in eV, calculated with SF-TDDFT.

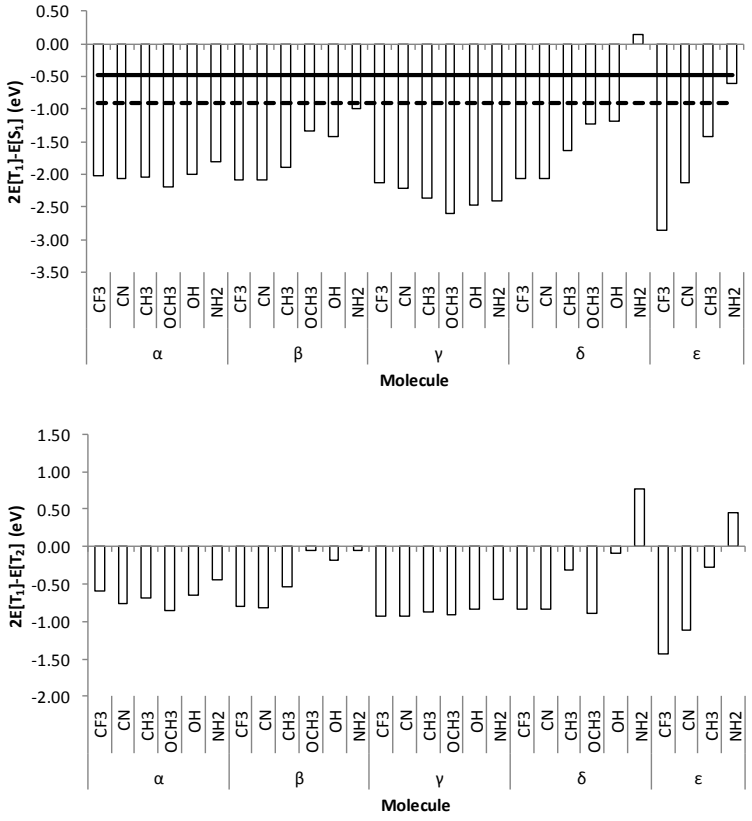

Figure 87: $2E[T_1]$-$E[S_1]$ and $2E[T_1]$-$E[T_2]$ energy differences, in eV, calculated with SF-TDDFT. Black straight and dashed lines represent the values for tetracene and pentacene, respectively.

Regarding the $2E[T_1]$-$E[S_1]$ and the $2E[T_1]$-$E[T_2]$ energy differences (see **Figure 86** and **Figure 87**), EWG groups show little effect in the C1 condition, independently of the position. Additionally, the effect of the substitution in α is also very small. The EDGs placed in β or δ positions shift C1 to more positive values, especially for the NH_2 group. It is important to note that the NH_2 group in δ position forms a

hydrogen bond with the carbonyl group, in a six-membered ring, which may have as a consequence a closed-shell structure and, then, shifting C1 to more positive values.Finally, the ε-substitution with EWD groups causes a shift of C1 to more negative values, while EDG groups shift that parameter to more positive values.

Comparing with the $2E[T_1]$-$E[S_1]$ value of 1,5-C(6+6+6)/Q (-2.12 eV), we may highlight the following molecules that show a less exoergic value: NH_2 in β, δ and ε, nevertheless the last two show positive C2 values (0.76 and 0.45 eV, respectively). Other promising molecules may be: OCH_3 and OH in δ positions, with C1 values close to -1 eV and negative C2 values.

4.4. Increase of the number of fused rings

In Chapter 4, thirty molecules were designed adding aromatic rings to the backbone of six different naphthoquinones and it was noted an enhancement of y_0 with the number of fused rings, although it was also related to the relative position of the carbonyl groups.

Table 52: Energies of the first singlet ($E[S_1]$) and two triplet ($E[T_1]$ and $E[T_2]$) excited states, and the $2E[T_1]$-$E[S_1]$ (C1) and $2E[T_1]$-$E[T_2]$ (C2) energy differences, in eV, calculated with SF-TDDFT. $E[Q_1]$ has been calculated with DFT.

		$E[S_1]$	$E[T_1]$	$E[T_2]$	$E[Q_1]$	$2E[T_1]$-$E[S_1]$	$2E[T_1]$-$E[T_2]$
Acenes	**2**	3.93	2.92	3.49	7.29	1.92	2.36
	3	3.47	1.95	2.46	6.46	0.43	1.45
	4	2.96	1.24	1.76	5.27	-0.48	0.72
	5	2.42	0.76	1.28	4.04	-0.91	0.24
	6	1.99	0.31	0.85	3.03	-1.36	-0.22
1,2	**2**	2.92	2.14	2.73	5.29	1.36	1.55
	3	3.11	2.16	2.77	4.43	1.21	1.55
	4	2.95	2.22	2.58	3.68	1.48	1.86
	5	2.33	1.24	1.74	3.14	0.14	0.73
	6	2.17	0.78	1.29	2.74	-0.60	0.28
1,4	**2**	3.39	2.74	3.43	6.76	2.09	2.04
	3	3.56	2.61	3.03	5.14	1.66	2.19
	4	2.95	2.27	2.66	4.34	1.59	1.87
	5	2.33	2.03	2.41	3.78	1.73	1.64
	6	1.89	1.86	2.25	3.38	1.84	1.48
1,5	**2**	2.28	0.73	1.38	4.98	-0.83	0.07
	3	2.10	-0.01	0.70	4.07	-2.12	-0.72
	4	1.60	-0.32	0.41	2.71	-2.24	-1.05
	5	1.15	-0.47	0.29	1.99	-2.09	-1.23
	6	0.79	-0.55	0.25	1.49	-1.89	-1.35
1,7	**2**	2.35	0.95	1.62	5.06	-0.46	0.27
	3	2.21	0.45	1.12	3.80	-1.32	-0.23
	4	1.87	-0.09	0.63	2.72	-2.06	-0.82
	5	1.34	-0.36	0.46	2.08	-2.06	-1.18
	6	1.12	-0.38	0.50	1.61	-1.88	-1.27
2,3	**2**	2.05	0.33	0.93	3.86	-1.38	-0.27
	3	1.33	-0.50	0.15	2.91	-2.33	-1.15
	4	1.15	-0.66	0.02	2.53	-2.46	-1.33
	5	1.14	-0.65	0.04	1.92	-2.44	-1.34
	6	0.83	-0.60	0.10	1.47	-2.03	-1.29
2,6	**2**	3.17	2.37	2.79	5.11	1.58	1.96
	3	2.45	1.93	2.36	3.84	1.41	1.49
	4	2.00	0.24	0.94	2.83	-1.53	-0.47
	5	1.64	-0.09	0.65	2.19	-1.82	-0.83
	6	1.26	-0.29	0.50	1.73	-1.83	-1.08

In **Table 52** are gathered the numerical values of the low-lying excited states, as well as the $2E[T_1]$-$E[S_1]$ and $2E[T_1]$-$E[T_2]$ energy differences for these 30 molecules. In **Figure 88** is represented the evolution of $E[S_1]$ and $E[T_1]$ as the size of the carbon backbone grows, compared with the acenes, from naphthalene to hexacene, and a general decreasing trend is observed.

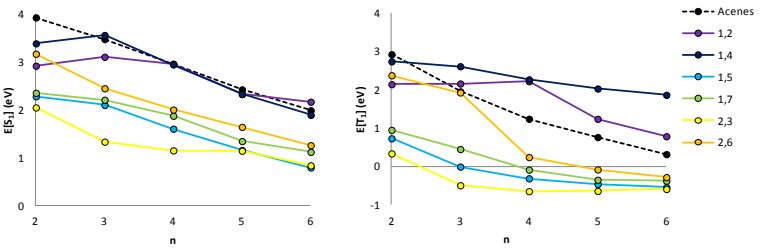

Figure 88: Variation of the first singlet ($E[S_1]$, left) and triplet ($E[T_1]$, right) excited states with the number of rings (*n*), in eV, at the SF-TDDFT level of theory.

The 1,2- and 1,4-substituted quinones, which are mainly closed-shell molecules, show almost the same $E[S_1]$ values than the corresponding acene for n>3, while for n=2,3 the energy gap is lower than in naphthalene and anthracene. The carbonyl groups placed in 1,5, 1,7, 2,3 and 2,6 positions lower $E[S_1]$, in accordance to a larger y_0 value than the parent acenes, following the trend: 2,6 > 1,7 > 1,5 > 2,3. The changes accounted for $E[T_1]$ are also in accordance with the variation of y_0. Thus, the lowest values are observed in the open-shell 1,5, 1,7, 2,3 and 2,6 derivatives. The fact that

some molecules show a triplet ground state may be ascribed to the SF-TDDFT method, which may underestimate the energy of the triplet, since the results obtained with DFT show that all the molecules have a singlet ground state.

In **Figure 89**, the variation of the C1 and C2 energy conditions is represented. As expected, the open-shell 1,5, 1,7 and 2,3 derivatives have negative C1 values, from n=2 to n=6, while for 2,6 is only exoergic for n>3 molecules. However, these values may be considered too exoergic, except for 1,5 and 1,7 molecules with n=2. In the other hand, 1,2 and 1,4 molecules show positive C1 values although, in the 1,2-quinones, C1 becomes more negative in larger structures, in such a way that, for n=6, a convenient value for C1 is obtained. All the 1,4-quinones have C1≈2 eV, independently of the molecular size. Nevertheless, using TDDFT calculations, both 1,4 and 1,2 derivatives show similar behavior.

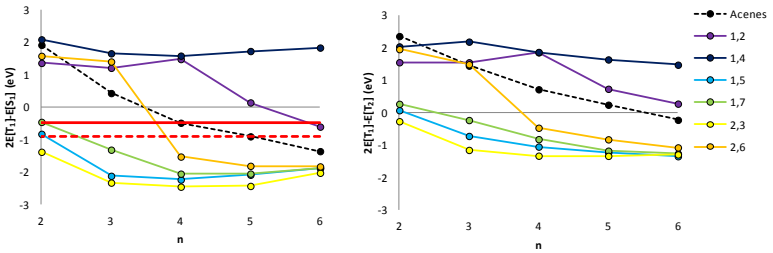

Figure 89: Variation of the $2E[T_1]$-$E[S_1]$ (C1) and $2E[T_1]$-$E[T_2]$ (C2) energy differences with the number of rings (*n*), in eV, at the SF-TDDFT level of theory. Red straight and dashed lines represent the values for tetracene and pentacene, respectively.

Regarding the second energy condition, 1,5, 1,7 and 2,3 derivatives show C2<0 for any value of n (slightly positive values are calculated for 1,5 and 1,7) and 2,6 derivative for n>3. For 1,2 with n=6 is slightly positive.

As a conclusion, the only molecules we may highlight as promising singlet fission sensitizers, using the tetracene and pentacene as references, are the 1,5- and 1,7-naphthoquinones (n=2), and the 1,7-anthraquinone (n=3). These molecules were already analyzed in section 3 by means of TDDFT and the same conclusion was obtained, except for 1,7-naphthoquinone, for which the spin contamination precluded its analysis. Besides, 2,6 derivatives for n=4-6, as well as 2,3- and 1,7-hexaquinone (n=6) show C1 values not exaggeratedly exoergic (≥ -2 eV) and could be considered as potential candidates for singlet fission

4.5. Summary and conclusions

In this section, we have analyzed the variation of the low-lying excited states after structural modifications, such as substitution of the oxygen in the carbonyl group, insertion of heteroatoms in the aromatic rings, addition of substituents and increase of the number of fused rings

As it was observed in section 3, the energy of the excited $E[S_1]$ and $E[T_1]$ states is decreased with larger y_0. Additionally, both the $2E[T_1]$-$E[S_1]$ (C1) and $2E[T_1]$-$E[T_2]$ (C2) energy conditions are more negative on strongly open-shell

structures. These trends are also recorded in this section, although some irregular behavior is observed. Finally, the quintet state could be a competing state in some cases, still already discarded due to a positive C1.

In summary, the C1 condition of a particular quinoid molecule may be tuned in many ways, in order to fulfill the requirements for an efficient SF process. Thus, the following molecules can be underlined as potential candidates for singlet fission:

- 1,5-C(6+6+6)/Q with the oxygen of the carbonyl substituted by S and Se
- 1,5-C(6+6+6)/Q with B in γ and β, as well as Si in β and δ positions of the backbone.
- 1,5-C(6+6+6+)/Q with an NH_2 group in β, δ or ε positions, as well as OCH_3 and OH groups in δ position.
- 2,6 dicarbonyl in tetracene, pentacene and hexacene (n=4-6), and the 2,3 and 1,7 dicarbonyls in hexacene (n=6)

5. Other diradical structures

Plenty of singlet open-shell molecules have been proposed in Chapter 4, and many of them have been studied in the literature, either experimentally or theoretically. However, for most of them, there is still a lack of information about their low-lying excited states, and their suitability to be

used as singlet fission materials is unknown. Thus, this section is focused in the calculation and analysis of the $S_0 \rightarrow S_1$, $S_0 \rightarrow T_1$ and $S_0 \rightarrow T_2$ transitions, and to evaluate the $2E[T_1]$-$E[S_1]$ and $2E[T_1]$-$E[T_2]$ energetic conditions (C1 and C2) to provide with a set of new promising candidates to be singlet fission sensitizers.

5.1. Croconate and squarate dyes

The optical activity of diradical croconate [449] and squarate[450,451] dyes has been extensively studied during the last decades due to the intense color and the narrow and strong band they present in the red to near-infrared (NIR) region of the absorption spectra, so that they have become very popular in the photovoltaic field.[212,222,223,224,225,226,227,452,453,454] For instance, in the design of dye-sensitized solar cells that could extend the range of absorption from the visible to the NIR,[380,455] enhancing the efficiency of the sunlight harvesting mechanism. Thus, both theoretical and experimental values for the singlet-singlet transition energies are available in the literature,[234,237,456,457] and it is well known that the presence of donor or acceptor moieties on the backbone,[386] π-conjugation,[458,459,460,461,462] or heavy atoms[463] may lead to modifications in the absorption energy. Additionally, it was observed that the introduction of alkoxy groups on squarate moieties could modify the crystal packaging,[382] which can be important for the consecution of an efficient singlet fission process.

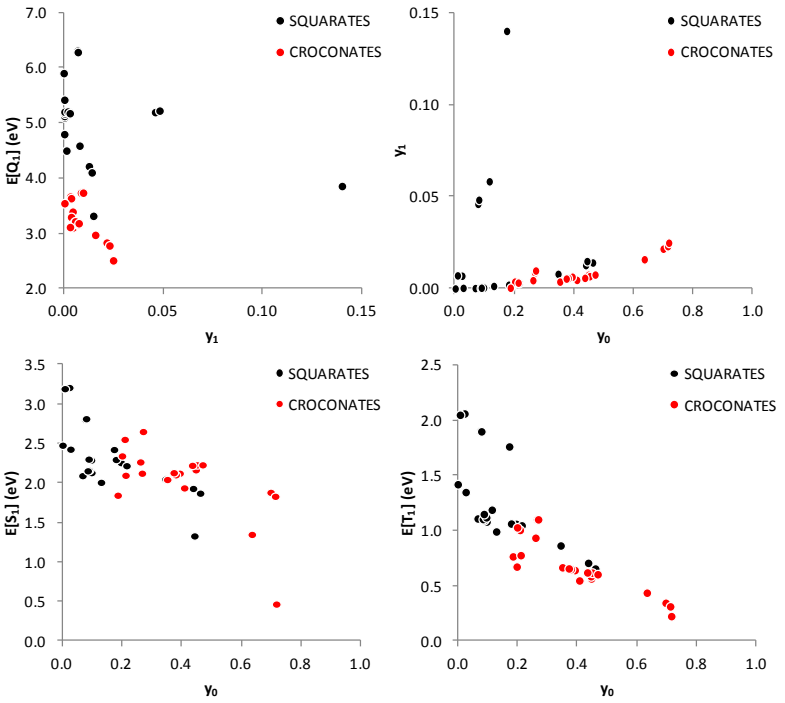

Figure 90: Relation between the tetraradical character (y_1) and the energy of the first quintet state (Q_1), top left, in eV; the diradical (y_0) and the tetraradical character, top right; y_0 and the energy of the first singlet state (S_1), in eV, bottom left, and y_0 and the singlet-triplet gap, in eV, bottom right, for squarates (black dots) and croconates (red dots).

No experimental data could be found regarding the singlet-triplet transition, although squarate dyes with relatively long-lived triplet states (>30 μs)[387,464] have been described, with lifetimes depending upon the medium and concentration, among other variables.

Tripathi et al. [233] or Thomas et al.[234] have calculated the transitions to both the first singlet ($S_0 \rightarrow S_1$) and triplet ($S_0 \rightarrow T_1$) excited states for a great variety of oxocarbon

derivatives, using density functional theory (DFT). Makowsy et al.[465,466] have investigated the low-lying excited states of the 1,3-dicyanomethylene croconate anion radical using both DFT and wavefunction-based methods (CASSCF). Srinivas et al.[237] investigated the effect of the diradical character as well as the low-lying singlet-singlet transitions on a broad number of derivatives. However, despite the availability of information regarding the lowest excited states in a variety of derivatives of squarates and croconates, there is a lack of fundamental research focused in the performance and suitability of these dyes in singlet fission processes.

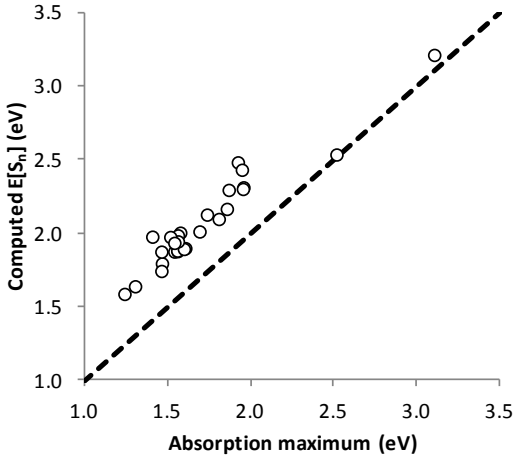

Figure 91: Representation of the TDDFT $S_0 \rightarrow S_1$ transitions against experimental values (eV).

In this section is presented a detailed analysis of a total of 44 derivatives (22 for each backbone, squarate and croconate). The selection of molecules is based on previous experimental and theoretical investigations. As a result, we will propose several molecules as possible candidates. This

implies, to our knowledge, a new use for these well-known dyes.

5.1.1. Low-lying excited states and frontier molecular orbitals.

Table 53: Energies of the singlet ($E[S_1]$), triplet ($E[T_1]$, $E[T_2]$), quintet ($E[Q_1]$) excited states, in eV, and oscillator strength (*f*) of the croconate derivatives, together with the available experimental values from references 233, 234. For those $S_0 \rightarrow S_1$ transitions with *f*=0.00, the energy of the lowest optical state ($E[S_n]$) is also included. The spin-contaminated values are substituted by those obtained by SF-TDDFT and highlighted in italics

	$E[S_1]$(f)		$E[S_n]$	$E[S_n]^{EXP}$	$E[T_1]$	$E[T_2]$	$E[Q_1]$	$2E[T_1]-E[S_1]$	$2E[T_1]-E[T_2]$
1	1.48	(0.00)	1.85	--	0.42	1.30	3.03	-0.64	-0.46
2	*2.05*	--	--	1.47	*0.11*	*0.50*	2.97	*-1.83*	*-0.29*
3	*1.88*	--	--	1.31	*0.01*	*0.39*	2.83	*-1.87*	*-0.38*
4	*1.83*	--	--	1.24	*-0.04*	*0.36*	2.78	*-1.91*	*-0.44*
5	1.74	(1.44)	--	1.46	0.23	1.73	3.11	-1.28	-1.27
6	2.45	(0.00)	2.53	2.52	0.84	2.09	3.74	-0.76	-0.41
7	2.22	(1.05)	--	--	0.74	1.99	3.67	-0.73	-0.50
8	1.90	(0.81)	--	--	0.65	1.52	3.39	-0.59	-0.21
9	2.42	(0.00)	2.56	--	0.84	2.12	3.74	-0.75	-0.44
10	2.30	(1.05)	--	--	0.76	2.07	3.63	-0.77	-0.54
11	*0.47*	--	--	--	*-0.38*	*0.32*	2.51	*-1.23*	*-1.08*
12	1.87	(1.29)	--	1.54	0.44	1.78	3.29	-0.99	-0.90
13	1.88	(1.29)	--	1.56	0.37	1.76	3.17	-1.13	-1.02
14	1.90	(1.29)	--	1.61	0.39	1.79	3.19	-1.12	-1.01
15	1.88	(1.45)	--	1.56	0.41	1.82	3.20	-1.06	-1.00
16	1.82	(0.00)	1.88	--	0.12	1.66	3.15	-1.59	-1.43
17	1.78	(0.00)	1.89	1.60	0.20	1.61	3.17	-1.38	-1.21
18	1.97	(0.00)	2.00	1.58	0.32	1.80	3.20	-1.33	-1.17
19	1.98	(1.25)	--	1.56	0.33	1.85	3.22	-1.32	-1.18
20	1.94	(0.02)	--	1.56	0.28	1.78	3.18	-1.38	-1.21
21	1.79	(0.00)	1.97	1.41	0.59	1.51	3.54	-0.60	-0.32
22	1.84	(0.00)	1.97	1.52	0.62	1.67	3.11	-0.60	-0.43

An increase of the tetraradical character (y_1) is related with the presence of low-lying quintet states (Q_1), which may

negatively interfere with an eventual SF process, reducing the efficiency as a competing state. In **Figure 90** top, are represented the relationship between $E[Q_1]$ and y_1 (left panel) and between y_0 and y_1 (right panel). In general, all the studied systems show very low y_1 values, although some of the squarates present notably larger values. Nevertheless, still they are very low (less than 0.15-0.10) and most of the molecules show $E[Q_1]$ over 3.0 eV.

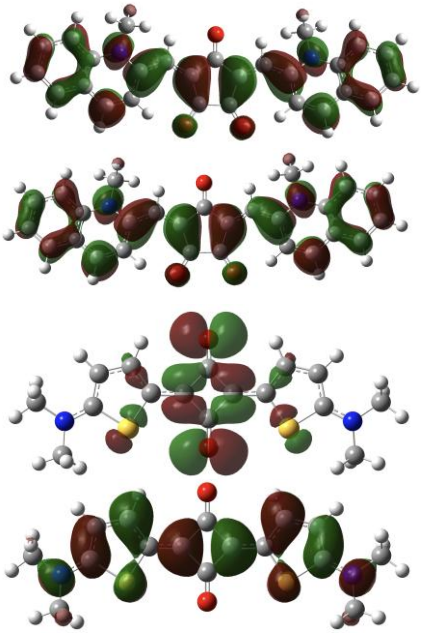

Figure 92: HOMO and LUMO molecular orbitals of the $\mathbf{R_5}$ croconate (top) and HOMO-1 and LUMO orbitals of the $\mathbf{R_{18}}$ squarate derivative (bottom).

Nevertheless, the experimental data have been obtained from absorption spectra in solution, which typically present redshifted values with respect to the gas phase. Analogously, a solution-to-crystal redshift has been also

observed in the case of hexacene, for instance, where the $E[S_1]$ value is reduced from 1.82 eV in solution to 1.48 eV in a polycrystalline film.[427] Therefore, the comparison with the calculated $E[S_1]$ should be carefully done. Nevertheless, good correlation is observed between the calculated and experimental values (**see Figure 91**).

Table 54: Energies of the singlet ($E[S_1]$), triplet ($E[T_1]$, $E[T_2]$), quintet ($E[Q_1]$) excited states, in eV, and oscillator strength (*f*) of the squarate derivatives, together with the available experimental values in references 237, 467,233, 378. For those $S_0 \rightarrow S_1$ transitions with *f*=0.00, the energy of the lowest optical state ($E[S_n]$) is also included. The spin-contaminated values are substituted by those obtained by SF-TDDFT and highlighted in italics.

	$E[S_1]$(f)	$E[S_n]$	$E[S_n]^{EXP}$	$E[T_1]$	$E[T_2]$	$E[Q_1]$	$2E[T_1]-E[S_1]$	$2E[T_1]-E[T_2]$
1	1.94 (0.00)	2.09	--	1.02	1.80	4.22	0.11	0.24
2	2.05 (0.00)	2.13	1.74	0.64	1.94	4.59	-0.77	-0.66
3	1.93 (1.15)	--	1.54	0.45	1.83	4.22	-1.02	-0.92
4	1.87 (1.18)	--	1.46	0.39	1.79	4.10	-1.09	-1.01
5	2.01 (1.39)	--	1.69	0.83	1.92	4.50	-0.36	-0.27
6	3.21 (0.87)	--	3.11	1.91	3.29	6.31	0.62	0.54
7	2.81 (0.95)	--	--	1.72	2.40	5.20	0.63	1.03
8	2.43 (0.77)	--	--	1.44	1.65	3.86	0.46	1.23
9	3.20 (0.79)	--	--	1.90	3.21	6.28	0.61	0.59
10	2.82 (0.89)	--	--	1.72	2.43	5.22	0.61	1.00
11	*1.03* --	--	--	*0.11*	*0.82*	3.32	*-0.82*	*-0.60*
12	2.10 (0.99)	--	1.81	0.99	2.32	5.16	-0.12	-0.34
13	2.13 (1.07)	--	--	0.93	2.10	5.10	-0.27	-0.24
14	2.16 (1.13)	--	1.86	0.95	2.14	5.13	-0.26	-0.24
15	2.16 (1.28)	--	--	0.97	2.18	4.80	-0.23	-0.25
16	2.29 (1.47)	--	--	0.96	2.21	5.17	-0.38	-0.29
17	2.30 (0.00)	2.31	1.96	0.99	2.17	5.20	-0.32	-0.18
18	2.26 (0.01)	--	--	0.90	2.13	5.19	-0.46	-0.33
19	2.30 (1.18)	--	1.96	0.91	2.18	5.21	-0.48	-0.36
20	2.22 (0.00)	2.29	1.87	0.88	2.09	5.18	-0.46	-0.33
21	2.48 (1.57)	--	1.93	1.35	2.18	5.90	0.23	0.53
22	2.43 (1.46)	--	1.95	1.27	2.48	5.42	0.10	0.05

Inspecting **Table 53**, we observe that the $S_0 \rightarrow S_1$ transitions in croconates take place between 1.03 and 2.42 eV. Those transitions with oscillator strength values of *f*=0 correspond to $n \rightarrow \pi^*$ transitions, involving the excitation of the oxygen lone pairs of the carbonyls. In **Figure 92** are represented the molecular orbitals involved in both $\pi \rightarrow \pi^*$ (top) and $n \rightarrow \pi^*$ (bottom) transitions. As it was stated in subsection 3.1, this feature may negatively affect the light harvesting power of the material. Thus, in such cases, the possibility to excite to a higher $S_0 \rightarrow S_n$ transition is also considered (E[S_n]), which may relax to the desired S_1 state. These S_n transitions are, in general, very close in energy, around 0.10 eV or less, and correspond to the second singlet excited state (S_2), except for **R_1**, where the S_n transition lies 0.37 eV above the lowest excited singlet and corresponds to the fourth singlet excited state (S_4). Thus, the energy losses by non-radiative relaxation from these optical states will be almost negligible. Finally, regarding the $S_0 \rightarrow T_1$ transitions, all of them appear below 1 eV.

In **Table 54** is collected the same information for the squarate derivatives. The $S_0 \rightarrow S_1$ transitions appear between 0.47 and 3.21 eV. As it has been mentioned before, those transitions corresponding to $n \rightarrow \pi^*$ excitations show an oscillator strength of *f*=0. The triplet states (T_1) are located around 1 eV, although several molecules show notably larger gaps, such as **R_6** (1.91 eV), **R_7** (1.72 eV), **R_9** (1.90 eV) or **R_{10}** (1.72 eV).

Thus, it is observed a general decrease of the $S_0 \rightarrow S_1$ and $S_0 \rightarrow T_1$ transition energies in croconates with respect to squarates that may be ascribed to the increase in the diradical character, leading to a stabilization of the S_1 and T_1 excited states (see **Figure 90**, bottom left and right). Experimentally, it has been observed a redshift of around 0.5 eV (100 nm) in the first visible excited state of croconates with respect to the corresponding squarates.[233] The shift of these transitions to lower energies due to the enhancement of y_0 may be used to tune the optoelectronic properties, to include a broader range of wavelengths.

5.1.2. Singlet fission suitability

In **Figure 93** is displayed the graphical representation of $2E[T_1]$-$E[S_1]$ and $2E[T_1]$-$E[T_2]$ values, together with the computed $2E[T_1]$-$E[S_1]$ values for tetracene (-0.35 eV) and pentacene (-0.95 eV). The practical implementation of the singlet fission mechanism into the solar cell harvesting technology requires the use of materials in the solid state and, therefore, a redshift of the $S_0 \rightarrow S_1$ transition energy is expected compared to the gas-phase energies calculated here. This suggests that the optimal $2E[T_1]$-$E[S_1]$ values will be more exoergic than the ones represented in **Figure 93**. In order to have a good reference to evaluate the C1 and C2 conditions for an optimal SF process, the calculated values of tetracene and pentacene are included. Besides, an efficient performance of this process within the solar cell harvesting technology would also require a $E[T_1]$ around 1.1 eV to match

the energy gap of the silicon, which implies a $E[S_1]$ slightly over 2.2 eV. Taking into account the redshift of the $E[S_1]$ in the solid state, theoretical gas-phase $S_0 \rightarrow S_1$ transitions higher than 2.4 eV, approximately, would be specially interesting. In this study, only those croconates substituted with **R_6**, **R_7**, **R_9** and **R_{10}** have $E[S_1] > 2.0$ eV. In the other hand, most of the squarates have $E[S_1] > 2.0$ eV, (**R_6**, **R_7**, **R_9** and **R_{10}** substituents show $E[S_1] > 2.5$ eV) with the only exception of **R_1**, **R_3**, **R_4** and **R_{11}**. However, although silicon is the most widely used semiconductor in the construction of solar cells, other materials with different energy gap may be also utilized.

Remarkable differences are observed between croconate (white bars) and squarate derivatives (black bars), that can amount more than 1 eV (0.75 eV in average). Thus, in derivatives such as **R_6** to **R_{10}**, corresponding to the aromatic amines, $2E[T_1]$-$E[S_1]$ is negative for croconates while it is positive for squarates. In general, the observed greater stabilization of the T_1 state in croconates may have as a consequence a more exoergic C1 condition, which, in some cases, can be detrimental. Despite the $S_0 \rightarrow S_1$ transition is forbidden for **R_6** and **R_9**, the optical $\pi \rightarrow \pi^*$ transition ($S_0 \rightarrow S_2$), appears only 0.08 eV and 0.14 eV over the first one, respectively. The values of $2E[T_1]$-$E[S_1]$ fluctuate, for croconates **$R_{6\text{-}10}$**, between -0.77 and -0.59 eV, located between the values of tetracene and pentacene, which make these compounds to be appropriated for singlet fission purposes. Similarly, derivatives **R_1**, **R_{21}** and **R_{22}** show

moderately negative $2E[T_1]$-$E[S_1]$ values, close to the Tc and Pc limits and, therefore, they could be considered as candidates for SF. Besides, the C2 condition is also fulfilled.

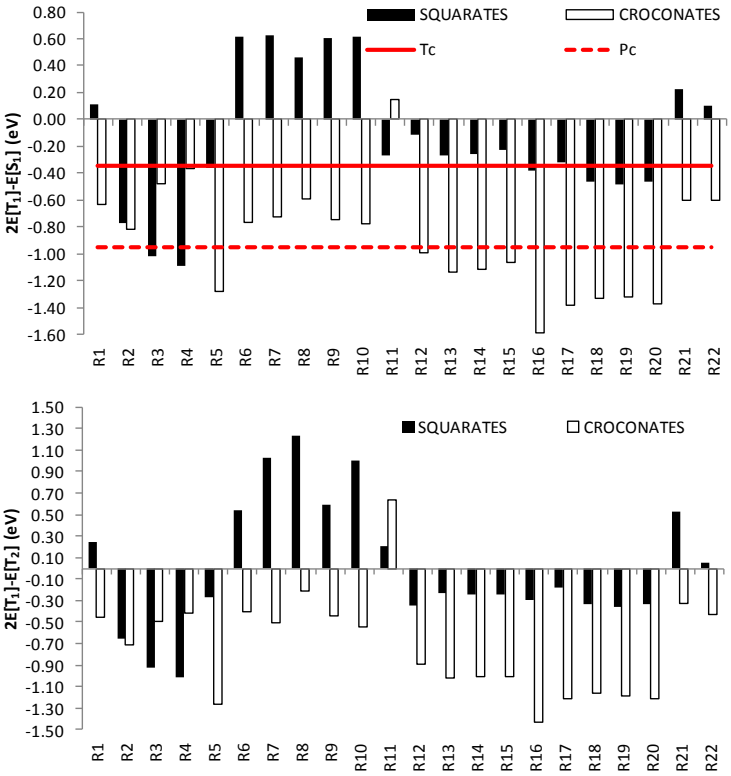

Figure 93: $2E[T_1]$-$E[S_1]$ and $2E[T_1]$-$E[T_2]$ energy differences, in eV, for croconates (white bars) and squarates (black bars), calculated with TDDFT. Red straight and dashed lines represent the values for tetracene (Tc) and pentacene (Pc), respectively.

The $\mathbf{R_5}$ and $\mathbf{R_{18\text{-}20}}$ croconate derivatives show rather negative $2E[T_1]$-$E[S_1]$ values, which is related to their large diradical character ($y_0 > 0.40$), a feature that may reduce the efficiency of the process.[468] Within the group $\mathbf{R_{12\text{-}17}}$, only those

molecules from **R_{12}** to **R_{15}** seem adequate for singlet fission, since **R_{16}** and **R_{17}** show too exoergic $2E[T_1]$-$E[S_1]$ values. However, for **$R_{12\text{-}15}$**, despite TDDFT yields slightly more negative than tetracene, SF-TDDFT provides much more negative values. Finally, the results for **$R_{2\text{-}4}$** and **R_{11}** showed remarkable spin contaminations and, therefore, should be carefully considered. Thus, despite the TDDFT calculations show that the C1 and the C2 conditions are fulfilled for **$R_{2\text{-}4}$**, the results calculated with SF-TDDFT show very exoergic $2E[T_1]$-$E[S_1]$ values.

The results obtained for squarates (black bars in **Figure 93**) show positive $2E[T_1]$-$E[S_1]$ values for the aromatic amine derivatives (**R_6** to **R_{10}**), which may be a consequence of less stabilized T_1 states, due to smaller diradical character. These molecules, therefore, should be excluded as potential candidates. **R_1**, **R_{12}**, **R_{21}** and **R_{22}** show a nearly isoergic process, nevertheless, the C2 condition is not fulfilled. The rest of the derivatives (**R_2** to **R_5**, **R_{11}** and **R_{13}** to **R_{20}**) fulfill both C1 and C2 conditions, with $2E[T_1]$-$E[S_1]$ energy differences close to those of pentacene and tetracene. Again, squarate **R_{11}** showed spin contamination, so the interpretation of these results might be done with care

In summary, within the croconate group 11 molecules can be considered as potential candidates: **$R_{1\text{-}4}$**, **$R_{6\text{-}10}$** and **$R_{21\text{-}22}$** have adequate $2E[T_1]$-$E[S_1]$ and $2E[T_1]$-$E[T_2]$ values. Besides, four additional derivatives, **$R_{12\text{-}15}$**, may also be considered, as the C1 condition is nearly fulfilled. It must be

emphasized that **R_{2-4}**, **R_6**, **R_{21}** and **R_{22}** have been already synthesized. [233, 234] Nevertheless, the E[S_1] values are, in general, lower than required for an optimal match with the silicon energy gap, and only the **R_6**, **R_7** , **R_9**, and **R_{10}** show E[S_1]>2 eV. Analogously, in the squarate set, a total of 13 derivatives have been found suitable for singlet fission: **R_{2-5}**, **R_{11}** and **R_{13-20}** fulfill both C1 and C2 conditions with 2E[T_1]-E[S_1] values within or close to the limits imposed by tetracene and pentacene. The following derivatives: **R_{2-5}**, **R_5**, **R_{14}**, **R_{17}**, **R_{21}** and **R_{22}** have been experimentally obtained.[237,378,467] Besides, the E[S_1] energies are, in general, higher for squarates than for croconates, suggesting that the E[T_1] energies should be closer to the silicon energy gap (1.1 eV). Then, from 28 potential sensitizers that may undergo this process efficiently, 15 are croconates and 13 are squarates.

5.2. Oligothiophenes

Some quinoidal oligothiophenes, fundamentally small chain molecules as the quinoidal bithiophene,[346,388,469] have been already studied during the last years due to their applicability in singlet fission. The main features of these molecular structures are the low separation between the ground and the T_1 states, which arises from the diradical character, [28,181,470,] as well as the strong absorption they show in the NIR.

Table 55: Energies of the first singlet (E[S_1]) and two triplet (E[T_1] and E[T_2]) excited states, and the 2E[T_1]-E[S_1] (C1) and 2E[T_1]-E[T_2] (C2)

energy conditions, in eV, calculated with SF-TDDFT. $E[Q_1]$ has been calculated with DFT.

		$E[S_1]$	$E[T_1]$	$E[T_2]$	$E[Q_1]$	$2E[T_1]-E[S_1]$	$2E[T_1]-E[T_2]$
A	**1**	3.41	1.25	1.87	6.16	-0.92	0.62
	2	2.50	0.70	1.28	4.47	-1.11	0.12
	3	1.64	0.16	0.74	3.26	-1.32	-0.43
	4	1.03	-0.31	0.33	2.60	-1.65	-0.96
B	**1**	4.25	1.97	2.58	7.56	-0.32	1.35
	2	3.05	1.01	1.67	5.40	-1.03	0.34
	3	2.23	0.50	1.20	3.85	-1.23	-0.19
	4	1.16	-0.31	0.47	2.79	-1.78	-1.10
C	**1**	3.37	1.57	2.13	5.55	-0.24	1.01
	2	2.96	1.56	2.01	4.52	0.16	1.11
	3	2.72	1.54	1.98	3.94	0.37	1.10
	4	2.64	1.63	2.05	3.62	0.63	1.22
D	**1**	4.17	2.06	2.68	7.07	-0.05	1.44
	2	3.52	1.89	2.44	5.59	0.26	1.34
	3	3.27	1.81	2.35	4.81	0.35	1.28
	4	1.95	0.53	1.27	4.37	-0.89	-0.21
E	**1**	2.19	0.34	1.04	4.40	-1.50	-0.36
	2	1.22	-0.57	0.23	3.09	-2.37	-1.38
	3	0.86	-0.56	0.25	2.50	-1.97	-1.36
	4	0.64	-0.74	0.10	2.18	-2.12	-1.57
F	**1**	1.71	0.23	0.86	3.43	-1.24	-0.40
	2	1.15	-0.20	0.47	2.72	-1.54	-0.86
	3	0.79	-0.50	0.22	2.32	-1.79	-1.22
	4	0.62	-0.67	0.09	2.08	-1.97	-1.43
G	**1**	1.34	0.71	1.19	3.35	0.08	0.23
	2	0.92	0.10	0.66	2.79	-0.72	-0.46
	3	0.39	-0.53	0.10	2.43	-1.45	-1.16
	4	0.31	-0.58	0.09	2.19	-1.47	-1.26
H	**1**	3.54	3.16	3.66	8.15	2.78	2.66
	2	3.44	1.43	2.05	6.11	-0.57	0.82
	3	2.60	0.81	1.33	4.62	-0.99	0.29
	4	1.65	0.19	0.78	3.31	-1.26	-0.40
I	**1**	3.30	2.47	3.01	6.60	1.65	1.94
	2	2.31	0.76	1.55	5.45	-0.79	-0.02
	3	1.32	-0.48	0.35	4.43	-2.29	-1.32
	4	0.98	-0.84	0.04	3.75	-2.67	-1.72

In this subsection, we analyze the 32 oligothiophenes proposed in Chapter 4 (groups from **A** to **H**), together with the **I** group of molecules, used as a reference (see **Figure 33**,

Chapter 4). The SF-TDDFT method is used due to spin contamination found for molecules **A_{3-4}**, **B_4**, **E_{1-4}**, **F_{1-4}**, **G_{2-4}**, **H_4** and **I_{3-4}**. **Table 55** collects the excited states of these systems. Both $S_0 \rightarrow S_1$ and $S_0 \rightarrow T_1$ transitions are reduced as the molecular chain grows, as expected, due to an increment in y_0. Experiments support this behavior and compare well with the calculated data.[242] This reduction of the $S_0 \rightarrow S_1$ transition allows strongly open-shell structures, as group **G**, to absorb in the NIR, with wavelengths larger than 900 nm, while closed-shell structures (group **C**) would absorb in the UV region.

A graphical representation of the $2E[T_1]$-$E[S_1]$ (C1) values is plotted on **Figure 94**. Closed-shell molecules, such as **$C_{3,4}$**, **H_1** or **I_1** have endoergic C1 values. In the other hand, a large number of molecules show too exoergic C1 values. However, some interesting features can be found. For instance, the n=1,2 molecules of group **A** meet the C1 energy requirement (-0.92 and -1.11 eV, respectively, comparable to those of the tetracene and pentacene). The excited states of the **A_2** molecule have already been investigated and the values calculated in this thesis are in rather good agreement with the values of 2.25 eV (TDDFT) or 2.06 eV (CASPT2) reported for the $S_0 \rightarrow S_1$ transition,[469] while the singlet-triplet gap was predicted to be 0.96 eV within TDDFT.[388]

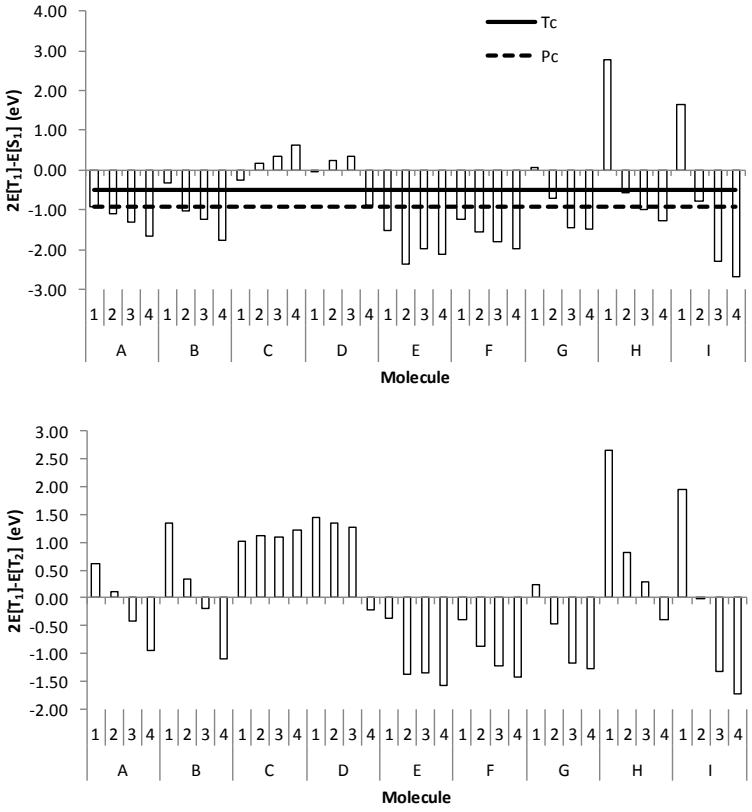

Figure 94: $2E[T_1]$-$E[S_1]$ (C1) and $2E[T_1]$-$E[T_2]$ (C2) energy differences, in eV, calculated with SF-TDDFT. Black straight and dashed lines represent the values for tetracene and pentacene, respectively.

The n=1,2 molecules of group **B** also show negative C1 values, while from **C** and **D** groups the only molecule that seems to meet this requirement is $\mathbf{D_4}$. The trend within **C** and **D** groups is the opposite as observed in the rest of the groups, and more endoergic C1 values are calculated as the molecular chain grows. Both **E** and **F** groups are composed

by molecules with too negative C1 condition, except **E_1**. From the rest of the groups, we may highlight **G_2**, **$H_{2,3}$** and **I_2**.

Table 56: Energies of the first singlet ($E[S_1]$) and two triplet ($E[T_1]$ and $E[T_2]$) excited states, and the $2E[T_1]$-$E[S_1]$ (C1) and $2E[T_1]$-$E[T_2]$ (C2) energy conditions, in eV, calculated with SF-TDDFT. $E[Q_1]$ has been calculated with DFT.

	$E[S_1]$	$E[T_1]$	$E[T_2]$	$E[Q_1]$	$2E[T_1]$-$E[S_1]$	$2E[T_1]$-$E[T_2]$
a	2.72	0.77	1.34	4.93	-1.19	0.19
b	2.50	0.70	1.28	6.11	-1.11	0.12
c	2.52	0.78	1.34	4.35	-0.96	0.23
d	2.92	1.31	1.86	4.62	-0.31	0.75
e	2.29	0.07	0.63	5.10	-2.16	-0.49
f	1.92	0.05	0.76	4.58	-1.83	-0.67
g	2.79	1.39	2.07	3.92	0.00	0.71

Finally, **Table 56** shows the effect exerted by the replacement of the sulfur atom by oxygen (**a**), carbonyl group (**b**), selenium (**c**), carbon (**d**) or nitrogen (**e**) (see Chapter 4). The reference molecule (**A_2**) is denoted as **f**. The value of the $S_0 \rightarrow S_1$ transition is slightly enhanced independently of the substitution, and is more evident for molecule **d**. The $S_0 \rightarrow T_1$ transition is also enhanced, especially in **d**. The only exception is **e**, in which the singlet-triplet gap is reduced.

Despite small differences are accounted for those transitions, stronger effects are shown in the C1 condition. Thus, the original -1.11 eV value might be enhanced to -1.19 or -1.47 eV when O or N are used (**a** and **e**). In the other hand, the molecules **c** and **d** slightly reduce the exoergicity of the system, while in **b** is greatly reduced.

In summary, from this subsection we can underline the following oligothiophenes as promising candidates, since they show intermediate diradical character and C1 values close to those of tetracene and pentacene: **A_1, B_1, C_1, D_1, E_1, G_2, H_2, H_3, b, c,** and **d.**

5.3. Aromatic Diimides

The preferred ground state on aromatic diimides is the closed shell, although some exceptions could be found, as sketched on Chapter 4. Thus, the diimides derived from zethrene moieties and oligorylene derivatives have small energy gaps and narrow and intense absorption bands in the NIR, converting these type of carbonyl molecules into an interesting group to investigate the singlet fission process. In fact, their parent molecules (zethrenes and oligorylenes) were recently predicted to host the singlet fission mechanism by the relative disposition of their low-lying excited states,[258,259, 471] and the presence of the diimide functional group does not seem to modify the ground state of the molecules. Actually, perylene diimide has been investigated for singlet fission purposes.[32,273,472,473]

The excitation energies are gathered on **Table 57** and good agreement is observed between the calculated E[S_1] and the experimental values obtained in solution, although a general overestimation is observed. As recognized in previous sections, those molecules with larger diradical character (y_0>0.15, molecules **10-14** and **18**-**19**) yield lower

$E[T_1]$ states (less than about 1.50 eV). Note that molecule **1** has an optically forbidden $S_0 \rightarrow S_1$ transition that could explain why in this case the experimental value is higher. Spin contamination was observed for molecules **15**, **20** and **21**, so that SF-TDDFT values ($E[S_1]^{SF\text{-}TDDFT}$) are used instead. As shown, both TDDFT and experimental results place the $E[S_1]$ near 2 eV, encouraging the investigation of these molecules, as they could match the energy gap of silicon.

Table 57: Energies of the first singlet ($E[S_1]$) and two triplet ($E[T_1]$ and $E[T_2]$) excited states, and the $2E[T_1]$-$E[S_1]$ (C1) and $2E[T_1]$-$E[T_2]$ (C2) energy conditions, in eV, calculated with TDDFT. $E[Q_1]$ has been calculated with DFT. Experimental values taken from references 254, 255, 257, 261, 407, 408, 409, 474 and 475. The spin-contaminated values are substituted by those obtained by SF-TDDFT and highlighted in italics.

	$E[S_1]$(f)	$E[S_n]$	$E[S_n]^{EXP}$	$E[T_1]$	$E[T_2]$	$E[Q_1]$	$2E[T_1]$-$E[S_1]$	$2E[T_1]$-$E[T_2]$
1	3.86 (0.00)	3.98	4.00	3.45	3.53	7.46	3.04	3.38
2	4.02 (0.14)	--	--	3.01	3.40	6.26	2.01	2.63
3	3.49 (0.05)	--	2.95	2.17	3.08	5.65	0.85	1.25
4	3.91 (0.00)	4.03	--	3.38	3.58	6.86	2.85	3.18
5	3.88 (0.00)	4.01	--	3.42	3.55	6.92	2.95	3.28
6	3.83 (0.00)	3.90	--	3.34	3.53	6.74	2.85	3.14
7	3.74 (0.35)	--	3.54	2.36	3.31	6.50	0.98	1.40
8	3.73 (0.36)	--	--	2.35	3.30	6.48	0.98	1.40
9	3.73 (0.42)	--	--	2.36	3.32	6.48	0.99	1.39
10	2.87 (0.24)	--	2.59	1.60	2.95	5.84	0.34	0.25
11	2.13 (0.15)	--	1.99	0.90	2.24	4.35	-0.32	-0.43
12	1.80 (0.12)	--	1.66	0.51	1.80	3.54	-0.79	-0.78
13	2.29 (0.01)	--	2.25	1.33	2.08	3.99	0.38	0.58
14	2.25 (1.22)	--	1.92	0.51	1.93	3.28	-1.23	-0.90
15	*0.82* --	--	1.16	*-0.91*	*0.03*	2.34	*-2.64*	*-1.85*
16	4.02 (0.00)	4.03	--	3.34	3.67	6.73	2.66	3.01
17	3.50 (0.00)	3.98	--	3.02	3.55	6.65	2.55	2.50
18	2.69 (0.74)	--	2.36	1.50	2.97	5.75	0.32	0.03
19	2.11 (0.95)	--	1.91	0.69	2.31	4.05	-0.72	-0.92
20	*1.75* --	--	1.50	*0.05*	*0.69*	2.90	*-1.66*	*-0.59*
21	*1.26* --	--	--	*-0.42*	*0.28*	2.14	*-2.10*	*-1.13*

The acene-derived diimides can be compared with the parent acene. Thus, the TDDFT $S_0 \rightarrow T_1$ transitions for acenes from naphthalene to pentacene are, respectively, 3.19, 2.20, 1.47, and 0.91 eV. In that manner, it is observed that the energy gap between the ground and the first triplet state is lower in the diimide, and also that this decrease is larger when the acene chain is placed in the perpendicular axis, as in molecules **7**, **10**, **11** and **12**. It is noted that this difference becomes smaller as long as the acene chain gets larger. In that manner, the $E[T_1]$ energies for naphthalene diimide (**7**) is -0.83 eV higher than that of naphthalene, while the difference observed on pentacene diimide (**12**) is only -0.40. Additionally, experimental results for molecule **18**, 1.1 or 1.2 eV,[476,477] match very well the calculated $E[T_1]^{DFT}$=1.11 eV value.

Finally, the C1 and C2 energy requirements for singlet fission are represented in **Figure 95**. As expected, molecules with low diradical character (molecules **1**-**9** and **16**-**17**) should not be recommended for the design of singlet fission materials. However, the comparison of the diimides with the corresponding PAH is still possible. The parent acenes from naphthalene to pentacene show $2E[T_1]$- $E[S_1]$ values of 1.71, 0.80, 0.14 and 0.42 eV. Thus, acene diimides with the acene chain placed in the longitudinal axis yield more positive C1 values (molecules **2** and **3**), while the placement of the acene chain in the perpendicular axis favors more exoergic C1 values (molecules **7**, **10**-**12**). In that manner, the tetracene

(**11**) and pentacene (**12**) derived diimides give negative values for both C1 and C2. The $2E[T_1]$-$E[S_1]$ value in the anthracene diimide (**10**) and in the substituted tetracene diimide (**13**) are slightly positive, and the singlet fission mechanism might appear anyway by heating those materials.

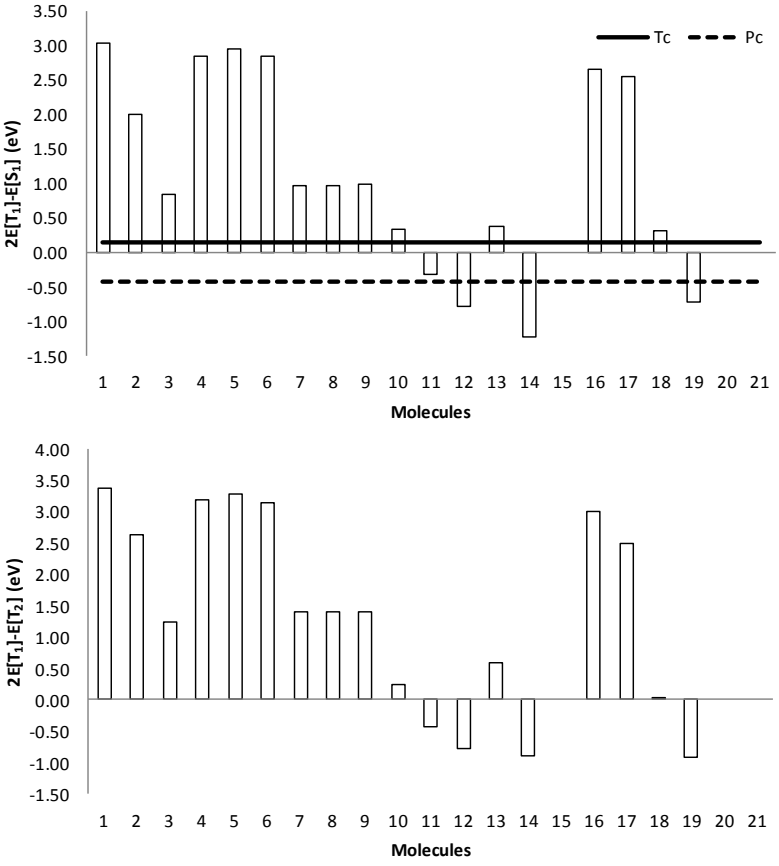

Figure 95: $2E[T_1]$-$E[S_1]$ (C1) and $2E[T_1]$-$E[T_2]$ (C2) energy differences, in eV, for the studied molecules calculated with TDDFT. Molecules **15**, **20** and **21** are not included due excessive spin contamination**.** Black straight and dashed lines represent the values for tetracene and pentacene, respectively.

Molecules **14** and **15** show very exoergic C1 values. The latter has been calculated using SF-TDDFT (C1=-2.64 eV). The perylene diimide (**18**) shows a C1 value of 0.32 eV, a bit far from the $2E[T_1]-E[S_1]\leq 0$ condition. Perylene and other rylene molecules (not diimides) have been already theoretically tested to know their singlet fission applicability, [258,259] obtaining $2E[T_1]-E[S_1]$ values of 0.31 eV for perylene, -0.08 for terrylene, -0.28 for quaterrylene and -0.44 eV for pentarylene. Those results point that the oligorylene diimide derivatives can also be used as singlet fission materials, favored by redshifted absorption maxima with respect their parent oligorylene.[260] Large zethrene-like diimides also give negative C1 values, supporting previous investigations that propose zethrenes as singlet fission materials.[471] However, zethrenes larger than **19** seem to have excessively negative C1 values, reducing the efficiency of the process. C1 values for **20** and **21** have been calculated with SF-TDDFT to be -1.66 and -2.10 eV, excessively negative. Regarding the C2 condition, the **10-14, 18** and **19** molecules show C2 < 0. In general, the quintet state is far of being a limitation. Only molecule **2** shows $2E[T_1]-E[Q_1] >0$.

As a summary, the following molecules may be selected from this study: **10, 11, 12** and **19.**

5.4. Indigo-based chromophores

The indigo molecule has been broadly used as dye since the ancient ages and has been synthesized in industrial

scale since the XIX century.[478] Thus, a large amount of experimental and theoretical work can be found in the literature focused in this molecule or in their numerous derivatives,[479,480] and the excited states of this molecule have also been widely investigated.

The experimental gas-phase value of the $S_0 \rightarrow S_1$ transition is 2.30 eV[481] and is redshifted to 2.03 eV in solution.[482] Additionally, the redshift from solution to solid state has also been reported: $E[S_1]$ energy is 1.94 eV for amorphous indigo and 1.82 eV for crystalline indigo.[483] In this section, all the experimental $E[S_1]$ values are obtained in solution. Besides, the $S_0 \rightarrow T_1$ transition has been also estimated from experimental data to be 1.04 eV on a benzene solution.[484] Thus, the C1 energy condition is fulfilled in this molecule ($2E[T_1]-E[S_1]\approx 0$) and, together with its low toxicity, high stability, availability and absorbance in the visible region, the indigo molecule is a perfect candidate to be a good singlet fission sensitizer. However, no data related to singlet fission is available for this molecule. This lack of information might be caused for the short S_1 lifetime that may hinder an efficient singlet fission process.[482] Nevertheless, derivatives of indigo as the cibalackrot have shown moderated singlet fission activity due low triplet yield.[273,485]

Thus, chemical modifications may be useful for the pursuit of indigo-like molecules as singlet fission sensitizers.

Table 58: Energies of the first singlet ($E[S_1]$) and two triplet ($E[T_1]$ and $E[T_2]$) excited states, and the $2E[T_1]$-$E[S_1]$ (C1) and $2E[T_1]$-$E[T_2]$ (C2) energy conditions, in eV, calculated with TDDFT. Experimental data were taken from Refs. 264, 269, 272, 481, 482, 486, 487 and 488. $E[Q_1]$ has been calculated with DFT. The spin-contaminated values are substituted by those obtained by SF-TDDFT and highlighted in italics.

	$E[S_1]$(f)		$E[S_n]$	$E[S_n]^{EXP}$	$E[T_1]$	$E[T_2]$	$E[Q_1]$	$2E[T_1]$-$E[S_1]$	$2E[T_1]$-$E[T_2]$
1	2.51	(0.34)	--	2.03	1.08	2.76	4.90	-0.35	-0.60
2	2.30	(0.25)	--	1.93	0.91	2.72	4.76	-0.49	-0.90
3	2.09	(0.24)	--	--	0.77	2.36	4.29	-0.56	-0.83
4	2.93	(0.00)	3.39	3.00	1.91	2.60	5.67	0.90	1.23
5	2.72	(0.26)	--	2.27	1.65	2.77	5.32	0.57	0.53
6	2.57	(0.23)	--	2.21	1.63	2.75	5.14	0.69	0.51
7	2.67	(0.00)	--	--	2.41	2.71	5.32	2.14	2.10
8	2.94	(0.00)	--	--	2.63	2.83	6.53	2.31	2.42
9	*1.56*	--	--	--	*0.42*	*0.80*	3.85	*-0.72*	*0.05*
10	2.89	(0.36)	--	--	1.37	2.91	4.89	-0.14	-0.17
11	2.57	(0.36)	--	2.08	1.06	2.86	4.82	-0.44	-0.73
12	*1.87*	--	--	1.66	*0.34*	*0.80*	3.71	*-1.20*	*-0.12*
13	*1.47*	--	--	--	*0.25*	*0.64*	3.37	*-0.97*	*-0.14*
14	2.11	(0.43)	--	1.65	0.58	2.32	4.32	-0.95	-1.16
15	*1.23*	--	--	--	*-0.50*	*0.20*	3.44	*-2.22*	*-1.20*
16	*1.05*	--	--	--	*-0.25*	*0.22*	3.35	*-1.54*	*-0.71*
17	2.75	(0.06)	--	--	1.60	2.50	5.18	0.44	0.69
18	2.71	(0.27)	--	2.25	1.53	2.73	5.61	0.36	0.34
19	3.47	(0.85)	--	3.00	2.00	3.76	6.48	0.52	0.23
20	3.12	(0.27)	--	2.40	1.83	3.07	5.72	0.54	0.59
21	3.34	(0.35)	--	2.73	2.12	3.45	5.89	0.90	0.79
22	2.84	(0.22)	--	2.53	1.73	2.71	6.12	0.63	0.76
23	3.59	(0.01)	--	3.49	2.95	3.30	6.29	2.31	2.61
24	2.79	(0.22)	--	2.30	1.13	2.51	5.46	-0.53	-0.25
25	2.52	(0.65)	--	2.16	0.99	2.46	4.39	-0.54	-0.48
26	2.24	(0.54)	--	--	0.80	1.72	4.03	-0.65	-0.13
27	3.17	(0.44)	--	2.76	2.07	3.52	6.07	0.97	0.63
28	2.60	(0.31)	--	2.01	1.57	2.91	5.20	0.54	0.23
29	2.15	(0.90)	--	1.70	1.31	2.02	3.57	0.47	0.60
30	2.62	(0.61)	--	2.12	1.88	2.13	3.87	1.15	1.63
31	2.37	(0.39)	--	--	1.29	2.57	4.64	0.21	0.01
32	2.79	(0.24)	--	2.28	1.45	2.84	5.16	0.11	0.07
33	2.68	(0.14)	--	2.29	1.44	2.37	4.62	0.19	0.50

In this sense, the low-lying excited states of 33 indigo derivatives have been calculated and gathered in **Table 58**.

Somewhat large discrepancies are observed with respect to the experimental values (MAEs of 0.62 and 0.43 eV for SF-TDDFT and TDDFT, respectively). However, both calculated and experimental values follow the same trend. The calculated $E[S_1]$ values range 2.09-3.59 eV, many of them near 2.70 eV. This places the absorption of these molecules between 344-620 nm, adequate for singlet fission purposes. These transition energies are reduced as the diradical character grows, as expected.

The calculated low-lying excited states of the indigo molecule (**1**) point to an exoergic singlet fission process and high absorption in the visible region, while this mechanism has not been experimentally observed for this molecule. The substitution of the amine hydrogen by methyl and alcohol moieties (**2** and **3**) enhances the diradical character, shifting the $2E[T_1]$-$E[S_1]$ energy difference to more negative values. Those features are more clearly shown on **Figure 96**.

Molecules from **4** to **8**, as the result of the substitution of the NH by O, S, Se, B and C, have C1 shifted to more positive values. Molecules **7** and **8** showed no optically active excitations in the studied range. Molecule **4** also has a forbidden S_1, but there is an available excitation at 3.39 eV.

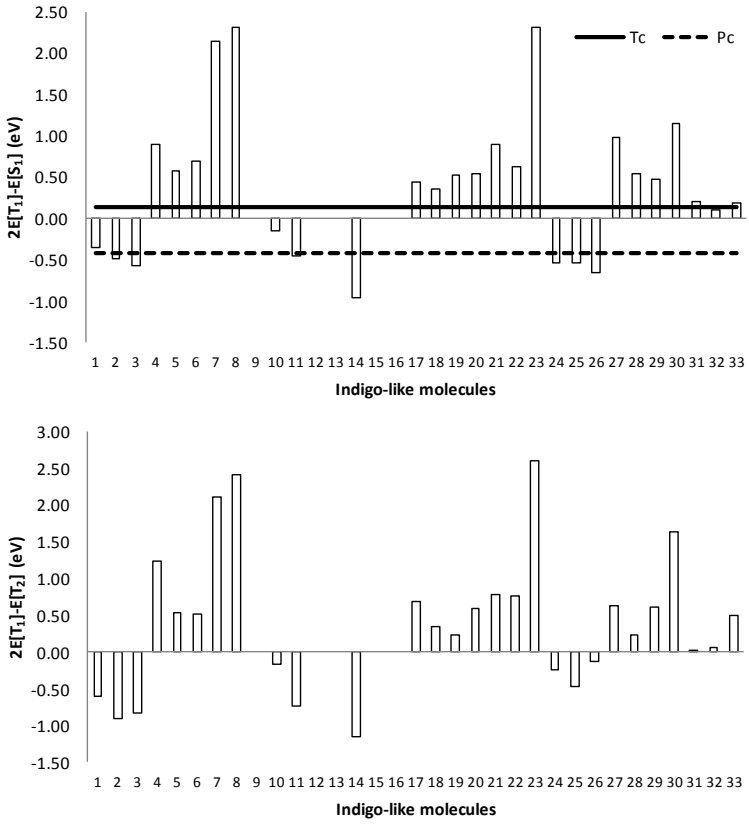

Figure 96: $2E[T_1]$-$E[S_1]$ (C1) and $2E[T_1]$-$E[T_2]$ (C2) energy differences, in eV, for the studied molecules calculated with TDDFT. Some molecules have been omitted due to excessive spin contamination. Black straight and dashed lines represent the values for tetracene and pentacene, respectively.

In molecules **9**-**14,** the carbonyl oxygen has been substituted by S, CH_2, NH, $C(CN)_2$, cyclopentadiene and NCN moieties. These structures show negative C1 values, some of them obtained with SF-TDDFT. However, these molecules (except **12**) could be valid anyway for singlet fission purposes. If the carbonyl is displaced from the five- to the six-membered

ring, the diradical character is greatly enhanced and then, $2E[T_1]$-$E[S_1]$ becomes too negative. Something similar occurs on molecule **16**, in which the hydrogen of the amino group is transferred to the carbonyl oxygen, generating an alcohol.

The modification of the position of the C=C linker, as well as the C=O and NH groups gives rise to molecules **17**-**23**, all of them calculated as near closed-shell molecules and, thus, positive C1 values are found.

Negative C1 values could be found on molecules **24**-**26**. Molecule **24** is an indigo molecule without the benzene-like rings, while **25** has two vinyl groups to enlarge the conjugated system. In the other hand, in molecule **26** the rings are interchanged, in such a way that the six-membered rings are linked with the double bond. Both **24** and **25** have been synthesized. Molecules **27**-**30** have positive C1 values, while in **31**-**33** are near the isoergicity. A derivative of **32**, cibalackrot, has been found as singlet fission material, and the $2E[T_1]$-$E[S_1]$ value is in agreement with our result. The innovative feature is the blockage of the central double bond, so molecule **33** (a simplified derivative of preCiba) is also calculated, and a slightly positive value of $2E[T_1]$-$E[S_1]$ is found. The $2E[T_1]$-$E[T_2]$ energy difference is negative for **1**, **2**, **3**, **10**, **11**, **14**, **24**, **25**, **26**, **31** and **32**, mostly the same molecules that fulfill the $2E[T_1]$-$E[S_1]$ condition, with the exception of **33**. Molecules **9**, **12**, **13**, **15** and **16** are excluded in the Figure due to spin contamination. However, SF-TDDFT calculations show that molecules **9** ($2E[T_1]$-$E[S_1]$=-0.72 eV)

and **13** ($2E[T_1]-E[S_1]$=-0.97 eV) fulfill the energy requirements. Nevertheless, they show too low values of $E[S_1]$.

As a summary, molecules **1, 2, 3, 10, 11, 24, 25** and **26** could be highlighted as possible candidates.

5.5. Other carbonyl-containing chromophores

The molecules studied in this section have been suggested for many applications. For instance, the quinacridone molecule (**1**)[489] has been applied in emitting diodes (OLEDs),[490,491] organic field-effect transistors (OFETs),[492,493] or organic solar cells (OSCs).[494] The trans-perinone (**3**) molecule has been investigated as an organic photoconductive (OPC) device.[495] Diketopyrrolopyrrole (**4**) derivatives have been proposed in OSCs technologies[496] and OFETs.[497] Dibromoanthranone (**10**) and flavanthrone yellow (**14**) were investigated due to their semiconductor properties.[498]

The energies of the low-lying excited states have been collected on **Table 59**. The $E[S_1]$ values are between 2.07 – 3.43 eV above the ground state, in the visible region of the spectrum. Some experimental absorption maxima (in solution) could be found in the literature: molecule **1** shows a transition at 2.37 eV,[499] **3** at 2.77 eV,[500] **9** at 2.09 eV,[417] **15** at 2.07 eV[501] and **17** at 2.00 eV.[501] The largest discrepancy is observed for the quinacridone molecule (**1**), still within the error previously observed in the calculation of the first excited states with several TDDFT functionals.[499] The only molecules with *f*=0 are

11 and **14**, with active $S_0 \rightarrow S_2$ transitions at 2.70 eV (f=0.57) and 3.14 eV (f=0.85) respectively.

Table 59: Energies of the first singlet ($E[S_1]$) and two triplet ($E[T_1]$ and $E[T_2]$) excited states, and the $2E[T_1]$-$E[S_1]$ (C1) and $2E[T_1]$-$E[T_2]$ (C2) energy conditions, in eV, calculated with TDDFT. Experimental values taken from Refs. 417, 499, 500 and 501. $E[Q_1]$ has been calculated with DFT.

	$E[S_1]$(f)	$E[S_n]^{EXP}$	$E[T_1]$	$E[T_2]$	$E[Q_1]$	$2E[T_1]$-$E[S_1]$	$2E[T_1]$-$E[T_2]$
1	3.43 (0.16)	2.37	2.12	3.20	6.11	0.81	1.04
2	2.33 (0.76)	--	1.39	2.23	3.85	0.44	0.54
3	2.95 (0.88)	2.77	1.91	2.64	5.23	0.88	1.18
4	2.81 (0.63)	--	1.24	3.06	5.88	-0.32	-0.57
5	2.07 (5.39)	--	0.52	0.99	2.31	-1.04	0.04
6	3.30 (0.64)	--	2.06	2.87	5.73	0.82	1.25
7	2.51 (1.31)	--	0.84	2.82	5.02	-0.83	-1.14
8	2.53 (2.15)	--	1.15	1.91	3.69	-0.22	0.40
9	2.12 (2.34)	2.09	-0.62	1.91	3.77	-3.37	-3.16
10	2.87 (0.31)	--	1.80	2.56	4.80	0.73	1.05
11	2.24 (0.00)	--	1.50	1.70	3.74	0.76	1.30
12	3.10 (0.56)	--	1.86	2.84	5.52	0.62	0.88
13	3.05 (0.80)	--	1.76	2.71	4.91	0.47	0.81
14	3.13 (0.00)	--	1.87	2.79	5.03	0.62	0.95
15	2.40 (1.02)	2.07	1.26	2.51	4.52	0.13	0.02
16	2.45 (0.76)	--	1.50	2.57	4.73	0.56	0.44
17	2.37 (0.97)	2.00	1.26	2.53	4.84	0.15	-0.01

Regarding the $S_0 \rightarrow T_1$ transition, molecules with clear open-shell character as **3-5**, **7**, **8** and **12-17** show values between 0.52 and 1.91 eV, an appropriate range for singlet fission. Molecule **9** shows a triplet ground state. However, further calculations with SF-TDDFT and DFT suggest that this transition should be positive.

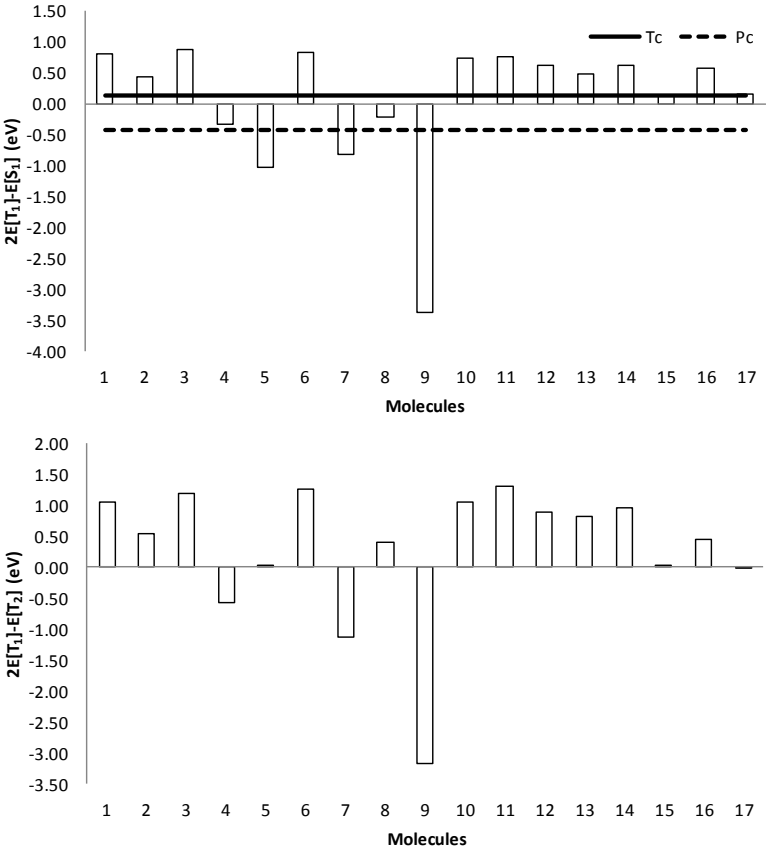

Figure 97: $2E[T_1]$-$E[S_1]$ (C1) and $2E[T_1]$-$E[T_2]$ (C2) conditions, in eV, for the studied molecules calculated with TDDFT. Black straight and dashed lines represent the values for tetracene and pentacene, respectively.

In **Figure 97** it is observed that molecules **4** and **8** show slightly exoergic $2E[T_1]$-$E[S_1]$ energy differences, while molecules **5** and **7** show a too negative value, arising from an excessive diradical character. For molecules **12-17** a slight endoergicity is observed, while molecules **15** and **16** have C1 values similar to tetracene. Regarding the C2 condition, those

molecules with appropriated C1 present negative C2 values. The only exception is molecule **8**, with $2E[T_1]-E[T_2]=0.40$ eV.

In summary, molecules **4**, **8**, **15** and **17** are found as possible candidates for singlet fission.

5.6. Derivatives of naphthalene, pentalene, heptalene and azulene

In the literature can be found a large number of applications for the acene molecules[185] derived from their unique optical properties (singlet fission, semiconductors, organic LEDs, solar energy devices, etc.). Similar linear conjugated compounds also share that interest, such as azulene-derived non-alternant hydrocarbons.[278,279,280,281] Additionally, the non-alternant hydrocarbons derived from the benzinterposition process applied in pentalene and heptalene can also be proposed.

The excited states of naphthalene (C(6+6)), anthracene (C(6+6+6)), tetracene (C(6+6+6+6)) and pentacene (C(6+6+6+6+6)) have been extensively studied and they will be used as reference. Inspecting **Table 60***,* it is observed that almost all of the molecules considered here show optically inactive $S_0 \rightarrow S_1$ transitions. One exception is azulene,[278,280, 502] (C(7+5), *f*=0.01), whose calculated value (2.37 eV) matches well with the experimental one (2.12 eV),[503] responsible of the observed blue color. However, in the literature can also be found articles that claim that the first

observable value transition is located at 3.65 eV, [504] matching the calculated energy of the $S_0 \rightarrow S_2$ transition (3.86 eV). According with these calculations, low absorption should be accounted for the $S_0 \rightarrow S_2$ transition, that shows *f*=0.003. Previous analysis of the excited states for heptalene (C(7+7)) shows a forbidden $S_0 \rightarrow S_1$ transition, while the $S_0 \rightarrow S_2$ absorbs in the near-UV (3.52 eV),[505,506] showing brownish red color. [506,507]

Table 60: Energies of the first singlet ($E[S_1]$) and two triplet ($E[T_1]$ and $E[T_2]$) excited states, and the $2E[T_1]$-$E[S_1]$ (C1) and $2E[T_1]$-$E[T_2]$ (C2) energy conditions, in eV, calculated with TDDFT. $E[Q_1]$ has been calculated with DFT. The spin-contaminated values are substituted by those obtained by SF-TDDFT and highlighted in italics.

	$E[S_1]$(f)		$E[S_n]$	$E[T_1]$	$E[T_2]$	$E[Q_1]$	$2E[T_1]$-$E[S_1]$	$2E[T_1]$-$E[T_2]$
C(6+6)	4.66	(0.00)	4.75	3.19	4.26	7.29	1.71	2.12
C(6+6+6)	3.59	(0.08)	--	2.20	3.69	6.46	0.80	0.70
C(6+6+6+6)	2.80	(0.08)	--	1.47	2.87	5.27	0.14	0.07
C(6+6+6+6+6)	2.25	(0.07)	--	0.91	2.23	4.04	-0.42	-0.40
C(5+5)	1.71	(0.00)	3.88	0.92	2.13	6.02	0.14	-0.28
C(5+6+5)	1.03	(0.00)	2.65	-0.44	0.80	3.92	-1.92	-1.69
C(5+6+6+5)	*0.87*	--	--	*-0.03*	*0.65*	3.30	*-0.94*	*-0.72*
C(5+6+6+6+5)	*1.13*	--	--	*-0.33*	*0.37*	2.94	*-1.79*	*-1.02*
C(7+7)	2.24	(0.00)	3.47	1.61	2.29	5.17	0.97	0.93
C(7+6+7)	0.86	(0.00)	2.02	-0.73	0.68	3.08	-2.32	-2.14
C(7+6+6+7)	*0.71*	--	--	*-0.31*	*0.43*	2.75	*-1.33*	*-1.04*
C(7+6+6+6+7)	*0.83*	--	--	*-0.49*	*0.27*	2.52	*-1.81*	*-1.24*
C(7+5)	2.37	(0.01)	--	2.00	2.44	5.15	1.63	1.56
C(7+6+5)	1.11	(0.00)	2.81	0.85	1.66	4.03	0.58	0.03
C(7+6+6+5)	*0.86*	--	--	*-0.09*	*0.49*	3.32	*-1.05*	*-0.68*
C(7+6+6+6+5)	*0.65*	--	--	*-0.73*	*-0.07*	2.01	*-2.11*	*-1.39*

For pentalene ((C(5+5)), previous CASPT2 calculations[277] claim that the only optically active transition is $S_0 \rightarrow S_3$. However, in this work is shown that the allowed

transition is $S_0 \rightarrow S_2$. In any case, the experimental value (3.48 eV) is close to the calculated one (3.88 eV). Finally, s-indacene (C(5+6+5)) can also be compared with experimental data,[284] and good agreement has been found: a forbidden band at 1.15 eV (1.03 eV with TDDFT) and an active transition at 2.25 eV (2.65 eV).

Few information is found about the triplet excited states. However, the azulene molecule and their elongated derivatives have been already theoretically studied giving singlet-triplet gaps matching the present values. Additionally, the same quantity has been calculated[274] referred to the larger molecule of each group (C(6+6+6+6+6), C(5+6+6+6+5), C(7+6+6+6+7) and C(5+6+6+6+7)), giving satisfactory results. The only experimental value refers to azulene, in which the singlet-triplet gap was measured to be 1.739 eV in solution, close to the results in the present study.[508] C(5+6+5) and C(7+6+7) show triplet ground states with TDDFT; however, DFT calculations show that their ground state is actually a singlet excepting C(7+6+6+6+5).

Irregular behavior is found on the $E[T_1]$ values calculated with both SF-TDDFT and TDDFT, and no clear trend is devised.

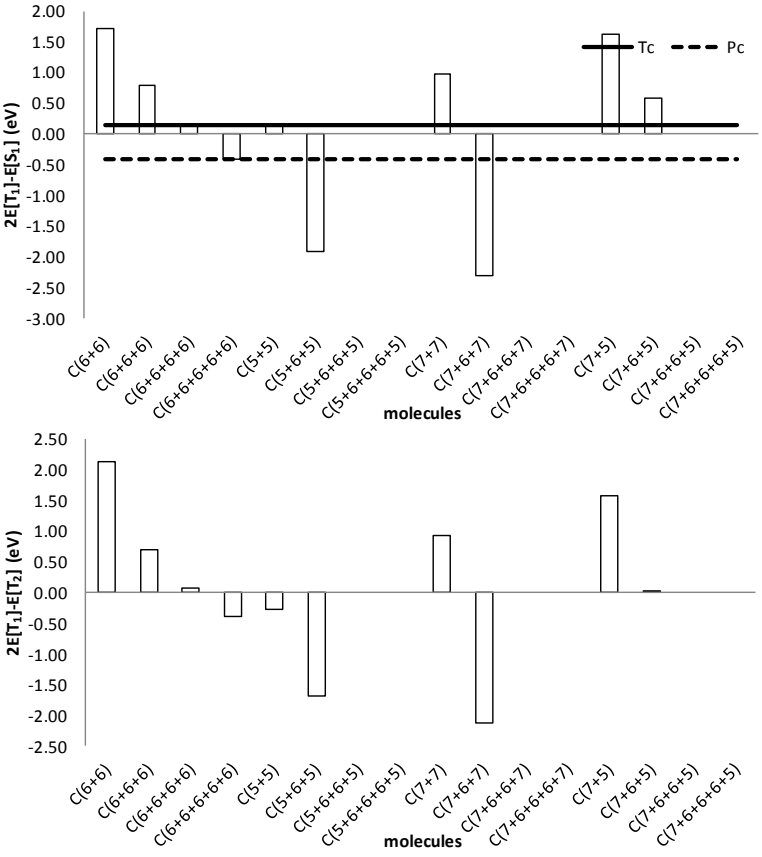

Figure 98: 2E[T_1]-E[S_1] (C1) and 2E[T_1]-E[T_2] (C2) conditions, in eV, for the studied molecules calculated with TDDFT. Some molecules have been omitted due to excessive spin contamination. Black straight and dashed lines represent the values for tetracene and pentacene, respectively.

In **Figure 98,** C1 positive values are found for all bicycles, while pentalene has an almost isoergic 2E[T_1]-E[S_1] value. Tricycles have more negative values than bicycles. The low values calculated for T_1 in molecules C(5+6+5) and C(7+6+7) are responsible for the observed too negative C1 values. Tetracycles are calculated to display C1 values

resembling the one of tetracene. However, such big systems are likely to have $S_0 \rightarrow S_1$ transitions lower than 1 eV, so the adequacy of these molecules for singlet fission purposes is not expected.

In summary, apart from the acene series of molecules, only pentalene combines a nearly isoergic C1. However, molecules C(5+6+6+5), C(5+6+6+7) and C(7+6+6+7) show C1 values near to the one of pentacene, so these could also be good candidates.

5.7. Indenofluorenes and indolocarbazoles

In Chapter 4, sixteen indenofluorenes (**1-16**) and five indolocarbazoles (**1-N**, **3-N**, **4-N**, **6-N** and **7-N**) were sketched as open-shell molecules. Despite this feature was already known for some of the proposed molecules, very little information is available regarding the singlet fission suitability of those molecules. To our knowledge, only the low-lying excited states of the indeno[1,2-b]fluorine molecule have been studied,[25] suggesting a slightly endoergic singlet fission process according with theoretical predictions.

In **Table 61** are summarized the electronic features of the proposed molecules. **1** and **4** molecules are investigated together with their mesityl derivatives (**2** and **5**). Interestingly, little differences are accounted for in the energy of their $S_0 \rightarrow S_n$ transitions. Additionally, UV-vis measurements of **2** and **4** have shown that their $S_0 \rightarrow S_n$ transitions are 2.41 and 1.70

eV, respectively. The mesityl derivative of **7** has also been measured to be 2.06 eV. The large open-shell character of **3**, **6**, **15** and **16** precluded the proper calculation of their excited states with TDDFT. The $S_0 \rightarrow S_1$ of molecules **1**-**7** fluctuate between 2.33 and 2.01 eV. SF-TDDFT calculations yield $S_0 \rightarrow S_1$ transitions of 0.66 and 0.57 eV for molecules **3** and **6,** respectively. Note that the nitrogen-containing molecules (indolocarbazoles) reduce the energy of the S_1 state 0.08-0.29 eV with respect to the parent indenofluorene.

From the whole set of 21 molecules, two of them were predicted to have triplet ground state from the $E[T_1]^{DFT}$ calculations: **6** and **6-N**. Besides, **3**, **3-N** and **16** have their triplet states only 0.12, 0.11 and 0.03 eV over the singlet, respectively. SQUID measurements on a molecule similar to **16** showed a triplet ground state only 14 meV below the singlet.[509]

The calculated C1 energy requirement is represented in **Figure 99**. The obtained $2E[T_1]$-$E[S_1]$ values are negative for indenofluorenes (from -0.09 to -0.55 eV), while the smallest C1 for the indolocarbazoles is 0.50 eV. SF-TDDFT shows that the molecules **3**, **3-N**, **6** and **6-N** yield excessively negative C1 values. The C2 condition is also fulfilled for molecules **2**, **4**, **5** and **7**, so these molecules are good choices for the accomplishment of efficient singlet fission. Molecules **8**, **9, 10** and **14** show high and optically active $S_0 \rightarrow S_1$ transitions, that combines well with the energy of the $S_0 \rightarrow T_1$

to get slightly endoergic C1 conditions. However, their $2E[T_1]$-$E[T_2]$ values are higher than 0.30 eV.

Table 61: Energies of the first singlet ($E[S_1]$) and two triplet ($E[T_1]$ and $E[T_2]$) excited states, and the $2E[T_1]$-$E[S_1]$ (C1) and $2E[T_1]$-$E[T_2]$ (C2) energy conditions, in eV, calculated with TDDFT. $E[Q_1]$ has been calculated with DFT. Reference values taken from Refs. 285, 287 and 298.

	$E[S_1](f)$		$E[S_n]$	$E[S_n]^{EXP}$	$E[T_1]$	$E[T_2]$	$E[Q_1]$	$2E[T_1]$-$E[S_1]$	$2E[T_1]$-$E[T_2]$
Indenofluorenes									
1	2.29	(0.00)	2.68	--	0.99	1.83	4.10	-0.31	0.16
2	2.33	(0.00)	2.57	2.41	0.89	1.87	4.04	-0.55	-0.09
3	*0.66*	--	--	--	*-0.51*	*0.20*	3.51	*-1.68*	*-1.21*
4	2.01	(0.08)	--	1.70	0.81	1.67	4.28	-0.39	-0.05
5	2.06	(0.11)	--	--	0.82	1.75	4.27	-0.42	-0.11
6	*0.57*	--	--	--	*-0.85*	*-0.17*	3.20	*-2.28*	*-1.53*
7	2.04	(0.07)	--	2.06	0.97	2.15	4.39	-0.09	-0.20
8	2.59	(0.31)	--	--	1.40	2.51	4.84	0.22	0.30
9	2.66	(0.33)	--	--	1.45	2.55	4.87	0.24	0.35
10	2.65	(0.29)	--	--	1.47	2.56	4.94	0.29	0.38
11	1.81	(0.23)	--	--	0.59	1.16	2.44	-0.63	0.02
12	2.20	(0.58)	--	--	0.59	2.28	3.85	-1.01	-1.10
13	2.39	(0.00)	2.49	--	1.55	1.76	5.11	0.70	1.33
14	2.79	(0.49)	--	--	1.53	2.69	5.38	0.26	0.37
15	*2.14*	--	--	--	*0.28*	*0.83*	4.50	*-1.57*	*-0.27*
16	*1.46*	--	--	--	*-0.61*	*0.05*	3.88	*-2.68*	*-1.26*
Indolocarbazoles									
1-N	2.00	(0.00)	2.76	--	1.38	1.48	4.38	0.76	1.28
3-N	*1.36*	--	--	--	*-0.54*	*0.12*	3.45	*-1.42*	*-1.20*
4-N	1.84	(0.00)	2.60	--	1.17	1.31	4.54	0.50	1.03
6-N	*0.36*	--	--	--	*-0.75*	*-0.06*	3.62	*-1.86*	*-1.44*
7-N	1.96	(0.01)	--	--	1.25	1.88	4.65	0.55	0.62

Similar features are accounted for molecules **11** and **12**, while their triplet states are only 0.59 eV over the ground state in both cases, originating too exoergic $2E[T_1]$-$E[S_1]$ values. Molecule **13** is apparently the less appropriated for singlet fission of the whole set. The absorption of the $S_0 \rightarrow S_n$ transitions (n=1,2) is small and the singlet-triplet gap is too large. Finally, regarding molecules **14**-**16**, only **14** could be

calculated with TDDFT methods. However, it shows a $2E[T_1]$-$E[S_1]$=0.26 eV.

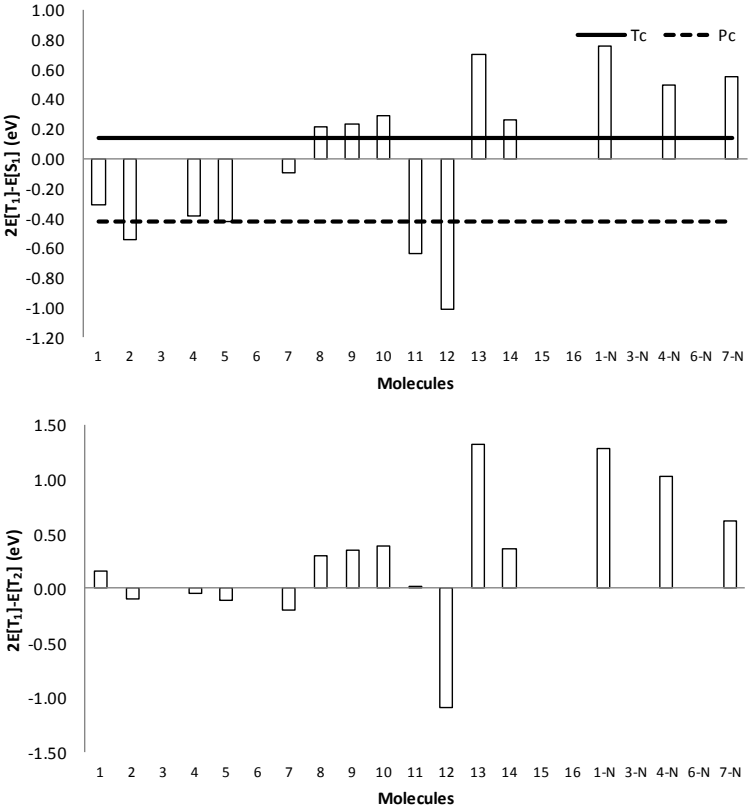

Figure 99: $2E[T_1]$-$E[S_1]$ (C1) and $2E[T_1]$-$E[T_2]$ (C2) conditions, in eV, for the studied molecules calculated with TDDFT. Some molecules have been omitted due to excessive spin contamination. Black straight and dashed lines represent the values for tetracene and pentacene, respectively.

In summary, molecules **2**, **4, 5** and **7** fulfill both C1 and C2 conditions and might be considered for future investigations as promising singlet fission materials due their

low-lying excited states as well as their experimental availability.

5.8. Derivatives of phenalenyl and acenaphthylene

The low-lying excited states of 23 phenalenyl and acenaphthylene derivatives have been studied in this subsection. In the literature, a few experimental values can be found. For instance, the singlet-triplet gaps of very similar structures to **2** and **3** (see **Figure 48**, Chapter 4) have been estimated to be 0.21 and 0.17 eV, respectively,[13] and their absorption spectra show a band at 1.66 eV and 1.43 eV, respectively.[13,319] With those results C1 can be estimated to be -1.24 and -1.10 eV respectively. Better values have been obtained for the singlet-triplet gap by means of DFT (0.23 and 0.12 eV respectively)

In **Table 62** are collected the excited states of the studied molecules, as well as the C1 and C2 energy requirements. Molecule **1** shows a triplet ground state, following TDDFT results. Nevertheless, $E[T_1]^{DFT}$ is 0.60 eV, suggesting a singlet ground state. Too negative $2E[T_1]-E[S_1]$ values are calculated for these molecules. Similar results are obtained for molecules **2**-**5**, **7** and **22**-**23,** using SF-TDDFT. Molecules **6**, **8** and **9** show too low $S_0 \rightarrow S_1$ to match the silicon energy gap.

Molecules **10**-**13** have $S_0 \rightarrow S_1$ between 1.84 and 2.07 eV, and only in case of **12** there is a forbidden transition (the

allowed one is only 0.01 eV above). The singlet-singlet transitions compare well with the experimental results. Molecules **14**-**17** have high $S_0 \rightarrow S_1$ transitions (higher than 2.75 eV) and high $S_0 \rightarrow T_1$ transitions (higher than 1.57 eV). Molecules **18-21** have $S_0 \rightarrow S_1$ transitions between 2.01 and 2.71 eV, apparently appropriated to match the ≈2.2 eV desired.

Table 62: Energies of the first singlet ($E[S_1]$) and two triplet ($E[T_1]$ and $E[T_2]$) excited states, and the $2E[T_1]$-$E[S_1]$ (C1) and $2E[T_1]$-$E[T_2]$ (C2) energy conditions, in eV, calculated with TDDFT. $E[Q_1]$ has been calculated with DFT. Experimental results from Refs. 13, 297 and 319. The spin-contaminated values are substituted by those obtained by SF-TDDFT and highlighted in italics.

	$E[S_1]$(f)		$E[S_n]$	$E[S_n]^{EXP}$	$E[T_1]$	$E[T_2]$	$E[Q_1]$	$2E[T_1]$-$E[S_1]$	$2E[T_1]$-$E[T_2]$
1	0.65	(0.00)	1.94	--	-0.47	0.51	3.05	-1.58	-1.44
2	*0.72*	--	--	1.66	*-0.40*	*0.38*	3.35	*-1.52*	*-1.18*
3	*1.13*	--	--	1.43	*-0.58*	*0.21*	3.08	*-2.29*	*-1.37*
4	*1.09*	--	--	--	*-0.67*	*0.12*	2.32	*-2.44*	*-1.47*
5	*0.74*	--	--	--	*-0.76*	*-0.02*	3.33	*-2.25*	*-2.44*
6	1.06	(0.11)	--	--	0.24	1.10	2.71	-0.59	-0.63
7	*0.50*	--	--	--	*-0.56*	*0.13*	2.70	*-1.61*	*-1.25*
8	1.48	(0.01)	--	--	0.83	1.25	2.43	0.18	0.42
9	1.51	(0.01)	--	--	0.86	1.08	2.39	0.20	0.63
10	1.89	(0.13)	--	1.63	1.17	1.71	3.12	0.45	0.62
11	2.01	(0.15)	--	1.54	1.18	1.70	3.04	0.35	0.66
12	2.07	(0.00)	2.08	--	1.62	1.69	3.17	1.17	1.56
13	1.84	(0.03)	--	--	1.46	1.84	3.54	1.08	1.07
14	3.49	(1.01)	--	--	2.21	2.44	4.53	0.93	1.98
15	3.65	(0.04)	--	--	2.63	2.91	5.45	1.60	2.35
16	3.39	(0.00)	3.41	--	2.22	2.90	4.88	1.05	1.55
17	2.75	(0.02)	--	--	1.57	2.72	4.46	0.39	0.43
18	2.71	(0.49)	--	--	1.09	2.62	4.73	-0.54	-0.45
19	2.67	(0.52)	--	--	1.08	2.59	4.60	-0.52	-0.44
20	2.01	(0.66)	--	--	0.67	1.97	3.87	-0.67	-0.64
21	2.08	(0.94)	--	--	0.64	1.92	3.70	-0.79	-0.63
22	*0.69*	--	--	--	*-0.63*	*0.28*	1.67	*-1.95*	*-1.53*

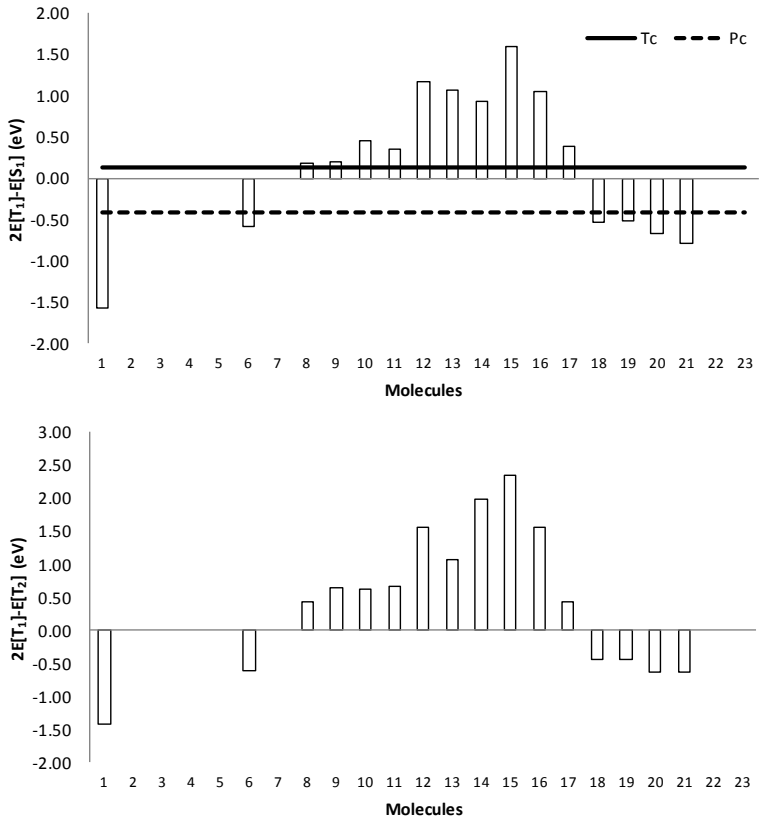

Figure 100: $2E[T_1]$-$E[S_1]$ and $2E[T_1]$-$E[T_2]$ energy differences, in eV, calculated with TDDFT. Black straight and dashed lines represent the values for tetracene and pentacene, respectively.

In **Figure 100** are represented the $2[T_1]$-$E[S_1]$ and $2E[T_1]$-$E[T_2]$ energy differences. The only molecules that fulfill C1 and C2 conditions are **6, 18, 19** and **20**, although the first one shows too low excited states to match the silicon energy gap. Molecules **8**-**11** present reasonable C1 conditions but C2 is too endoergic. In summary, the selected molecules in this group would be: **6**, **18, 19** and **20**.

5.9. Zethrenes

As it was previously advanced, zethrene diimides show endoergic values for the $2E[T_1]$-$E[S_1]$ condition. Zethrene, heptazethrene and octazethrene have been previously presented for their use in singlet fission devices.[471,510] Nevertheless, the research focused on these systems still represents a very small fraction compared to that focused on the acenes, whose applicability is still limited by low extinction coefficients and instability.[511] Thus, in this subsection are evaluated a set of zethrene derivatives that can be described as quinoidal derivatives. Their excited states are investigated using SF-TDDFT method, since large spin contamination precluded the use of TDDFT.

The excited states are gathered on **Table 63**, together with the $2E[T_1]$-$E[S_1]$ and $2E[T_1]$-$E[T_2]$ energy differences. Molecules **1**-**4** (perylene, zethrene, hexazethrene and heptazethrene) show decreasing $E[S_1]$ and $E[T_1]$ energies as long as the molecular size grows. For instance, from perylene to octazethrene, the calculated singlet-singlet transition is reduced in 1.71 eV, larger than the reduction of 0.99 eV observed experimentally. This might be related to an overestimation of the $S_0 \rightarrow S_1$ transitions. Thus, a large molecule such as **5** shows $E[S_1]$ as low as 1.45 eV, while the experimental value is 2.00 eV. Molecules **3**, **6**, **11** and **12** have a structure formed by seven benzene-like rings and similar $E[S_1]$ energies can be noted, except for molecule **12**, which has been already described as an almost perfect

diradical molecule and shows $E[S_1]$=1.61 eV. In the same way, molecules with the same size as octazethrene (**7**, **9** and **13**) can be compared and low $E[S_1]$ are found (1.36-1.57 eV), with the only exception of molecule **9** (2.12 eV), which can be related to larger diradical character. Finally, molecules **8** and **10** are comparable to nonazethrene, and very low $E[S_1]$ energies are found (1.18 and 1.51 eV, respectively, very close to the experimental data). In general, although large diradical characters are calculated for this group of molecules, which would correspond to low-energy excited states, molecules like **1**, **2**, **3**, **6**, **9** and **11** show values of $E[S_1]$>2 eV.

Table 63: Energies of the first singlet ($E[S_1]$) and two triplet ($E[T_1]$ and $E[T_2]$) excited states, and the $2E[T_1]$-$E[S_1]$ (C1) and $2E[T_1]$-$E[T_2]$ (C2) energy conditions, in eV, calculated with SF-TDDFT. $E[Q_1]$ has been calculated with DFT. Experimental results taken from Refs from 512, 254, 326, 298 and 513.

	$E[S_1]$	$E[S_n]^{EXP}$	$E[T_1]$	$E[T_2]$	$E[Q_1]$	$2E[T_1]$-$E[S_1]$	$2E[T_1]$-$E[T_2]$
1	3.21	2.85	1.58	2.14	6.17	-0.04	1.02
2	2.64	2.27	0.74	1.40	4.57	-1.17	0.07
3	2.03	2.11	0.14	0.86	3.19	-1.75	-0.58
4	1.50	1.86	-0.21	0.56	2.32	-1.92	-0.98
5	1.45	2.00	0.39	1.19	1.78	-0.68	-0.41
6	2.23	2.03	0.43	1.07	4.08	-1.38	-0.22
7	1.57	--	-0.11	0.60	3.42	-1.78	-0.81
8	1.18	1.25	-0.44	0.35	2.59	-2.05	-1.23
9	2.12	--	0.57	1.23	3.29	-0.97	-0.08
10	1.51	1.51	-0.08	0.70	2.42	-1.66	-0.85
11	2.12	--	0.15	0.85	3.55	-1.82	-0.56
12	1.61	--	-0.36	0.40	3.96	-2.32	-1.11
13	1.36	--	-0.75	0.08	3.18	-2.87	-1.58

Some negative TDDFT $E[T_1]$ energies have been found for molecules **4**, **7**, **8**, **10**, **12** and **13** but, according to

DFT calculations, singlet ground states are predicted. Nevertheless, $E[T_1]^{DFT}$ values as low as 0.05 eV (**13**) or 0.19 eV (**8**) were found. Additionally, SQUID experiments provide a $S_0 \rightarrow T_1$ transition of a close derivative of molecule **4** equal to 0.17 eV,[256] far from the -0.21 eV computed with SF-TDDFT, but not so far from the 0.32 eV predicted by DFT. Nonazene has also been determined to have a singlet ground state 0.22 eV lower than the triplet state.[337]

In **Figure 101** is observed that all the molecules have negative C1 and, with the exception of **1** and **2**, also negative C2 values. As the zethrene chain length grows (molecules from **1** to **4**), the C1 values become more negative, as expected, due to the reduction of the $S_0 \rightarrow S_1$ and $S_0 \rightarrow T_1$ excitations. Molecule **5** also shows negative C1 and C2 conditions, although rather large tetraradical character is observed (y_1=0.28). Nevertheless, the quintet state is high enough in energy to be problematic. The obtained C1 value is located between the limits of tetracene and pentacene. Thus, considering the C1 of these molecules (-0.48 and -0.91 eV, respectively), it can be asserted that molecules **2**, **5** and **9** have the most adequate $2E[T_1]$-$E[S_1]$ values, combined with negative (or almost negative) $2E[T_1]$-$E[T_2]$ quantities. Nevertheless, it should not be neglected the rather large diradical character they possess.

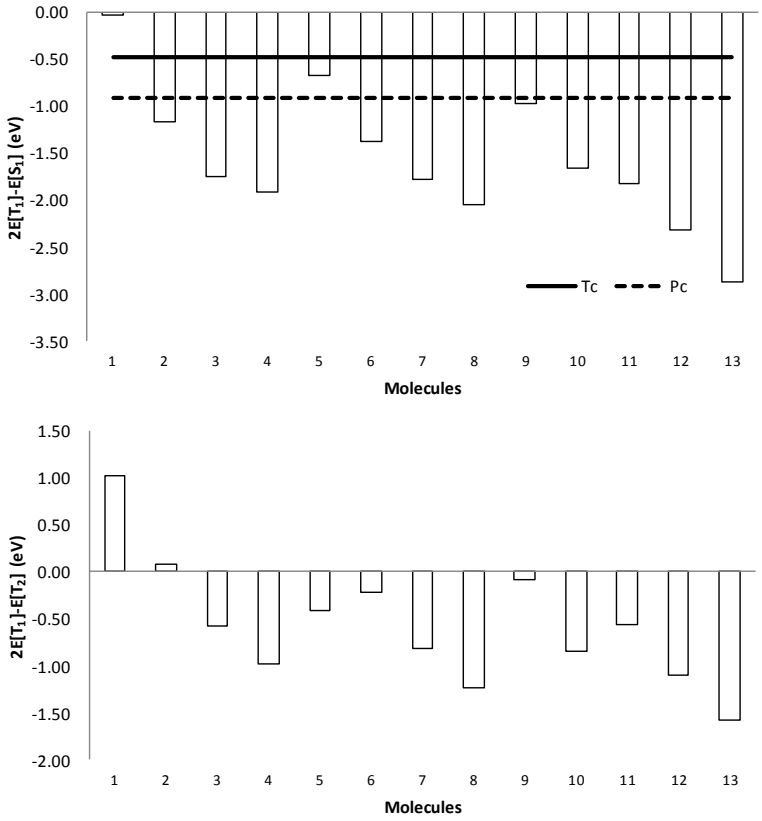

Figure 101: $2E[T_1]$-$E[S_1]$ and $2E[T_1]$-$E[T_2]$ energy differences, in eV, calculated with SF-TDDFT. Black straight and dashed lines represent the values for tetracene and pentacene, respectively.

Besides, in the literature can be found several quinone derivatives based on the zethrene backbone (see Chapter 4). The data of the excited states are collected in **Table 64**. Experimental UV-Vis data are available for zethrene quinones derived from molecules **4**, **5** and **13**. Thus, it is observed that the conversion to zethrene quinones leads to the diminution of the diradical character and then, the low-lying excited

states are shifted to higher energies. Molecules **1**, **2** and **4** show $E[S_1]$ values above the desired 2 eV. The C1 energy requirement is fulfilled for molecules **2** and **4**, while in case of molecule **1** is close to the fulfillment. .

Table 64: Energies of the first singlet ($E[S_1]$) and two triplet ($E[T_1]$ and $E[T_2]$) excited states, and the $2E[T_1]$-$E[S_1]$ (C1) and $2E[T_1]$-$E[T_2]$ (C2) energy conditions, in eV, calculated with SF-TDDFT. $E[Q_1]$ has been calculated with DFT. Experimental data from Refs. 298 and 331.

	$E[S_1]$	$E[S_n]^{EXP}$	$E[T_1]$	$E[T_2]$	$E[Q_1]$	$2E[T_1]$-$E[S_1]$	$2E[T_1]$-$E[T_2]$
1	2.59	2.00	1.10	1.66	3.53	-0.39	0.54
2	2.02	1.86	0.76	1.38	3.56	-0.51	0.13
3	1.75	--	0.44	0.88	2.47	-0.88	-0.01
4	2.60	2.24	1.78	2.18	3.45	0.96	1.38

As a conclusion, zethrenes **2**, **5** and **9** as well as the zethrene quinones **1**, **2** and **3** might be good candidates for singlet fission sensitizers.

5.10. Polycyclic aromatic hydrocarbons

In this subsection, the low-lying excited states of thirteen polycyclic aromatic hydrocarbons (PAH) have been investigated. Among them, molecules **1**-**7** are well described and have been selected from the analysis carried out by Parac and Grimme,[336] in which the lowest excitation energies were calculated by means of TDDFT and compared with experimental data. Additionally, six of the cyclopenta-fused PAHs (CP-PAHs) investigated by Naskar and Das (**8**-**13**)[333] may provide a starting point for further considerations, as these authors have observed that molecule (**8**), pyracylene, might match the $2E[T_1]$-$E[S_1]$ requirement.

Table 65: Energies of the first singlet ($E[S_1]$) and two triplet ($E[T_1]$ and $E[T_2]$) excited states, and the $2E[T_1]$-$E[S_1]$ (C1) and $2E[T_1]$-$E[T_2]$ (C2) energy conditions, in eV, calculated with TDDFT. $E[Q_1]$ has been calculated with DFT. Experimental data from references 514 and 515.

	$E[S_1]$(f)	$E[S_n]$	$E[S_n]^{EXP}$	$E[T_1]$	$E[T_2]$	$E[Q_1]$	$2E[T_1]$-$E[S_1]$	$2E[T_1]$-$E[T_2]$
1	3.98 (0.00)	4.02	3.53	2.51	3.76	6.39	1.04	1.27
2	2.57 (0.81)	--	--	0.98	2.27	3.81	-0.61	-0.31
3	1.95 (0.32)	--	1.87	0.58	2.35	4.15	-0.78	-1.18
4	3.49 (0.00)	--	3.72	2.77	3.32	5.66	2.04	2.22
5	3.50 (0.36)	--	3.06	2.15	3.37	5.69	0.81	0.93
6	3.54 (0.11)	--	3.23	2.30	3.16	5.50	1.07	1.45
7	3.12 (0.44)	--	2.87	1.67	3.04	5.66	0.22	0.30
8	2.26 (0.00)	3.44	2.56	1.57	2.58	5.95	0.87	0.55
9	2.34 (0.00)	3.21	--	1.58	2.23	4.88	0.82	0.93
10	0.89 (0.01)	--	0.90	0.43	1.30	3.44	-0.04	-0.45
11	2.07 (0.01)	--	1.61	1.55	1.72	3.40	1.03	1.38
12	1.21 (0.01)	--	--	0.59	1.47	3.20	-0.04	-0.30
13	1.25 (0.01)	--	--	0.57	1.16	2.73	-0.12	-0.03

The lowest excited states of molecules **1**-**13** are gathered on **Table 65**. The $S_0 \rightarrow S_1$ transitions are characterized as $\pi \rightarrow \pi^*$ transitions, and high oscillator strengths could be found for molecules from **1** to **7**. These molecules show large $E[S_1]$ values that, in some cases, exceeds 3 eV. As it has been already commented, the change of aggregation state from gas to the solid results on the redshift of the absorption band and, therefore, more reasonable values (around 2 eV) may be expected in these molecules. Additionally, experimental data could be found regarding the $E[T_1]$ values. Thus, molecules **1**, **4** and **5** have T_1 states 2.08, 2.40 and 1.82 eV higher than the values predicted by TDDFT, respectively. Some optically forbidden transitions can be found (**1**, **4**, **8**, **9**). Among them, no active

transition could be found on molecule **4**, although an experimental absorption maximum is present at 3.72 eV.

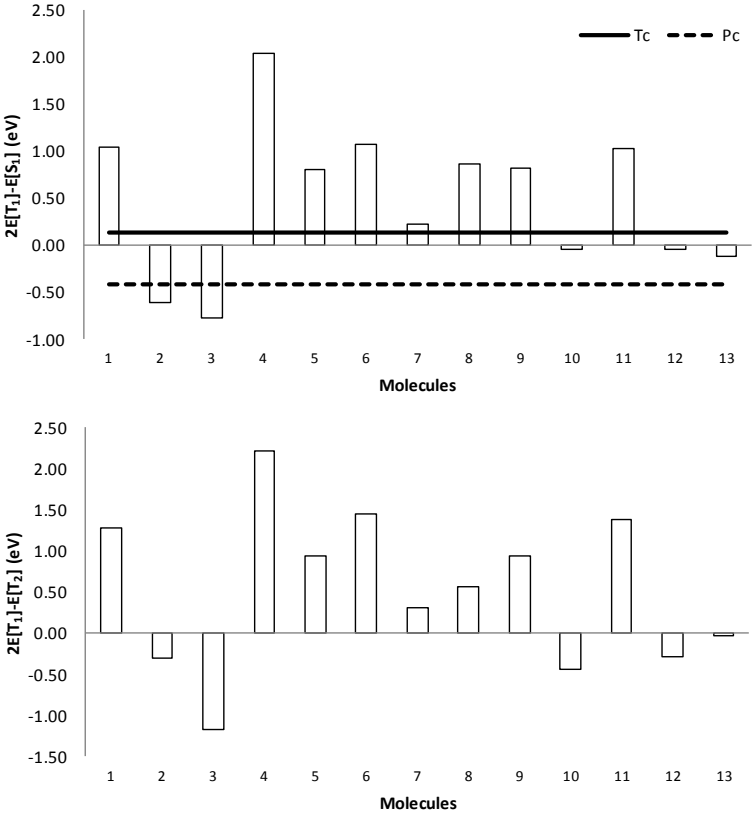

Figure 102: $2E[T_1]$-$E[S_1]$ and $2E[T_1]$-$E[T_2]$ energy differences, in eV, calculated with TDDFT. Black straight and dashed lines represent the values for tetracene and pentacene, respectively.

The $2E[T_1]$-$E[S_1]$ and $2E[T_1]$-$E[T_2]$ conditions are depicted on **Figure 102**. Only five molecules show negative C1 and C2, PAHs **2** and **7,** as well as CP-PAHs **10**, **12** and **13**. While these CP-PAHs show $2E[T_1]$-$E[S_1]$ values between the boundaries set by tetracene and pentacene, molecules **2**

and **3** show excessively negative C1 values. In the other hand, molecule **7** has a slightly endoergic C2 condition (0.22 eV), but this molecule will be included in the final selection because the soft application of heat could overcome this disadvantage. Regarding molecules **10, 12** and **13,** they show low $S_0 \rightarrow S_1$ absorptions that could negatively affect the efficiency of the process.

In summary, five promising candidates for singlet fission have been found in this group: **2**, **7**, **10**, **12** and **13**.

5.11. Summary and conclusions

To conclude, the low-lying excited states of up to 538 molecules have been analyzed in this chapter in order to establish their ability to undergo the singlet fission mechanism. Two energy conditions have been used to select promising candidates: (i) the energy of the first singlet state ($E[S_1]$) should be at least double of that of the first triplet state ($E[T_1]$). (ii) The energy of the second triplet state ($E[T_2]$) should be at least double of that of $E[T_1]$. This two conditions can be expressed as $2E[T_1]-E[S_1] \leq 0$ and $2E[T_1]-E[T_2]$ 0. Note that slight endoergicity in the first condition ($2E[T_1]-E[S_1]>0$) can be accepted.

Additionally, other considerations have also been inspected in this chapter. These features should be taken into account as recommendations, rather than compulsory requirements. They are listed as follows:

i. An optimal efficiency on the transformation of sunlight into electrical energy by means of singlet fission mechanism connected with a solar cell would require a T_1 state matching the bandgap of the semiconductor. In general, crystalline silicon is used (1.1 eV), but other semiconductor with bandgaps up to 1.8 eV can be used instead.

ii. The diradical character is intimately related with the energy of the T_1 state, and optimal $E[T_1]$ values are found for intermediate y_0, such as in pentacene (y_0=0.42).

iii. The tetraradical character (y_1), which is related to low Q_1 states that may diminish the efficiency of the process, might also be studied. The y_1/y_0 ratio should be lower than 0.2.

From the exhaustive TDDFT and SF-TDDFT analysis, we have found up to 126 molecules (around 23% from the total) that match the energy requirements and can be considered as potential singlet fission sensitizers:

- 32 conjugated quinones and methylene derivatives (14 Q, 14 QDM and 4 QM)
- 11 molecules resulting from structural modifications of the 1,5-anthraquinone: a) the oxygen of the carbonyl substituted by S and Se; b) substitution of boron in β and γ positions; c) substitution of silicon in β and δ positions; d) insertion of NH_2 in β, δ and ε positions; e) insertion of OCH_3 and OH in δ position.

- 2,6 dicarbonyl in tetracene, pentacene and hexacene
- 2,3 and 1,7 dicarbonyl in hexacene
- 15 croconates and 13 squarates
- 11 oligothiophenes
- 4 aromatic diimides
- 8 indigo-like cromophores
- 4 other carbonyl-containing chromophores
- 4 derivatives of naphthalene, pentalene, heptalene and azulene
- 4 indenofluorenes
- 4 phenalenyl and acenaphthylene derivatives
- 6 zethrenes and quinone derivatives
- 2 PAHs and 3 CP-PAHs

From section 3, 32 molecules have been selected and some of them are experimentally available, such as 1,7-C(6+6)/Q, 6-C(6+7)/Q or 1,2-C6/QDM and 1,4-C6/QDM. Following, many croconates and squarates have been already experimentally studied and, inspecting their low-lying excited states, croconates as **6** or squarates as **2**, **5**, **17**, **19** and **20** should be highlighted**.** From the aromatic diimides, molecule **11** matches both C1 and C2 conditions, has an optically active $S_0 \rightarrow S_1$ transition and it has already been synthesized. This molecule is structurally related with tetracene. Indigo-related structure **11** nicely fulfills the singlet fission requirements. Indenofluorenes **2**, **4** and **7** have been synthesized and the calculations performed suggest that they should be further investigated from an experimental point of

view. Zethrene quinones seem appropriated for SF like their zethrene counterparts and zethrene quinone **1** is the most attractive.

Chapter 7

Final conclusions

Organic open-shell diradicals have motivated intense consideration of experimentalists and theoreticians in the search of molecular materials with new and intriguing properties. Nevertheless, many of their features remain elusive due to difficulties to obtain experimental data. In this context, computational approaches have emerged as a valuable tool to unravel some of the otherwise inaccessible characteristics. In this thesis, a detailed analysis of the diradical nature and its influence in features such as low-lying excited states and redox chemistry has been performed in a large number of diradical structures.

Firstly, an assessment of a set of recently developed DFT functionals including long-range corrected, dispersion corrected and screened-exchange functionals has been carried out to define an efficient and computationally less demanding method to study these complicated electronic structures. Besides, four high-level composite methods designed for the study of radical species (G3n-RAD) have been tested. The main conclusion is that, in general, the studied functionals represent fairly well the diradical nature, although the incorporation of a certain amount of Hartree-Fock exchange is essential to calculate certain parameters. Functionals such as B3PW91, SOGGA11-X, M11 and ωB97X-D are suggested as good candidates for the calculation of features like EA, IP and $E[T_1]^{DFT}$. Besides, M06-2X functional is highlighted for the calculation of low-lying excited states using TDDFT.

A representative selection of molecules has been selected to characterize their ground state and analyze their diradical character (y_0). Firstly, a set of conjugated quinones and methylene derivatives formed by one, two or three fused rings with sizes between three and seven carbons is proposed. Then, the 1,5-anthraquinone is selected as a probe molecule to introduce modifications such as substitution of the carbonyl oxygen, substitution of carbons in the backbone by heteroatoms, addition of substituents and elongation of the conjugated chain. Large dependences have been found with the studied modifications. For instance, in the substitution of the carbonyl oxygen, y_0 is generally increased with the atomic number. The presence of heteroatoms in the carbon backbone modifies the diradical character depending both on the nature and the position of the heteroatom. Additionally, the effect of EWG or EDG substituents mainly relies upon the position rather than in their nature. Finally, increasing the chain length leads to an enhancement of y_0.

Next, a large screening of potential diradicals available in the literature has been performed and new derivatives have been proposed in order to study the nature of their ground state and expand the number of open-shell molecules, in the pursuit of promising candidates to be used in organic cathode materials and as singlet fission sensitizers. Most of the analyzed molecules show non-negligible diradical character and it is remarkable for groups like croconates, diimides, indolocarbazoles, zethrenes, oligothiophenes and derivatives of pentalene, azulene and hepatalene. Indigo-based and

carbonyl-containing chromophores show moderate to low diradical character.

The electrochemical features of the previously studied carbonyls have been investigated, including the first and second reduction potentials, first oxidation potential, electron affinity, ionization potential, and energy density. It is found that, in general, larger diradical characters accomplish larger EAs and redox potentials, suggesting that this feature may be used as a new, unexplored variable for tuning redox potentials. The addition of EWG substituents increases the reduction potentials, nevertheless lower energy densities are obtained due to the increase of the molecular weight. Additionally, the substitution of carbonyl oxygen by S and Se, as well as N and P in the carbon backbone (in α and γ positions) lead to derivatives with larger reduction potentials that may be good candidates for improved cathode materials. From the experimentally available carbonyl-containing molecules investigated, many of them show high reduction potentials, such as croconates, diimides, indigo-based dyes or carbazoloquinones, and may be proposed for further investigations. Thus, although the large size of some of them might be detrimental, an eventual experimental design with some of these materials might overcome the limitations of the traditional inorganic battery catodes.

The low-lying excited states of the whole set of molecules proposed in this thesis have been analyzed in order to establish their ability to undergo singlet fission, in the

pursuit of new sensitizers that may improve the performance of archetype molecules such as tetracene and pentacene. Two energy conditions have been used to select promising candidates: (i) $2E[T_1]-E[S_1]\leq 0$ and (ii) $2E[T_1]-E[T_2]<0$. The energies of the singlet and triplet states are, in general, decreased with larger y_0. Besides, it is known that adequate singlet fission materials require moderate diradical character, singlet-triplet gaps around 1.1 eV, and separation between the S_0 and S_1 around 2.2 eV. Thus, from the exhaustive TDDFT and SF-TDDFT analysis, up to 126 molecules from all the studied groups match the energetic requirements and can be selected as potential singlet fission sensitizers, including more than 40 carbonyls and methylene derivatives, 15 croconates, 13 squarates, 11 oligothiophenes and more than 10 chromophores, to mention some.

To conclude, although part of the results presented here are still unpublished, this thesis has contributed, up to now, to the following publications:

- López-Carballeira, D. and Ruipérez, F. (2016). Evaluation of modern DFT functionals and G3n-RAD composite methods in the modelization of organic singlet diradicals. Journal of Molecular Modeling, 22(4):76. doi: 10.1007/s00894-016-2950-z
- López-Carballeira, D. and Ruipérez, F. (2017). Singlet open-shell diradical nature and redox properties of conjugated carbonyls: a quantum chemical study.

Theoretical Chemistry Accounts, 136(3):32. doi: 10.1007/s00214-017-2061-7

- López-Carballeira, D., Casanova, D. and Ruipérez, F. (2017). Theoretical design of conjugated diradicaloids as singlet fission sensitizers: quinones and methylene derivatives. Physical Chemistry Chemical Physics, 19(44), 30227–30238. doi: 10.1039/c7cp05120d
- López-Carballeira, D., Casanova, D. and Ruipérez, F. Potential use of squarates and croconates as singlet fission sensitizers. *Submitted*

Resumen

Se usa el término *dirradical* para designar a aquellas moléculas que tienen dos electrones desapareados en su última capa y, por tanto, son moléculas de capa abierta. Cuando estos electrones están localizados en dos orbitales moleculares no enlazantes, el dirradical se puede representar por medio de seis configuraciones electrónicas: dos tripletes, dos singletes de capa cerrada y dos singletes de capa abierta. Según la regla de Hund, el dirradical más estable será aquél cuya multiplicidad es triplete, seguido por el singlete de capa abierta, de modo que el singlete de capa cerrada es el más inestable, debido a la repulsión interelectrónica. Sin embargo, si el valor de la integral de solapamiento entre los orbitales moleculares donde se encuentran los electrones desapareados es muy pequeño o despreciable, es posible que la regla de Hund no se cumpla y la multiplicidad más estable sea el singlete de capa abierta. .

Actualmente, hay un gran interés en el estudio de estos dirradicales debido a las extraordinarias propiedades ópticas y magnéticas que muestran, siendo de gran relevancia en optoelectrónica y espintrónica. Algunas de estas propiedades son estados excitados de baja energía, alto rendimiento en procesos de fisión de singlete, absorción en el infrarrojo cercano, diferencias de energía modulables entre alto y bajo espín, mejora de las propiedades ópticas no lineales, etc., cuyo origen está en el carácter dirradical de su

estructura electrónica singlete de capa abierta. De este modo, este tipo de moléculas representan una alternativa prometedora a los materiales orgánicos convencionales, en particular para su aplicación en dispositivos fotovoltaicos o en cátodos de baterías orgánicas.

A pesar de los esfuerzos llevados a cabo para la caracterización experimental de estos sistemas, muchas de sus propiedades siguen estando sin dilucidar debido a su inestabilidad y reactividad. En este contexto, los enfoques computacionales han surgido como una herramienta valiosa para desentrañar algunas de las características que de otro modo serían inaccesibles. Sin embargo, la descripción teórica de dirradicales singlete es muy complicada, ya que métodos como la Teoría del Funcional de la Densidad (DFT) o métodos monoconfiguracionales Hartree-Fock (HF) o post-HF no son capaces de representar correctamente una configuración singlete de capa abierta. Así, una descripción precisa de esta situación debería llevarse a cabo con métodos multiconfiguracionales como CASSCF/CASPT2, MR-CI o MR-AQCC, cuyo uso está muy limitado para el análisis de sistemas moleculares grandes o para el análisis sistemático de muchos sistemas, por el alto coste computacional que suponen.

Una alternativa para superar las limitaciones inherentes de DFT es el uso del formalismo *broken symmetry* (BS), donde la función de onda es una combinación de las funciones de onda del singlete de capa cerrada y del triplete,

y ya no es autofunción del operador total de espín $\langle \widehat{S^2} \rangle$, lo que se denomina como contaminación de espín. Así, para obtener valores representativos de las energías del estado singlete, esta contaminación de espín debe corregirse y, para ello, la aproximación de Yamaguchi es particularmente útil.

Esta tesis representa una contribución al cálculo y entendimiento de propiedades relevantes en dirradicales orgánicos singlete. Para ello, se ha realizado un análisis detallado de la naturaleza dirradical y la influencia que pueda tener sobre los estados excitados y la electroquímica de un gran número de estructuras donde el carácter diradical (y_0) sea distinto a cero.

En primer lugar, se ha llevado a cabo una evaluación de un conjunto de funcionales DFT recientemente desarrollados, que incluyen correcciones de largo alcance, de dispersión y funcionales conocidos como *screened-exchange*, con la finalidad de definir un método eficiente y que demande menos recursos desde un punto de visto computacional, para el estudio estos sistemas complicados. Además, se han evaluado cuatro métodos compuestos de alto nivel diseñados especialmente para el estudio de especies radicalarias (G3n-RAD). La conclusión principal es que, en general, los funcionales estudiados representan bastante bien la naturaleza de capa abierta de estos sistemas, aunque la incorporación de una cierta cantidad de intercambio Hartree-Fock es esencial para calcular ciertas magnitudes. Se sugieren funcionales tales como B3PW91,

SOGGA11-X, M11 y ωB97X-D como buenos candidatos para los cálculos de afinidad electrónica (EA), potencial de ionización (IP) y *singlet-triplet gap* (STG). Además, el funcional M06-2X destaca para el cálculo de estados excitados en combinación con TDDFT.

Se ha realizado una selección de un conjunto representativo de moléculas para caracterizar la naturaleza del estado fundamental y su carácter dirradical. Primero, se ha propuesto un conjunto de quinonas conjugadas y derivados de metileno formados por uno, dos o tres anillos fusionados con tamaño de anillo de entre 3 y 7 carbonos. A continuación, la 1,5-antraquinona es seleccionada para realizar modificaciones en su estructura y analizar sus efectos en el carácter dirradical. Estas modificaciones incluyen la sustitución del oxígeno carbonílico, la sustitución de carbonos por heteroátomos, la adición de grupos funcionales y la elongación de la cadena conjugada. Se han observado importantes modificaciones del carácter dirradical; por ejemplo, al sustituir el oxígeno carbonílico, y_0 suele aumentar con el número atómico. La presencia de heteroátomos en la cadena conjugada modifica esta propiedad dependiendo tanto de la naturaleza del heteroátomo como su posición. Además, el efecto de la presencia de grupos funcionales se basa fundamentalmente en su posición más que en su naturaleza dadora o aceptora de electrones. Finalmente, el aumentar la longitud de la cadena conduce a un aumento del carácter dirradical de la molécula.

A continuación, se ha realizado una amplia selección de posibles dirradicales disponibles en la literatura y se han propuesto nuevos derivados para estudiar la naturaleza de su estado fundamental y expandir el número de moléculas de capa abierta. Esto ayudará a encontrar nuevas y prometedoras moléculas que puedan ser utilizadas como cátodo en nuevas baterías orgánicas y como sensibilizadores en células solares basadas en fisión de singlete. La mayoría de las moléculas analizadas muestran un carácter diradical apreciable que incluso llega a ser muy notable para grupos como croconatos, diimidas, indolocarbazoles, zetrenos, oligotiofenos y derivados de pentaleno, azuleno y heptaleno. Por otro lado, cromóforos que contienen grupos carbonilo (como el índigo) muestran un carácter dirradical bajo o moderado.

Se han investigado las características electroquímicas de los compuestos carbonílicos estudiados previamente, incluyendo el primer y segundo potencial de reducción (E_R^1 y E_R^2), el primer potencial de oxidación (E_O^1), la afinidad electrónica (EA), el potencial de ionización (IP) y la densidad de energía (E_{DEN}). Se ha encontrado que, en general, un carácter dirradical alto se relaciona con valores altos de afinidad electrónica y potencial de reducción, lo que sugiere que esta característica se puede utilizar como una nueva variable no explorada para modificar los potenciales redox. La adición de sustituyentes dadores de electrones aumenta los potenciales de reducción; sin embargo, se obtienen densidades de energía más bajas debido al aumento del

peso molecular. Además, la sustitución del oxígeno de carbonilo por azufre y selenio, así como nitrógeno y potasio en la cadena principal de carbono (en las posiciones denominadas como α y γ), conduce a derivados con altos potenciales de reducción y que, por tanto, pueden ser buenas opciones para el diseño de baterías orgánicas más eficientes.

Se han investigado derivados carbonílicos que están experimentalmente disponibles, y muchos de ellos muestran potenciales de reducción altos. Ejemplos de ello son los croconatos, diimidas, índigo y sus derivados o las carbazoloquinonas. Por tanto, algunas de las moléculas propuestas pueden, por sus propiedades, ser un buen punto de partida para futuras investigaciones ya que, aunque el gran tamaño de algunos de ellos podría influir negativamente en propiedades como la densidad de energía, un diseño específico molecular podría superar las limitaciones de los cátodos inorgánicos tradicionales.

Los estados excitados más bajos de todo el conjunto de moléculas propuesto en esta tesis han sido analizados para establecer su capacidad de experimentar el proceso de fisión de singlete, para así poder diseñar sistemas que puedan mejorar el rendimiento de moléculas arquetípicas en fisión de singlete como tetraceno y pentaceno. Se han utilizado las siguientes dos condiciones de energía para seleccionar candidatos óptimos: (i) la energía del primer estado excitado singlete debe ser ligeramente mayor, o al menos similar al doble de la energía del primer estado

excitado triplete: $2E[T_1]-E[S_1]\leq 0$; (ii) la energía del segundo estado excitado triplete debe ser mayor del doble de la energía del primer triplete: $2E[T_1]-E[T_2]<0$.

Previamente a este estudio, moléculas con carácter dirradical intermedio han sido propuestas como candidatos prometedores para experimentar fisión de singlete, debido a sus pequeñas diferencias de energía entre el singlete y el triplete (*singlet-triplet gap*) que favorecen el cumplimiento de las dos condiciones mencionadas. Como las energías de los estados excitados singlete y triplete están relacionados con el carácter dirradical, esta propiedad es sugerida como una pauta para el diseño de nuevos sensibilizadores de fisión de singlete. Se ha observado que las energías de los estados singlete y triplete disminuyen, en general, al aumentar y_0, por lo que ambas condiciones serán satisfechas preferentemente por aquellas moléculas con cierto carácter dirradical, si bien un carácter dirradical demasiado alto daría lugar a que la condición (i) fuera demasiado negativa, lo que también tendría un efecto negativo. Además de las dos condiciones energéticas citadas anteriormente, se sabe que los materiales adecuados para fisión de singlete requieren una energía entre el estado fundamental (S_0) y el primer triplete (T_1) de alrededor de 1.1 eV y una separación entre S_0 y S_1 alrededor de 2.2 eV.

Gracias a un exhaustivo análisis en el que se han analizado los estados excitados obtenidos mediante cálculos TDDFT y SF-TDDFT, hasta 126 moléculas propicias para

fisión de singlete han sido seleccionadas, entre las que se pueden destacar 40 carbonilos y derivados de metileno, 15 croconatos, 13 escuaratos, 11 oligotiofenos y más de 10 cromóforos.

References

[1] Gomberg, M. (1897). Berichte Der Deutschen Chemischen Gesellschaft, 30(2), 2043–2047. doi:10.1002/cber.189703002177

[2] Gomberg, M. (1898). Journal of the American Chemical Society, 20(10), 773–780. doi:10.1021/ja02072a009

[3] Gomberg, M. (1900). Journal of the American Chemical Society, 22(11), 757–771. doi:10.1021/ja02049a006

[4] Tomlinson, E. P., Hay, M. E., and Boudouris, B. W. (2014). Macromolecules, 47(18), 6145–6158. doi:10.1021/ma5014572

[5] Nishide, H., Koshika, K., and Oyaizu, K. (2009). Pure and Applied Chemistry, 81(11), 1961–1970. doi:10.1351/pac-con-08-12-03

[6] Nakahara, K., Oyaizu, K., and Nishide, H. (2011). Chemistry Letters, 40(3), 222–227. doi:10.1246/cl.2011.222

[7] Muench, S., Wild, A., Friebe, C., Häupler, B., Janoschka, T., and Schubert, U. S. (2016). Chemical Reviews, 116(16), 9438–9484. doi:10.1021/acs.chemrev.6b00070

[8] Rajca, A. (2001). Science, 294(5546), 1503–1505. doi:10.1126/science.1065477

[9] Rajca, A. (2002). Chemistry - A European Journal, 8(21), 4834–4841. doi:10.1002/1521-3765(20021104)8:21<4834::aid-chem4834>3.0.co;2-e

[10] Griller, D., and Ingold, K. U. (1976). Accounts of Chemical Research, 9(1), 13–19. doi:10.1021/ar50097a003

[11] Hund, F. (1925). Zeitschrift Für Physik, 33(1), 345–371. doi:10.1007/bf01328319

[12] Bonačić-Koutecký, V., Koutecký, J., and Michl, J. (1987). Angewandte Chemie International Edition in English, 26(3), 170–189. doi:10.1002/anie.198701701

[13] Abe, M. (2013). Chemical Reviews, 113(9), 7011–7088. doi:10.1021/cr400056a

[14] Borden, W. T. (2015). In The Foundations of Physical Organic Chemistry: Fifty Years of the James Flack Norris Award (pp. 251–303). American Chemical Society. doi:10.1021/bk-2015-1209.ch011

[15] Zhang, K., Monteiro, M. J., and Jia, Z. (2016). Polymer Chemistry, 7(36), 5589–5614. doi:10.1039/c6py00996d

[16] Chandra Mondal, K., Roy, S., and Roesky, H. W. (2016). Chemical Society Reviews, 45(4), 1080–1111. doi:10.1039/c5cs00739a

[17] Trinquier, G., and Malrieu, J.-P. (2014). Chemistry - A European Journal, 21(2), 814–828. doi:10.1002/chem.201403952

[18] Zeng, Z., Shi, X., Chi, C., López Navarrete, J. T., Casado, J., and Wu, J. (2015). Chemical Society Reviews, 44(18), 6578–6596. doi:10.1039/c5cs00051c

[19] Thiele, J., and Balhorn, H. (1904). Berichte Der Deutschen Chemischen Gesellschaft, 37(2), 1463–1470. doi:10.1002/cber.19040370245

[20] Tschitschibabin, A. E. (1907). Berichte Der Deutschen Chemischen Gesellschaft, 40(2), 1810–1819. doi:10.1002/cber.19070400282

[21] Quinkert, G., Wiersdorff, W.-W., Finke, M., and Opitz, K. (1966). Tetrahedron Letters, 7(20), 2193–2200. doi:10.1016/s0040-4039(00)72400-2

[22] Montgomery, L. K., Huffman, J. C., Jurczak, E. A., and Grendze, M. P. (1986). Journal of the American Chemical Society, 108(19), 6004–6011. doi:10.1021/ja00279a056

[23] Hicks RG (2010) Stable Radicals – Fundamentals and Applied Aspects of Odd-electron Compounds. John Wiley & Sons, Chichester

[24] Nagai, H., Nakano, M., Yoneda, K., Kishi, R., Takahashi, H., Shimizu, A., … Champagne, B. (2010). Chemical Physics Letters, 489(4–6), 212–218. doi:10.1016/j.cplett.2010.03.013

[25] Ito, S., Minami, T., and Nakano, M. (2012). The Journal of Physical Chemistry C, 116(37), 19729–19736. doi:10.1021/jp3072684

[26] Lambert, C. (2011). Angewandte Chemie International Edition, 50(8), 1756–1758. doi:10.1002/anie.201006705

[27] Sun, Z., and Wu, J. (2012). J. Mater. Chem., 22(10), 4151–4160. doi:10.1039/c1jm14786b

[28] Di Motta, S., Negri, F., Fazzi, D., Castiglioni, C., and Canesi, E. V. (2010). The Journal of Physical Chemistry Letters, 1(23), 3334–3339. doi:10.1021/jz101400d

[29] Ponce Ortiz, R., Casado, J., Hernández, V., López Navarrete, J. T., Viruela, P. M., Ortí, E., … Otsubo, T. (2007). Angewandte Chemie International Edition, 46(47), 9057–9061. doi:10.1002/anie.200703244

[30] Boratyński, P. J., Pink, M., Rajca, S., and Rajca, A. (2010). Angewandte Chemie International Edition, 49(32), 5459–5462. doi:10.1002/anie.201002811

[31] Trinquier, G., Suaud, N., and Malrieu, J.-P. (2010). Chemistry - A European Journal, 16(29), 8762–8772. doi:10.1002/chem.201000044

[32] Paci, I., Johnson, J. C., Chen, X., Rana, G., Popović, D., David, D. E., … Michl, J. (2006). Journal of the American Chemical Society, 128(51), 16546–16553. doi:10.1021/ja063980h

[33] Smith, M. B., and Michl, J. (2010). Chemical Reviews, 110(11), 6891–6936. doi:10.1021/cr1002613

[34] Minami, T., and Nakano, M. (2011). The Journal of Physical Chemistry Letters, 3(2), 145–150. doi:10.1021/jz2015346

[35] Shimizu, A., Uruichi, M., Yakushi, K., Matsuzaki, H., Okamoto, H., Nakano, M., … Kubo, T. (2009). Angewandte Chemie International Edition, 48(30), 5482–5486. doi:10.1002/anie.200901382

[36] Tian, Y.-H., and Kertesz, M. (2010). Journal of the American Chemical Society, 132(31), 10648–10649. doi:10.1021/ja103396h

[37] Kamada, K., Ohta, K., Kubo, T., Shimizu, A., Morita, Y., Nakasuji, K., … Nakano, M. (2007). Angewandte Chemie International Edition, 46(19), 3544–3546. doi:10.1002/anie.200605061

[38] Quast, H., Fuß, A., and Jakobi, H. (1991). Chemische Berichte, 124(8), 1747–1755. doi:10.1002/cber.19911240813

[39] Shang, Y., Hao, S., Yang, C., and Chen, G. (2015). Nanomaterials, 5(4), 1782–1809. doi:10.3390/nano5041782

[40] https://www.nrel.gov/

[41] Shockley, W., and Queisser, H. J. (1961). Journal of Applied Physics, 32(3), 510–519. doi:10.1063/1.1736034

[42] Delgado, J. L., Bouit, P.-A., Filippone, S., Herranz, M., and Martín, N. (2010). Chemical Communications, 46(27), 4853. doi:10.1039/c003088k

[43] Hagfeldt, A., Boschloo, G., Sun, L., Kloo, L., and Pettersson, H. (2010). Chemical Reviews, 110(11), 6595–6663. doi:10.1021/cr900356p

[44] Shin, S. S., Yeom, E. J., Yang, W. S., Hur, S., Kim, M. G., Im, J., … Seok, S. I. (2017). Science, 356(6334), 167–171. doi:10.1126/science.aam6620

[45] Simon, Y. C., and Weder, C. (2012). Journal of Materials Chemistry, 22(39), 20817. doi:10.1039/c2jm33654e

[46] Zhou, J., Liu, Q., Feng, W., Sun, Y., and Li, F. (2014). Chemical Reviews, 115(1), 395–465. doi:10.1021/cr400478f

[47] Cates, E. L., Chinnapongse, S. L., Kim, J.-H., and Kim, J.-H. (2012). Environmental Science & Technology, 46(22), 12316–12328. doi:10.1021/es303612p

[48] Burdett, J. J., Müller, A. M., Gosztola, D., and Bardeen, C. J. (2010). The Journal of Chemical Physics, 133(14), 144506. doi:10.1063/1.3495764

[49] Lee, J., Jadhav, P., and Baldo, M. A. (2009). Applied Physics Letters, 95(3), 33301. doi:10.1063/1.3182787

[50] Rao, A., Wilson, M. W. B., Hodgkiss, J. M., Albert-Seifried, S., Bässler, H., and Friend, R. H. (2010). Journal of the American Chemical Society, 132(36), 12698–12703. doi:10.1021/ja1042462

[51] Congreve, D. N., Lee, J., Thompson, N. J., Hontz, E., Yost, S. R., Reusswig, P. D., … Baldo, M. A. (2013). Science, 340(6130), 334–337. doi:10.1126/science.1232994

[52] Yost, S. R., Lee, J., Wilson, M. W. B., Wu, T., McMahon, D. P., Parkhurst, R. R., … Van Voorhis, T. (2014). Nature Chemistry, 6(6), 492–497. doi:10.1038/nchem.1945

[53] Busby, E., Xia, J., Low, J. Z., Wu, Q., Hoy, J., Campos, L. M., and Sfeir, M. Y. (2015). The Journal of Physical Chemistry B, 119(24), 7644–7650. doi:10.1021/jp511704r

[54] Yoshino, A. (2012). Angewandte Chemie International Edition, 51(24), 5798–5800. doi:10.1002/anie.201105006

[55] Poizot, P., and Dolhem, F. (2011). Energy & Environmental Science, 4(6), 2003. doi:10.1039/c0ee00731e

[56] Song, Z., and Zhou, H. (2013). Energy & Environmental Science, 6(8), 2280. doi:10.1039/c3ee40709h

[57] Gracia, R., and Mecerreyes, D. (2013). Polymer Chemistry, 4(7), 2206. doi:10.1039/c3py21118e

[58] Janoschka, T., Hager, M. D., and Schubert, U. S. (2012). Applications. Advanced Materials, 24(48), 6397–6409. doi:10.1002/adma.201203119

[59] Tarascon, J.-M., and Armand, M. (2001). Nature, 414(6861), 359–367. doi:10.1038/35104644

[60] Choi, N.-S., Chen, Z., Freunberger, S. A., Ji, X., Sun, Y.-K., Amine, K., … Bruce, P. G. (2012). Angewandte Chemie International Edition, 51(40), 9994–10024. doi:10.1002/anie.201201429

[61] Williams, D. L., Byrne, J. J., and Driscoll, J. S. (1969). Journal of The Electrochemical Society, 116(1), 2. doi:10.1149/1.2411755

[62] Alt, H., Binder, H., Köhling, A., and Sandstede, G. (1972). Electrochimica Acta, 17(5), 873–887. doi:10.1016/0013-4686(72)90010-2

[63] Guin, P. S., Das, S., and Mandal, P. C. (2011). International Journal of Electrochemistry, 2011, 1–22. doi:10.4061/2011/816202

[64] Zhu, Z., Hong, M., Guo, D., Shi, J., Tao, Z., and Chen, J. (2014). Journal of the American Chemical Society, 136(47), 16461–16464. Doi:10.1021/ja507852t

[65] Wei, W., Li, L., Zhang, L., Hong, J., and He, G. (2018). Electrochemistry Communications, 90, 21–25. doi:10.1016/j.elecom.2018.03.006

[66] Schrödinger, E. (1926). Annalen Der Physik, 386(18), 109–139. doi:10.1002/andp.19263861802

[67] Born, M., and Oppenheimer, R. (1927). Annalen Der Physik, 389(20), 457–484. doi:10.1002/andp.19273892002

[68] Szabo, A.; Ostlund, N. S.; “Modern Quantum Chemistry. Introduction to Advanced Electronic Structure Theory”, Dover, New York, 1996.

[69] Hartree, D. R. (1928). Mathematical Proceedings of the Cambridge Philosophical Society, 24(1), 89. doi:10.1017/s0305004100011919

[70] Fock, V. (1930). Zeitschrift Für Physik, 61(1–2), 126–148. doi:10.1007/bf01340294

[71] Kutzelnigg, W. (1988). Theochem, 181(1–2), 33–54. doi:10.1016/0166-1280(88)80028-9

[72] Møller, C., and Plesset, M. S. (1934). Physical Review, 46(7), 618–622. doi:10.1103/physrev.46.618

[73] Bartlett, R. J.; "Recent Advances in Coupled-Cluster Methods", World Scientific, Singapore, 1997.

[74] Hohenberg, P., and Kohn, W. (1964). Physical Review, 136(3B), B864–B871. doi:10.1103/physrev.136.b864

[75] Kohn, W., and Sham, L. J. (1965). Physical Review, 140(4A), A1133–A1138. doi:10.1103/physrev.140.a1133

[76] Becke, A. D. (1988). Physical Review A, 38(6), 3098–3100. doi:10.1103/physreva.38.3098

[77] Becke, A. D. (1986). The Journal of Chemical Physics, 84(8), 4524–4529. doi:10.1063/1.450025

[78] Perdew, J. P. (1986). Physical Review B, 33(12), 8822–8824. doi:10.1103/physrevb.33.8822

[79] Perdew, J. P., Burke, K., and Ernzerhof, M. (1996). Physical Review Letters, 77(18), 3865–3868. doi:10.1103/physrevlett.77.3865

[80] Perdew, J. P., and Wang, Y. (1992). Physical Review B, 45(23), 13244–13249. doi:10.1103/physrevb.45.13244

[81] Lee, C., Yang, W., and Parr, R. G. (1988). Physical Review B, 37(2), 785–789. doi:10.1103/physrevb.37.785

[82] Becke, A. D. (1993). The Journal of Chemical Physics, 98(7), 5648–5652. doi:10.1063/1.464913

[83] Perdew, J. P.; in "Electronic Structure of Solids '91", Akademie Verlag, Berlin, 1991.

[84] Burke, K. Perdew, J. P. Wang, Y. in "Electronic Density Functional Theory: Recent Progress and New Directions", Plenum, New York, 1998.

[85] Vosko, S. H., Wilk, L., and Nusair, M. (1980). Canadian Journal of Physics, 58(8), 1200–1211. doi:10.1139/p80-159

[86] Zhao, Y., and Truhlar, D. G. (2007). Theoretical Chemistry Accounts, 120(1–3), 215–241. doi:10.1007/s00214-007-0310-x

[87] Runge, E., and Gross, E. K. U. (1984). Physical Review Letters, 52(12), 997–1000. doi:10.1103/physrevlett.52.997

[88] Casida, M. E. Recent Advances in Density Functional Methods; World Scientific: Singapore, 1995; Vol. 1.

[89] Shao, Y., Head-Gordon, M., and Krylov, A. I. (2003). The Journal of Chemical Physics, 118(11), 4807–4818. doi:10.1063/1.1545679

[90] Krylov, A. I. (2006). Accounts of Chemical Research, 39(2), 83–91. doi:10.1021/ar0402006

[91] Krylov, A. I. (2008). Annual Review of Physical Chemistry, 59(1), 433–462. doi:10.1146/annurev.physchem.59.032607.093602

[92] Krylov, A. I. (2001). Chemical Physics Letters, 350(5–6), 522–530. doi:10.1016/s0009-2614(01)01316-1

[93] Andersson, K., Malmqvist, P. A., Roos, B. O., Sadlej, A. J., and Wolinski, K. (1990). The Journal of Physical Chemistry, 94(14), 5483–5488. doi:10.1021/j100377a012

[94] Andersson, K., Malmqvist, P., and Roos, B. O. (1992). The Journal of Chemical Physics, 96(2), 1218–1226. doi:10.1063/1.462209

[95] Gdanitz, R. J., and Ahlrichs, R. (1988). Chemical Physics Letters, 143(5), 413–420. doi:10.1016/0009-2614(88)87388-3

[96] Szalay, P. G.; in “Modern Ideas in Coupled-Cluster Methods”, World Scientific, Singapore, 1997.

[97] Noodleman, L. (1981). The Journal of Chemical Physics, 74(10), 5737–5743. doi:10.1063/1.440939

[98] Noodleman, L., and Baerends, E. J. (1984). Journal of the American Chemical Society, 106(8), 2316–2327. doi:10.1021/ja00320a017

[99] Yamaguchi, K., Takahara, Y., Fueno, T., and Nasu, K. (1987). Japanese Journal of Applied Physics, 26(Part 2, No. 8), L1362–L1364. doi:10.1143/jjap.26.l1362

[100] Yamaguchi, K., Jensen, F., Dorigo, A., and Houk, K. N. (1988). Chemical Physics Letters, 149(5–6), 537–542. doi:10.1016/0009-2614(88)80378-6

[101] Noodleman, L., and Davidson, E. R. (1986). Chemical Physics, 109(1), 131–143. doi:10.1016/0301-0104(86)80192-6

[102] Illas, F., de P. R. Moreira, I., Bofill, J. M., and Filatov, M. (2004). Physical Review B, 70(13). doi:10.1103/physrevb.70.132414

[103] Gilbert, T. L. (1975). Physical Review B, 12(6), 2111–2120. doi:10.1103/physrevb.12.2111

[104] Levy, M. (1979). Proceedings of the National Academy of Sciences, 76(12), 6062–6065. doi:10.1073/pnas.76.12.6062

[105] Valone, S. M. (1980). The Journal of Chemical Physics, 73(3), 1344–1349. doi:10.1063/1.440249

[106] Piris, M., and Ugalde, J. M. (2014). International Journal of Quantum Chemistry, 114(18), 1169–1175. doi:10.1002/qua.24663

[107] Lopez, X., Ruipérez, F., Piris, M., Matxain, J. M., and Ugalde, J. M. (2011). ChemPhysChem, 12(6), 1061–1065. doi:10.1002/cphc.201100136

[108] Lopez, X., Piris, M., Matxain, J. M., Ruipérez, F., and Ugalde, J. M. (2011). ChemPhysChem, 12(9), 1673–1676. doi:10.1002/cphc.201100190

[109] Pople, J. A., Head-Gordon, M., Fox, D. J., Raghavachari, K., and Curtiss, L. A. (1989). The Journal of Chemical Physics, 90(10), 5622–5629. doi:10.1063/1.456415

[110] Curtiss, L. A., Jones, C., Trucks, G. W., Raghavachari, K., and Pople, J. A. (1990). The Journal of Chemical Physics, 93(4), 2537–2545. doi:10.1063/1.458892

[111] Curtiss, L. A., Raghavachari, K., Trucks, G. W., and Pople, J. A. (1991). The Journal of Chemical Physics, 94(11), 7221–7230. doi:10.1063/1.460205

[112] Curtiss, L. A., Raghavachari, K., Redfern, P. C., Rassolov, V., and Pople, J. A. (1998). The Journal of Chemical Physics, 109(18), 7764–7776. doi:10.1063/1.477422

[113] Curtiss, L. A., Redfern, P. C, and Raghavachari, K. (2007). The Journal of Chemical Physics, 126(8), 84108. doi:10.1063/1.2436888

[114] Henry, D. J., Sullivan, M. B, and Radom, L. (2003). The Journal of Chemical Physics, 118(11), 4849–4860. doi:10.1063/1.1544731

[115] Hemelsoet, K., Moran, D., Van Speybroeck, V., Waroquier, M, and Radom, L. (2006). The Journal of Physical Chemistry A, 110(28), 8942–8951. doi:10.1021/jp061823z

[116] Henry, D. J., Parkinson, C. J, and Radom, L. (2002). The Journal of Physical Chemistry A, 106(34), 7927–7936. doi:10.1021/jp0260752

[117] Perdew, J. P., Chevary, J. A., Vosko, S. H., Jackson, K. A., Pederson, M. R., Singh, D. J., and Fiolhais, C. (1992). Physical Review B, 46(11), 6671–6687. doi:10.1103/physrevb.46.6671

[118] Peverati, R, and Truhlar, D. G. (2012). Journal of Chemical Theory and Computation, 8(7), 2310–2319. doi:10.1021/ct3002656

[119] Peverati, R., and Truhlar, D. G. (2011). The Journal of Physical Chemistry Letters, 3(1), 117–124. doi: 10.1021/jz201525m

[120] Zhao, Y, and Truhlar, D. G. (2006). The Journal of Chemical Physics, 125(19), 194101. doi:10.1063/1.2370993

[121] Peverati, R, and Truhlar, D. G. (2012). Physical Chemistry Chemical Physics, 14(38), 13171. doi:10.1039/c2cp42025b

[122] Peverati, R, and Truhlar, D. G. (2011). The Journal of Chemical Physics, 135(19), 191102. doi:10.1063/1.3663871

[123] Zhao, Y, and Truhlar, D. G. (2006). The Journal of Physical Chemistry A, 110(49), 13126–13130. doi:10.1021/jp066479k

[124] Vydrov, O. A., Heyd, J., Krukau, A. V, and Scuseria, G. E. (2006). The Journal of Chemical Physics, 125(7), 74106. doi:10.1063/1.2244560

[125] Peverati, R, and Truhlar, D. G. (2011). The Journal of Physical Chemistry Letters, 2(21), 2810–2817. doi:10.1021/jz201170d

[126] Chai, J.-D, and Head-Gordon, M. (2008). The Journal of Chemical Physics, 128(8), 84106. doi:10.1063/1.2834918

[127] Chai, J.-D, and Head-Gordon, M. (2008). Physical Chemistry Chemical Physics, 10(44), 6615. doi:10.1039/b810189b

[128] Grimme, S. (2006). Journal of Computational Chemistry, 27(15), 1787–1799. doi:10.1002/jcc.20495

[129] Yanai, T., Tew, D. P, and Handy, N. C. (2004). Chemical Physics Letters, 393(1–3), 51–57. doi:10.1016/j.cplett.2004.06.011

[130] Peverati, R, and Truhlar, D. G. (2012). Physical Chemistry Chemical Physics, 14(47), 16187. doi:10.1039/c2cp42576a

[131] Hehre, W. J., Ditchfield, R, and Pople, J. A. (1972). The Journal of Chemical Physics, 56(5), 2257–2261. doi:10.1063/1.1677527

[132] Dunning, T. H., Jr. (1989). The Journal of Chemical Physics, 90(2), 1007–1023. doi:10.1063/1.456153

[133] Frisch, MJ, Trucks, GW, Schlegel, HB, Scuseria, GE, Robb, MA, Cheeseman, J.R., Scalmani, G., Barone, V., Mennucci, B., Petersson, G.A., Nakatsuji, H., Caricato, M. Li X., Hratchian, H.P., Izmaylov, A.F., Bloino, J., Zheng, G., Sonnenberg, J.L., Hada, M., Ehara, M., Toyota, K., Fukuda, R., Hasegawa, J., Ishida, M., Nakajima, T., Honda, Y., Kitao, O., Nakai, H., Vreven, T., Montgomery Jr., J.A., Peralta, J.E., Ogliaro, F., Bearpark, M., Heyd, J.J., Brothers, E., Kudin, K.N., Staroverov, V.N., Kobayashi, R., Normand, J., Raghavachari, K., Rendell, A., Burant, J.C., Iyengar, S.S., Tomasi, J., Cossi, M., Rega, N., Millam, J.M., Klene, M., Knox, J.E., Cross, J.B., Bakken, V, Adamo, C., Jaramillo, J., Gomperts, R., Stratmann, R.E., Yazyev, O., Austin, A.J., Cammi, R., Pomelli, C., Ochterski, J.W., Martin, R.L., Morokuma, K., Zakrzewski, V.G., Voth, G.A., Salvador, P., Dannenberg, J.J., Dapprich, S., Daniels, A.D., Farkas, Ö., Foresman, J.B., Ortiz J.V., Cioslowski, J., Fox DJ (2009). Gaussian 09, Revision A.1.Gaussian Inc., Wallingford CT

[134] Roos, B. O., Taylor, P. R, and Sigbahn, P. E. M. (1980). Chemical Physics, 48(2), 157–173. doi:10.1016/0301-0104(80)80045-0

[135] Siegbahn, P. E. M., Almlöf, J., Heiberg, A, and Roos, B. O. (1981). The Journal of Chemical Physics, 74(4), 2384–2396. doi:10.1063/1.441359

[136] Siegbahn, P., Heiberg, A., Roos, B, and Levy, B. (1980). Physica Scripta, 21(3–4), 323–327. doi:10.1088/0031-8949/21/3-4/014

[137] Aquilante, F., De Vico, L., Ferré, N., Ghigo, G., Malmqvist, P.-å., Neogrády, P., … Lindh, R. (2010). Journal of Computational Chemistry, 31(1), 224–247. doi:10.1002/jcc.21318

[138] Herebian, D., Wieghardt, K. E, and Neese, F. (2003). Journal of the American Chemical Society, 125(36), 10997–11005. doi:10.1021/ja030124m

[139] Mozhayskiy, V., Goebbert, D. J., Velarde, L., Sanov, A, and Krylov, A. I. (2010). The Journal of Physical Chemistry A, 114(26), 6935–6943. doi:10.1021/jp102183z

[140] Šimsa, D., Demel, O., Bhaskaran-Nair, K., Hubač, I., Mach, P, and Pittner, J. (2012). Chemical Physics, 401, 203–207. doi:10.1016/j.chemphys.2011.08.018

[141] Schalley, C. A., Blanksby, S., Harvey, J. N., Schröder, D., Zummack, W., Bowie, J. H, and Schwarz, H. (1998). European Journal of Organic Chemistry, 1998(6), 987–1009. doi:10.1002/(sici)1099-0690(199806)1998:6<987::aid-ejoc987>3.0.co;2-g

[142] Ichino, T., Villano, S. M., Gianola, A. J., Goebbert, D. J., Velarde, L., Sanov, A., … Lineberger, W. C. (2011). The Journal of Physical Chemistry A, 115(9), 1634–1649. doi:10.1021/jp111311k

[143] Vanovschi, V., Krylov, A. I, and Wenthold, P. G. (2007). Theoretical Chemistry Accounts, 120(1–3), 45–58. doi:10.1007/s00214-007-0305-7

[144] Li, H, and Huang, M.-B. (2008). Physical Chemistry Chemical Physics, 10(35), 5381. doi:10.1039/b805938a

[145] Sander, W., Exner, M., Winkler, M., Balster, A., Hjerpe, A., Kraka, E, and Cremer, D. (2002). Journal of the American Chemical Society, 124(44), 13072–13079. doi:10.1021/ja012686g

[146] Wenthold, PG, Hu, J, Squires, RR (1996) Journal of the American Chemical Society 118(47), 11865-11871.

[147] Nash, J. J, and Squires, R. R. (1996). Journal of the American Chemical Society, 118(47), 11872–11883. doi:10.1021/ja9606642

[148] Wenthold, P. G., Squires, R. R, and Lineberger, W. C. (1998). Journal of the American Chemical Society, 120(21), 5279–5290. doi:10.1021/ja9803355

[149] Perera, A., Molt, R. W., Lotrich, V. F., and Bartlett, R. J. (2014). Theoretical Chemistry Accounts, 133(8). doi: 10.1007/s00214-014-1514-5

[150] Chattopadhyay, S., Chaudhuri, R. K, and Freed, K. F. (2011). Physical Chemistry Chemical Physics, 13(16), 7514. doi:10.1039/c0cp02106g

[151] LI, X, and PALDUS, J. (2008). Journal of Theoretical and Computational Chemistry, 7(4), 805–820. doi:10.1142/s0219633608004131

[152] Nam, H. H., Leroi, G. E, and Harrison, J. F. (1991). The Journal of Physical Chemistry, 95(17), 6514–6519. doi:10.1021/j100170a026

[153] Cramer, C. J, and Debbert, S. (1998). Chemical Physics Letters, 287(3–4), 320–326. doi:10.1016/s0009-2614(98)00192-4

[154] Kraka, E, and Cremer, D. (1994). Journal of the American Chemical Society, 116(11), 4929–4936. doi:10.1021/ja00090a043

[155] Kraka, E., Cremer, D., Bucher, G., Wandel, H, and Sander, W. (1997). Chemical Physics Letters, 268(5–6), 313–320. doi:10.1016/s0009-2614(97)00233-9

[156] Opik, U, and Pryce, M. H. L. (1957). Proceedings of the Royal Society A: Mathematical, Physical and Engineering Sciences, 238(1215), 425–447. doi:10.1098/rspa.1957.0010

[157] Borden, W. T., Davidson, E. R., and Feller, D. (1982). Tetrahedron, 38(6), 737–739. doi: 10.1016/0040-4020(82)80153-1

[158] Cramer, C. J., Nash, J. J., and Squires, R. R. (1997). Chemical Physics Letters, 277(4), 311–320. doi: 10.1016/s0009-2614(97)00855-5

[159] Hrovat, D. A., Hou, G.-L., Wang, X.-B., and Borden, W. T. (2015). Journal of the American Chemical Society, 137(28), 9094–9099. doi:10.1021/jacs.5b04416

[160] Cramer, C. J., and Squires, R. R. (1997). The Journal of Physical Chemistry A, 101(49), 9191–9194. doi:10.1021/jp973119b

[161] Tozer, D. J., and De Proft, F. (2005). The Journal of Physical Chemistry A, 109(39), 8923–8929. doi:10.1021/jp053504y

[162] Izgorodina, E. I., Brittain, D. R. B., Hodgson, J. L., Krenske, E. H., Lin, C. Y., Namazian, M., and Coote, M. L. (2007). The Journal of Physical Chemistry A, 111(42), 10754–10768. doi:10.1021/jp075837w

[163] Grützmacher, H.-F., and Lohmann, J. (1970). Justus Liebigs Annalen Der Chemie, 733(1), 88–100. doi:10.1002/jlac.19707330109

[164] Adamo, C., and Barone, V. (1999). The Journal of Chemical Physics, 110(13), 6158–6170. doi:10.1063/1.478522

[165] Shao, Y.; Molnar, L. F.; Jung, Y.; Kussmann, J.; Ochsenfeld, C.; Brown, S. T.; Gilbert, A. T. B.; Slipchenko, L. V.; Levchenko, S. V.; O'Neill, D. P.; DiStasio, R. A., Jr; Lochan, R. C.; Wang, T.; Beran, G. J. O.; Besley, N. A.;

Herbert, J. M.; Lin, C. Y.; Voorhis, T. V.; Chien, S. H.; Sodt, A.; Steele, R. P.; Rassolov, V. A.; Maslen, P. E.; Korambath, P. P.; Adamson, R. D.; Austin, B.; Baker, J.; Byrd, E. F. C.; Dachsel, H.; Doerksen, R. J.; Dreuw, A.; Dunietz, B. D.; Dutoi, A. D.; Furlani, T. R.; Gwaltney, S. R.; Heyden, A.; Hirata, S.; Hsu, C.-P.; Kedziora, G.; Khalliulin, R. Z.; Klunzinger, P.; Lee, A. M.; Lee, M. S.; Liang, W.; Lotan, I.; Nair, N.; Peters, B.; Proynov, E. I.; Pieniazek, P. A.; Rhee, Y. M.; Ritchie, J.; Rosta, E.; Sherrill, C. D.; Simmonett, A. C.; Subotnik, J. E.; Iii, H. L. W.; Zhang, W.; Bell, A. T.; (2006). Physical Chemistry Chemical Physics, 8(27), 3172–3191. doi:10.1039/b517914a

[166] Bernard, Y. A., Shao, Y., and Krylov, A. I. (2012). The Journal of Chemical Physics, 136(20), 204103. doi:10.1063/1.4714499

[167] Conrad, M. P., Pitzer, R. M., and Schaefer, H. F. (1979). Journal of the American Chemical Society, 101(8), 2245–2246. doi:10.1021/ja00502a073

[168] Getty, S. J., Hrovat, D. A., and Borden, W. T. (1994). Journal of the American Chemical Society, 116(4), 1521–1527. doi:10.1021/ja00083a041

[169] Xu, J. D., Hrovat, D. A., and Borden, W. T. (1994). Journal of the American Chemical Society, 116(12), 5425–5427. doi:10.1021/ja00091a054

[170] Ma, J., Ding, Y., Hattori, K., and Inagaki, S. (2004). The Journal of Organic Chemistry, 69(12), 4245–4255. doi:10.1021/jo035687v

[171] Abe, M., Ishihara, C., and Tagegami, A. (2004). The Journal of Organic Chemistry, 69(21), 7250–7255. doi:10.1021/jo0490447

[172] Abe, M., Kubo, E., Nozaki, K., Matsuo, T., and Hayashi, T. (2006). Angewandte Chemie International Edition, 45(46), 7828–7831. doi:10.1002/anie.200603287

[173] Zhang, G., Li, S., and Jiang, Y. (2003). The Journal of Physical Chemistry A, 107(29), 5573–5582. doi:10.1021/jp022596d

[174] Fort, R. C., Getty, S. J., Hrovat, D. A., Lahti, P. M., and Borden, W. T. (1992). Journal of the American Chemical Society, 114(19), 7549–7552. doi:10.1021/ja00045a031

[175] Latif, I. A., Hansda, S., and Datta, S. N. (2012). The Journal of Physical Chemistry A, 116(33), 8599–8607. doi:10.1021/jp3033879

[176] Bachman, J. E., Curtiss, L. A., and Assary, R. S. (2014). The Journal of Physical Chemistry A, 118(38), 8852–8860. doi:10.1021/jp5060777

[177] Er, S., Suh, C., Marshak, M. P., and Aspuru-Guzik, A. (2015). Chemical Science, 6(2), 885–893. doi:10.1039/c4sc03030c

[178] Nourmohammadian, F.; Yavari, I.; Mohtat, B.; Shafaei, S.Z.; (2007). Dyes and Pigments, 75(2), 479–482. doi:10.1016/j.dyepig.2006.06.028

[179] Ohkita, M., Sano, K., Suzuki, T., Tsuji, T., Sato, T., and Niino, H. (2004). Organic & Biomolecular Chemistry, 2(7), 1044–1050. doi:10.1039/b400080n

[180] Golas, E., Lewars, E., and F. Liebman, J. (2009). The Journal of Physical Chemistry A, 113(34), 9485–9500. doi:10.1021/jp902868h

[181] Canesi, E. V., Fazzi, D., Colella, L., Bertarelli, C., and Castiglioni, C. (2012). Journal of the American Chemical Society, 134(46), 19070–19083. doi:10.1021/ja3072385

[182] Amiri, S., and Schreiner, P. R. (2009). The Journal of Physical Chemistry A, 113(43), 11750–11757. doi:10.1021/jp9028672

[183] Bunz, U. H. F. (2015). Accounts of Chemical Research, 48(6), 1676–1686. doi:10.1021/acs.accounts.5b00118

[184] Zeng, T., Ananth, N., and Hoffmann, R. (2014). Journal of the American Chemical Society, 136(36), 12638–12647. doi:10.1021/ja505275m

[185] Yang, Y., Davidson, E. R., and Yang, W. (2016). Proceedings of the National Academy of Sciences, 113(35), E5098–E5107. doi:10.1073/pnas.1606021113

[186] Radenković, S., Marković, S., Kuč, R., and Stanković, N. (2011). Monatshefte Für Chemie - Chemical Monthly, 142(10), 1013–1019. doi:10.1007/s00706-011-0557-8

[187] Shi, X., and Chi, C. (2017). Topics in Current Chemistry, 375(4). doi:10.1007/s41061-017-0154-3

[188] Acker, D. S., and Hertler, W. R. (1962). Journal of the American Chemical Society, 84(17), 3370–3374. doi:10.1021/ja00876a028

[189] Yanagimoto, T., Takimiya, K., Otsubo, T., and Ogura, F. (1993). Journal of the Chemical Society, Chemical Communications, (6), 519. doi:10.1039/c39930000519

[190] Yamanaka, S., Kawamura, T., Noro, T., and Yamaguchi, K. (1994). Journal of Molecular Structure, 310, 185–196. doi:10.1016/s0022-2860(10)80069-9

[191] Nakano, M., Kishi, R., Nakagawa, N., Ohta, S., Takahashi, H., Furukawa, S., … Yamaguchi, K. (2006). The Journal of Physical Chemistry A, 110(12), 4238–4243. doi:10.1021/jp056672z

[192] Nakano, M., Kishi, R., Ohta, S., Takebe, A., Takahashi, H., Furukawa, S., … Botek, E. (2006). The Journal of Chemical Physics, 125(7), 74113. doi:10.1063/1.2213974

[193] Ditchfield, R. (1974). Molecular Physics, 27(4), 789–807. doi:10.1080/00268977400100711

[194] Wolinski, K., Hinton, J. F., and Pulay, P. (1990). Journal of the American Chemical Society, 112(23), 8251–8260. doi:10.1021/ja00179a005

[195] Schleyer, P. von R., Maerker, C., Dransfeld, A., Jiao, H., and van Eikema Hommes, N. J. R. (1996). Journal of the American Chemical Society, 118(26), 6317–6318. doi:10.1021/ja960582d

[196] Schleyer, P. von R., Manoharan, M., Wang, Z.-X., Kiran, B., Jiao, H., Puchta, R., and van Eikema Hommes, N. J. R. (2001). Organic Letters, 3(16), 2465–2468. doi:10.1021/ol016217v

[197] Corminboeuf, C., Heine, T., Seifert, G., Schleyer, P. von R., and Weber, J. (2004). Physical Chemistry Chemical Physics, 6(2), 273–276. doi:10.1039/b313383b

[198] Gomes, J. A. N. F., and Mallion, R. B. (2001). Chemical Reviews, 101(5), 1349–1384. doi:10.1021/cr990323h

[199] Szatylowicz, H., Krygowski, T. M., Solà, M., Palusiak, M., Dominikowska, J., Stasyuk, O. A., and Poater, J. (2015). Theoretical Chemistry Accounts, 134(3). doi:10.1007/s00214-015-1635-5

[200] Motomura, S., Nakano, M., Fukui, H., Yoneda, K., Kubo, T., Carion, R., and Champagne, B. (2011). Physical Chemistry Chemical Physics, 13(46), 20575. doi:10.1039/c1cp20773c

[201] Tomerini, D., Gatti, C., and Frayret, C. (2016). Physical Chemistry Chemical Physics, 18(4), 2442–2448. doi:10.1039/c5cp05786h

[202]Yavari, I., and Zabarjad-Shiraz, N. (2007). Dyes and Pigments, 75(3), 669–674. doi:10.1016/j.dyepig.2006.06.034

[203] Hückel, W. (1937) Zeitschrift für Elektrochemie, 43, 827-849. doi: 10.1002/bbpc.19370431016

[204] Nishida, J., Fujiwara, Y., and Yamashita, Y. (2009). Organic Letters, 11(8), 1813–1816. doi:10.1021/ol9003838

[205] Anthony, J. E. (2006). Chemical Reviews, 106(12), 5028–5048. doi:10.1021/cr050966z

[206] Tang, Q., Liu, J., Chan, H. S., and Miao, Q. (2009). Chemistry - A European Journal, 15(16), 3965–3969. doi:10.1002/chem.200900160

[207] Miao, S., Brombosz, S. M., Schleyer, P. v. R., Wu, J. I., Barlow, S., Marder, S. R., … Bunz, U. H. F. (2008). Journal of the American Chemical Society, 130(23), 7339–7344. doi:10.1021/ja077614p

[208] Minami, T., Ito, S., and Nakano, M. (2013). The Journal of Physical Chemistry Letters, 4(13), 2133–2137. doi:10.1021/jz400931b

[209] Lynch, D. (2015). Metals, 5(3), 1349–1370. doi:10.3390/met5031349

[210] Lynch, D. E., and Hamilton, D. G. (2017). Australian Journal of Chemistry, 70(8), 857. doi:10.1071/ch16383

[211] Beverina, L., and Sassi, M. (2014). Synlett, 25(4), 477–490. doi:10.1055/s-0033-1340482

[212] Law, K. Y. (1993). Chemical Reviews, 93(1), 449–486. doi:10.1021/cr00017a020

[213] Emmelius, M., Pawlowski, G., and Vollmann, H. W. (1989). Angewandte Chemie International Edition in English, 28(11), 1445–1471. doi:10.1002/anie.198914453

[214] Gassensmith, J. J., Arunkumar, E., Barr, L., Baumes, J. M., DiVittorio, K. M., Johnson, J. R., … Smith, B. D. (2007). Journal of the American Chemical Society, 129(48), 15054–15059. doi:10.1021/ja075567v

[215] Arunkumar, E., Fu, N., and Smith, B. D. (2006). Chemistry - A European Journal, 12(17), 4684–4690. doi:10.1002/chem.200501541

[216] Gonçalves, M. S. T. (2009). Chemical Reviews, 109(1), 190–212. doi:10.1021/cr0783840

[217] Xiang, Z., Nesterov, E. E., Skoch, J., Lin, T., Hyman, B. T., Swager, T. M., … Reeves, S. A. (2005). Journal of Histochemistry & Cytochemistry, 53(12), 1511–1516. doi:10.1369/jhc.5a6704.2005

[218] Ashwell, G. J., Ewington, J., and Moczko, K. (2005). Journal of Materials Chemistry, 15(11), 1154. doi:10.1039/b413480j

[219] Collini, E., Carlotto, S., Ferrante, C., Bozio, R., Polimeno, A., Bloino, J., … Pagani, G. A. (2011). Physical Chemistry Chemical Physics, 13(25), 12087. doi:10.1039/c1cp20945k

[220] Shi, Q., Chen, W.-Q., Xiang, J., Duan, X.-M., and Zhan, X. (2011). Macromolecules, 44(10), 3759–3765. doi:10.1021/ma200386f

[221] Webster, S., Fu, J., Padilha, L. A., Przhonska, O. V., Hagan, D. J., Van Stryland, E. W., … Kachkovski, A. D. (2008). Chemical Physics, 348(1–3), 143–151. doi:10.1016/j.chemphys.2008.02.062

[222] Maeda, T., Nakao, H., Kito, H., Ichinose, H., Yagi, S., and Nakazumi, H. (2011). Dyes and Pigments, 90(3), 275–283. doi:10.1016/j.dyepig.2011.01.006

[223] Mayerhöffer, U., Deing, K., Gruß, K., Braunschweig, H., Meerholz, K., and Würthner, F. (2009). Angewandte Chemie International Edition, 48(46), 8776–8779. doi:10.1002/anie.200903125

[224] Völker, S. F., Uemura, S., Limpinsel, M., Mingebach, M., Deibel, C., Dyakonov, V., and Lambert, C. (2010). Macromolecular Chemistry and Physics, 211(10), 1098–1108. doi:10.1002/macp.200900670

[225] Wang, S., Hall, L., Diev, V. V., Haiges, R., Wei, G., Xiao, X., … Thompson, M. E. (2011). Chemistry of Materials, 23(21), 4789–4798. doi:10.1021/cm2020803

[226] Wei, G., Wang, S., Renshaw, K., Thompson, M. E., and Forrest, S. R. (2010). ACS Nano, 4(4), 1927–1934. doi:10.1021/nn100195j

[227] Wei, G., Xiao, X., Wang, S., Sun, K., Bergemann, K. J., Thompson, M. E., and Forrest, S. R. (2011). ACS Nano, 6(1), 972–978. doi:10.1021/nn204676j

[228] Beverina, L., and Salice, P. (2010). European Journal of Organic Chemistry, 2010(7), 1207–1225. doi:10.1002/ejoc.200901297

[229] Yagi, S., and Nakazumi, H., (2008) Topics in Heterocyclic Chemistry, 14,133–181.

[230] Ajayaghosh, A. (2005). Accounts of Chemical Research, 38(6), 449–459. doi:10.1021/ar0401000

[231] Sreejith, S., Carol, P., Chithra, P., and Ajayaghosh, A. (2008). Journals of Materials Chemistry, 18(3), 264–274. doi:10.1039/b707734c

[232] Lynch, D. E., and Hamilton, D. G. (2017). European Journal of Organic Chemistry, 2017(27), 3897–3911. doi:10.1002/ejoc.201700218

[233] Tripathi, A., Promila, and Prabhakar, C. (2016). Journal of Physical Organic Chemistry, 30(10), e3673. doi:10.1002/poc.3673

[234] Thomas, A., Srinivas, K., Prabhakar, C., Bhanuprakash, K., and Rao, V. J. (2008). Chemical Physics Letters, 454(1–3), 36–41. doi:10.1016/j.cplett.2008.01.074

[235] Seitz, G., and Imming, P. (1992). Chemical Reviews, 92(6), 1227–1260. doi:10.1021/cr00014a004

[236] Chitumalla, R. K., Lim, M., Gao, X., and Jang, J. (2015). Journal of Molecular Modeling, 21(11). doi:10.1007/s00894-015-2845-4

[237] Srinivas, K., Prabhakar, C., Devi, C. L., Yesudas, K., Bhanuprakash, K., and Rao, V. J. (2007). The Journal of Physical Chemistry A, 111(17), 3378–3386. doi:10.1021/jp067410f

[238] Yesudas, K., and Bhanuprakash, K. (2007). The Journal of Physical Chemistry A, 111(10), 1943–1952. doi:10.1021/jp068900a

[239] Fazzi, D., Canesi, E. V., Negri, F., Bertarelli, C., and Castiglioni, C. (2010). ChemPhysChem, 11(17), 3685–3695. doi:10.1002/cphc.201000675

[240] Koerner, C., Ziehlke, H., Fitzner, R., Riede, M., Mishra, A., Bäuerle, P., and Leo, K. (2016). Dicyanovinylene-Substituted Oligothiophenes for Organic Solar Cells. In Elementary Processes in Organic Photovoltaics (pp. 51–75). Springer International Publishing. doi:10.1007/978-3-319-28338-8_3

[241] Kishi, R., Ochi, S., Izumi, S., Makino, A., Nagami, T., Fujiyoshi, J., … Nakano, M. (2015Chemistry - A European Journal, 22(4), 1493–1500. doi:10.1002/chem.201503705

[242] Takahashi, T., Matsuoka, K., Takimiya, K., Otsubo, T., and Aso, Y. (2005). Journal of the American Chemical Society, 127(25), 8928–8929. doi:10.1021/ja051840m

[243] Takahashi, K., Suzuki, T., Akiyama, K., Ikegami, Y., and Fukazawa, Y. (1991). Journal of the American Chemical Society, 113(12), 4576–4583. doi:10.1021/ja00012a029

[244] Takahashi, K., Fujita, S., Akiyama, K., Miki, M., and Yanagi, K. (1998). Angewandte Chemie International Edition, 37(18), 2484–2487. doi:10.1002/(sici)1521-3773(19981002)37:18<2484::aid-anie2484>3.0.co;2-b

[245] D'Amore, F., Lanata, M., Gallazzi, M. C., and Zerbi, G. (2003). Chemical Physics Letters, 377(1–2), 243–248. doi:10.1016/s0009-2614(03)01152-7

[246] Lanata, M., Bertarelli, C., Gallazzi, M. C., Bianco, A., Del Zoppo, M., and Zerbi, G. (2003). Synthetic Metals, 138(1–2), 357–362. doi:10.1016/s0379-6779(03)00036-5

[247] Zhang, K., Huang, K.-W., Li, J., Luo, J., Chi, C., and Wu, J. (2009). Organic Letters, 11(21), 4854–4857. doi:10.1021/ol902241u

[248] Ishida, H., Yui, K., Aso, Y., Otsubo, T., and Ogura, F. (1990). Bulletin of the Chemical Society of Japan, 63(10), 2828–2835. doi:10.1246/bcsj.63.2828

[249] Fatiadi, A. J. (1978). Journal of the American Chemical Society, 100(8), 2586–2587. doi:10.1021/ja00476a073

[250] Takimiya, K., Kunugi, Y., Konda, Y., Niihara, N., and Otsubo, T. (2004). Journal of the American Chemical Society, 126(16), 5084–5085. doi:10.1021/ja0496930

[251] Batsanov, A. S., Bryce, M. R., Davies, S. R., Howard, J. A. K., Whitehead, R., and Tanner, B. K. (1993). Journal of the Chemical Society, Perkin Transactions 2, (3), 313–319. doi:10.1039/p29930000313

[252] Crean, C., Gallagher, J. F., and Pratt, A. C. (2001). Acta Crystallographica Section E Structure Reports Online, 57(3), o236–o238. doi:10.1107/s1600536801002598

[253] Song, Z., Zhan, H., and Zhou, Y. (2010). Angewandte Chemie, 122(45), 8622–8626. doi:10.1002/ange.201002439

[254] Ni, Y., and Wu, J. (2016). Tetrahedron Letters, 57(49), 5426–5434. doi:10.1016/j.tetlet.2016.10.100

[255] Sun, Z., Huang, K.-W., and Wu, J. (2011). Journal of the American Chemical Society, 133(31), 11896–11899. doi:10.1021/ja204501m

[256] Li, Y., Heng, W.-K., Lee, B. S., Aratani, N., Zafra, J. L., Bao, N., … Wu, J. (2012). Journal of the American Chemical Society, 134(36), 14913–14922. doi:10.1021/ja304618v

[257] Lee, S., Miao, F., Phan, H., Herng, T. S., Ding, J., Wu, J., and Kim, D. (2017). ChemPhysChem, 18(6), 591–595. doi:10.1002/cphc.201700015

[258] Minami, T., Ito, S., and Nakano, M. (2012). The Journal of Physical Chemistry Letters, 3(18), 2719–2723. doi:10.1021/jz3011749

[259] Nagami, T., Ito, S., Kubo, T., and Nakano, M. (2017). ACS Omega, 2(8), 5095–5103. doi:10.1021/acsomega.7b00655

[260] Zhao, X., Xiong, Y., Ma, J., and Yuan, Z. (2016). The Journal of Physical Chemistry A, 120(38), 7554–7560. doi:10.1021/acs.jpca.6b07552

[261] Cai, K., Xie, J., Yang, X., and Zhao, D. (2014). Organic Letters, 16(7), 1852–1855. doi:10.1021/ol500116z

[262] Li, C., Lin, Z., Li, Y., and Wang, Z. (2016). The Chemical Record, 16(2), 873–885. doi:10.1002/tcr.201500246

[263] Köytepe, S., Erdoğan, S., and Seçkin, T. (2009). Journal of Hazardous Materials, 162(2–3), 695–702. doi:10.1016/j.jhazmat.2008.05.126

[264] Fabian, J. (2010). Dyes and Pigments, 84(1), 36–53. doi:10.1016/j.dyepig.2009.06.008

[265] Viehe, H. G., Janousek, Z., Merenyi, R., and Stella, L. (1985). Accounts of Chemical Research, 18(5), 148–154. doi:10.1021/ar00113a004

[266] Xu, L., Sugiyama, T., Huang, H., Song, Z., Meng, J., and Matsuura, T. (2002). Chemical Communications, (20), 2328–2329. doi:10.1039/b206876a

[267] Oakley, S. R., Nawn, G., Waldie, K. M., MacInnis, T. D., Patrick, B. O., and Hicks, R. G. (2010). Chemical Communications, 46(36), 6753. doi:10.1039/c0cc01736a

[268] Thoburn, J. D., Lüttke, W., Benedict, C., and Limbach, H.-H. (1996). Journal of the American Chemical Society, 118(49), 12459–12460. doi:10.1021/ja962515p

[269] Gompper, R., Hartmann, K., Kellner, R., and Polborn, K. (1995). Angewandte Chemie International Edition in English, 34(4), 464–467. doi:10.1002/anie.199504641

[270] Buchsbaum, C., Paulus, E. F., and Schmidt, M. U. (2011). Zeitschrift Für Kristallographie, 226(11), 822–831. doi:10.1524/zkri.2011.1411

[271] Velezheva, V. S., Gunar, V. I., Balyakina, M. V., and Suvorov, N. N. (1978). Chemistry of Heterocyclic Compounds, 14(7), 757–760. doi:10.1007/bf00471645

[272] Seixas de Melo, J., Rondão, R., Burrows, H. D., Melo, M. J., Navaratnam, S., Edge, R., and Voss, G. (2006). The Journal of Physical Chemistry A, 110(51), 13653–13661. doi:10.1021/jp057451w

[273] Smith, M. B., and Michl, J. (2013). Annual Review of Physical Chemistry, 64(1), 361–386. doi:10.1146/annurev-physchem-040412-110130

[274] Nakano, M., Fukuda, K., and Champagne, B. (2016). The Journal of Physical Chemistry C, 120(2), 1193–1207. doi:10.1021/acs.jpcc.5b10503

[275] Boyd, G. V. (1966). Tetrahedron, 22(10), 3409–3416. doi:10.1016/s0040-4020(01)92529-3

[276] De Mayo, P., Bloch, R., and Marty, R. A. (1971). Journal of the American Chemical Society, 93(12), 3071–3072. doi:10.1021/ja00741a056

[277] Bally, T., Chai, S., Neuenschwander, M., and Zhu, Z. (1997). Journal of the American Chemical Society, 119(8), 1869–1875. doi:10.1021/ja963439t

[278] Xin, H., and Gao, X. (2017). ChemPlusChem, 82(7), 945–956. doi:10.1002/cplu.201700039

[279] Vosskötter, S., Konieczny, P., Marian, C. M., and Weinkauf, R. (2015). Physical Chemistry Chemical Physics, 17(36), 23573–23581. doi:10.1039/c5cp01826a

[280] Koch, M., Blacque, O., and Venkatesan, K. (2013). Journal of Materials Chemistry C, 1(44), 7400. doi:10.1039/c3tc31610f

[281] Radenković, S., Marković, S., and Milenković, V. (2012). Chemical Physics Letters, 545, 132–137. doi:10.1016/j.cplett.2012.07.021

[282] Peters, D. (1958). Journal of the Chemical Society (Resumed), 1023. doi:10.1039/jr9580001023

[283] Peters, D. (1958). Journal of the Chemical Society (Resumed), 1039. doi:10.1039/jr9580001039

[284] Gellini, C., Angeloni, L., Salvi, P. R., and Marconi, G. (1995). The Journal of Physical Chemistry, 99(1), 85–93. doi:10.1021/j100001a016

[285] Shimizu, A., and Tobe, Y. (2011). Angewandte Chemie International Edition, 50(30), 6906–6910. doi:10.1002/anie.201101950

[286] Chase, D. T., Rose, B. D., McClintock, S. P., Zakharov, L. N., and Haley, M. M. (2010). Angewandte Chemie International Edition, 50(5), 1127–1130. doi:10.1002/anie.201006312

[287] Fix, A. G., Deal, P. E., Vonnegut, C. L., Rose, B. D., Zakharov, L. N., and Haley, M. M. (2013). Organic Letters, 15(6), 1362–1365. doi:10.1021/ol400318z

[288] Miyoshi, H., Miki, M., Hirano, S., Shimizu, A., Kishi, R., Fukuda, K., … Tobe, Y. (2017). The Journal of Organic Chemistry, 82(3), 1380–1388. doi:10.1021/acs.joc.6b02500

[289] Miyoshi, H., Nobusue, S., Shimizu, A., Hisaki, I., Miyata, M., and Tobe, Y. (2014). Chemical Science, 5(1), 163–168. doi:10.1039/c3sc52622d

[290] Rudebusch, G. E., Zafra, J. L., Jorner, K., Fukuda, K., Marshall, J. L., Arrechea-Marcos, I., … Haley, M. M. (2016). Nature Chemistry, 8(8), 753–759. doi:10.1038/nchem.2518

[291] Rudebusch, G. E., Espejo, G. L., Zafra, J. L., Peña-Alvarez, M., Spisak, S. N., Fukuda, K., … Haley, M. M. (2016). Journal of the American Chemical Society, 138(38), 12648–12654. doi:10.1021/jacs.6b07882

[292] Fukuda, K., Fujiyoshi, J., Matsui, H., Nagami, T., Takamuku, S., Kitagawa, Y., … Nakano, M. (2017). Organic Chemistry Frontiers, 4(5), 779–789. doi:10.1039/c7qo00108h

[293] Miyoshi, H., Miki, M., Hirano, S., Shimizu, A., Kishi, R., Fukuda, K., … Tobe, Y. (2017). The Journal of Organic Chemistry, 82(3), 1380–1388. doi:10.1021/acs.joc.6b02500

[294] Chase, D. T., Fix, A. G., Rose, B. D., Weber, C. D., Nobusue, S., Stockwell, C. E., … Haley, M. M. (2011). Angewandte Chemie International Edition, 50(47), 11103–11106. doi:10.1002/anie.201104797

[295] Rose, B. D., Vonnegut, C. L., Zakharov, L. N., and Haley, M. M. (2012). Organic Letters, 14(9), 2426–2429. doi:10.1021/ol300942z

[296] Minami, T., Ito, S., and Nakano, M. (2013). The Journal of Physical Chemistry A, 117(9), 2000–2006. doi:10.1021/jp311965k

[297] Hibi, D., Kitabayashi, K., Fujita, K., Takeda, T., and Tobe, Y. (2016). The Journal of Organic Chemistry, 81(9), 3735–3743. doi:10.1021/acs.joc.6b00389

[298] Hu, P., Lee, S., Herng, T. S., Aratani, N., Gonçalves, T. P., Qi, Q., … Wu, J. (2016). Journal of the American Chemical Society, 138(3), 1065–1077. doi:10.1021/jacs.5b12532

[299] de la Harpe, C., and van Dorp, W. A. (1875). Berichte Der Deutschen Chemischen Gesellschaft, 8(2), 1048–1050. doi:10.1002/cber.18750080248

[300] Brunetti, F. G., Gong, X., Tong, M., Heeger, A. J., and Wudl, F. (2009). Angewandte Chemie International Edition, 49(3), 532–536. doi:10.1002/anie.200905117

[301] Hünig, S., and Steinmetzer, H.-C. (1976). Justus Liebigs Annalen Der Chemie, 1976(6), 1090–1102. doi:10.1002/jlac.197619760611

[302] Yudina, L. N., Preobrazhenskaya, M. N., and Korolev, A. M. (2000). Chemistry of Heterocyclic Compounds, 36(9), 1112–1113. doi:10.1023/a:1002754503680

[303] Gu, R., Robeyns, K., Van Meervelt, L., Toppet, S., and Dehaen, W. (2008). Organic & Biomolecular Chemistry, 6(14), 2484. doi:10.1039/b807255h

[304] Luo, D., Lee, S., Zheng, B., Sun, Z., Zeng, W., Huang, K.-W., … Wu, J. (2014). Chemical Science, 5(12), 4944–4952. doi:10.1039/c4sc01843e

[305] Zhang, B., Hu, X., Wang, M., Xiao, H., Gong, X., Yang, W., and Cao, Y. (2012). New Journal of Chemistry, 36(10), 2042. doi:10.1039/c2nj40309a

[306] Nie, H., Sun, G., Zhang, M., Baumgarten, M., and Müllen, K. (2012). Journal of Materials Chemistry, 22(5), 2129–2132. doi:10.1039/c1jm14691b

[307] Pei, Q., Yu, G., Zhang, C., Yang, Y., and Heeger, A. J. (1995). Science, 269(5227), 1086–1088. doi:10.1126/science.269.5227.1086

[308] Siove, A., and Adès, D. (2004). Polymer, 45(12), 4045–4049. doi:10.1016/j.polymer.2004.03.048

[309] Norcott, P., and McErlean, C. S. P. (2015). Organic & Biomolecular Chemistry, 13(24), 6866–6878. doi:10.1039/c5ob00852b

[310] Rickards, R. W., Rothschild, J. M., Willis, A. C., de Chazal, N. M., Kirk, J., Kirk, K., … Smith, G. D. (1999). Tetrahedron, 55(47), 13513–13520. doi:10.1016/s0040-4020(99)00833-9

[311] Furukawa, H.; Wu, T. S.; Ohta, T.; Kuoh, C. S.; (1985) Chemical and Pharmaceutical Bulletin, 33(10), 4132–4138. doi:10.1248/cpb.33.4132

[312] Saha, C., and Chowdhury, B. K. (1998). Phytochemistry, 48(2), 363–366. doi:10.1016/s0031-9422(97)01135-7

[313] Aouacheria, A., Néel, B., Bouaziz, Z., Dominique, R., Walchshofer, N., Paris, J., … Gillet, G. (2002). Biochemical Pharmacology, 64(11), 1605–1616. doi:10.1016/s0006-2952(02)01385-0

[314] Sánchez, J. D., Egris, R., Perumal, S., Villacampa, M., and Menéndez, J. C. (2012). European Journal of Organic Chemistry, 2012(12), 2375–2385. doi:10.1002/ejoc.201101848

[315] Benzies, D. W. M., and Jones, R. A. (1986). Journal of the Chemical Society, Chemical Communications, (13), 1019. doi:10.1039/c39860001019

[316] Compain-Batissou, M., Latreche, D., Gentili, J., Walchshofer, N., and Bouaziz, Z. (2004). Chemical & Pharmaceutical Bulletin, 52(9), 1114–1116. doi:10.1248/cpb.52.1114

[317] Kubo, T., Sakamoto, M., Akabane, M., Fujiwara, Y., Yamamoto, K., Akita, M., … Nakasuji, K. (2004). Angewandte Chemie, 116(47), 6636–6641. doi:10.1002/ange.200460565

[318] Ohashi, K., Kubo, T., Masui, T., Yamamoto, K., Nakasuji, K., Takui, T., … Murata, I. (1998). Journal of the American Chemical Society, 120(9), 2018–2027. doi:10.1021/ja970961m

[319] Kubo, T., Shimizu, A., Sakamoto, M., Uruichi, M., Yakushi, K., Nakano, M., … Nakasuji, K. (2005). Angewandte Chemie, 117(40), 6722–6726. doi:10.1002/ange.200502303

[320] Chikamatsu, M., Mikami, T., Chisaka, J., Yoshida, Y., Azumi, R., Yase, K., … Nakasuji, K. (2007). Applied Physics Letters, 91(4), 43506. doi:10.1063/1.2766696

[321] Kubo, T., Shimizu, A., Uruichi, M., Yakushi, K., Nakano, M., Shiomi, D., … Nakasuji, K. (2007). Organic Letters, 9(1), 81–84. doi:10.1021/ol062604z

[322] Shimizu, A., Kubo, T., Uruichi, M., Yakushi, K., Nakano, M., Shiomi, D., … Nakasuji, K. (2010). Journal of the American Chemical Society, 132(41), 14421–14428. doi:10.1021/ja1037287

[323] Nakano, M., and Champagne, B. (2015). The Journal of Physical Chemistry Letters, 6(16), 3236–3256. doi:10.1021/acs.jpclett.5b00956

[324] Sugiura, K., Mikami, S., Iwasaki, K., Hino, S., Asato, E., and Sakata, Y. (2000). Journal of Materials Chemistry, 10(2), 315–319. doi:10.1039/a907251i

[325] Sun, Z., Zeng, Z., and Wu, J. (2014). Accounts of Chemical Research, 47(8), 2582–2591. doi:10.1021/ar5001692

[326] Hu, P., and Wu, J. (2017). Canadian Journal of Chemistry, 95(3), 223–233. doi:10.1139/cjc-2016-0568

[327] Wu, T.-C., Chen, C.-H., Hibi, D., Shimizu, A., Tobe, Y., and Wu, Y.-T. (2010). Angewandte Chemie, 122(39), 7213–7216. doi:10.1002/ange.201001929

[328] Clar, E., Lang, K. F., and Schulz-Kiesow, H. (1955). Chemische Berichte, 88(10), 1520–1527. doi:10.1002/cber.19550881008

[329] Clar, E., and Macpherson, I. A. (1962). Tetrahedron, 18(12), 1411–1416. doi:10.1016/s0040-4020(01)99296-8

[330] Kemalettin Erünlü, R. (1969). Justus Liebigs Annalen Der Chemie, 721(1), 43–47. doi:10.1002/jlac.19697210107

[331] Hu, P., Lee, S., Park, K. H., Das, S., Herng, T. S., Gonçalves, T. P., … Wu, J. (2016). The Journal of Organic Chemistry, 81(7), 2911–2919. doi:10.1021/acs.joc.6b00172

[332] Sun, Z., Lee, S., Park, K. H., Zhu, X., Zhang, W., Zheng, B., … Wu, J. (2013). Journal of the American Chemical Society, 135(48), 18229–18236. doi:10.1021/ja410279j

[333] Naskar, S., and Das, M. (2017). ACS Omega, 2(5), 1795–1803. doi:10.1021/acsomega.7b00278

[334] Choi, Y., Chatterjee, T., Kim, J., Kim, J. S., and Cho, E. J. (2016). Organic & Biomolecular Chemistry, 14(28), 6804–6810. doi:10.1039/c6ob01235c

[335] Tsuneda, T., Singh, R. K., and Nakata, A. (2017). Journal of Computational Chemistry, 38(23), 2020–2029. doi:10.1002/jcc.24846

[336] Parac, M., and Grimme, S. (2003). Chemical Physics, 292(1), 11–21. doi:10.1016/s0301-0104(03)00250-7

[337] Huang, R., Phan, H., Herng, T. S., Hu, P., Zeng, W., Dong, S., … Wu, J. (2016). Journal of the American Chemical Society, 138(32), 10323–10330. doi:10.1021/jacs.6b06188

[338] Qu, Z., Zhang, D., Liu, C., and Jiang, Y. (2009). The Journal of Physical Chemistry A, 113(27), 7909–7914. doi:10.1021/jp9015728

[339] Bendikov, M., Duong, H. M., Starkey, K., Houk, K. N., Carter, E. A., and Wudl, F. (2004). Journal of the American Chemical Society, 126(24), 7416–7417. doi:10.1021/ja048919w

[340] Hod, O., Peralta, J. E., and Scuseria, G. E. (2007). Physical Review B, 76(23). doi:10.1103/physrevb.76.233401

[341] Wang, J., Zubarev, D. Y., Philpott, M. R., Vukovic, S., Lester, W. A., Cui, T., and Kawazoe, Y. (2010). Physical Chemistry Chemical Physics, 12(33), 9839. doi:10.1039/c003708g

[342] Reta Mañeru, D., Pal, A. K., Moreira, I. de P. R., Datta, S. N., and Illas, F. (2013). Journal of Chemical Theory and Computation, 10(1), 335–345. doi:10.1021/ct400883m

[343] Saito, T., Nishihara, S., Yamanaka, S., Kitagawa, Y., Kawakami, T., Yamada, S., … Yamaguchi, K. (2011). Theoretical Chemistry Accounts, 130(4–6), 739–748. doi:10.1007/s00214-011-0914-z

[344] Nakamura, T., Gagliardi, L., and Abe, M. (2010). Journal of Physical Organic Chemistry, n/a-n/a. doi:10.1002/poc.1643

[345] Cramer, C. J. (1998). Journal of the American Chemical Society, 120(25), 6261–6269. doi:10.1021/ja9806579

[346] Casado, J., Ponce Ortiz, R., and López Navarrete, J. T. (2012). Chemical Society Reviews, 41(17), 5672. doi:10.1039/c2cs35079c

[347] Yang, H., Song, Q., Li, W., Song, X., and Bu, Y. (2012). The Journal of Physical Chemistry C, 116(9), 5900–5907. doi:10.1021/jp2107654

[348] Romanova, J., Liégeois, V., and Champagne, B. (2014). Physical Chemistry Chemical Physics, 16(39), 21721–21731. doi:10.1039/c4cp02977a

[349] Liang, Y., Tao, Z., and Chen, J. (2012). Advanced Energy Materials, 2(7), 742–769. doi:10.1002/aenm.201100795

[350] Song, Z., Zhan, H., and Zhou, Y. (2009). Chem. Commun., (4), 448–450. doi:10.1039/b814515f

[351] Chen, H., Armand, M., Courty, M., Jiang, M., Grey, C. P., Dolhem, F., … Poizot, P. (2009). Journal of the American Chemical Society, 131(25), 8984–8988. doi:10.1021/ja9024897

[352] Choi, W., Harada, D., Oyaizu, K., and Nishide, H. (2011). Journal of the American Chemical Society, 133(49), 19839–19843. doi:10.1021/ja206961t

[353] Zhou, W., Hernández-Burgos, K., Burkhardt, S. E., Qian, H., and Abruña, H. D. (2013). The Journal of Physical Chemistry C, 117(12), 6022–6032. doi:10.1021/jp310555b

[354] Genorio, B., Pirnat, K., Cerc-Korosec, R., Dominko, R., and Gaberscek, M. (2010). Angewandte Chemie International Edition, 49(40), 7222–7224. doi:10.1002/anie.201001539

[355] Namazian, M., and Coote, M. L. (2007). The Journal of Physical Chemistry A, 111(30), 7227–7232. doi:10.1021/jp0725883

[356] Zhu, X.-Q., and Wang, C.-H. (2010). The Journal of Organic Chemistry, 75(15), 5037–5047. doi:10.1021/jo100735s

[357] Pakiari, A. H., Siahrostami, S., and Mohajeri, A. (2008). Journal of Molecular Structure: THEOCHEM, 870(1–3), 10–14. doi:10.1016/j.theochem.2008.08.030

[358] Namazian, M., Siahrostami, S., Noorbala, M. R., and Coote, M. L. (2006). THEOCHEM, 759(1–3), 245–247. doi:10.1016/j.theochem.2005.11.011

[359] Cheng, J., Sulpizi, M., and Sprik, M. (2009). The Journal of Chemical Physics, 131(15), 154504. doi:10.1063/1.3250438

[360] Johnsson Wass, J. R. T., Ahlberg, E., Panas, I., and Schiffrin, D. J. (2006). The Journal of Physical Chemistry A, 110(5), 2005–2020. doi:10.1021/jp055414z

[361] Hernández-Burgos, K., Burkhardt, S. E., Rodríguez-Calero, G. G., Hennig, R. G., and Abruña, H. D. (2014). The Journal of Physical Chemistry C, 118(12), 6046–6051. doi:10.1021/jp4117613

[362] Beheshti, A., Norouzi, P., Ganjali, M. R. (2012) International Journal of Electrochemical Science, 7:4811-4821

[363] Yao, M., Senoh, H., Araki, M., Sakai, T., and Yasuda, K. (2010). Presented at the 217th ECS Meeting, ECS. doi:10.1149/1.3490677

[364] Assary, R. S., Brushett, F. R., and Curtiss, L. A. (2014). RSC Adv., 4(101), 57442–57451. doi:10.1039/c4ra08563a

[365] Kim, K. C., Liu, T., Lee, S. W., and Jang, S. S. (2016). Journal of the American Chemical Society, 138(7), 2374–2382. doi:10.1021/jacs.5b13279

[366] Isse, A. A., and Gennaro, A. (2010). The Journal of Physical Chemistry B, 114(23), 7894–7899. doi:10.1021/jp100402x

[367] Namazian, M., Lin, C. Y., and Coote, M. L. (2010). Journal of Chemical Theory and Computation, 6(9), 2721–2725. doi:10.1021/ct1003252

[368] Nokami, T., Matsuo, T., Inatomi, Y., Hojo, N., Tsukagoshi, T., Yoshizawa, H., … Yoshida, J. (2012). Journal of the American Chemical Society, 134(48), 19694–19700. doi:10.1021/ja306663g

[369] Fu, Q., Yang, J., and Wang, X.-B. (2011). The Journal of Physical Chemistry A, 115(15), 3201–3207. doi:10.1021/jp1120542

[370] Heinis, T., Chowdhury, S., Scott, S. L., and Kebarle, P. (1988). Journal of the American Chemical Society, 110(2), 400–407. doi:10.1021/ja00210a015

[371] Lauer, G., Schäfer, W., and Schweig, A. (1975). Chemical Physics Letters, 33(2), 312–315. doi:10.1016/0009-2614(75)80164-3

[372] Millefiori, S., Gulino, A., and Casarin, M. (1990). Journal de Chimie Physique, 87, 317–330. doi:10.1051/jcp/1990870317

[373] Rothgery, E. F., Holt, R. J., and McGee, H. A. (1975). Journal of the American Chemical Society, 97(17), 4971–4973. doi:10.1021/ja00850a034

[374] Koenig, T., Smith, M., and Snell, W. (1977). Journal of the American Chemical Society, 99(20), 6663–6667. doi:10.1021/ja00462a031

[375] Peover ME (1965) Journal of the Chemical Society, 4540-4549.

[376] Scott, L. T. (1983). Pure and Applied Chemistry, 55(2), 363–368. doi:10.1351/pac198855020363

[377] Fabre, P.-L., Dumestre, F., Soula, B., and Galibert, A.-M. (2000). Electrochimica Acta, 45(17), 2697–2705. doi:10.1016/s0013-4686(00)00324-8

[378] Simard, T. P., Yu, J. H., Zebrowski-Young, J. M., Haley, N. F., and Detty, M. R. (2000). The Journal of Organic Chemistry, 65(7), 2236–2238. doi:10.1021/jo9916939

[379] Punzi, A., Capozzi, M. A. M., Fino, V., Carlucci, C., Suriano, M., Mesto, E., … Farinola, G. M. (2016). Journal of Materials Chemistry C, 4(15), 3138–3142. doi:10.1039/c6tc00264a

[380] Pradhan, A., Morimoto, T., Saikiran, M., Kapil, G., Hayase, S., and Pandey, S. S. (2017). Journal of Materials Chemistry A, 5(43), 22672–22682. doi:10.1039/c7ta06990a

[381] Büschel, M., Ajayaghosh, A., Arunkumar, E., and Daub, J. (2003). Organic Letters, 5(17), 2975–2978. doi:10.1021/ol034841x

[382] Chen, G., Sasabe, H., Sasaki, Y., Katagiri, H., Wang, X.-F., Sano, T., … Kido, J. (2014). Chemistry of Materials, 26(3), 1356–1364. doi:10.1021/cm4034929

[383] Ravet, N., Michot, C., and Armand, M. (1997). MRS Proceedings, 496. doi:10.1557/proc-496-263

[384] Luo, C., Huang, R., Kevorkyants, R., Pavanello, M., He, H., and Wang, C. (2014). Nano Letters, 14(3), 1596–1602. doi:10.1021/nl500026j

[385] Payne, A.-J., and Welch, G. C. (2017). Organic & Biomolecular Chemistry, 15(15), 3310–3319. doi:10.1039/c7ob00362e

[386] Völker, S. F., Renz, M., Kaupp, M., and Lambert, C. (2011). Chemistry - A European Journal, 17(50), 14147–14163. doi:10.1002/chem.201102227

[387] Wojcik, A., Nicolaescu, R., Kamat, P. V., Chandrasekaran, Y., and Patil, S. (2010). The Journal of Physical Chemistry A, 114(8), 2744–2750. doi:10.1021/jp9118887

[388] Varnavski, O., Abeyasinghe, N., Aragó, J., Serrano-Pérez, J. J., Ortí, E., López Navarrete, J. T., … Goodson, T., III. (2015). The Journal of Physical Chemistry Letters, 6(8), 1375–1384. doi:10.1021/acs.jpclett.5b00198

[389] Ray, S., Sharma, S., Salzner, U., and Patil, S. (2017). The Journal of Physical Chemistry C, 121(30), 16088–16097. doi:10.1021/acs.jpcc.7b04085

[390] Kishi, R., Katsurayama, T., Ochi, S., Makino, A., Matsushita, N., Saito, M., … Nakano, M. (2017). ChemistryOpen, 6(4), 506–513. doi:10.1002/open.201700083

[391] Casado, J., Miller, L. L., Mann, K. R., Pappenfus, T. M., Higuchi, H., Ortí, E., … López Navarrete, J. T. (2002). Journal of the American Chemical Society, 124(41), 12380–12388. doi:10.1021/ja027161i

[392] Zhou, J., and Rieker, A. (1997). Journal of the Chemical Society, Perkin Transactions 2, (5), 931–938. doi:10.1039/a607113i

[393] Schon, T. B., McAllister, B. T., Li, P.-F., and Seferos, D. S. (2016). Chemical Society Reviews, 45(22), 6345–6404. doi:10.1039/c6cs00173d

[394] Miroshnikov, M., Divya, K. P., Babu, G., Meiyazhagan, A., Reddy Arava, L. M., Ajayan, P. M., and John, G. (2016). Journal of Materials Chemistry A, 4(32), 12370–12386. doi:10.1039/c6ta03166h

[395] Zhao, Q., Zhu, Z., and Chen, J. (2017). Advanced Materials, 29(48), 1607007. doi:10.1002/adma.201607007

[396] Li, C., and Wonneberger, H. (2012). Advanced Materials, 24(5), 613–636. doi:10.1002/adma.201104447

[397] Vadehra, G. S., Maloney, R. P., Garcia-Garibay, M. A., and Dunn, B. (2014). Chemistry of Materials, 26(24), 7151–7157. doi:10.1021/cm503800r

[398] Kim, D. J., Je, S. H., Sampath, S., Choi, J. W., and Coskun, A. (2012). RSC Advances, 2(21), 7968. doi:10.1039/c2ra21239k

[399] Chen, D., Avestro, A.-J., Chen, Z., Sun, J., Wang, S., Xiao, M., … Stoddart, J. F. (2015). Advanced Materials, 27(18), 2907–2912. doi:10.1002/adma.201405416

[400] DeBlase, C. R., Hernández-Burgos, K., Rotter, J. M., Fortman, D. J., dos S. Abreu, D., Timm, R. A., … Dichtel, W. R. (2015). Angewandte Chemie International Edition, 54(45), 13225–13229. doi:10.1002/anie.201505289

[401] Xu, F., Jin, S., Zhong, H., Wu, D., Yang, X., Chen, X., … Jiang, D. (2015). Scientific Reports, 5(1). doi:10.1038/srep08225

[402] Veerababu, M., Varadaraju, U. ., and Kothandaraman, R. (2016). Electrochimica Acta, 193, 80–87. doi:10.1016/j.electacta.2016.02.030

[403] Banda, H., Damien, D., Nagarajan, K., Raj, A., Hariharan, M., and Shaijumon, M. M. (2017). Advanced Energy Materials, 7(20), 1701316. doi:10.1002/aenm.201701316

[404] Oltean, V.-A., Renault, S., Valvo, M., and Brandell, D. (2016). Materials, 9(3), 142. doi:10.3390/ma9030142

[405] Renault, S., Oltean, V. A., Araujo, C. M., Grigoriev, A., Edström, K., and Brandell, D. (2016). Chemistry of Materials, 28(6), 1920–1926. doi:10.1021/acs.chemmater.6b00267

[406] Pearce, N., Davies, E. S., Horvath, R., Pfeiffer, C. R., Sun, X.-Z., Lewis, W., … Champness, N. R. (2018). Physical Chemistry Chemical Physics, 20(2), 752–764. doi:10.1039/c7cp06952a

[407] Katsuta, S., Tanaka, K., Maruya, Y., Mori, S., Masuo, S., Okujima, T., … Yamada, H. (2011). Chemical Communications, 47(36), 10112. doi:10.1039/c1cc13980k

[408] Ye, Q., Chang, J., Huang, K.-W., Shi, X., Wu, J., and Chi, C. (2013). Organic Letters, 15(6), 1194–1197. doi:10.1021/ol400082c

[409] Tilley, A. J., Pensack, R. D., Lee, T. S., Djukic, B., Scholes, G. D., and Seferos, D. S. (2014). The Journal of Physical Chemistry C, 118(19), 9996–10004. doi:10.1021/jp503708d

[410] Würthner, F., and Stolte, M. (2011). Chemical Communications, 47(18), 5109. doi:10.1039/c1cc10321k

[411] Röger, C., and Würthner, F. (2007). The Journal of Organic Chemistry, 72(21), 8070–8075. doi:10.1021/jo7015357

[412] Míšek, J., Vargas Jentzsch, A., Sakurai, S., Emery, D., Mareda, J., and Matile, S. (2010). Angewandte Chemie International Edition, 49(42), 7680–7683. doi:10.1002/anie.201003722

[413] Yao, M., Kuratani, K., Kojima, T., Takeichi, N., Senoh, H., and Kiyobayashi, T. (2014). Scientific Reports, 4(1). doi:10.1038/srep03650

[414] Cao, R., Qian, J., Zhang, J.-G., and Xu, W. (2015). Organic Cathode Materials for Rechargeable Batteries. In Rechargeable Batteries (pp. 637–671). Springer International Publishing. doi:10.1007/978-3-319-15458-9_23

[415] Luo, W., Allen, M., Raju, V., and Ji, X. (2014). Advanced Energy Materials, 4(15), 1400554. doi:10.1002/aenm.201400554

[416] Slattery, D. (2001). Dyes and Pigments, 49(1), 21–27. doi:10.1016/s0143-7208(01)00009-2

[417] Takahashi, K., and Ogiyama, M. (1990). Journal of the Chemical Society, Chemical Communications, (17), 1196. doi:10.1039/c39900001196

[418] Akdag, A., Havlas, Z., and Michl, J. (2012). Journal of the American Chemical Society, 134(35), 14624–14631. doi:10.1021/ja3063327

[419] Wen, J., Havlas, Z., and Michl, J. (2014). Journal of the American Chemical Society, 137(1), 165–172. doi:10.1021/ja5070476

[420] Zimmerman, P. M., Bell, F., Casanova, D., and Head-Gordon, M. (2011). Journal of the American Chemical Society, 133(49), 19944–19952. doi:10.1021/ja208431r

[421] Margulies, E. A., Kerisit, N., Gawel, P., Mauck, C. M., Ma, L., Miller, C. E., … Wasielewski, M. R. (2017). The Journal of Physical Chemistry C, 121(39), 21262–21271. doi:10.1021/acs.jpcc.7b07870

[422] Bhattacharyya, K., Pratik, S. M., and Datta, A. (2015). The Journal of Physical Chemistry C, 119(46), 25696–25702. doi:10.1021/acs.jpcc.5b06960

[423] Sardar, S. (2017). Journal of Molecular Graphics and Modelling, 74, 24–37. doi:10.1016/j.jmgm.2017.01.020

[424] Chen, Y., Shen, L., and Li, X. (2014). The Journal of Physical Chemistry A, 118(30), 5700–5708. doi:10.1021/jp503114b

[425] Shen, L., Chen, Y., Li, X., and Gao, J. (2014). Journal of Molecular Graphics and Modelling, 51, 86–96. doi:10.1016/j.jmgm.2014.04.017

[426] Shen, L., Chen, Y., Li, X., and Li, C. (2016). Journal of Molecular Graphics and Modelling, 66, 187–195. doi:10.1016/j.jmgm.2016.04.007

[427] Busby, E., Berkelbach, T. C., Kumar, B., Chernikov, A., Zhong, Y., Hlaing, H., … Yaffe, O. (2014). Journal of the American Chemical Society, 136(30), 10654–10660. doi:10.1021/ja503980c

[428] Tomkiewicz, Y., Groff, R. P., and Avakian, P. (1971). The Journal of Chemical Physics, 54(10), 4504–4507. doi:10.1063/1.1674702

[429] Willstätter, R., and Parnas, J. (1907). Berichte Der Deutschen Chemischen Gesellschaft, 40(2), 1406–1415. doi:10.1002/cber.19070400224

[430] Menting, K. H., Eichel, W., Schmand, H. L. K., and Boldt, P. (1983). The Journal of Organic Chemistry, 48(17), 2814–2820. doi:10.1021/jo00165a006

[431] Schmand, H. L. K., and Boldt, P. (1975). Journal of the American Chemical Society, 97(2), 447–448. doi:10.1021/ja00835a052

[432] Horak, V., Foster, F. V., de Levie, R., Jones, J. W., and Svoronos, P. (1981). Tetrahedron Letters, 22(37), 3577–3578. doi:10.1016/s0040-4039(01)81962-6

[433] Boldt, P.; Zippel, S.; Ratzkowsky, M. (1996) Journal of the Chemical Society - Perkin Transactions 1, 21, 2615-2617.

[434] Verga, D., Nadai, M., Doria, F., Percivalle, C., Di Antonio, M., Palumbo, M., … Freccero, M. (2010). Journal of the American Chemical Society, 132(41), 14625–14637. doi:10.1021/ja1063857

[435] Škalamera, Đ., Mlinarić-Majerski, K., Uzelac, L., Kralj, M., Wan, P., and Basarić, N. (2013). Photochemical & Photobiological Sciences, 12(11), 2043. doi:10.1039/c3pp50190f

[436] Cava, M. P., and Napier, D. R. (1957). Journal of the American Chemical Society, 79(7), 1701–1705. doi:10.1021/ja01564a048

[437] Scott, L. T., and Adams, C. M. (1984). Journal of the American Chemical Society, 106(17), 4857–4861. doi:10.1021/ja00329a037

[438] Hafner, K., Häfner, K. H., König, C., Kreuder, M., Ploss, G., Schulz, G., … Vöpel, K. H. (1963). Angewandte Chemie International Edition in English, 2(3), 123–134. doi:10.1002/anie.196301231

[439] Morita, T., and Takase, K. (1977). Chemistry Letters, 6(5), 513–516. doi:10.1246/cl.1977.513

[440] Schore, N. E., La Belle, B. E., Knudsen, M. J., Hope, H., and Xu, X.-J. (1984). Journal of Organometallic Chemistry, 272(3), 435–446. doi:10.1016/0022-328x(84)80487-8

[441] Gross, G., Schulz, R., Schweig, A., and Wentrup, C. (1981). Angewandte Chemie, 93(12), 1078–1079. doi:10.1002/ange.19810931216

[442] Fukuzumi, S., Ohkubo, K., Ortiz, J., Gutiérrez, A. M., Fernández-Lázaro, F., and Sastre-Santos, A. (2008). The Journal of Physical Chemistry A, 112(43), 10744–10752. doi:10.1021/jp805464e

[443] Kazlauskas, K., Kreiza, G., Radiunas, E., Adomėnas, P., Adomėnienė, O., Karpavičius, K., … Juršėnas, S. (2015). Physical Chemistry Chemical Physics, 17(19), 12935–12948. doi:10.1039/c5cp01325a

[444] Zheng, S., Tan, H., Zhang, X., Yu, C., and Shen, Z. (2014). Tetrahedron Letters, 55(5), 975–978. doi:10.1016/j.tetlet.2013.11.081

[445] Ohkita, M., Nishida, S., and Tsuji, T. (1999). Journal of the American Chemical Society, 121(19), 4589–4597. doi:10.1021/ja984348u

[446] Johnson, J. C., Nozik, A. J., and Michl, J. (2010). Journal of the American Chemical Society, 132(46), 16302–16303. doi:10.1021/ja104123r

[447] Johnson, J. C., Akdag, A., Zamadar, M., Chen, X., Schwerin, A. F., Paci, I., … Michl, J. (2013). The Journal of Physical Chemistry B, 117(16), 4680–4695. doi:10.1021/jp310979q

[448] Schrauben, J. N., Akdag, A., Wen, J., Havlas, Z., Ryerson, J. L., Smith, M. B., … Johnson, J. C. (2016). The Journal of Physical Chemistry A, 120(20), 3473–3483. doi:10.1021/acs.jpca.6b00826

[449] Treibs, A., and Jacob, K. (1965). Angewandte Chemie International Edition in English, 4(8), 694–694. doi:10.1002/anie.196506941

[450] G. A. Rillaers, H. Depoorter, DE 1930224, (1970**),** 72, 122944

[451] Treibs, A., and Schulze, L. (1973). Justus Liebigs Annalen Der Chemie, 1973(2), 201–206. doi:10.1002/jlac.197319730205

[452] Takechi, K., Kamat, P. V., Avirah, R. R., Jyothish, K., and Ramaiah, D. (2008). Chemistry of Materials, 20(1), 265–272. doi:10.1021/cm7018668

[453] Silvestri, F., Irwin, M. D., Beverina, L., Facchetti, A., Pagani, G. A., and Marks, T. J. (2008). Journal of the American Chemical Society, 130(52), 17640–17641. doi:10.1021/ja8067879

[454] Tian, M., Furuki, M., Iwasa, I., Sato, Y., Pu, L. S., and Tatsuura, S. (2002). The Journal of Physical Chemistry B, 106(17), 4370–4376. doi:10.1021/jp013698r

[455] Chen, G., Sasabe, H., Igarashi, T., Hong, Z., and Kido, J. (2015). Journal of Materials Chemistry A, 3(28), 14517–14534. doi:10.1039/c5ta01879j

[456] Prabhakar, C., Promila, Tripathi, A., Bhanuprakash, K., and Jayathirtharao, V. (2017). Journal of Molecular Structure, 1146, 684–691. doi:10.1016/j.molstruc.2017.06.005

[457] Prabhakar, C., Yesudas, K., Krishna Chaitanya, G., Sitha, S., Bhanuprakash, K., and Rao, V. J. (2005). The Journal of Physical Chemistry A, 109(38), 8604–8616. doi:10.1021/jp0516184

[458] Meier, H., and Dullweber, U. (1997). The Journal of Organic Chemistry, 62(14), 4821–4826. doi:10.1021/jo970284e

[459] Petermann, R., Tian, M., Tatsuura, S., and Furuki, M. (2003). Dyes and Pigments, 57(1), 43–54. doi:10.1016/s0143-7208(03)00003-2

[460] Meier, H., and Petermann, R. (2004). Helvetica Chimica Acta, 87(5), 1109–1118. doi:10.1002/hlca.200490101

[461] Meier, H., and Dullweber, U. (1996). Tetrahedron Letters, 37(8), 1191–1194. doi:10.1016/0040-4039(95)02414-x

[462] Pschirer, N. G., Kohl, C., Nolde, F., Qu, J., and Müllen, K. (2006). Angewandte Chemie International Edition, 45(9), 1401–1404. doi:10.1002/anie.200502998

[463] G. A. Casay, N. Narayanan, L. Evans-III, T. Czuppon, G. Patonay, (1996). Talanta, 43(11), 1997–2005. doi:10.1016/0039-9140(96)01989-3

[464] Sauve, G., Kamat, P. V., Thomas, K. G., Thomas, K. J., Das, S., and George, M. V. (1996). The Journal of Physical Chemistry, 100(6), 2117–2124. doi:10.1021/jp9520815

[465] Makowski, M., and Pawlikowski, M. T. (2003). Chemical Physics Letters, 376(5–6), 631–637. doi:10.1016/s0009-2614(03)01039-x

[466] Makowski, M., and Pawlikowski, M. T. (2003). The Journal of Chemical Physics, 119(24), 12795–12804. doi:10.1063/1.1626544

[467] Zhang, X., Li, C., Cheng, X., Wang, X., and Zhang, B. (2008). Sensors and Actuators B: Chemical, 129(1), 152–157. doi:10.1016/j.snb.2007.07.094

[468] Minami, T., and Nakano, M. (2011). The Journal of Physical Chemistry Letters, 3(2), 145–150. doi:10.1021/jz2015346

[469] Elfers, N., Lyskov, I., Spiegel, J. D., and Marian, C. M. (2016). The Journal of Physical Chemistry C, 120(26), 13901–13910. doi:10.1021/acs.jpcc.6b02263

[470] Naoda, K., Shimizu, D., Kim, J. O., Furukawa, K., Kim, D., and Osuka, A. (2017). Chemistry - A European Journal, 23(37), 8969–8979. doi:10.1002/chem.201701355

[471] Lukman, S., Richter, J. M., Yang, L., Hu, P., Wu, J., Greenham, N. C., and Musser, A. J. (2017). Journal of the American Chemical Society, 139(50), 18376–18385. doi:10.1021/jacs.7b10762

[472] Le, A. K., Bender, J. A., Arias, D. H., Cotton, D. E., Johnson, J. C., and Roberts, S. T. (2018). Journal of the American Chemical Society, 140(2), 814–826. doi:10.1021/jacs.7b11888

[473] Eaton, S. W., Shoer, L. E., Karlen, S. D., Dyar, S. M., Margulies, E. A., Veldkamp, B. S., … Wasielewski, M. R. (2013). Journal of the American Chemical Society, 135(39), 14701–14712. doi:10.1021/ja4053174

[474] Zhan, X., Facchetti, A., Barlow, S., Marks, T. J., Ratner, M. A., Wasielewski, M. R., and Marder, S. R. (2010). Advanced Materials, 23(2), 268–284. doi:10.1002/adma.201001402

[475] Chao, C.-C., Leung, M., Su, Y. O., Chiu, K.-Y., Lin, T.-H., Shieh, S.-J., and Lin, S.-C. (2005). The Journal of Organic Chemistry, 70(11), 4323–4331. doi:10.1021/jo050001f

[476] Ford, W. E., and Kamat, P. V. (1987). The Journal of Physical Chemistry, 91(25), 6373–6380. doi:10.1021/j100309a012

[477] Fukuzumi, S., Ohkubo, K., Ortiz, J., Gutiérrez, A. M., Fernández-Lázaro, F., and Sastre-Santos, A. (2008). The Journal of Physical Chemistry A, 112(43), 10744–10752. doi:10.1021/jp805464e

[478] A.S. Travis, in: Z. Rappoport (Ed.), The Chemistry of Anilines, 2007, Part 1, Chapter 1, pp. 1–74.

[479] Lei, T., Wang, J.-Y., and Pei, J. (2014). Accounts of Chemical Research, 47(4), 1117–1126. doi:10.1021/ar400254j

[480] Clark, R. J. ., Cooksey, C. J., Daniels, M. A. ., and Withnall, R. (1993). Endeavour, 17(4), 191–199. doi:10.1016/0160-9327(93)90062-8

[481] Christie, R. (2007). Biotechnic & Histochemistry, 82(2), 51–56. doi:10.1080/00958970701267276

[482] de Melo, J. S. S., Rondão, R., Burrows, H. D., Melo, M. J., Navaratnam, S., Edge, R., and Voss, G. (2006). ChemPhysChem, 7(11), 2303–2311. doi:10.1002/cphc.200600203

[483] Monahan, A. R., and Kuder, J. E. (1972). The Journal of Organic Chemistry, 37(25), 4182–4184. doi:10.1021/jo00798a048

[484] Seixas de Melo, J. S., Burrows, H. D., Serpa, C., and Arnaut, L. G. (2007). Angewandte Chemie International Edition, 46(12), 2094–2096. doi:10.1002/anie.200604679

[485] Josef Michl's lecture at the Molecular Frontiers Symposium at Chalmers University of Technology, Sweden, Dec 2017.

[486] Jacquemin, D., Perpète, E. A., Scuseria, G. E., Ciofini, I., and Adamo, C. (2008). Journal of Chemical Theory and Computation, 4(1), 123–135. doi:10.1021/ct700187z

[487] Nawn, G., Waldie, K. M., Oakley, S. R., Peters, B. D., Mandel, D., Patrick, B. O., … Hicks, R. G. (2011). Inorganic Chemistry, 50(20), 9826–9837. doi:10.1021/ic200388y

[488] Perpète, E. A., Preat, J., André, J.-M., and Jacquemin, D. (2006). The Journal of Physical Chemistry A, 110(17), 5629–5635. doi:10.1021/jp060069e

[489] Wang, C., Zhang, Z., and Wang, Y. (2016). Journal of Materials Chemistry C, 4(42), 9918–9936. doi:10.1039/c6tc03621j

[490] Shi, J., and Tang, C. W. (1997). Applied Physics Letters, 70(13), 1665–1667. doi:10.1063/1.118664

[491] Wang, S., Zhang, Y., Chen, W., Wei, J., Liu, Y., and Wang, Y. (2015). Chemical Communications, 51(60), 11972–11975. doi:10.1039/c5cc04469c

[492] Daniel Głowacki, E., Leonat, L., Irimia-Vladu, M., Schwödiauer, R., Ullah, M., Sitter, H., … Serdar Sariciftci, N. (2012). Applied Physics Letters, 101(2), 23305. doi:10.1063/1.4736579

[493] Osaka, I., Akita, M., Koganezawa, T., and Takimiya, K. (2012). Chemistry of Materials, 24(6), 1235–1243. doi:10.1021/cm300514z

[494] Song, H.-J., Kim, D.-H., Lee, E.-J., Heo, S.-W., Lee, J.-Y., and Moon, D.-K. (2012). Macromolecules, 45(19), 7815–7822. doi:10.1021/ma301466m

[495] Loutfy, R. (1991). Dyes and Pigments, 15(2), 139–156. doi:10.1016/0143-7208(91)87013-d

[496] Li, W., Hendriks, K. H., Wienk, M. M., and Janssen, R. A. J. (2015). Accounts of Chemical Research, 49(1), 78–85. doi:10.1021/acs.accounts.5b00334

[497] Kim, N.-K., Shin, E.-S., Noh, Y.-Y., and Kim, D.-Y. (2018). Organic Electronics, 55, 6–14. doi:10.1016/j.orgel.2018.01.006

[498] Irimia-Vladu, M., Troshin, P. A., Reisinger, M., Schwabegger, G., Ullah, M., Schwoediauer, R., … Razumov, V. F. (2010). Organic Electronics, 11(12), 1974–1990. doi:10.1016/j.orgel.2010.09.007

[499] Champagne, B., Liégeois, V., and Zutterman, F. (2015). Photochemical & Photobiological Sciences, 14(2), 444–456. doi:10.1039/c4pp00317a

[500] Mizuguchi, J. (2004). The Journal of Physical Chemistry B, 108(26), 8926–8930. doi:10.1021/jp031351d

[501] Gruen, H., and Görner, H. (2011). Photochemical & Photobiological Sciences, 10(10), 1527. doi:10.1039/c1pp05086a

[502] Pariser, R. (1956). The Journal of Chemical Physics, 25(6), 1112–1116. doi:10.1063/1.1743159

[503] Tobe, Y. (2014). The Chemical Record, 15(1), 86–96. doi:10.1002/tcr.201402077

[504] Koch, M., Blacque, O., and Venkatesan, K. (2012). Organic Letters, 14(6), 1580–1583. doi:10.1021/ol300327b

[505] Nakajima, T., Yaguchi, Y., Kaeriyama, R., and Nemoto, Y. (1964). Bulletin of the Chemical Society of Japan, 37(2), 272–276. doi:10.1246/bcsj.37.272

[506] Dauben, H. J., Jr., and Bertelli, D. J. (1961). Journal of the American Chemical Society, 83(22), 4659–4660. doi:10.1021/ja01483a038

[507] Paquette, L. A., Browne, A. R., and Chamot, E. (1979). Angewandte Chemie International Edition in English, 18(7), 546–547. doi:10.1002/anie.197905461

[508] Nickel, B., and Klemp, D. (1993). Chemical Physics, 174(2), 297–318. doi:10.1016/0301-0104(93)87014-e

[509] Zeng, Z., Sung, Y. M., Bao, N., Tan, D., Lee, R., Zafra, J. L., … Wu, J. (2012). Journal of the American Chemical Society, 134(35), 14513–14525. doi:10.1021/ja3050579

[510] Zafra, J. L., González Cano, R. C., Ruiz Delgado, M. C., Sun, Z., Li, Y., López Navarrete, J. T., … Casado, J. (2014). The Journal of Chemical Physics, 140(5), 54706. doi:10.1063/1.4863557

[511] Anthony, J. E. (2008). Angewandte Chemie International Edition, 47(3), 452–483. doi:10.1002/anie.200604045

[512] http://omlc.org/

[513] Sun, Z., Lee, S., Park, K. H., Zhu, X., Zhang, W., Zheng, B., … Wu, J. (2013). Journal of the American Chemical Society, 135(48), 18229–18236. doi:10.1021/ja410279j

[514] J.B. Birks, Photophysics of Aromatic Molecules, Wiley, New York, 1970.

[515] Oda, M., Sakamoto, Y., Kajioka, T., Uchiyama, T., Miyatake, R., and Kuroda, S. (2001). Angewandte Chemie International Edition, 40(14), 2660–2662. doi:10.1002/1521-3773(20010716)40:14<2660::aid-anie2660>3.0.co;2-6